UNCLASSIFIED

| AD NUMBER: | AD0909224 |
|---|---|

## LIMITATION CHANGES

TO:

Approved for public release; distribution is unlimited.

FROM:

Distribution authorized to US Government Agencies only; Test and Evaluation; 20 Dec 1971 May 1942. Other requests shall be referred to Space and Missile Systems Organization, Los Angeles, CA 90045.

## AUTHORITY

SAMSO ltr dtd 29 Sep 1976

THIS PAGE IS UNCLASSIFIED

# (U) Proceedings of the Boundary Layer Transition Workshop Held 3-5 November 1971

## Volume IV

Prepared by W. D. McCauley
Technology Division

71 DEC 20

D D C
APR 23 1973

San Bernardino Operations
THE AEROSPACE CORPORATION

Technical operating rept.,

# PROCEEDINGS OF THE BOUNDARY LAYER TRANSITION WORKSHOP HELD 3-5 NOVEMBER 1971.

## Volume IV,

Prepared by

W. D. McCauley
Technology Division

20 Dec 71          220 p.

71 DEC 20

San Bernardino Operations
THE AEROSPACE CORPORATION
San Bernardino, California

D D C

RECEIVED
APR 23 1973
E

Prepared for

SPACE AND MISSILE SYSTEMS ORGANIZATION
AIR FORCE SYSTEMS COMMAND
Air Force Unit Post Office
Los Angeles, California 90045

402 067

(U) PROCEEDINGS OF THE BOUNDARY LAYER
TRANSITION WORKSHOP HELD 3-5 NOVEMBER 1971

Volume IV

Prepared

*W. D. McCauley*

W. D. McCauley
Flight Performance Evaluation

Approved

*T. A. Bergstralh*

T. A. Bergstralh, General Manager
Technology Division

# FOREWORD

(U)   The Boundary Layer Transition Specialists Workshop was held on November 3-5, 1971 at Aerospace Corporation, San Bernardino, California. The objective of the meeting was to make transition specialists aware of the most recent data and techniques for transition prediction and to focus on the solution of design problems associated with boundary layer transition.

(U)   The Proceedings of the meeting have been compiled by Aerospace Corporation, San Bernardino Operations, under Contract No. F04701-71-C-0172 as TOR-0172(S2816-16)-5. The Air Force program monitor is Col. C. Zimmerman, USAF (SAMSO/RNS). The Proceedings were edited by William D. McCauley and submitted for publication in December 1971.

(U)   The chairman and co-chairmen of the meeting were Dr. Richard A. Hartunian, Dr. Frank L. Fernandez and William D. McCauley of the Aerospace Corporation, respectively. Principle contributors selected for their demonstrated expertise in the field of Boundary Layer Transition include those listed as authors in the Table of Contents. The session and committee chairmen are indicated in the meeting notes which follow.

(U)   The proceedings consist of four volumes. Volume I contains the Keynote address on the NASA Transition Study Group and the session on Transition Design Problems and Information Needed for Their solution. Volume II contains the session on Recent Flight Test Transition Data and Correlations. Volume III contains the session on Recent Ground Test Transition Data and Correlations. Volume IV contains the session on Boundary Layer Stability Theory, Tests and Transition Modeling, and the recommendations of four committees for future efforts on boundary layer transition.

(U) BOUNDARY LAYER TRANSITION
SPECIALISTS WORKSHOP, Volumes I
through IV, Edited by W. D. McCauley

TOR-0172(S2816-16)-5
Volumes I-IV
December 1971

The workshop consisted of introductory remarks, a keynote address, four reporting investigation sessions and a session involving all participants on four committees. The objective of the meeting was to make transition specialists aware of the most recent data and techniques for transition prediction and to focus on the solution of design problems associated with boundary layer transition. The first session showed how transition affects reentry vehicle design in terms of nosetip thermostress and ablation, transpiration cooled nosetips, frustum ablation, reentry observables, plasma attenuation, vehicle dynamics and space shuttle design. The second session presented ABRES reentry vehicle transition data and prediction techniques obtained since the previous meeting four years ago. The third session presented recent data obtained from government laboratories. The fourth session presented recent applications of stability theory, additional confirmation of the theory and work toward transition modeling. In the last session the meeting participants worked on four committees to arrive at recommendations for future efforts on boundary layer transition.
(Secret Formerly Restricted Data Report)

# MEETING NOTES

(U)     About four years ago SAMSO/Aerospace held a similar meeting to make transition specialists aware of the recent flight test data, discrepancies between laboratory and flight data and correlations of flight transition data which were being used for transition prediction but were not compatible with all of the trends of the laboratory investigations.  Since that meeting, a significant amount of additional flight data has been obtained by SAMSO/Aerospace and a variety of transition correlations have been developed utilizing the seemingly abundant data.*  Unfortunately, none of these correlations has resulted in completely successful prediction of transition occurrence on flight vehicles and some surprises in the low altitude occurrence of transition during reentry were obtained most notably on the SAMAST and RVTO-2B vehicles which are shown in detail in the proceedings.

(U)     Dr. Mark Morkovin attempted to instigate a similar type of meeting through the NASA committee on which he served over a year ago.  Though this meeting did not materialize it was probably instrumental in establishing the NASA Transition Study Group.  Dr. Eli Reshotko reports on the activities of this group in the proceedings as our keynote speaker.  This approach of integrating theoretical and ground test efforts, understanding facility limitations and developing quiet tunnels for transition research should ultimately yield a more complete understanding of transition phenomena.

(U)     The success of the meeting can really be attributed to the caliber and efforts of the chairmen, speakers, and attendees who were invited to participate.  The meeting was organized around five primary sessions.  Introductory remarks by Dr. Brian D. Henshall, Associate General Manager, Aerospace Corporation, San Bernardino Operations, and a keynote address by Dr. Eli Reshotko on the NASA Transition Study Group set the stage for the meeting.  The first session Transition Design Problems and Information

---

*Though abundant data exist it is with few sensors per flight, different types of sensors, different configurations and different materials making separation of the variables which affect transition difficult.

v

Needed for Their Solution, chaired by E. Hertler of Aerospace, was organized to show how transition affects reentry vehicle design in terms of nosetip thermostructure and ablation, transpiration cooled nosetips, frustum ablation, reentry observables, plasma attenuation, vehicle dynamics and space shuttle design. The second session, Recent Flight Test Transition Data and Correlations chaired by Dr. N. Jaffe of Aerospace, was used to present the ABRES flight transition data and flight data correlations obtained since the meeting which occurred four years ago. Since the results of the first two sessions were for the most part classified, they are presented in the classified Volumes I and II of the proceedings. The third session, Recent Ground Test Data and Correlation chaired by Dr. W. R. Warren of the Aerospace Laboratory, presented the most recent work obtained throughout the government laboratories. Examination of these papers in the proceedings shows the significant influence of the NASA Transition Study Group already being made on quiet tunnel development and resolving discrepancies between transition results from the various government facilities.

(U)    The fourth session, Boundary Layer Stability Theory, Transition Modeling, and Confirming tests, chaired by Dr. John Laufer of the University of Southern California, gave the most recent results of stability theory applications, additional confirmation of the theory by supporting tests, and an attempt to construct an analytic model of transition. In the fifth session, Workshop Committees and Recommendations, was chaired by Dr. R. Kenneth Lobb of the Naval Ordnance Laboratory; all of the attendees and speakers of the workshop were invited to participate on committees of their specialties, and considering the many problems associated with their specialties, to come up with recommendations for studies or approaches for solutions to these problems. There were four committees in this session including:

Committee A:  Theoretical Approaches
    Dr. Eli Reshotho, Chairman
Committee B:  Transition Data Correlation Approaches
    Dr. Leith Potter, Chairman
Committee C:  Transition Flight Test Efforts Needed
    Dr. Frank Fernandez, Chairman
Committee D:  Transition Ground Test Efforts Needed
    Dr. Mark Morkovin, Chairman

The results of these committee meetings were summarized by the committee chairmen to all of the workshop participants. These summaries were taped at the meeting, have been transcribed and are presented in Volume IV of the Proceedings.

(U)     In the organization of the meeting, many individuals contributed to its success. Most notable was our secretary, Shirley Jelen, the Technology Division Administrator Gordon Lamb and the projectionist Bob Lemke. Publication of the proceedings occurred in a timely manner through the dedicated efforts of George Waggoner in our publications department.

# VOLUME IV

## CONTENTS

## SESSION IV   BOUNDARY LAYER STABILITY THEORY, TESTS, AND TRANSITION MODES

CONTENTS (Continued)

cont on
p. x

CONTENTS (Continued)

CONTENTS (Continued)

## SESSION V WORKSHOP COMMITTEE RECOMMENDATIONS —
### Dr. Kenneth Lobb, Chairman

# FIGURES

## SESSION IV

FIGURES (Continued)

## TABLES

## SESSION IV

(This page intentionally left blank)

# SESSION IV

## BOUNDARY LAYER STABILITY THEORY, TESTS, AND TRANSITION MODELS

# SECTION 1

# PROGRESS IN COMPRESSIBLE BOUNDARY LAYER STABILITY COMPUTATIONS[*]
## (Unclassified)

by Leslie M. Mack

Jet Propulsion Laboratory, Pasadena, Calif.

## ABSTRACT

Progress made since the first San Bernardino Transition Workshop in 1967 in the computation of the stability of laminar compressible boundary layers on the basis of the linearized parallel-flow theory is described. Both the viscous and inviscid computer programs in use at that time have been improved. Eigenvalues and eigenfunctions of two- and three-dimensional temporal or spatial disturbances in either two- or three-dimensional boundary layers can be computed. The use of the Gram-Schmidt orthonormalization technique permits the viscous problem to be solved at extremely high Reynolds numbers. As one example of a stability calculation, the three-dimensional frequency response is computed as a function of downstream position at three unit Reynolds numbers for a given input disturbance spectrum. As another example, it is shown that damped disturbances which travel faster than the free stream lead to a temperature reversal phenomenon for highly cooled boundary layers.

In addition to the self-excited disturbances of the usual stability theory, the forced response of the boundary layer to externally imposed disturbances is of interest, particularly in connection with studies of transition in conventional supersonic wind tunnels. The viscous and inviscid stability programs have been modified to compute the forced response of a boundary layer to an external pressure disturbance of specified wave length and phase velocity. When the phase velocity is supersonic with respect to

the free stream, this disturbance is a sound wave. The calculations show that according to the viscous theory, but not the inviscid, there is a region starting at the leading edge in which disturbances of all frequencies grow as they travel downstream. The length of this region is inversely proportional to the frequency, and can extend well into the region of instability of self-excited disturbances. Results are given as a function of Mach number; as a function of frequency, phase velocity and wave angle at $M_1 = 4.5$; and as a function of wall temperature at $M_1 = 5.8$.

## INTRODUCTION

At the present time the linear stability theory is the only theoretical tool available for studying boundary-layer transition. When this theory is applied to the undisturbed laminar profiles of velocity and temperature, it provides the frequency response of the boundary layer. The unstable frequency range and the growth of each frequency are given as functions of $R_x$, the free-stream x Reynolds number, where x is the downstream distance from the origin of the boundary layer. With the unstable frequencies known it is possible to assess the probable importance to transition of various sources of external disturbances. Computations of the disturbance amplitude as a function of mean-flow parameters such as Mach number, wall temperature, pressure gradient, etc. give some information as to the effect of each of these quantities on transition.

The asymptotic stability theory has proved to be inadequate for Mach numbers above about 1.5, and recourse is made to direct numerical solutions of the linearized stability equations, which are further reduced to ordinary differential equations by the parallel-flow assumption. Even at low speeds, where the asymptotic theory can yield useful results, ease of computation and the completeness and accuracy of the numerical results has led to increasing use of direct numerical computations. Versatile computer programs such as those of Landahl (Ref. 1) and Reynolds (Ref. 2) are in common use. A key development in the numerical integration of the stability equations was made by Kaplan (Ref. 3) and is incorporated in both of these programs. This development makes it possible to carry out the numerical integration at virtually any Reynolds number, no matter how large.

Computer programs for the integration f the compressible stability equations have been developed by Brown (Ref. 4) and the present author (Ref. 5). The extensive numerical results obtained from the latter program and a companion program for the integration of the inviscid stability equations have been collected together in a single volume (Ref. 6), which also includes an exposition of the theory. These calculations, based on the parallel-flow theory, give excellent agreement with the stability experiments of Kendall (Ref. 7). Later work by Brown (Ref. 8), which attempted to remove the parallel-flow restriction, does not agree with these experiments.

In the present paper, after a description of both the inviscid and viscous computer programs, the principal results of the stability theory are reviewed. Then two topics of particular importance to the transition problem are taken up, the growth of a disturbance whose power spectrum is known, and the effect of wall cooling on the maximum disturbance amplitude at $M_1 = 5.8$. The remainder of the paper is devoted to a problem that lies outside of the usual stability theory, but which can be treated by similar methods. This problem is the forced response of a laminar boundary to a moving sound wave, and it has direct bearing on the question of transition in supersonic wind tunnels.

## DESCRIPTION OF COMPUTER PROGRAMS

### Inviscid Equations

A system of two linear first-order ordinary differential equations is integrated from the free stream to the wall by a variable step size, variable order Adams-Moulton integrator. For neutral and damped disturbances the integration proceeds along a contour with a rectangular indentation at the critical point. The proper contour is chosen automatically, but can be specified as input if desired.

The disturbances are of the form

$$q'(x,y,z,t) = q(y) \exp\left[i(\alpha x + \beta z - \omega t)\right]$$

where $q(y)$ is a complex amplitude function with $y$ the coordinate normal to the wall, $\alpha$ and $\beta$ are dimensionless wave numbers, and $\omega$ is the dimensionless

frequency. The reference velocity is the free-stream velocity $U_1^*$ and the reference length is

$$L^* = (x^* v_1^* / U_1^*)^{\frac{1}{2}} = x^* / \langle$$

where the asterisks refer to dimensional quantities, the subscript 1 refers to free-stream quantities, and $v^*$ is the kinematic viscosity coefficient. Also

$$R = U_1^* L^* / v_1^* = R_x^{\frac{1}{2}} .$$

Either $\alpha$ (and $\beta$) or $\omega$, or both, can be complex. When $\alpha$ and $\beta$ are real and $\omega$ complex, the disturbance grows temporally; when $\alpha$ and $\beta$ are complex and $\omega$ is real, the disturbance grows spatially; when $\alpha$, $\beta$ and $\omega$ are all complex, the disturbance grows both temporally and spatially. When $\beta = 0$, the disturbance is two-dimensional; when $\beta \neq 0$, the line of constant phase in the x-z plane is oblique to the x direction and the disturbance is three-dimensional. The angle $\psi$ between the normal to the constant-phase line and the x direction is the wave obliqueness angle. The oblique spatial disturbances are required to have constant amplitude along the constant phase line.

There are three basic options in the program:

1) The equations are integrated for any specified values of $\alpha$, $\omega$ (or $c = \omega/\alpha$) and $\psi$.

2) The following eigenvalue searches can be carried out:

| Type of Disturbance | | Constant |
|---|---|---|
| Temporal: | a) | $\omega_i$ |
| | b) | $\alpha$ |
| | c) | $c_r$ $(= \omega_r/\alpha)$ |
| | d) | $\omega_r$ |
| Spatial: | a) | $\alpha_i$ |
| | b) | phase velocity $= \omega_r/\alpha_r$ |
| | c) | $\alpha_r$ |
| | d) | $\omega_r$ |

Temporal/Spatial:     a)     $\alpha = \alpha_r + i\alpha_i$

                      b)     $\omega = \omega_r + i\omega_i$

The eigenvalue searches are completely automated, and may be operated either for a fixed number of iterations, or until preset convergence criteria have been satisfied.

3) **Response to external pressure field** (see final section).

For every specified $\alpha$, c and $\psi$ there is a solution. Both $\alpha$ and c are real (neutral disturbances only). When $c < 1 - 1/M_1$, the external pressure field is a sound wave.

Detailed output can be provided at the conclusion of the eigenvalue search, or during the integrations of options (1) and (3), as a function of $\eta$, where

$$\eta = y^* (U_1^* / x^* v_1^*)^{\frac{1}{2}} .$$

is the Blasius variable. The output is given at increments $h = \Delta\eta$, and up to 10 different values of h can be assigned for selected intervals of $y/\delta$. Besides the dependent variables and their derivatives, the rms amplitudes and phases of the following quantities are computed: $u'$, $v'$, $w'$, $T'$ (all referred to both the local mean flow and the free-stream flow), $p'$, $\rho'$, $m'$ (mass-flow fluctuation) and $T_o'$ (stagnation-temperature fluctuation). In addition, the terms of the local energy balance

$$\frac{\partial E}{\partial t} + U \frac{\partial E}{\partial x} + W \frac{\partial E}{\partial z} = \tau_x \frac{dU}{dy} + \tau_z \frac{dW}{dy} - \frac{1}{\gamma M_1^2}\left[ \frac{\partial}{\partial x}\overline{(p'u')} + \frac{\partial}{\partial y}\overline{(p'v')} + \frac{\partial}{\partial z}\overline{(p'w')} \right]$$

are computed, where $\tau_x$ and $\tau_z$ are the components of the Reynolds stress, and E is the sum of the kinetic and potential energies.

$$E = \frac{1}{2}\rho(\overline{u'^2} + \overline{v'^2} + \overline{w'^2}) + \frac{1}{2}M_1^2 \overline{(p'/\gamma M_1^2)^2}$$

The eigenfunction output can be normalized if desired so that $m'$ at the boundary-layer edge is equal to 1.0 (or any other value if provided as input). The boundary-layer thickness is computed by the program to be

the 0.999 $U_1^*$ point, but can be assigned to be any value. For the forced case, the output is normalized such that $p'/\gamma M_1^2$ of the incoming pressure field at $\eta = 0$ with no boundary layer is 0.00025 (or any desired value can be assigned).

## Viscous Equations

A system of four, six or eight linear first-order ordinary differential equations, depending upon the particular problem under consideration, is integrated from the free stream to the wall. The mean boundary-layer profiles may be incompressible or compressible and two- or three-dimensional. The disturbances may be temporal, spatial or temporal/spatial, and may be two- or three-dimensional. The program has the same three basic options as the inviscid program: (1) integration of equations only, (2) eigenvalue searches, and (3) response to an external pressure field. In addition to the parameters $\alpha$, $\omega$ (or c) and $\psi$ of the inviscid theory, there are two additional parameters: the Reynolds number R, and a new dimensionless frequency F which is independent of $x^*$ for a given frequency when the free stream is independent of $x^*$.

$$F = \frac{\omega^* \nu_1^*}{U_1^{*2}} = \frac{\omega}{R} .$$

The possible eigenvalue searches are:

| Type of Disturbance | | Constant |
|---|---|---|
| Temporal: | a) | $\omega_i$, R |
| | b) | $\omega_i$, $\alpha$ |
| | c) | $\alpha$, R |
| | d) | $F_r$, R |
| | e) | $F_r$, $c_i (= 0)$ |
| Spatial: | a) | $\alpha_i$, R |
| | b) | $\alpha_r$, $\alpha_i$ |
| | c) | $\alpha_r$, R |
| | d) | $F_r$, R |

Temporal/Spatial:      a)    $\alpha$, R

                                b)    F, R

The detailed output is the same as given by the inviscid program except that the amplitudes and phases of the three vorticity components are also computed. This output can be supplied at the same points and is normalized in the same way as in the inviscid program.

The program contains three separate integrators: (1) a fourth-order Runge-Kutta fixed step size integrator; (2) an Adams-Moulton fixed step size integrator with a fixed order that can be specified to be from one to eight, and with either a Runge-Kutta or analytic start; (3) the same variable step size, variable order Adams-Moulton integrator (or a full double-precision equivalent) used in the inviscid program. The problem of rapid error growth, which is usually circumvented in incompressible computations by Kaplan's purification method, is taken care of in this program by the Gram-Schmidt orthonormalization procedure used by Wazzan, Okamura and Smith (Ref. 9). Eigenvalues and eigenfunctions can thus be computed at virtually any Reynolds number desired. The orthonormalization, which can be bypassed completely when not needed, always takes place at the initial and final point and either after an assigned number of integration steps in the fixed step size integrators, or in all integrators when the largest component of the independent solutions has grown greater than an assigned magnitude. Eigenvalues have been successfully computed at $\alpha R = 31,000$ ($\alpha_\delta * R_\delta * = 3.3 \times 10^6$) where the largest viscous solution grows to $10^{210}$, and even higher values of $\alpha R$ can be reached.

## RESULTS OF STABILITY COMPUTATIONS

### Summary of Principal Results

For a comprehensive review of the results obtained from numerical studies of the stability of flat-plate laminar boundary layers, the reader is referred to the report by the author mentioned in the Introduction (Ref. 6). A few of the more important results will be summarized here before going on to a brief discussion of two investigations carried out since the first San Bernardino Transition Meeting.

1. The flat-plate laminar boundary layer on an insulated wall is unstable to inviscid disturbances at all Mach numbers above zero, and to viscous disturbances at all Mach numbers.

2. Whenever the local Mach number of the flow relative to the disturbance phase velocity, $\hat{M} = M_1 (U - c)/T^{\frac{1}{2}}$, is supersonic somewhere in the boundary layer, an infinite number of instability modes exists. In a wind tunnel this situation first occurs at about $M_1 = 2.2$ for neutral disturbances. The first mode is the same as in incompressible flow. In the inviscid theory the second mode is always the most unstable, and except near its critical Reynolds number is also the most unstable in the viscous theory.

3. The well-known destabilizing effect of viscosity at $M_1 = 0$ persists up to about $M_1 = 3.0$. Above this Mach number, inviscid stability dominates and the effect of viscosity is only stabilizing, i.e., the maximum amplification rate increases monotonically to its inviscid value as $R \to \infty$. The effect of viscosity on the second and higher modes is stabilizing at all Mach numbers.

4. First-mode three-dimensional disturbances are more unstable than two-dimensional disturbances at all supersonic Mach numbers. This effect is a maximum near $M_1 = 3.0$, where the most unstable disturbance is at $\psi = 65°$ and has a temporal amplification rate at $R = 1000$ about 20 times larger than the most unstable two-dimensional disturbance.

5. The effect of cooling the wall is to stabilize the first-mode disturbances, but not the higher-mode disturbances. The effect on the higher modes is to increase their unstable frequency range with little effect on their maximum amplification rates.

Effect of Mach Number on Amplification Rate, Amplitude Ratio and Unstable Frequencies

Figure 1 gives the maximum spatial amplification rate at $R = 1500$ as a function of Mach number for the first and second modes. The wave angle of the most unstable first-mode disturbances is marked on the figure. The first-mode curve ends at $M_1 = 8$ because beyond that point there is no longer a discernible maximum amplification rate in the first-mode region. The fractional change in amplitude can be written

$$\frac{\delta A}{A} = - 2\, \alpha_i\, \delta R$$

so the amplification rate $-\alpha_i$ is a measure of the relative instability of two boundary layers for equal changes in R.

Since the maximum amplification rate exists only at a single Reynolds number for each frequency, Fig. 1 gives an incomplete idea of how the actual amplitude of the most unstable disturbance changes with Mach number. More complete information is obtained by integrating the amplification rate to obtain the amplitude ratio $A/A_1$, where $A_1$ is the reference amplitude at the neutral stability point. Figure 2 gives the maximum amplitude ratio at $R = 1500$ as a function of $M_1$ for both the first and second modes. The two-dimensional first-mode results are also shown to emphasize the necessity of considering three-dimensional disturbances in order to obtain a correct idea of the instability of a supersonic boundary layer, and also to show how much smaller are the amplitude ratios at supersonic speeds than at low speeds when the Reynolds number is held constant. Of course, indefinitely large amplitude ratios can be produced at any Mach number by going to sufficiently large Reynolds numbers.

Of almost equal importance as the maximum amplitude ratios are the frequencies of the disturbances which have these amplitude ratios. If these frequencies are not present in a boundary layer, then their large amplitude ratios are irrelevant to the transition problem. In order to give an idea of what the dangerous frequencies are in various situations, Fig. 3 presents numerical values of the frequency of the most amplified[*] disturbances in the wind tunnel and also in atmospheric flight at two altitudes. It can be seen that even second-mode disturbances can be of rather low frequency at sufficiently high altitude.

---

[*] The term most amplified disturbance refers to the disturbance for which $A/A_1$ is a maximum, and is to be distinguished from the most unstable disturbance which is the disturbance for which the amplification rate is a maximum.

## Response of Boundary Layer to a Specified Input Disturbance

A boundary layer disturbance does not have a single frequency and wave angle, but has its energy distributed over both of these quantities. If the spectrum of the input disturbance is known, then the stability theory can be used to calculate the downstream development of the spectrum and thus the disturbance amplitude as a function of $R_x$. In order to carry out this calculation, it is first necessary to obtain boundary-la, r response functions, $A/A_1$ vs. $\omega^* \nu_1^*/U_1^{*2}$, for several wave angles and at a number of Reynolds numbers. Typical response functions are shown in Fig. 4 for a 60° disturbance at $M_1 = 4.5$.

With $E(\omega, \psi)$ the power spectral energy density of the input disturbance, the input amplitude is given by

$$A_1^2 = \frac{2}{\pi} \int_0^\infty d\omega \int_0^{\pi/2} E(\omega, \psi) d\psi$$

It is assumed that $A_1$ is independent of R so that in the absence of instability the entire boundary layer has a uniform disturbance level. As a result of instability, the disturbance amplitude at Reynolds number R in the unstable region is given by

$$A^2(R) = \frac{2}{\pi} \int_0^\infty d\omega \int_0^{\pi/2} \left[ \frac{A}{A_1} (\psi, \omega) \right]^2 E(\omega, \psi) d\psi .$$

In the boundary-layer response function $A_1$ is the amplitude at the neutral-stability point.

As an example, the source of the boundary-layer disturbances is considered to be the sound radiated from the side-wall turbulent boundary layers of a wind tunnel. The idea here is that the sound field plays only a passive role. It provides disturbances in the boundary layer to be amplified or damped by the stability mechanism, but does not otherwise interact with the boundary layer. Since $E(\omega, \psi)$ is not known, it is assumed that E is independent of $\psi$, and that $E(\omega)$ is identical to the free-stream power-spectral density measured by Laufer (Ref. 10). The above expression for $A^2(R)$ then simplifies to

$$A^2(R) = \frac{2}{\pi} \int_0^\infty E(\omega) \, d\omega \int_0^{\pi/2} \left[ \frac{A}{A_1} (\psi, \omega) \right]^2 d\psi .$$

In this calculation, $A/A_1$ was computed in an approximate manner. Instead of the true spatial amplification rate, temporal amplification rates were computed and transformed to spatial rates by using the phase velocity instead of the group velocity. As a result, the numerical values that follow are somewhat in error. If the response curves are cross-plotted as functions of $\psi$ for fixed values of dimensionless frequency F, then the $\psi$ integral can be evaluated once and for all as a function of F. Since $E(\omega)$ is not a function of F, but of some other dimensionless frequency proper to the radiating turbulent boundary layer, the $\omega$ integral must be evaluated in dimensional terms. $E(\omega)$ actually varies slightly with unit Reynolds number, but since this dependence is not well established, E will be assumed to be independent of unit Reynolds number. Consequently $A(R)$ is a function of $U_1^{*2}/\nu_1^{*}$, which in a wind tunnel is equivalent to the unit Reynolds number $U_1^{*}/\nu_1^{*}$.

The results of the calculation of the energy density E at $R_x/in = 10^5$ are shown in Fig. 5, where $L_x$ and $U_s$ are the turbulence integral scale and average source velocity, respectively, used by Laufer as reference scales. It is clearly seen that a peak develops in the power spectrum at the most amplified frequency. This peak grows rapidly and shifts to lower frequencies as the Reynolds number increases.

The area under each spectral density curve in Fig. 5 is equal to $A^2$. Laufer's spectrum is normalized so that $A_1 = 1$. In Fig. 6, where A is plotted as a function of R, three different results are shown. The uppermost curve gives $(A/A_1)_{max}$, i.e. all of the energy is in the most amplified frequency. The wave angle is $60°$ and the frequency at each Reynolds number is different. This curve gives the largest amplitude that can be produced by the instability. The group of three curves immediately below this curve gives the disturbance amplitude at three different unit Reynolds numbers when the input energy is distributed with frequency in accordance with Laufer's spectrum, but at the same time is concentrated at the single wave angle of $60°$. The other group of three curves gives the disturbance amplitude when the energy is distributed uniformly over all wave angles as well as with frequency by Laufer's spectrum.

From Fig. 6 it can be seen that with the energy distributed both in frequency and wave angle, it is necessary to reach a $R_x$ of about $5 \times 10^6$ for

the disturbance amplitude to increase 100 times when $R_x$/in $= 10^5$. In the
same wind tunnel in which Laufer made his measurements, transition is
observed to start at about $R_x = 7 \times 10^5$ at this unit Reynolds number.
Clearly some other mechanism in addition to or in place of linear instabil-
ity amplification must be present in a supersonic wind tunnel to account
for such low transition Reynolds numbers. This mechanism is believed to
be the forced response of the boundary layer to the sound field and is dis-
cussed in detail in the final section of this paper.

## Effect of Cooling on Maximum Disturbance Amplitude at $M_1 = 5.8$

As previously mentioned, cooling the wall stabilizes the first mode
but not the second and higher modes. Indeed at $M_1 = 5.8$ the second-mode
amplification rate increases with cooling. Experimental measurements of the
effect of cooling on the transition Reynolds number have given a mixed picture
of the actual situation. In some facilities, no effect of cooling could be
found, while in others an initial stabilization was found only to be followed
at lower wall temperatures by a destabilization. The latter effect has been
termed temperature reversal. Occasionally, further cooling caused a second
stabilization, an effect called re-reversal.

If input disturbances have frequencies only in the first-mode range,
then cooling is certainly stabilizing. However, if there exists in addition a
band of high frequency disturbances, these disturbances could become excited as
the boundary layer is cooled and the second-mode unstable frequency range shifted
to higher frequencies. Further cooling might then make the unstable frequencies
higher than the input disturbance frequencies and re-reversal would occur. With
a wide band of second-mode frequencies present, one might at first expect little
effect from cooling. A calculation at $M_1 = 5.8$ of the maximum amplitude ratio
$(A/A_1)_{max}$ at $R = 1500$ as a function of the ratio of wall to recovery temperature,
$T_w/T_R$, confirms this expectation. With $A_1$ considered to be independent of $R$,
the maximum amplitude is almost constant with $T_w/T_R$.

Instead of considering the input disturbances to exist uniformly
throughout the boundary layer, an alternate view is to consider that they
are introduced into the boundary layer at some fixed point, or fixed $R_x$, near

the leading edge. In such a case, the damping region upstream of the instability region is as important in determining the disturbance amplitude at a downstream position as is the instability region itself. The results obtained with both assumptions are shown in Fig. 7. (Again the phase velocity has been used in place of the group velocity.) The upper curve gives $(A/A_1)_{max}$, which is almost independent of $T_w/T_R$. The lower curve gives $(A/A_o)_{max}$, where $A_o$ is the input amplitude at $R = 100$, and $(A/A_o)_{max}$ is strongly dependent upon $T_w/T_R$. As $T_w/T_R$ is reduced from unity, the first-mode region through which the disturbance must pass before reaching the unstable second-mode region is stabilized, i.e., the maximum amplification rate at each Reynolds number decreases monotonically with decreasing $T_w/T_R$. The result is that $(A/A_o)_{max}$ also decreases, and eventually $A_{max}$ becomes equal to $A_o$ at $T_w/T_R = 0.25$.

The existence of multiple unstable modes means that there are multiple solutions present for all $\alpha$ and $R$. As cooling proceeds below $T_w/T_R = 0.25$, the unstable second-mode solutions change from the family of solutions for which damping in the first-mode region increases with cooling to a second family for which damping decreases with cooling. This second family is notable for the fact that near the leading edge the phase velocity is greater than the free-stream velocity. Indeed at $F \times 10^4 = 2.0$, the most amplified frequency at $R = 1500$ for $T_w/T_R = 0.05$, the phase velocity is greater than unity from the leading edge to $R = 1050$. With the disturbance following this second family, a further decrease in $T_w/T_R$ means an increase in $(A/A_o)_{max}$, and the second portion of the lower curve in Fig. 7 is the result. Consequently, a reversal phenomenon exists for highly cooled boundary layers provided the input disturbance is introduced at a fixed point.

RESPONSE OF BOUNDARY LAYER TO A MOVING SOUND WAVE

The prediction from the stability theory of only small disturbance growths at $M_1 = 4.5$ at the point where transition has been observed to start suggested that another transition mechanism must be present in supersonic wind tunnels. Measurements by Kendall (Ref. 11) show that all frequencies grow monotonically from the leading edge, and the source of these disturbances has been identified as the sound field radiated from the turbulent side-wall boundary layers. Thus, the sound field, instead of being confined to the passive role envisaged in a previous section of just providing disturbances to be amplified by the instability

mechanism, must actively interact with the boundary layer to provide the observed growing disturbances in a region that is stable according to stability theory.

The problem is now one of forced oscillation, rather than the free-oscillation stability problem. The boundary layer is driven by the external sound field, and what is to be calculated is the steady-state, not the transient, response of the boundary layer to the individual frequency components of the sound field. Each frequency component moves with a phase velocity that can be determined by experiment. The boundary layer response is a neutral solution of the linearized, parallel-flow stability equations which has the same frequency and phase velocity as the particular external frequency component under consideration. In the free stream, this solution must include the external frequency component, which will be referred to as the incoming sound wave, and in addition it will also have a second part which is the outgoing, or reflected, sound wave. At the wall the same boundary conditions as in the stability theory are to be satisfied.

Method of Solution

The method of solution used in the stability theory can be readily adapted to solve the forced problem. In the stability theory, independent solutions are obtained analytically, and the ones which satisfy the boundary conditions at $y \to \infty$ are integrated numerically across the boundary layer to obtain the wall values of the dependent variables which are needed to satisfy the wall boundary conditions and to carry out the eigenvalue search. Two of the independent solutions are of direct application to the present problem. In the inviscid theory, they give the flow over or under a moving wavy wall. When the wavy wall moves supersonically with respect to the free stream, then the flow over the wavy wall is an outward propagating sound field with respect to a position below the wavy wall, and the flow under the wavy wall is an inward propagating sound field with respect to the same position. Consequently, these two solutions are just what is needed to represent the reflected and incoming sound waves. With respect to the receiving laminar boundary layer the incoming sound wave is produced in a turbulent boundary layer at $y \to \infty$ and moves inward; the reflected wave originates in the laminar boundary layer itself and moves outward to $y \to \infty$. Figure 8 shows the radiating

turbulent boundary layer, the receiving laminar boundary layer, and the
Mach waves of the incoming and reflected sound fields. If $c_r > 1 - 1/M_1$,
then the disturbances are no longer sound waves, but two exponentially
decaying pressure fields.

In the viscous theory, two of the independent solutions are almost
identical to the inviscid solutions except for a small viscous decay term.
In the stability problem, the incoming sound wave solution, which for
$c_r > 1 - 1/M_1$ increases exponentially with increasing y, is not used as
it does not satisfy the boundary conditions at $y \to \infty$. Therefore, all that
is necessary to do to solve the forced problem is to add this solution to
those already used in the stability theory. Since the boundary conditions
at the wall are unchanged and one more solution is available, there are
enough solutions to satisfy the boundary conditions for all values of $\alpha$,
$c_r$ and $\psi$ and there is no longer an eigenvalue problem to solve.

## Effect of Frequency at $M_1 = 4.5$

Numerous viscous and inviscid calculations have been carried out for
a series of frequencies in the measured frequency range of the wind tunnel
sound field and with phase velocities also in the measured range. Figure 9
gives the results of the viscous calculations at $M_1 = 4.5$ for two-dimensional
disturbances and $c_r = 0.65$. The ratio of $m'_p$, the peak rms mass-flow fluc-
tuation in the boundary layer to $m'_I(0)$, the rms mass-flow fluctuation of the
incoming wave at $y = 0$ in the absence of the boundary layer, is used to char-
acterize the boundary-layer response and is given as a function of Reynolds
number. It is seen that disturbances of all frequencies grow starting at
the leading edge, reach a peak at a Reynolds number that varies inversely
with frequency, and then decline in amplitude. The lower the frequency,
the higher the maximum value of $m'_p/m'_I(0)$.

In the inviscid theory, once $c_r$ and $\psi$ have been specified, the only
remaining parameter is $\alpha$. In Fig. 10 the mass-flow fluctuation ratio is
plotted against $\alpha$ for $c_r = 0.65$, $\psi = 0$. A significantly different result
is obtained than from the viscous theory. Since $F = \alpha c_r/R$, a disturbance
of given frequency traveling at a constant $c_r$ will have the dimensionless
value of $\alpha$ increase linearly with R. Consequently, according to Fig. 10

a purely inviscid disturbance would experience no growth in traveling down-
stream through the boundary layer for $\alpha > 0.0075$, and the growth for smaller
$\alpha$ is insignificant compared to a viscous disturbance. The initial growth of
Fig. 9, which is just what is found in experiment, is a purely viscous phenomenon.
The response curves for the five frequencies of Fig. 9 are also given in Fig. 10,
and they show that for a viscous disturbance the decrease in amplitude which
follows the region of growth is described closely by the inviscid theory. This
result is in contrast to the stability theory, where inviscid amplification
or damping rates are only approached by the viscous theory in the limit $R \to \infty$.
Another quantity marked in Fig. 10 is the Reynolds number of the point of largest
$\alpha$ which is plotted on each viscous curve. It is seen that the higher the fre-
quency, the lower the Reynolds number at which the inviscid curve is attained.

## Effect of Phase Velocity at $M_1 = 4.5$

The effect of the phase velocity on the boundary-layer response is shown
in Fig. 11. The upper group of curves are viscous results for five values of
$c_r$ at the single frequency of $F \times 10^4 = 0.08125$. At low Reynolds numbers, where
the growth is almost linear in R, the response increases monotonically with
increasing $c_r$. (At $M_1 = 4.5$, the largest $c_r$ for which a two-dimensional dis-
turbance is supersonic is 0.778.) At $R = 200$, there is a 35% decrease in $m'_p$
as $c_r$ decreases from 0.75 to 0.50. The situation is different at $R = 1000$
where the maximum response is produced by the $c_r = 0.65$ disturbance, and the
response for $c_r = 0.75$ is 10% lower.

The results of inviscid calculations for $\alpha = 0.04$ are given by the lower
curve. Since this curve continues to rise to the right as $c_r$ is increased
beyond 0.40, the viscous curves must rearrange themselves in the same order
as at low Reynolds numbers. Figure 10 shows that for $c_r = 0.65$ the viscous
curve for $F \times 10^4 = 0.08125$ merges with the inviscid curve at about $R = 1000$,
and the shapes of the $c_r = 0.40$ and 0.50 curves in Fig. 11 suggest that their
merger Reynolds number may be even lower. Therefore, the inviscid results
suggest that the maximum response continues to decrease as $c_r$ is reduced below
0.40.

## Effect of Wave Angle at $M_1 = 4.5$

The effect of the wave angle on the growth of the mass-flow fluctuation ratio is shown in Fig. 12 for $c_r = 0.65$ and $F \times 10^4 = 0.08125$. For $\psi \leq 45°$ there is less than a 15% change from the growth of a two-dimensional disturbance. However, above $\psi = 45°$ there is a sharp drop in the response until at $\psi = 50°$ the maximum $m'_p$ is only 52% of the maximum at $\psi = 45°$. The relative free-stream Mach number of a 50° disturbance is 1.0124, so this disturbance is the most oblique supersonic disturbance. All disturbances with $c_r = 0.65$ are subsonic at larger wave angles. The limiting wave angles are, of course, larger for smaller $c_r$. For example, with $c_r = 0.40$ the limiting value of $\psi$ is 68°.

## Amplitude of Reflected Sound Wave and Wall Pressure Fluctuation

The present calculation gives not only the details of the response of the boundary layer to an external sound wave, but also the strength of the reflected sound wave and the pressure fluctuation at the wall. Figure 13 gives the ratio of the amplitude of the reflected wave to the amplitude of the incoming wave as a function of $\alpha$ for $c_r = 0.65$. Figure 14 gives the ratio of the pressure fluctuation at the wall to the pressure fluctuation of the incoming wave at the wall position with no boundary layer present. In each figure the upper curve is the inviscid result and the other curves are the viscous results for a series of frequencies. According to the inviscid theory, when $\alpha = 0$, $A_R/A_I = 1.0$ and $p'(0)/p'_I(0) = 2.0$; when $\alpha \to \infty$, $A_R/A_I = 1.0$ and $p'(0)/p'_I(0) = 0$. The dimensionless wave number $\alpha$ can be written

$$\alpha = \frac{2\pi}{\eta_\delta} \frac{\delta}{\lambda^*} \, ,$$

where $\eta_\delta$ is $R\delta/x^*$, the Blasius variable at the edge of the boundary layer, and $\delta/\lambda^*$ is the ratio of boundary-layer thickness to wave length. Thus at $\alpha = 0$, the boundary layer effectively has zero thickness and the sound wave reflects as from a solid surface in the absence of a boundary layer. The reflected wave has the same amplitude and phase (at $\eta = 0$) as the incoming wave so that the wall pressure fluctuation is twice $p'_I(0)$. At the other limit, $\alpha \to \infty$, the boundary layer is infinitely thick compared to the wave length and the reflection is the same as from a constant pressure surface. The amplitude

of the reflected wave is again equal to that of the incoming wave, but its phase at $\eta = 0$ differs by $180°$ from the incoming wave. Thus the pressure fluctuation at the wall is zero. Between these two limits the amplitude of the reflected wave is always greater than the amplitude of the incoming wave.

The viscous results are quite different. For small $\alpha$, $A_R$ is always less than $A_1$. A minimum exists in $A_R$ for each frequency, and the magnitude of $A_R$ at the minimum decreases with increasing frequency. A similar minimum exists in $p'(0)$, but it is located at a larger $\alpha$ than is the $A_R$ minimum. If the $A_R$ minimum were to reach zero, then that particular $\alpha$ would constitute a stability eigenvalue for the family of incoming neutral waves. In the stability theory this type of disturbance is not considered because for $c > 1 - 1/M_1$ it becomes a subsonic disturbance whose amplitude increases exponentially with increasing y. However, if there is such an eigenvalue, Fig. 13 indicates that it would be for a high frequency and a low Reynolds number. The minimum $A_R$ for $F \times 10^4 = 1.3$ occurs at $R = 75$.

## Effect of Mach Number and Wall Cooling at $M_1 = 5.8$

A few calculations have been made for a disturbance of frequency $F \times 10^4 = 0.08125$ and phase velocity $c_r = 0.65$ in other than the $M_1 = 4.5$ insulated-wall boundary layer. In Fig. 15 the disturbance growth in the insulated-wall boundary layers is shown for $M_1 = 4.5$, 5.8 and 7.0. The maximum value of the ratio $m'_p/m'_I(0)$ increases with increasing Mach number, and the location of the maximum moves to lower Reynolds numbers. At $R = 600$, $m'_p/m'_I(0)$ increases by 30% from $M_1 = 4.5$ to 7.0, and the percentage increase is probably higher at lower Reynolds numbers. Since in a supersonic wind tunnel $m'_I(0)$ also increases with Mach number, the magnitude of $m'_p$ increases even more than does the ratio.

The effect on $m'_p/m'_I(0)$ of cooling the wall is shown in Fig. 16. Cooling has a large effect on the response and lowers the maximum mass-flow fluctuation ratio by 46% as $T_w/T_R$ is decreased from unity to 0.40. Also the response as a function of Reynolds number is considerably flattened so that a value of $m'_p$ close to the maximum persists over a wider Reynolds number range than for the insulated-wall boundary layer.

REFERENCES

1.  M. Landahl, _A Time-Shared Program for the Stability Problem for Parallel Flow over Rigid or Flexible Surfaces_, Massachusetts Institute of Technology, ASRL TR 116-4 (1966).

2.  W. C. Reynolds, _Orrsom, A Fortran-IV Program for Solution of the Orr-Sommerfeld Equation_, Tech. Rept. No. FM-4, Dept. of Mechanical Engineering, Stanford Univ. (1969).

3.  R. E. Kaplan, _The Stability of Laminar Incompressible Boundary Layers in the Presence of Compliant Boundaries_, Massachusetts Institute of Technology, ASRL TR 116-1 (1964).

4.  W. B. Brown, _Exact Numerical Solutions of the Complete Linearized Equations for the Stability of Compressible Boundary Layers_, Northrop Aircraft Inc., Norair Division Report NOR-62-15 (1962).

5.  L. M. Mack, _Computation of the Stability of the Laminar Compressible Boundary Layer_, in "Methods in Computational Physics" (B. Alder, ed.), Vol. 4, pp. 247-299, Academic Press, New York (1965).

6.  L. M. Mack, _Boundary-Layer Stability Theory_, Jet Propulsion Laboratory Report No. 900-277 (Rev. A) (1969).

7.  J. M. Kendall, Jr., _Supersonic Boundary-Layer Stability Experiments_, in "Proceedings of Boundary Layer Transition Study Group Meeting," (W. D. McCauley, ed.), Air Force Report No. BSO-TR-67-213, Vol. II (1967).

8.  W. B. Brown, _Stability of Compressible Boundary Layers_, AIAA Journal, Vol. 5, pp. 1753-1759 (1967).

9.  A. R. Wazzan, T. T. Okamura and A. M. O. Smith, _Spatial and Temporal Stability Charts for the Falkner-Skan Boundary Layer Profiles_, Douglas Aircraft Co., Report No. DAC-67086 (1968).

10. J. Laufer, _Some Statistical Properties of the Pressure Field Radiated by a Turbulent Boundary Layer_, Phys. Fl., Vol. 7, pp. 1191-1197 (1964).

11. J. M. Kendall, Jr., _Supersonic Boundary Layer Transition Studies_, Space Programs Summary 37-62, Vol. III, Jet Propulsion Laboratory, Pasadena, Calif. (1970).
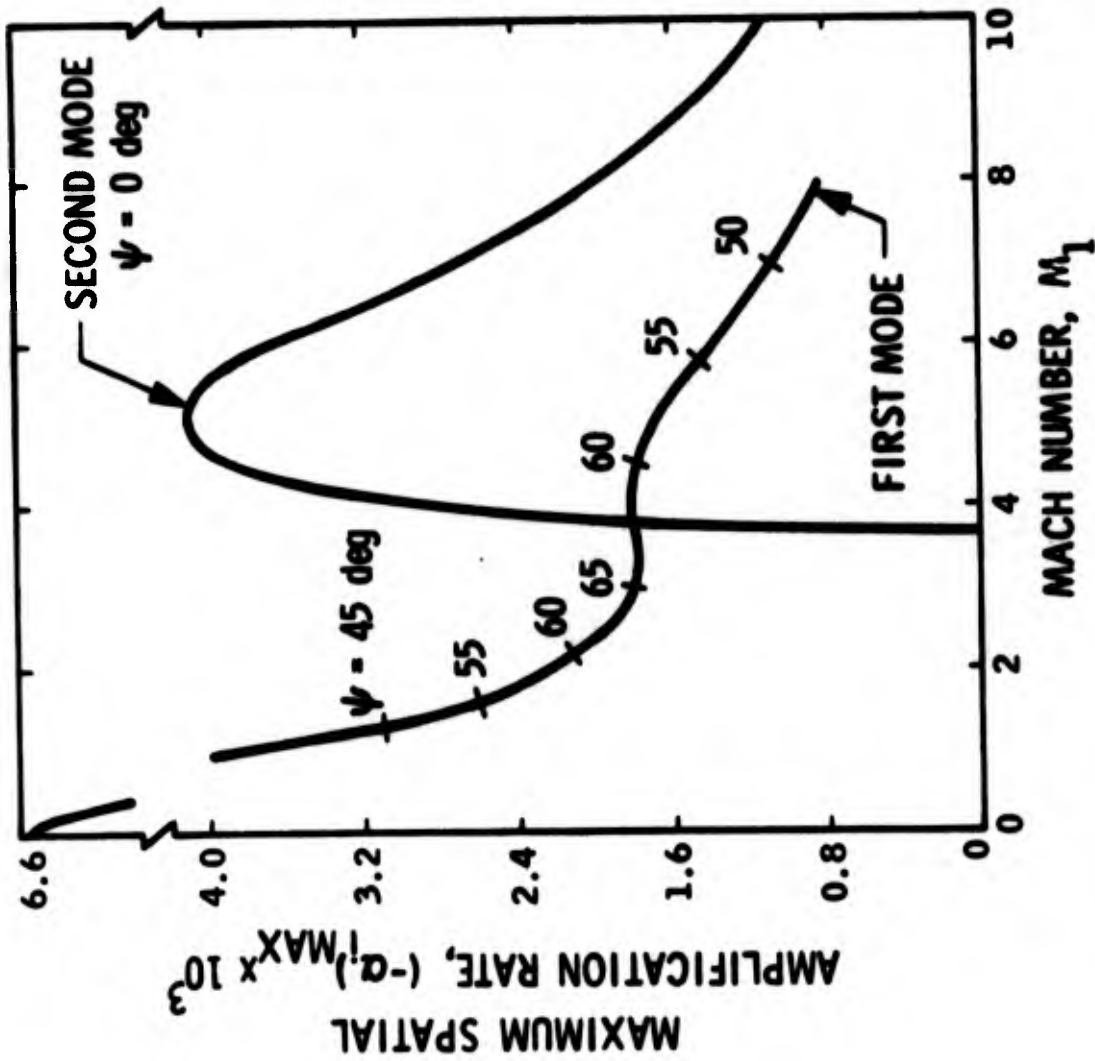
Fig. 1.  Effect of Mach Number on Spatial Amplification Rate of Most Unstable First and Second Mode Disturbances at R = 1500. Insulated Wall, Wind-Tunnel Temperatures
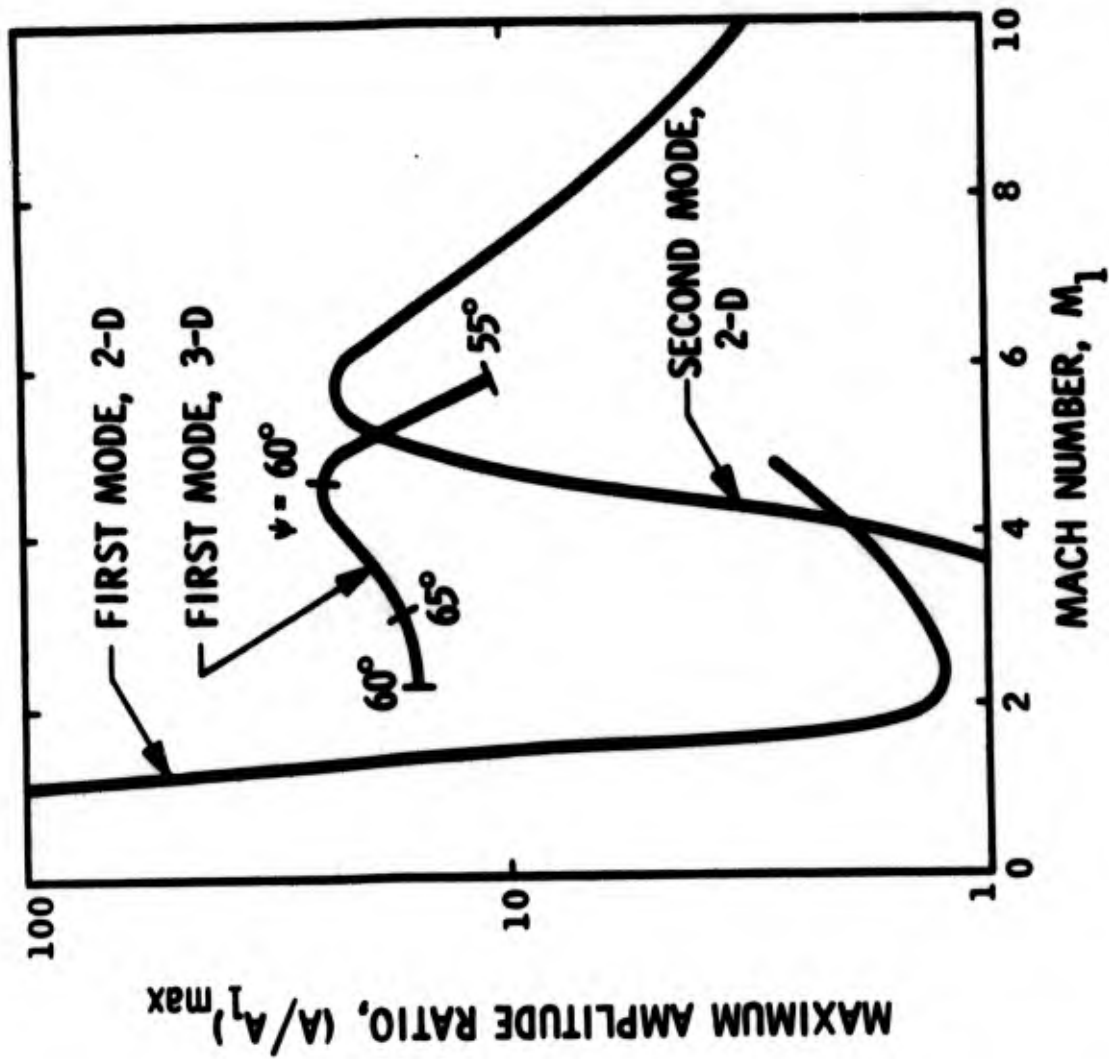
Fig. 2. Effect of Mach Number on Maximum Amplitude Ratio of Two- and Three-Dimensional Disturbances at R = 1500.

1-21

**WIND TUNNEL[1]**

R = 1500

| $M_1$ | 1[2] | 2 |
|---|---|---|
| 2.2 | 6,900 | — |
| 3.8 | 15,000 | |
| 4.5 | 17,800 | 67,800 |
| 5.8 | 26,000 | 56,800 |
| 7.0 | 25,000 | 56,800 |
| 10.0 | — | 62,200 |

**ATM., 50,000 ft**

R = 1500

| $M_1$ | 1 | 2 |
|---|---|---|
| 2.2 | 17,700 | — |
| 3.8 | 92,500 | |
| 4.5 | 148,000 | 561,000 |
| 5.8 | 307,000 | 676,000 |
| 7.0 | 358,000 | 818,000 |
| 10.0 | — | 1,280,000 |

R = 5000 (EST.)

| $M_1$ | 1 | 2 |
|---|---|---|
| 2.2 | 6,200 | — |
| 3.8 | 29,000 | |
| 4.5 | 48,000 | 170,000 |
| 5.8 | 92,000 | 203,000 |
| 7.0 | 107,000 | 242,000 |
| 10.0 | — | 385,000 |

**ATM., 100,000 ft**

R = 1500

| $M_1$ | 1 | 2 |
|---|---|---|
| 2.2 | 1,630 | — |
| 3.8 | 8,530 | |
| 4.5 | 13,600 | 51,800 |
| 5.8 | 28,300 | 62,200 |
| 7.0 | 33,000 | 75,500 |
| 10.0 | — | 118,000 |

R = 5000 (EST.)

| $M_1$ | 1 | 2 |
|---|---|---|
| 2.2 | 570 | — |
| 3.8 | 2,670 | |
| 4.5 | 4,420 | 15,700 |
| 5.8 | 8,470 | 18,700 |
| 7.0 | 9,900 | 22,300 |
| 10.0 | — | 35,400 |

[1] $R_x$/in. = 1 × $10^5$

[2] MODE NUMBER

Fig. 3. Frequency of Most-Amplified Disturbance in Cycles/Sec for Some Typical Cases
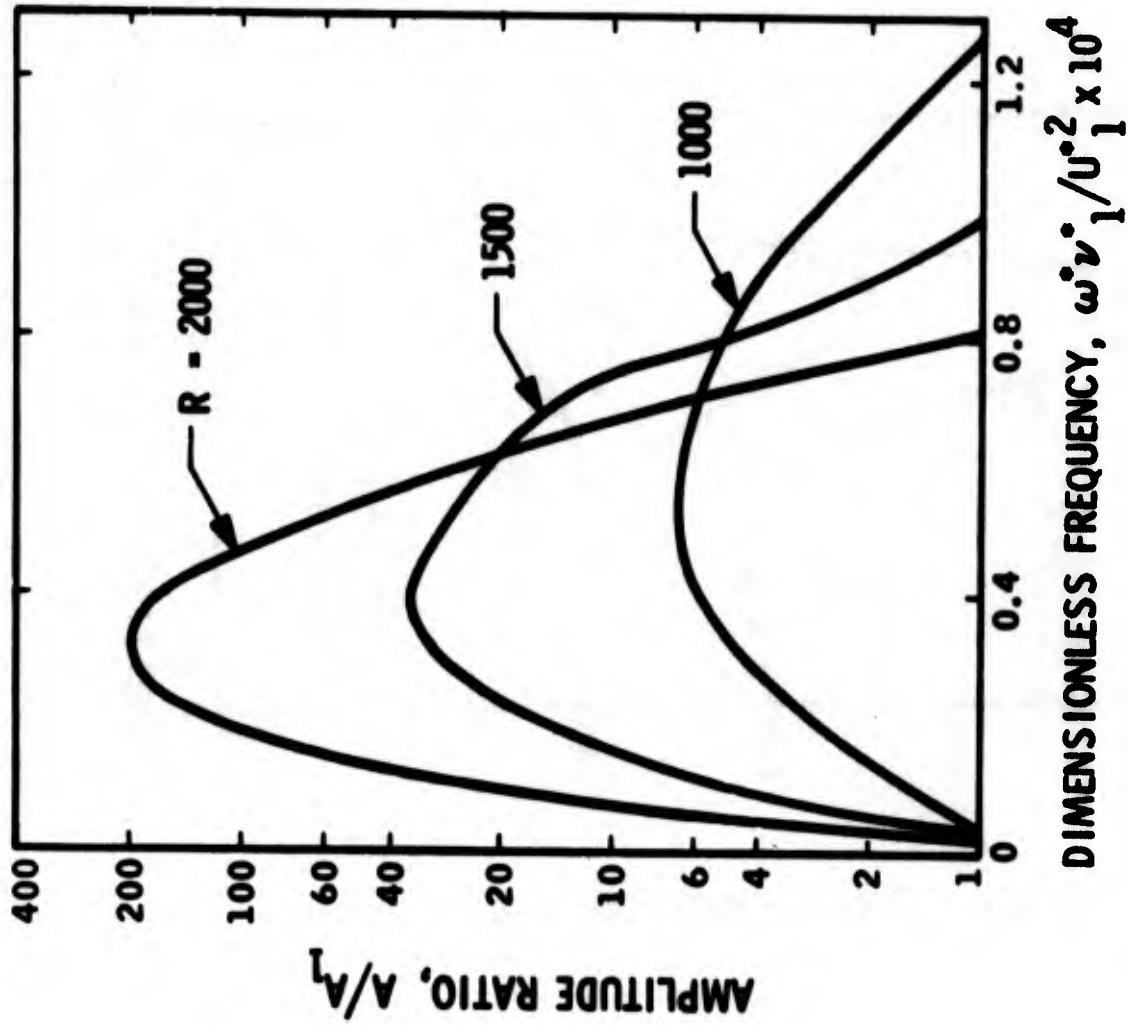
Fig. 4. Boundary-Layer Response Functions, $M_1 = 4.5$, $\psi = 60$ deg. Insulated Wall (Approximate Calculation)

1-23
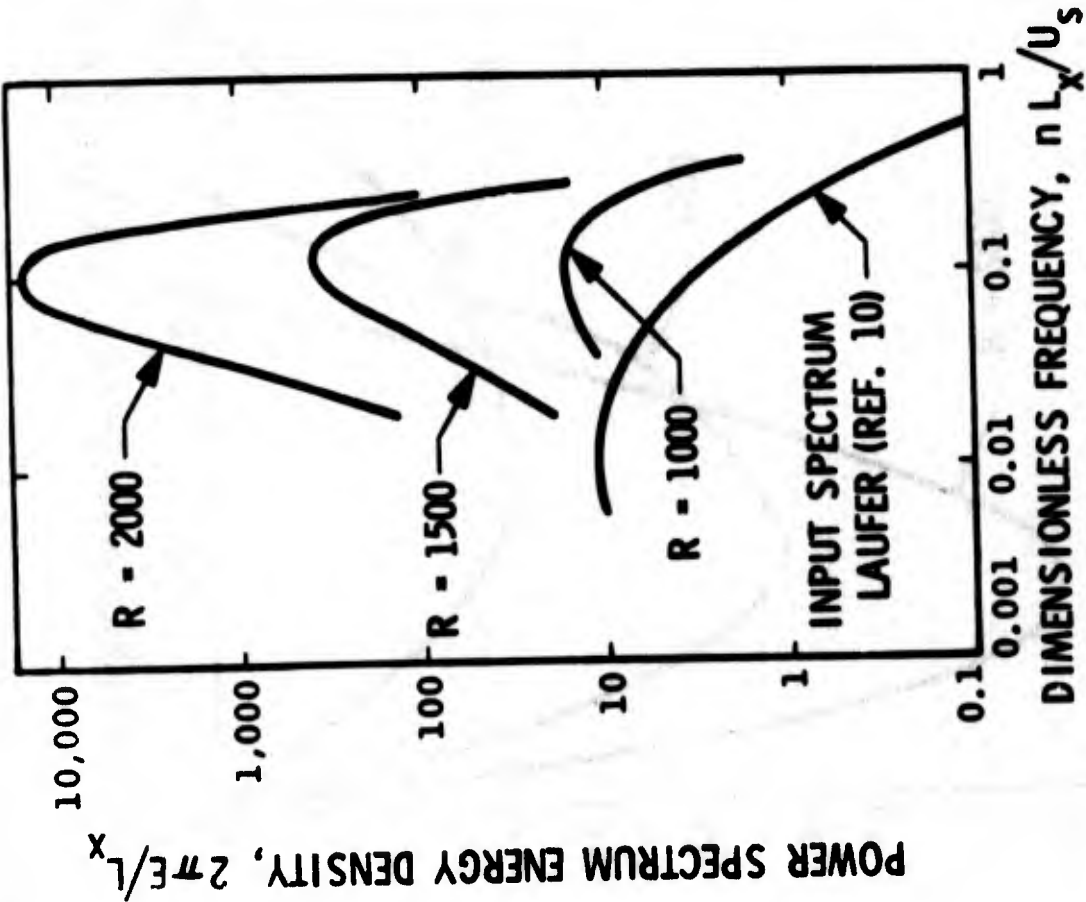
Fig. 5. Input and Output Disturbance Spectra, $M_1 = 4.5$, $R_x/in. = 1 \times 10^5$, Insulated Wall (Approximate Calculation)

1-24
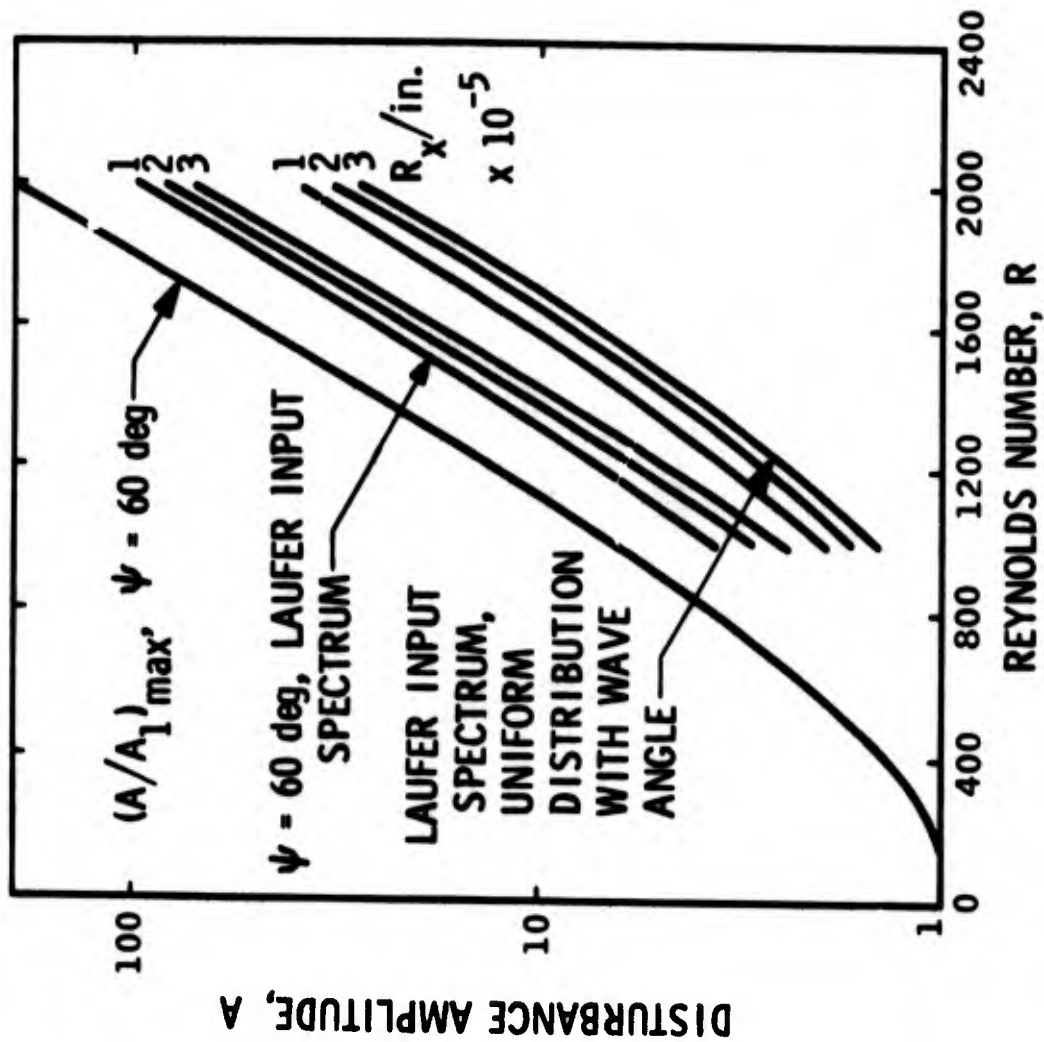
Fig. 6. Effect of Various Assumptions Concerning Distribution of Input Energy with Frequency and Wave Angle on Disturbance Amplitude. $M_1 = 4.5$, Insulated Wall (Approximate Calculation)
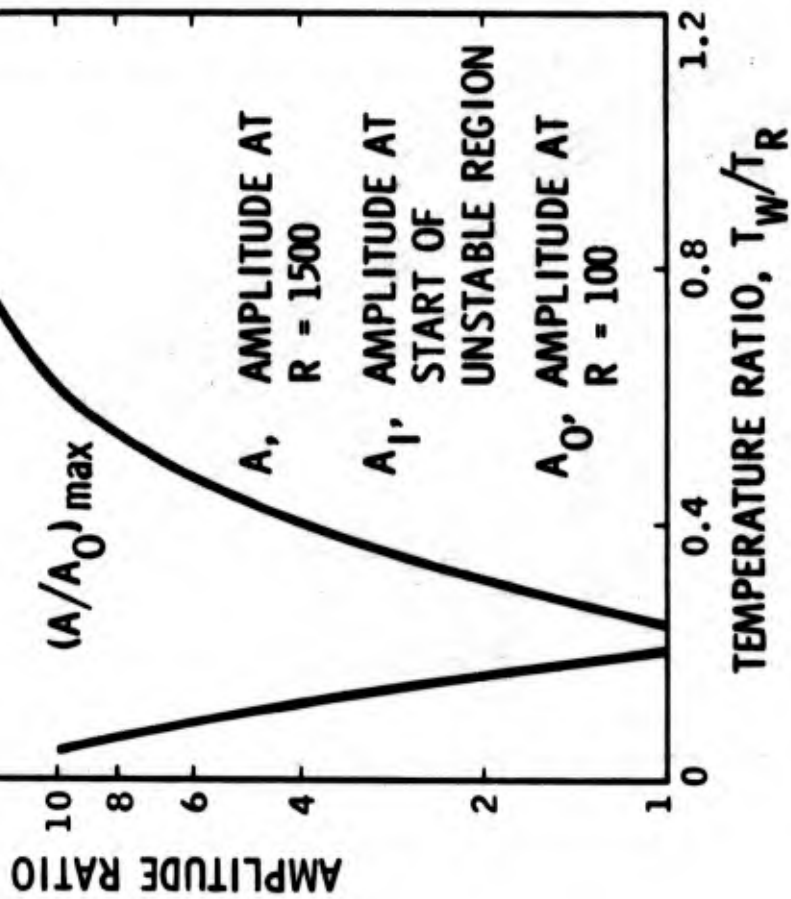
Fig. 7.  Effect of Wall Cooling at $M_1 = 5.8$ on the Maximum Amplitude Ratio at R = 1500 for Two Different Initial Conditions (Approximate Calculation)
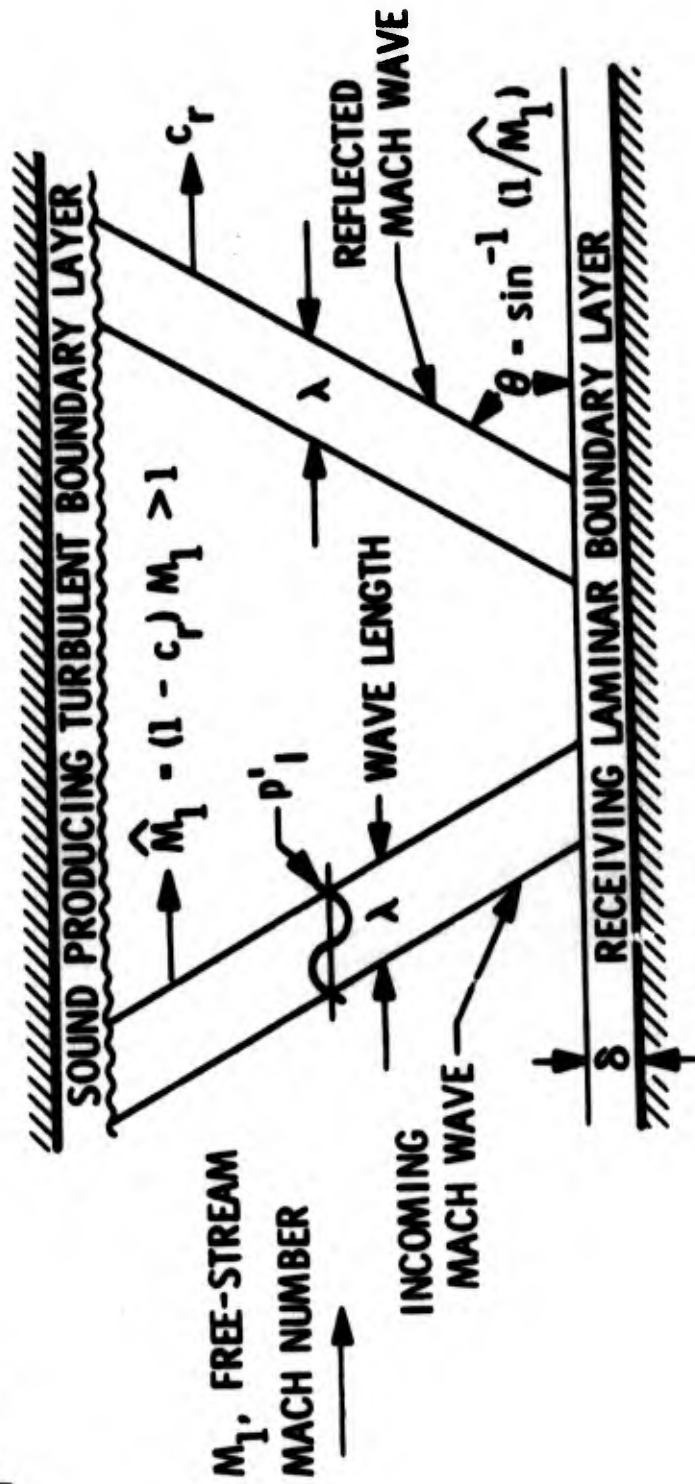
Fig. 8. Simplified Model of Sound Field Outside of Laminar Boundary Layer in Supersonic Wind Tunnel
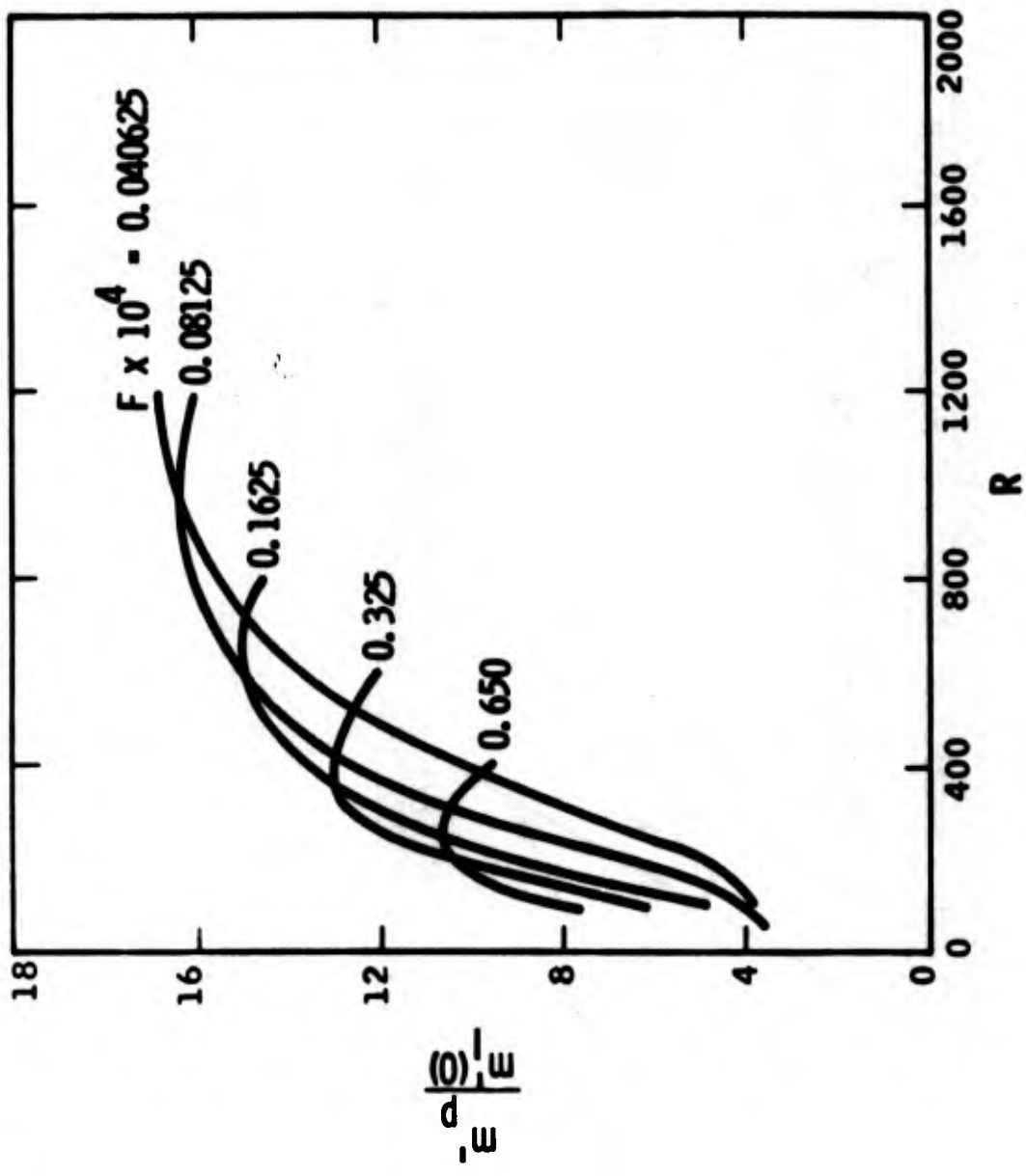
Fig. 9.   Effect of Frequency on Peak Mass-Flow Fluctuation
$M_1 = 4.5$, Insulated Wall, $\psi = 0°$, $c_r = 0.65$
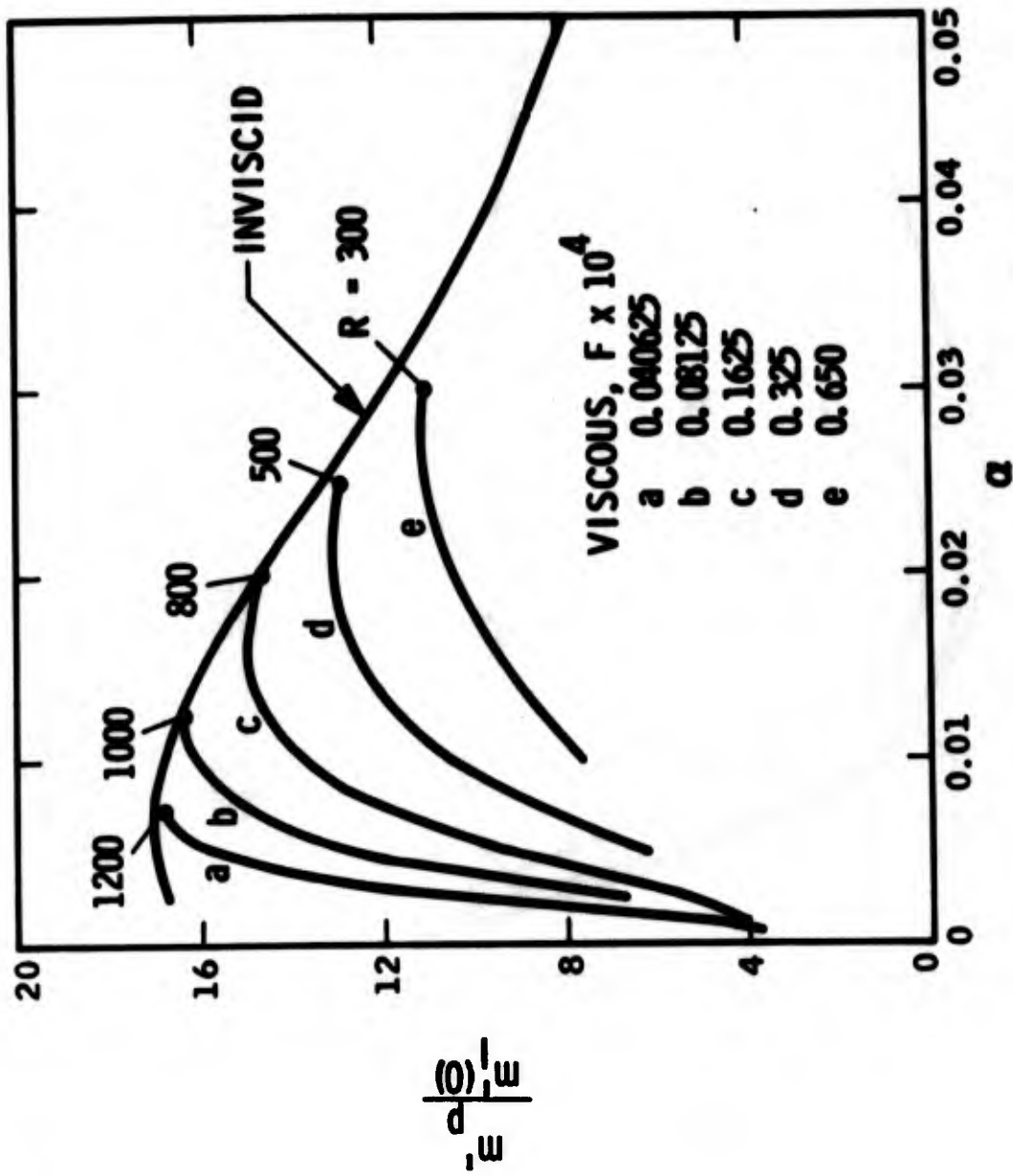
Fig. 10. Comparison of Viscous and Inviscid Peak Mass-Flow Fluctuations
$M_1 = 4.5$, Insulated Wall, $\psi = 0°$, $c_r = 0.65$
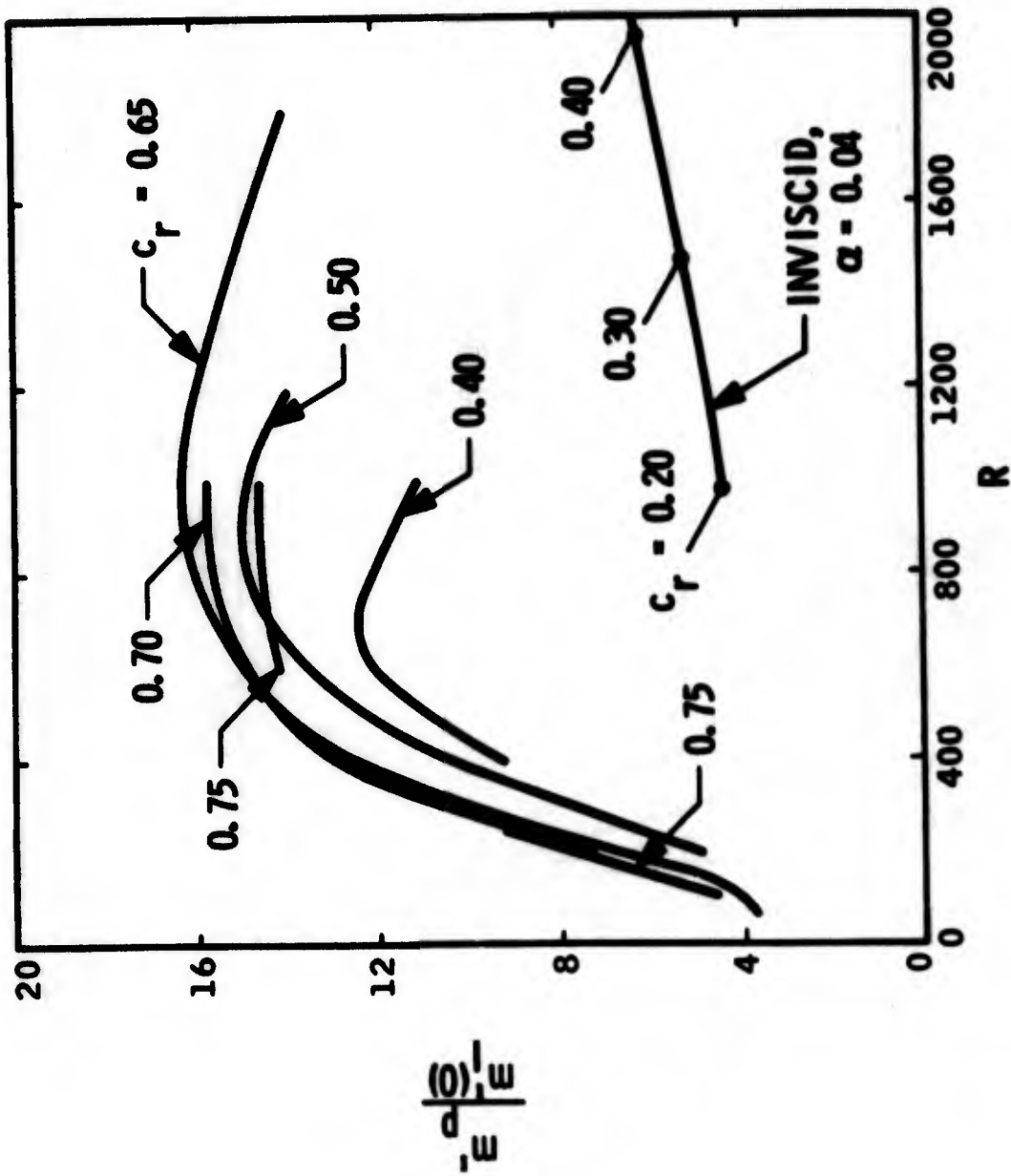
Fig. 11. Effect of Phase Velocity on Peak Mass-Flow Fluctuation
$M_1 = 4.5$, Insulated Wall, $\psi = 0°$, $F = 0.08125 \times 10^{-4}$
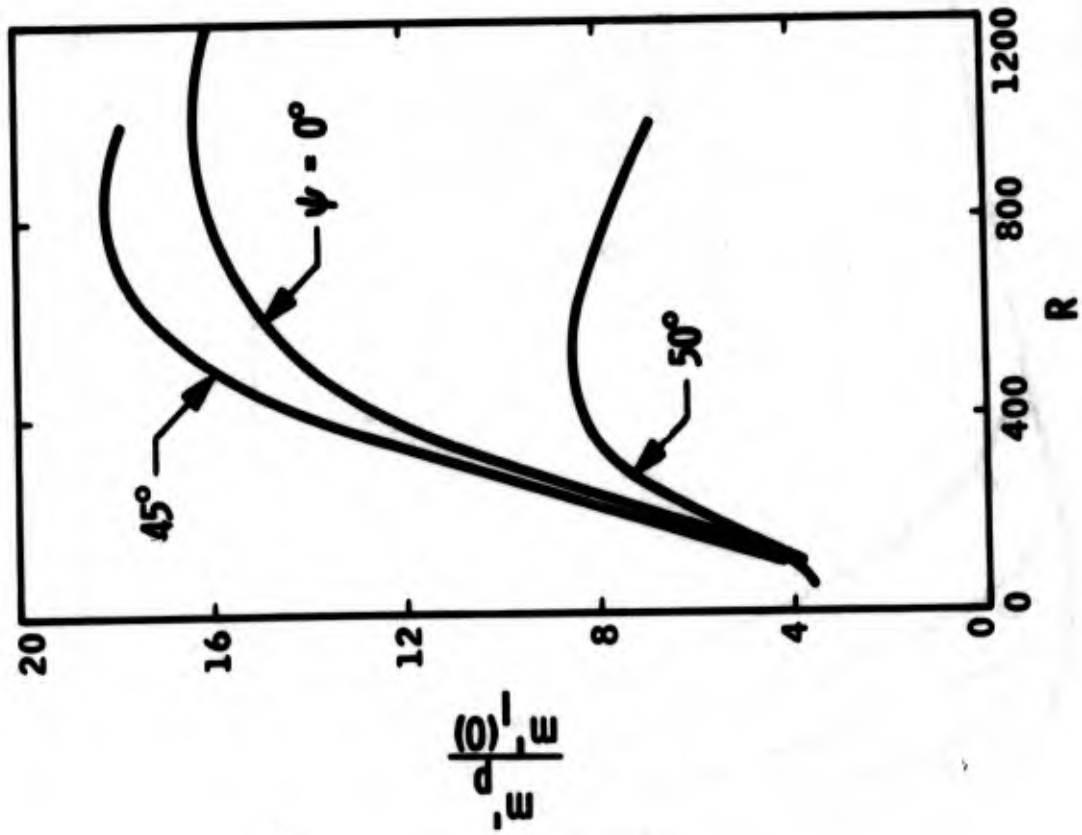
Fig. 12. Effect of Wave Angle on Peak Mass-Flow Fluctuation, $M_1 = 4.5$. Insulated Wall, $c_r = 0.65$, $F = 0.08125 \times 10^{-4}$
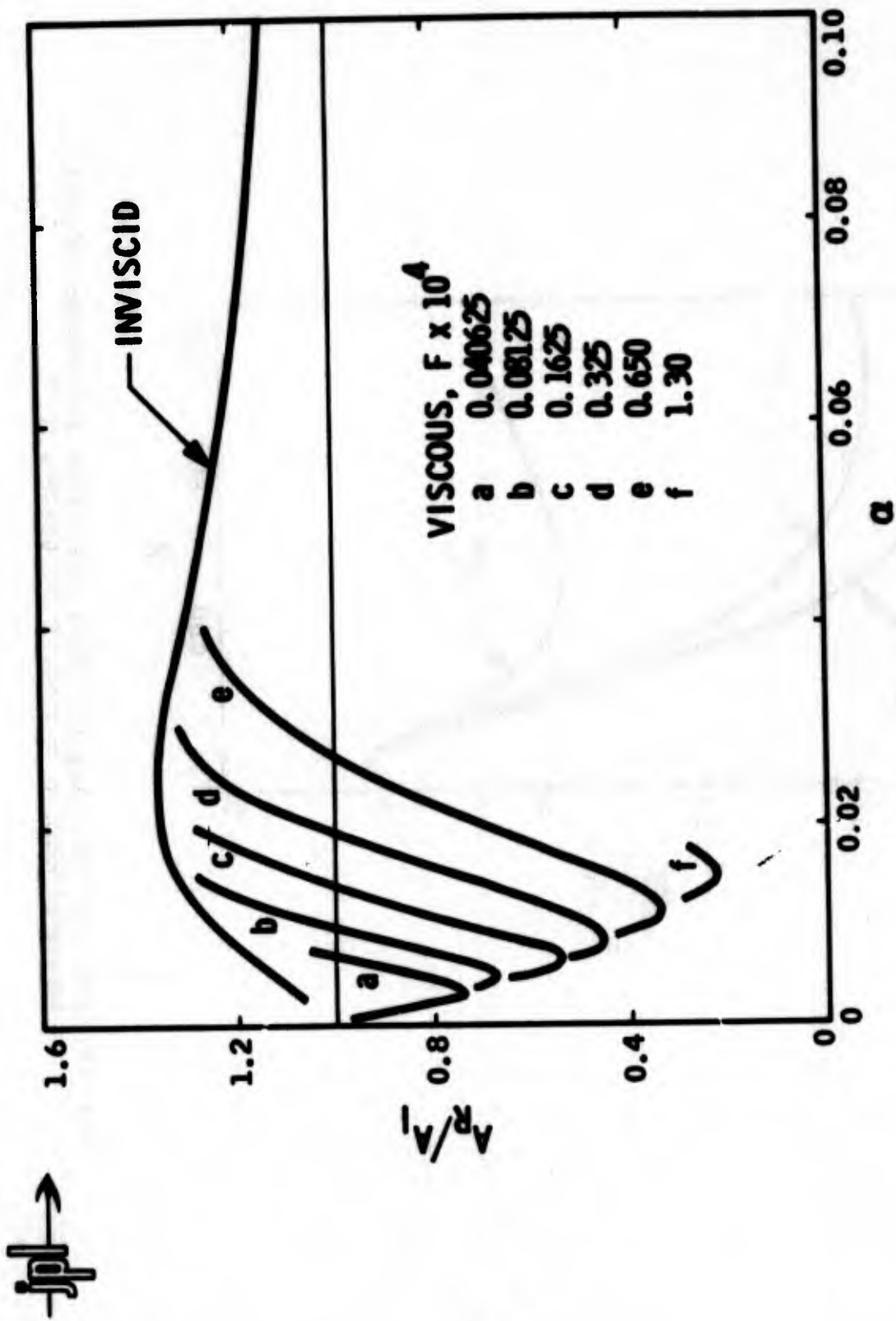
Fig. 13.   Comparison of Viscous and Inviscid Reflected-Wave Amplitudes. $M_1 = 4.5$, Insulated Wall. $\psi = 0°$, $c_r = 0.65$
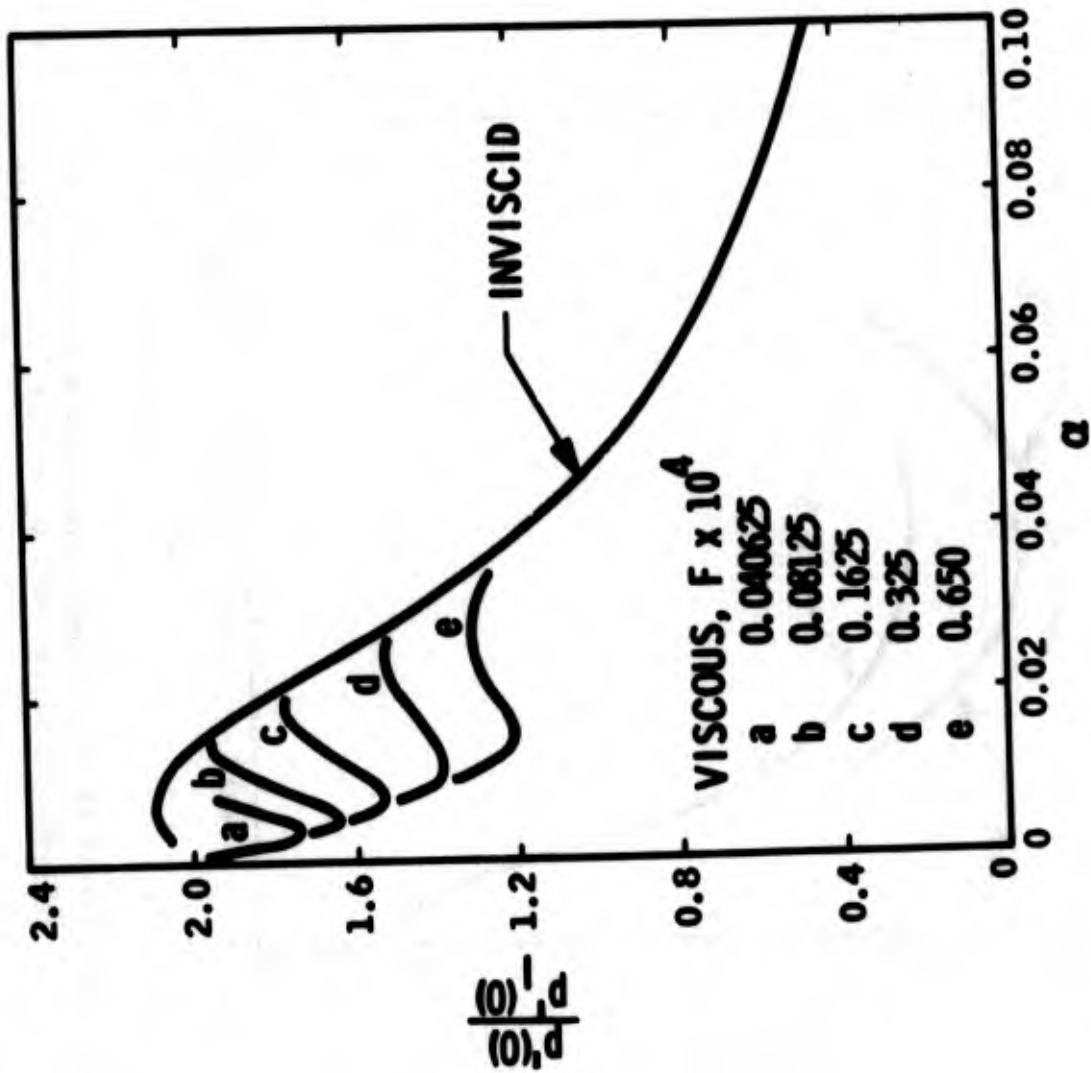
Fig. 14.   Comparison of Viscous and Inviscid Wall Pressure Fluctuations.
$M_1 = 4.5$, Insulated Wall, $\psi = 0°$, $c_r = 0.65$
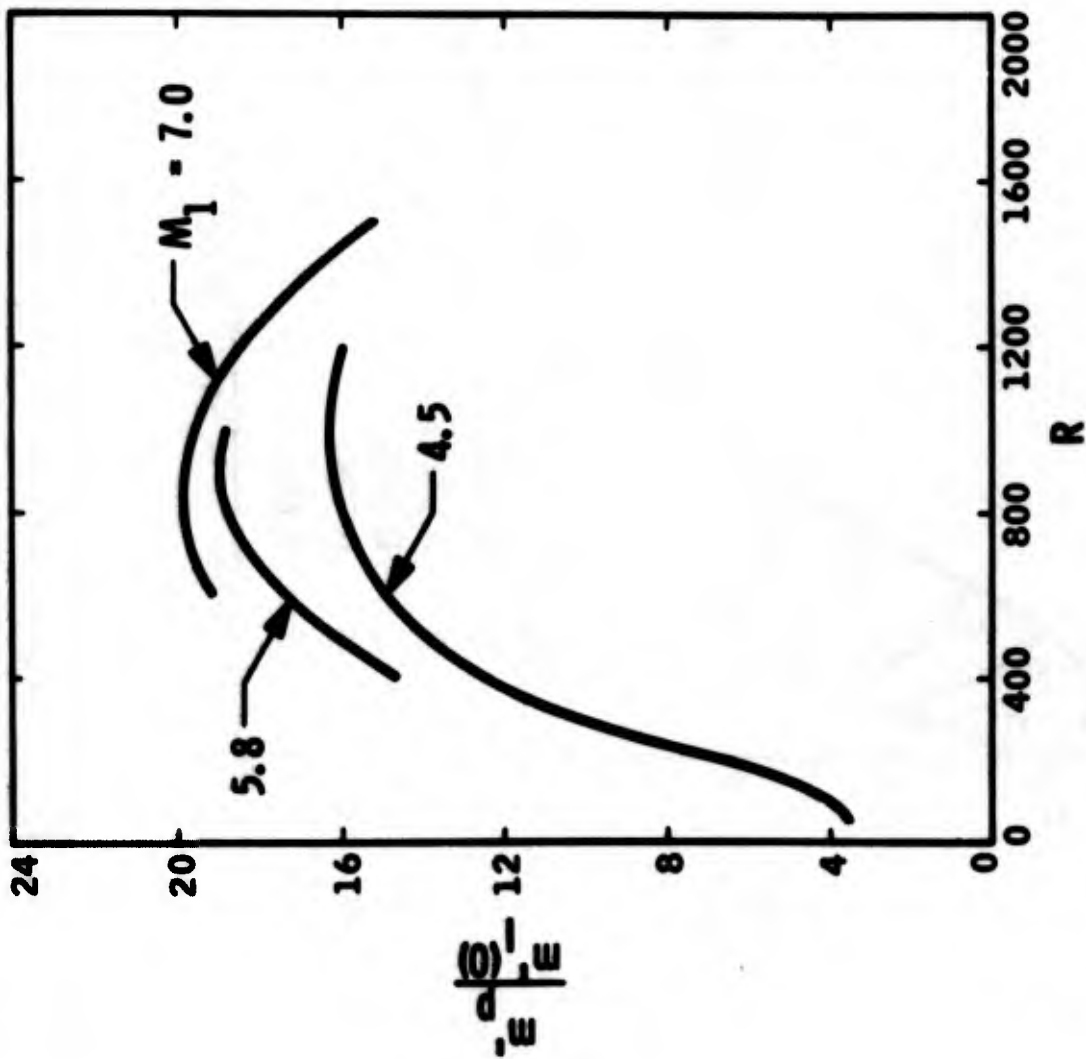
Fig. 15. Effect of Mach Number on Peak Mass-Flow Fluctuation. Insulated Wall, $\psi = 0°$, $c_r = 0.65$, $F = 0.09125 \times 10^{-4}$
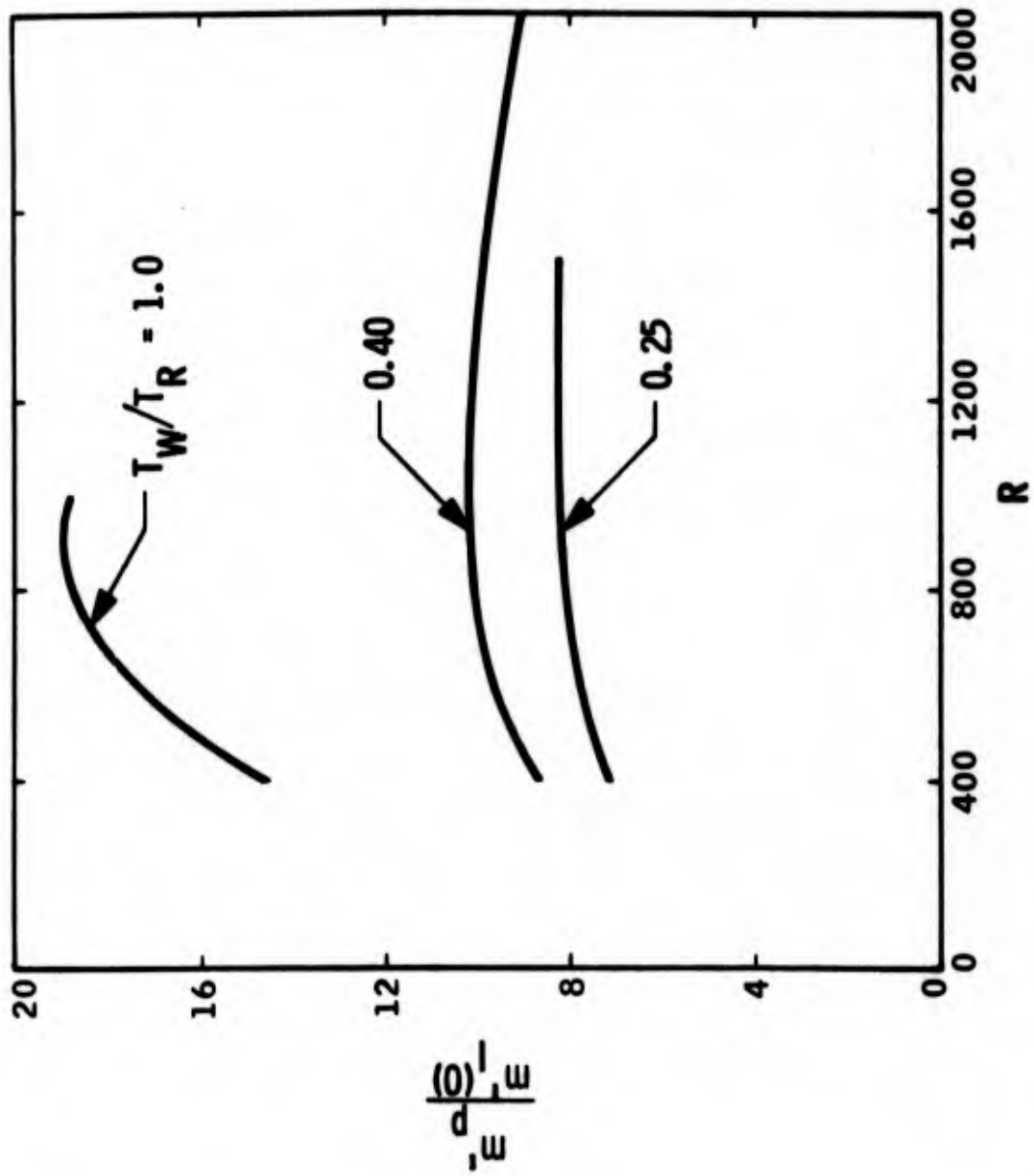
Fig. 16. Effect of Wall Cooling on Peak Mass-Flow Fluctuation, $M_1 = 5.8$. $\psi = 0°$, $c_r = 0.65$, $F = 0.08125 \times 10^{-4}$

(This page intentionally left blank)

# SECTION 2

## J.P.L. EXPERIMENTAL INVESTIGATIONS[*]

### (Unclassified)

James M. Kendall, Jr.

Jet Propulsion Laboratory, Pasadena, Calif.

## ABSTRACT

Experiments relating to boundary layer transition at Mach numbers between 1.6 and 5.6 are described. Hot-wire anemometry is used to obtain detailed information on the origin and growth of flow fluctuations in the region of the boundary layer ahead of transition. The results, which apply specifically to wind tunnel flows, indicate several important differences between the processes at the higher Mach numbers and at the lower ones.

## INTRODUCTION

It has been recognized for several years that boundary layer transition on test models in supersonic wind tunnels is influenced by turbulence-produced sound in che tunnel stream. The defect that this represents is not unimportant, for there is even now no laboratory facility which has proven satisfactory for transition testing. The realization of a suitable facility and the reconciliation of laboratory data with flight results will require a much deeper understanding than exists at present.

The mechanism of transition has been far less thoroughly explored for supersonic flows than for subsonic ones, partly because theoretical guidance has been lacking. During the recent years, however, Mack has developed the stability theory for compressible flows and given extensive numerical results. These are presented in Ref. 1 and summarized elsewhere in these proceedings. The theory has been experimentally confirmed for a Mach number $M_\infty = 4.5$, Ref. 2.

---

With theoretical results thus available, the present experiments were undertaken to investigate the relationship between stability and transition. Hot-wire anemometry is being used to study the flow fluctuations naturally present in laminar boundary layers in the region preceding transition. $M_\infty = 4.5$ was selected for the initial experiments because the stability theory is known to be correct. It quickly became apparent that a mechanism other than that of instability was operative at this Mach number, and the program was directed toward an exploration of the new effect and toward determination of the range of Mach number where it is important.

Some of the early results of the program have been reported in Ref. 3. It is indicated there that for $M_\infty = 4.5$, and probably for $M_\infty = 3.0$, the tunnel sound field forces fluctuation energy into the boundary layer in a region immediately aft of the leading edge of a test plate. The energy is observed to grow several-fold larger ahead of the station for which stability theory predicts the onset of amplification. Some results for $M_\infty = 2.2$ are also included in (3), and these indicate that the situation is rather different than at the higher speeds.

Recently, Mack has developed a program for the numerical computation of the response of a boundary layer to an external sound field. This is described elsewhere in these proceedings. In addition, the experiments have been extended in several directions. The principal emphasis of this paper is upon interpretation of the $M_\infty = 4.5$ flat plate results, including a qualitative comparison with the new theory, but various other results are described as well.

EQUIPMENT AND TECHNIQUES

The experiments were carried out in the JPL 45 x 50 cm supersonic wind tunnel. The flat plate tests were made on a 35 cm long, 1.27 cm thick steel plate that spanned the tunnel width. The bottom edge was bevelled 10 deg. The top or working surface was ground and lapped to bring the leading edge thickness to a value less than $10^{-3}$ cm. In some experiments reported here, the thickness was temporarily increased by affixing a strip of 0.025 cm thick steel strip to the bevelled surface, flush with the leading edge. Some measurements were also made on a sharp-tipped, 4.0-degree half angle steel cone 42 cm long.

All measurements were obtained by the use of constant-current hot-wire anemometers. The signal-to-noise ratio remained acceptably high to frequencies of about $0.5 \times 10^5$ to $1.0 \times 10^5$ Hz, depending on flow conditions. The hot-wire overheat was maintained at a pre-selected value by a current-controlling servomechanism. As the wire was traversed through a boundary layer normal to the plate or cone surface, a location of maximum voltage fluctuation was recorded, except at $M_\infty = 3.0$ where two nearly equal peaks were found. The profile of signal energy was approximately self-similar for all stations along the layer not too close to transition. All measurements in the layer were made at the location of the peak, and the signal there was taken to represent the fluctuation level throughout the layer.

Two types of hot-wire measurement were made. In the first kind, obtained only at $M_\infty = 4.5$, the hot-wire overheat was varied for a particular location in the flow in order to obtain mode-diagram plots. Straight-line plots were obtained for both the free stream and the boundary layer fluctuations. The intercept of the line with the ordinate indicates the numerical value of the total temperature fluctuation, and the slope indicates the mass-flow fluctuation. For the higher overheats, the hot-wire voltage is proportional to the mass-flow fluctuation to within a few percent. In the second kind of measurement, this result is used for the interpretation of comparative voltage measurements made in the free stream and along the boundary layer length.

Auxiliary equipment used with the hot-wire sets included a wave analyzer (Hewlett-Packard 310A), a 100 point correlator (Princeton Applied Research 101A), a correlator consisting of a 0-600 μsec delay line and analog multiplier, and a voltage comparator circuit for probability density measurements.

RESULTS AND DISCUSSION

A. Flat Plate Results, $M_\infty = 4.5$

Among the data of Ref. 3 are the fluctuation energy spectra measured in the tunnel stream and at various stations along the boundary layer length. These data were converted to an amplitude ratio $A/A_\infty$ for comparison with the

stability theory. A is the square root of the energy at any dimensionless frequency $F = \omega\nu/u_\infty^2$, and $A_\infty$ is the same quantity in the stream ahead of the plate; $\omega$, $\nu$, and $u$ are the frequency in radians, the kinematic viscosity and the stream speed. Amplitude ratio data are presented in Fig. 1 for a flow with twice the unit Reynolds number, Re, of that for which data were given in Ref. 3. The stations of measurement are denoted in terms of R, the square root of the x-Reynolds number. A principal difference between the two sets of data is that the aft-most station is at the location of maximum fluctuation energy in the transition zone for the case presented here.

The stability theory does not predict the results well. It indicates that the highest and lowest frequency waves are unamplified, whereas it is seen that waves of all frequencies grow more or less in parallel. The theory predicts that the fluctuation growth is not appreciable at any frequency for $R \gtrsim 400$, even for the most amplified 60-deg waves. Experimentally, a several-fold growth exists at $R \cong 400$.

In contrast, the forcing theory predicts a substantial amplitude ratio at low values of R. The ratio increases monotonically with R up to $R \simeq 700\text{-}1000$, depending on frequency. The fastest growth occurs at $R \simeq 300$, where ratios of the order of 10 are indicated. The results are reasonably insensitive to the parameters of frequency, wave speed, and wave obliqueness.

Figure 1 includes the prediction of the forcing theory taken directly from Mack's results for the case R = 300, wave angle $\psi$ = 0, and wave speed 0.65 $u_\infty$. The predicted values exceed the experimental ones at a corresponding R by about a factor of two. It is expected that when account is taken of the wave obliqueness and of the fact that the reference level $A_\infty$ contains the contribution of waves from the bottom half of the tunnel and which do not impinge upon the plate, that closer agreement will result.

It is added here that amplitude ratio results obtained at $M_\infty$ = 3.0 and 5.6 resemble those of Fig. 1.

Information about the source and about the development of the boundary layer waves has been gained by the use of the cross-correlation technique. For the measurements described here, one hot-wire probe was affixed to the

bevelled bottom edge of the test plate with the wire being 0.1 cm directly below the leading edge. A second probe was in the boundary layer on top of the plate in lateral alignment with the first. Examples of the cross correlation coefficient $R_{12} = \overline{e_1 e_2} / \sqrt{\overline{e_1^2 e_2^2}}$ are given for three positions of the second probe in Fig. 2a. Here, $e_1$ and $e_2$ are the fluctuating voltages of the two probes.

The relatively high degree of correlation represents direct evidence that the boundary layer waves are caused by the free stream sound field. For the smallest value of x, $R_{12}$ takes a maximum value of about 0.5. This is believed to reflect the fact that the reference wire below the plate is exposed to waves approaching from all directions, whereas only waves from the top half of the tunnel should induce boundary layer disturbances. Although results are given only for stations to x = 7.5 cm, measurements were carried out at close intervals to x = 30 cm, near the end of the transition zone. Even here, the correlation was significant, as will be shown below.

Similar measurements were also carried out in the empty tunnel. The two probes were offset laterally just enough to avoid wake or wave interference. The results, presented in Fig. 3, show that the correlation nearly vanishes within a length much shorter than the 30 cm length over which boundary layer waves continue.

The Fourier transform of the correlation data yields a somewhat more direct understanding of the wave development in that it gives the spectral decomposition and eliminates the need to compare curves whose shape varies with distance. Cross-power spectra computed from the correlation curves are presented in Fig. 4. The reduction of gain required in consequence of signal growth is indicated.

It is seen that most of the energy is contained in the low frequency waves, as is true of the individual signals. The spectra remain approximately invariant with distance to at least x = 10 cm, R = 850, indicating that those waves coherent with the sound field at the leading edge grow no faster nor slower than do any others making up the total signal. Beyond this station, the coherent waves do not maintain their relative growth.

The phase of a transformed correlation curve yields a determination of the wave speed. The wave speed, expressed as a fraction of the stream speed, is shown in Fig. 5 as a function of frequency for several stations along the boundary layer, and for one separation distance in the empty tunnel. The speeds indicated are the average prevailing over the interval of measurement rather than the local value.

It is seen that the waves accelerate during their streamwise travel, approaching a speed approximately equal to that predicted by stability theory. The theoretical result is included in the figure. The acceleration is regarded as significant. The forcing process yields boundary layer waves that move in register with the sound field. Because the sound field is necessarily supersonic with respect to the stream, as can be seen from the empty tunnel result, the forced waves are also supersonic initially, and, according to stability theory, are unable to self-amplify regardless of the Reynolds number. However, the sound field has been shown to have a very finite coherence length, and thus any particular wave is subsequently free to propagate without influence, i.e., in accordance with stability theory. The instability amplification favors waves of a certain speed. The trend of the wave speed toward the stability value has already been noted.

It is of interest to determine the limits over which linear theory might be applicable. For the particular case just described, several results taken together indicate the onset of nonlinearity to occur in the vicinity of $x = 15$ cm. These are as follows:

a) As reported in Ref. 3, the probability density of the hot-wire signal in the stream and in the forward stations of the boundary layer is approximately Gaussian-distributed. At $x = 20$ cm, it is strongly non-Gaussian, resembling that of a sine wave, although the signal itself does not resemble a sine wave.

b) As reported in Ref. 3, the lateral scale of the fluctuations in the forward stations of the boundary layer corresponds to that of the free stream. In recent experiments, it was found that for $x \lesssim 17$ cm the scale became much smaller.

c) The cross-correlation power spectra of Fig. 4 remain nearly constant to $x \simeq 15$ cm and then decline. The uncorrelated fluctuations responsible for the decline may arise from nonlinear processes.

d) Coles' experiments in the same tunnel, Ref. 4, show the minimum shear stress to occur at $x \simeq 15$ cm for the present value of $M_\infty$ and Re.

The final process of transition seems to be different at this Mach number than at the lower speeds described later. Here, the fluctuations grow larger along the plate length until their peak-to-peak mass-flow fluctuation becomes a major fraction of the mean mass flow of the stream. No isolated turbulent spots or bursts have been observed in the hot-wire signal.

## B. Cone Results, $M_\infty = 4.5$

A limited number of measurements similar to those for the flat plate have been carried out on a 4.0 degree half-angle cone, mostly at $M_\infty = 4.5$, but at lower speeds also.

As a general result for the case of zero incidence, no particularly important differences between the plate and cone flows have been noted. Fluctuation spectra on the cone at $M_\infty = 4.5$ were analyzed to obtain amplification ratio data to compare with Fig. 1. The dimensionless frequencies and values of R were reduced by $\sqrt{3}$ to account for the thinner layer on the cone. The results resembled those of Fig. 1 except that the ratio at any R was approximately twice that on the plate.

The effect of angle of incidence was investigated by comparing the wide-band hot-wire signal growth along any ray of the cone with the results for zero incidence. The most pronounced change was noted on the windward and leeward rays, where the growth was suppressed and enhanced, respectively. The signal energy along the leeward ray for a 1.5 deg pitch angle is compared with that for zero pitch angle in Fig. 6. The difference in growth, with corresponding movement of the transition point, is attributed to an alteration of the mean flow profile, which in turn affects both the sound forcing and instability mechanisms.

## C. Low Mach Number Results

Measurements were made at $M_\infty = 1.6$ and 2.2. These are the speeds at which Laufer and Vrebalovich carried out their boundary layer stability experiments, Ref. 5. Both the Laufer-Vrebalovich results and the present ones, some of which are presented in Ref. 3, indicate important differences from the $M_\infty = 4.5$ case. Here, it is found that the fluctuation energy at the closest approach behind the plate leading edge exceeds that of the stream. Laufer and Vrebalovich suggested that this is the result of an interaction between the stream fluctuations and the leading edge shock wave. The subsequent development of the boundary layer fluctuations, not too close to transition, is in nominal accordance with stability theory. That is, growth or damping occurs at frequencies so indicated by the stability theory.

The sound-field forcing mechanism does not seem to be very effective. Correlation measurements like those for $M_\infty = 4.5$ were repeated for $M_\infty = 1.6$ and 2.2. The $M_\infty = 2.2$ results are shown in Fig. 2b. Although a disturbance incident upon the leading edge produces a boundary layer wave, the relative response is only about a third of that at $M_\infty = 4.5$. The reduced sound intensity prevailing at this Mach number is already accounted for in taking the coefficient of correlation. For $M_\infty = 1.6$, the correlation was virtually undetectable, and is not presented. This does not indicate that the boundary layer fluctuations are not the result of free-stream ones, but rather that the reference hot wire primarily senses a component of the stream fluctuation to which the boundary layer response is indirect.

An indication of nonlinearity in the production of fluctuation energy near the leading edge of a plate or tip of a cone has been observed at $M_\infty = 1.6$. The tunnel stream fluctuation level was intentionally increased by means of an air jet in the tunnel settling chamber. The stream fluctuation energy at the model location was approximately doubled by the jet. The boundary layer on the plate and on the cone showed an order-of-magnitude increase in energy.

An attempt to check the Laufer-Vrebalovich suggestion concerning the origin of fluctuations was made by comparing the fluctuation behavior on a flat plate with and without a leading edge blunting strip 0.025 cm thick at

$M_\infty$ = 1.6. As indicated in Ref. 3, bluntness strongly suppressed the fluctuation growth at $M_\infty$ = 4.5. Here, virtually no change in the fluctuation level at any station along the plate was detected.

One of the more significant differences between low and high Mach number flows concerns the production of isolated turbulent spots. As indicated above, no such spots were observed for $M_\infty$ = 4.5. For $M_\infty$ = 1.6 and 2.2, very intense turbulent bursts were clearly evident on the oscilloscope at x-stations less than half way to transition. The production rate and propagation speed of such spots have been reported by Spangenberg and Rowland for $M_\infty$ = 1.96 in Ref. 6.

## SUMMARY OF FLAT PLATE RESULTS

For $M_\infty$ = 4.5 a several-fold fluctuation growth is observed ahead of the station R = 300, and can be accounted for by sound-forcing theory. Instability amplification becomes effective at about this R and may account for subsequent growth, but detailed comparison with linear theory has not been made. The onset of nonlinearity occurs at $R \cong 1000$. The breakdown of large amplitude laminar fluctuations occurs without evidence of turbulent spots. A similar chain of events appears to prevail at $M_\infty$ = 3.0 and 5.6.

For $M_\infty$ = 1.6 and 2.2, fluctuation energy is produced at the leading edge, but this may not be important in comparison with the subsequent amplification, which takes place in nominal accordance with stability theory. There is little evidence of sound-forcing. Turbulent spots are probably an important part of the transition process.

## REFERENCES

1. L. Mack, Boundary Layer Stability Theory, Document 900-277, Rev. A, Jet Propulsion Laboratory, Pasadena, Calif. (Nov. 1969).

2. J. M. Kendall, Jr., Supersonic Boundary Layer Stability Experiments, Proceedings, Boundary Layer Transition Study Group Meeting; Aerospace Report No. TR 0158 (S 3816-63)-1, Vol. II, W. D. McCauley, ed., pp. 10-11, (Aug. 1967).

3. J. M. Kendall, Jr., Supersonic Boundary Layer Transition Studies, Space Programs Summary 37-62, Vol. III, Jet Propulsion Laboratory, Pasadena, Calif., p. 43 (April 1970).

REFERENCES (CONT.)

4. D. Coles, <u>Measurements of Turbulent Friction on a Smooth Flat Plate in Supersonic Flow</u>, J. Aero. Sci., Vol. 21, No. 7, p. 433 (July 1954).

5. J. Laufer and T. Vrebalovich, <u>Stability and Transition of a Supersonic Laminar Boundary Layer on an Insulated Flat Plate</u>, J. Fluid Mech., Vol. 9, p. 257 (1960).

6. W. G. Spangenberg and W. R. Rowland, <u>Optical Study of Boundary Layer Transition Processes in a Supersonic Air Stream</u>, The Physics of Fluids, Vol. 3, No. 5, p. 667 (Sept. 1960).
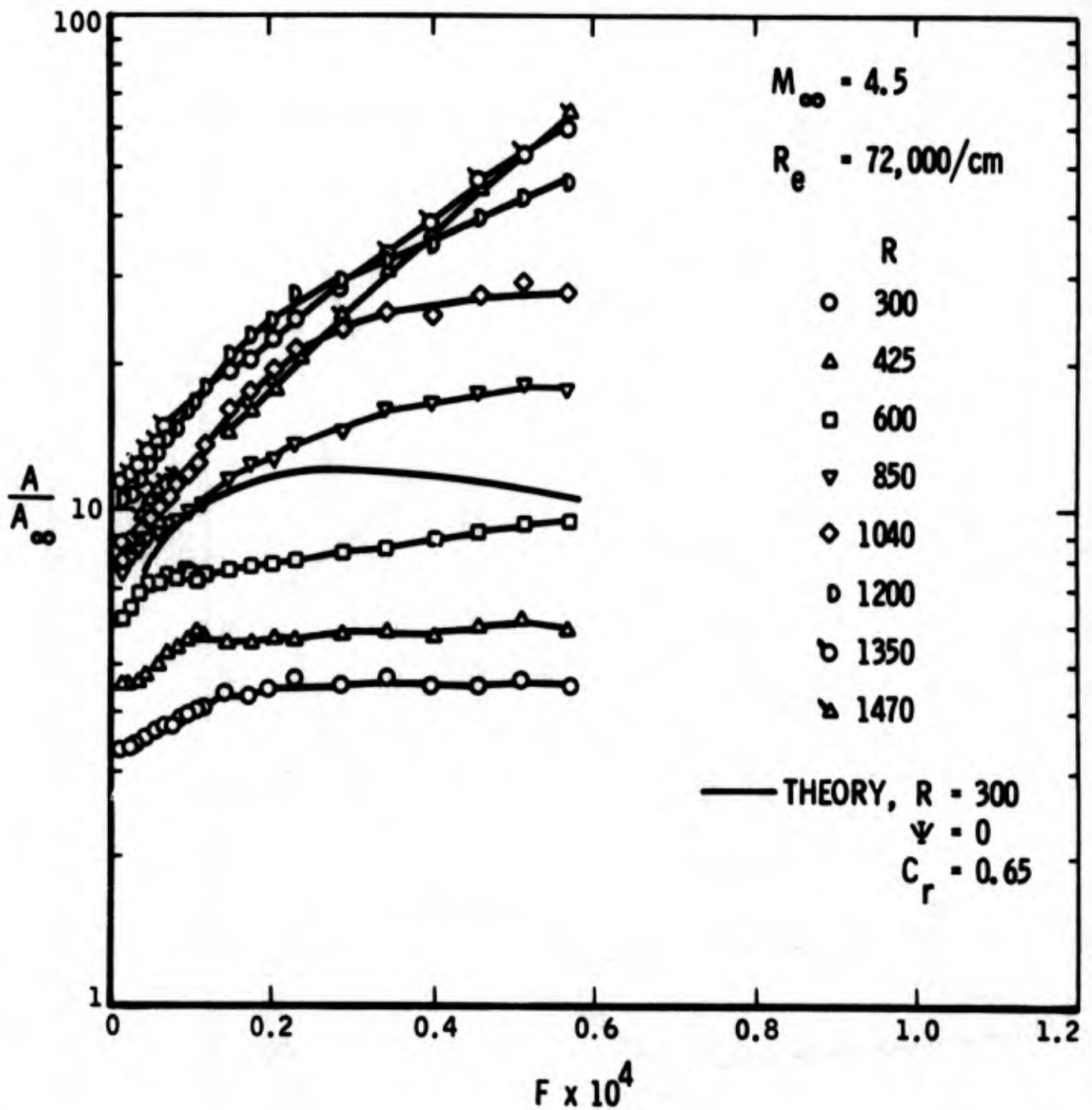
Figure 2-1. Fluctuation Amplitude in a Flat Plate Boundary Layer
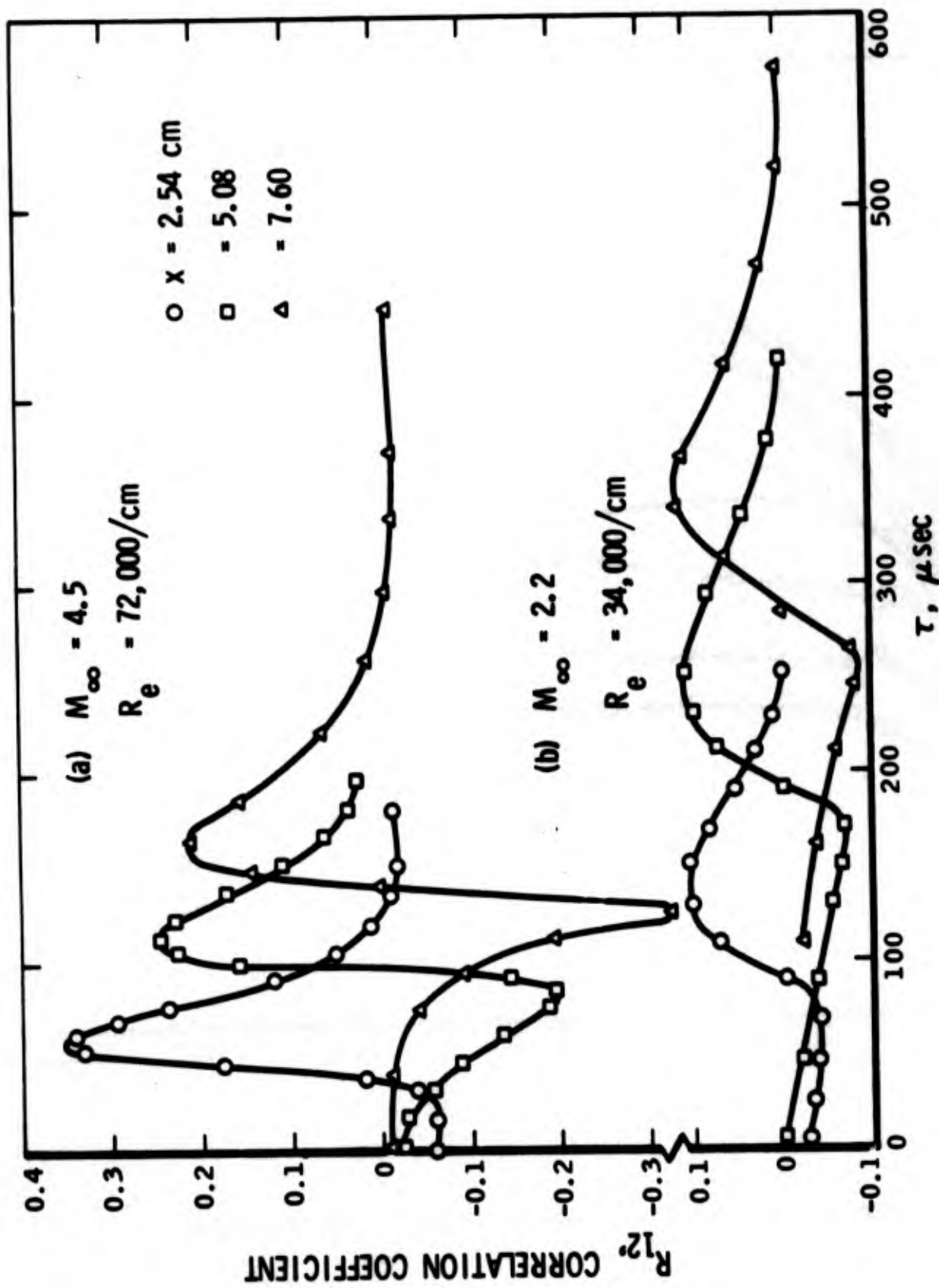
Figure 2-2. Cross-Correlation of Free-Stream and Boundary Layer Fluctuations
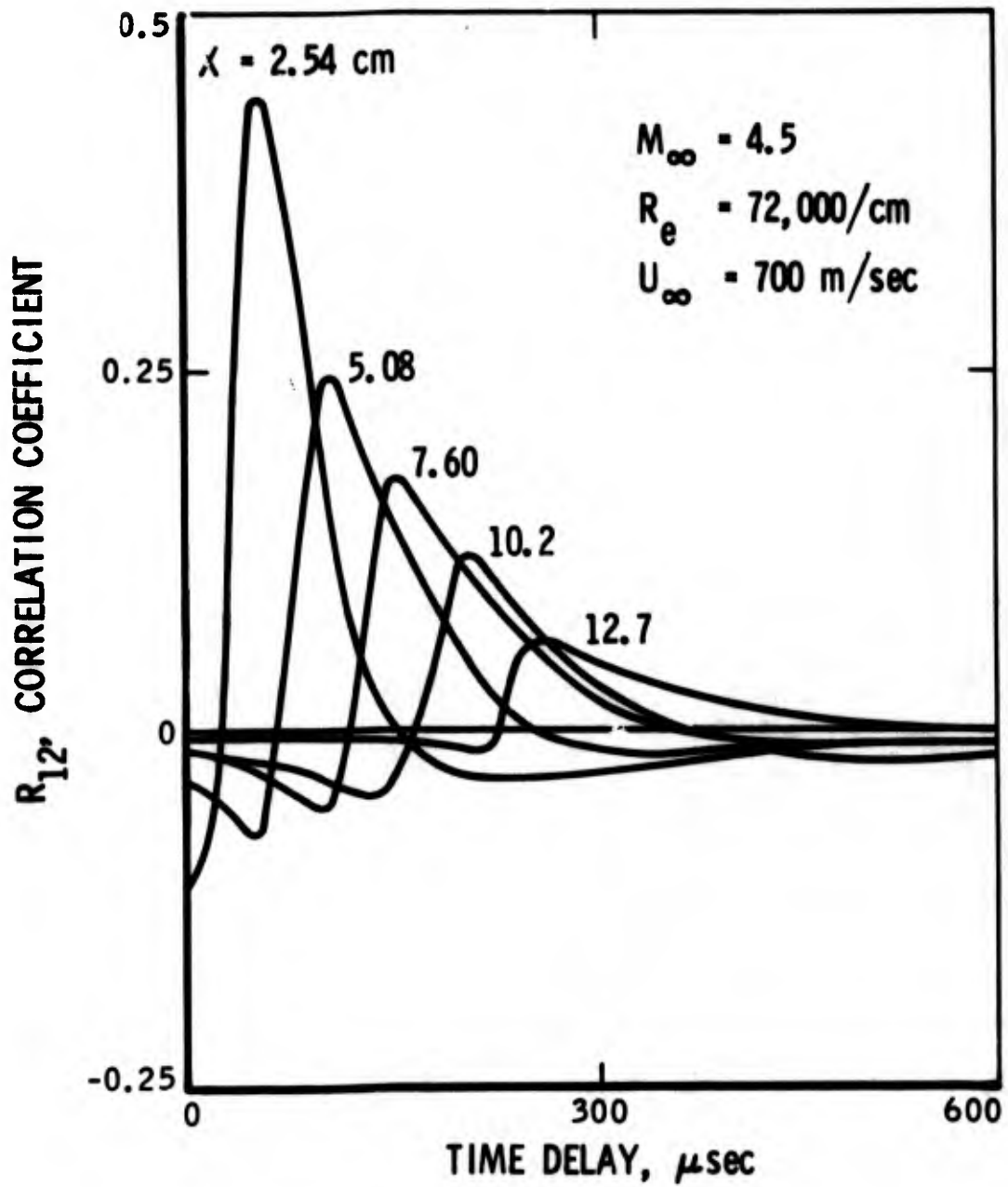
Figure 2-3. Cross-Correlation of Fluctuations in the Empty Tunnel
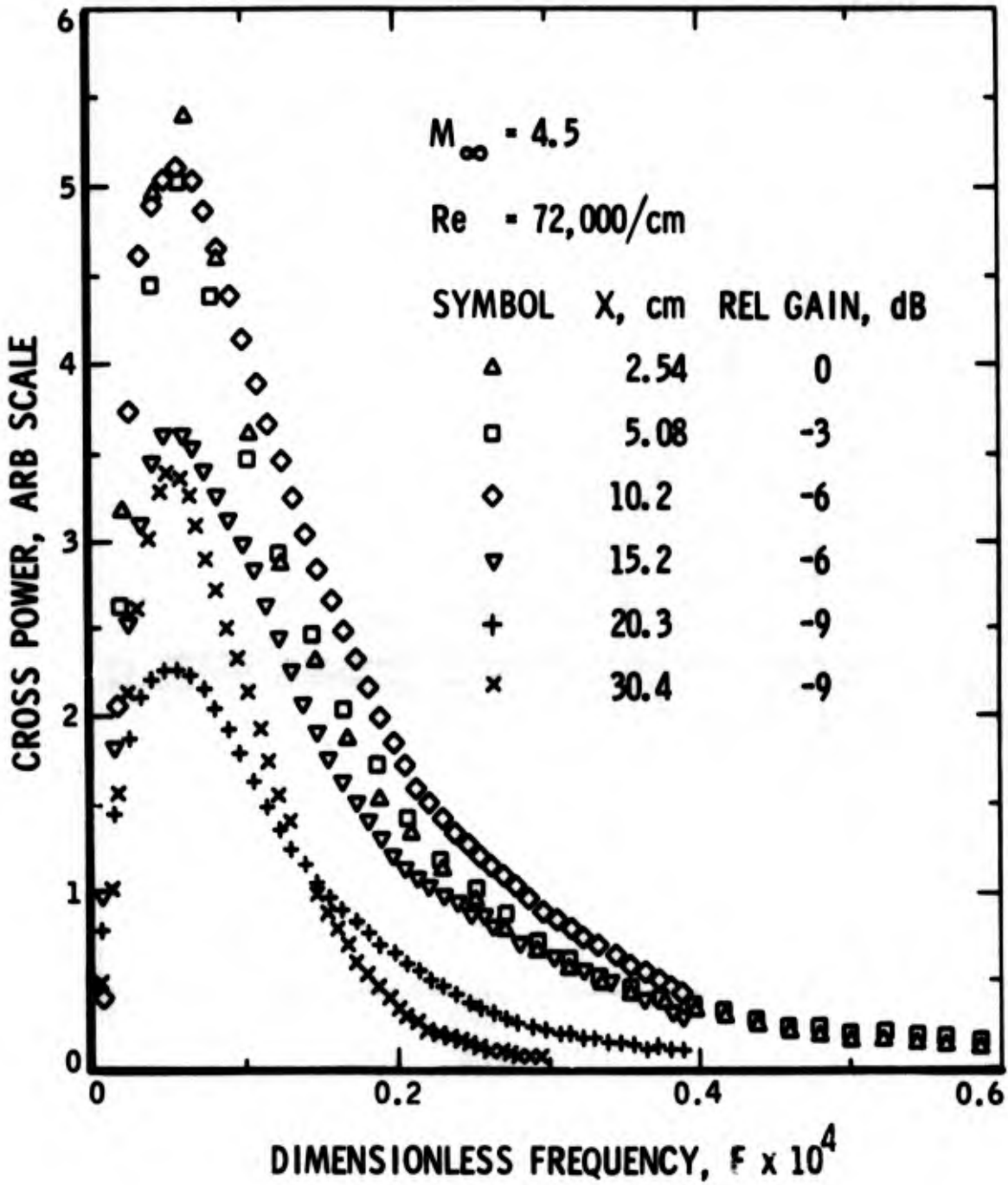
Figure 2-4. Spectra of Cross-Correlation Coefficient
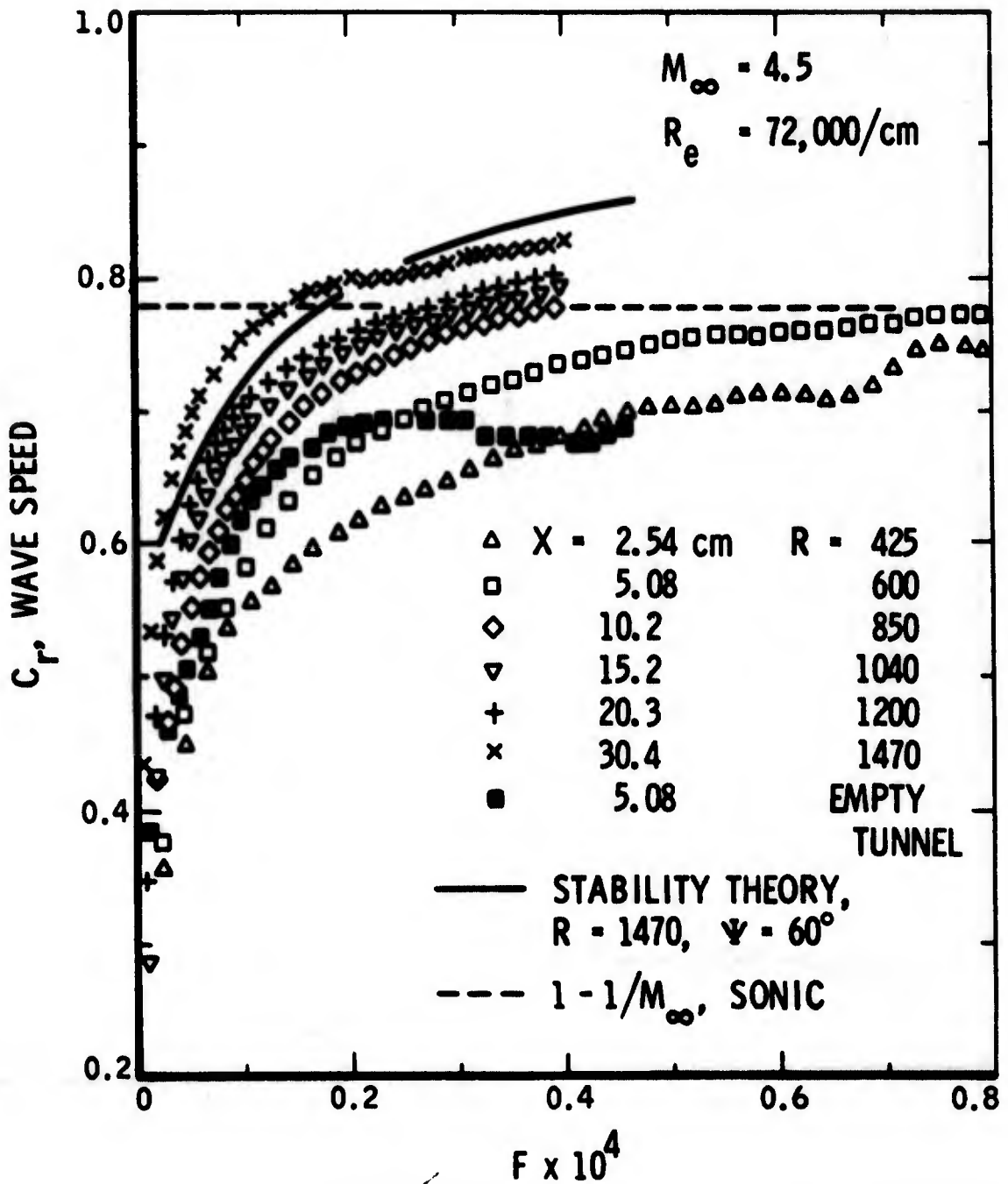
Figure 2-5. Wave Speed
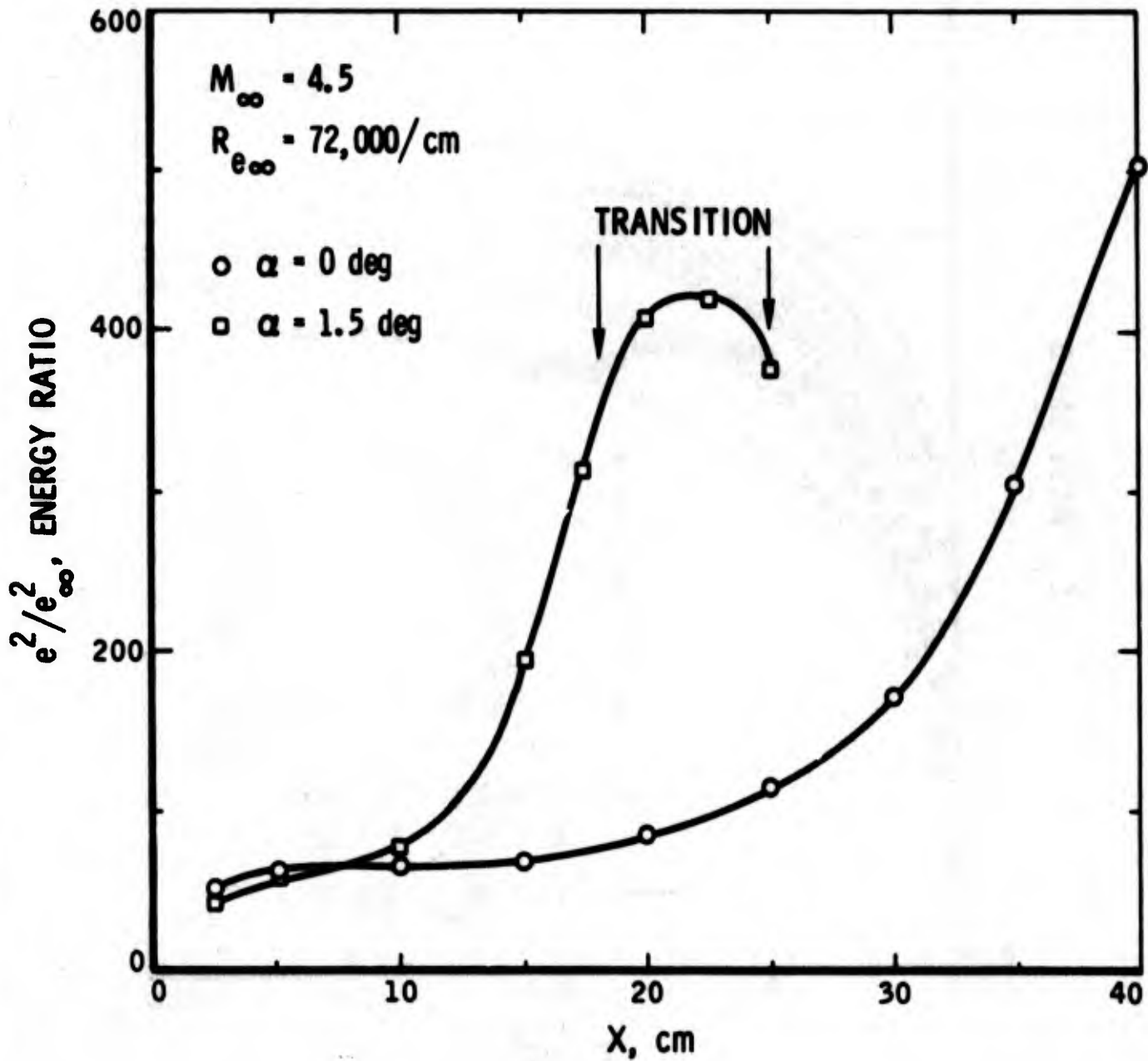
Figure 2-6. Fluctuation Energy along Leeward Ray of a Cone at Incidence

# SECTION 3

# RECALCULATION OF BROWN'S STABILITY RESULTS
(Unclassified)

by Louis I. Boehman

University of Dayton, Dayton, Ohio

## ABSTRACT

A number of investigators have questioned the validity of W. B. Brown's boundary layer stability calculations for the case when the terms involving the mean flow velocity component normal to the surface (v-component) are included in the stability equations. Brown's results for M=5 have been recalculated using improved numerical techniques. These calculations and calculations with the parallel flow equations show that Brown's results are incorrect and that, contrary to his predictions, the use of stability equations which include the v-terms does not lead to improved agreement between theory and experiment. The maximum amplification rate obtained with the augmented stability equations is considerably less than that obtained with the parallel flow equations and thus does not agree with the experimental data of Kendall.

INTRODUCTION

At the 1967 Boundary Layer Transition Study Group Meeting, W. B. Brown (Reference 1) presented a paper which concluded that at M=5 good agreement between boundary layer stability theory and experiment can be obtained only if the mean normal velocity terms (v-terms) are included in the stability equations and if all three momentum equations are used in the stability equations. Brown's conclusions were drawn on the basis of comparison of his calculations to the M=5.8 neutral stability data of Demetriades (Reference 2). At the same meeting Kendall (Reference 3) presented experimental amplification rate data at M=4.5 which showed good agreement with theoretical calculations of L. M. Mack based on

inviscid oblique first-mode waves. Later in 1967, Mack (Reference 4) calculated an amplification rate curve for viscous oblique first mode waves using the full set of parallel-flow stability equations and obtained even better agreement with Kendall's data. Mack (Reference 4) compared the upper-branch neutral point computed by Brown at M=5 with his calculations and concluded that, "It appears that if one accepts the Kendall experiment as decisive, then, in the absence of something dramatic occurring between M=4.5 and 5.8, the validity of the results of both Brown and Demetriades are suspect." Morkovin (Reference 5), noting the discrepancy between the calculations of Brown and Mack, argued that the inclusion of the v-terms without including the streamwise derivatives of mean flow quantities may be the reason why Brown's results do not agree with Kendall's data since the equation of continuity of the mean flow is not satisfied when only the v-terms are included. Morkovin (Reference 5) has also questioned the appropriateness of using the Demetriades data to justify linear stability theory predictions.

In Reference 6, an extensive analysis of Brown's work was presented by Boehman. We concluded that there were a number of reasons why Brown's results were probably in error. It was shown that the streamwise (x) derivatives of mean flow quantities could very easily be included into the stability equations and that on the basis of the effect that these terms had on certain coefficients in the stability equations at M=5, Morkovin's objection did not appear to be the reason why Brown's results were in error. In Reference 6, serious questions concerning the accuracy of Brown's numerical procedures were raised, and in addition, Brown's apparently inadvertant use of a negative value of the bulk viscosity coefficient in most of his calculations was noted. The main conclusion of Reference 6 was that Brown's calculations should be redone in order to conclusively demonstrate the relative importance of including the v-terms and the streamwise derivatives of mean flow quantities.

Improved numerical procedures were developed in order that Brown's calculations could be redone with confidence in the results. In the present paper, these improved numerical procedures are described and calculations with the complete set of linear stability equations with all of the v-terms included are presented along with calculations at M=4.5 and M=5 with the v-terms neglected. The results are compared to the calculations of both Brown and Mack and to the measurements of Demetriades and Kendall.

ANALYSIS

Except for numerical procedures, the analysis used in this paper is identical to that used by Brown as described in References 7 and 8. The stability equations are not, however, identical to Brown's, since as noted in Reference 6, his system of equations is not complete. The derivation of the stability equations including both the v-terms and the streamwise derivatives of mean flow quantities is given in Reference 6 and will not be repeated here. A ninth-order system of linear first order differential equations is obtained when the v-terms are included and following the procedure of Brown (Reference 1, 7 or 8), the ninth order system is reduced to an eighth order system. The eighth order system is set up as follows:

$$\sum_{j=1}^{8} a_{ij} Z_j' = \sum_{j=1}^{8} b_{ij} Z_j \qquad (i=1, 2, \ldots, 8) \qquad (1)$$

where

$$Z_1 = f, \qquad Z_2 = f' = Z_1', \qquad Z_3 = \phi, \qquad Z_4 = \pi/M^2, \qquad Z_5 = \theta,$$

$$Z_6 = \theta' = Z_5', \qquad Z_7 = h, \qquad Z_8 = h' = Z_7'$$

and where the row index, i, in Equation (1) is set up in the following order

| Row Index | Equation |
|-----------|----------|
| 1 | $Z_1' = Z_2$ |
| 2 | First momentum (x-direction) |
| 3 | Continuity |
| 4 | Second momentum (y-direction) |
| 5 | $Z_5' = Z_6$ |
| 6 | Energy |
| 7 | $Z_7' = Z_8$ |
| 8 | Third momentum (z-direction) |

The matrix coefficients $a_{ij}$ and $b_{ij}$ used in the present calculations are given in Appendix I of this paper since not all of these coefficients can easily be deduced from those given in Reference 6 where the $a_{ij}$ and $b_{ij}$ are given for the eighth-order system when both the v-terms and the streamwise derivatives of mean flow quantities are included in the stability equations. The terms missing in Brown's system of equations correspond to $a_{83}$, $b_{27}$, $b_{47}$, $b_{48}$, $b_{81}$, $b_{83}$, and $b_{85}$ of this paper.

The system of equations (Equation (1)) is written in the form

$$Z_i' = \sum_{i=1}^{8} C_{ij} Z_j \qquad (i=1, \ldots, 8) \qquad (2)$$

where

$$C_{ij} = \sum_{k=1}^{8} d_{ik} b_{kj}$$

$$d_{ik} = [a_{ik}]^{-1} \qquad (3)$$

In Reference 6, it was noted that Brown's method of solution to this system of equations for the region outside of the boundary layer probably was not sufficiently accurate for the case when the characteristic equation of the system had repeated roots or very nearly repeated roots. One of

the greatest difficulties that arises when the v- and/or the x-derivatives of mean flow quantities are added to the stability equations is that the characteristic equation corresponding to the stability equations can no longer be solved analytically and, thus, the characteristic values and character- istic solutions must be obtained numerically. In Reference 6, a typical set of characteristic values was presented for the system of equations which included only the v-terms and which definitely indicated that there were repeated or very nearly repeated roots; at least two pairs of roots differed only in the 9th and 10th significant figures. The presence of repeated or very nearly repeated roots requires that the numerical method used to obtain the characteristic values be highly accurate. A further complication arises because most elementary methods for solving for the characteristic vectors corresponding to the characteristic values do not generate a system of linearly independent characteristic vectors when repeated or nearly repeated characteristic values exist.

The ALLMAT Arbitrary Matrix Eigensystem Solver algorithm (Reference 9) was used to generate the characteristic values for the calculations presented herein. ALLMAT does not however generate independent characteristic vectors corresponding to repeated or very nearly repeated characteristic values. Before one can select a method for solving for the characteristic vectors corresponding to repeated characteristic values, one must first determine if independent charac- teristic vectors exist. Let $\lambda_1 = \lambda_2$ be a pair of repeated characteristic values. If there is only one independent characteristic vector a solution of the form

$$Z_i = K_1 k_i^{(1)} e^{\lambda_1 y} + K_2 [k_i^{(2)} + y k_i^{(1)}] e^{\lambda_1 y} \qquad (4)$$

must be used for a pair of repeated roots (see Reference 10, page 204), where $k_i^{(1)}$ is a solution to

$$(C_{ij}^* - \lambda_1 \delta_{ij}) k_j^{(1)} = 0 \qquad (5)$$

where $C_{ij}^*$ denotes $C_{ij}$ for $y \geq \delta$, and $k_i^{(2)}$ is a solution to

$$(C_{ij}^* - \lambda_1 \delta_{ij}) k_j^{(2)} = k_i^{(1)} \qquad . \qquad (6)$$

If there are two independent characteristic vectors, then the usual form
of the solution

$$Z_i = K_1 k_i^{(1)} e^{\lambda_1 y} + K_2 k_i^{(2)} e^{\lambda_1 y} \qquad (7)$$

is used (Reference 11) where $k_i^{(1)}$ and $k_i^{(2)}$ are the two linearly independent
solutions to

$$(C_{ij}^* - \lambda_1 \delta_{ij}) k_j^{(m)} = 0 \quad (m=1, 2) \qquad (8)$$

The rank of the $(C_{ij}^* - \lambda_1 \delta_{ij})$ determinant can be used to decide if one or two
independent characteristic vectors exist for the pair of repeated roots. If
the rank is one less than the order of the system, independent characteristic
vector exists. If the rank is two less than the order of the system, then
there are two independent characteristic vectors.

The MFGR subroutine (Reference 12) is used to determine the rank
of the $(C_{ij}^* - \lambda_1 \delta_{ij})$ determinant. For all calculations performed to date,
the rank of this determinant has always been 2 less than the order of the
system for all pairs of repeated characteristic values. In addition to
determining the rank of a determinant, the MFGR subroutine is ideally
suited to the task of calculating characteristic vectors since the normal
output of this subroutine includes information on which elements of a
characteristic vector can be arbitrarily specified and expresses the
remaining elements in terms of the arbitrarily specified ones.

It is recognized that the determination of the rank of a matrix is subject to numerical error and that an independent check should be performed on the accuracy of characteristic vectors obtained with an algorithm based on rank determination. Accordingly, after all characteristic values and corresponding characteristic vectors have been obtained, they are substituted into Equation (8) and the residuals are calculated. In all cases to date, these residuals have always been less than $10^{-10}$ indicating an acceptable degree of accuracy in determining both the characteristic values and their corresponding characteristic vectors. It is interesting to note that the characteristic vector obtained from the output of the MFGR subroutine for a non-repeated characteristic value yields considerably smaller residuals in Equation (8) than the characteristic vector obtained from the ALLMAT subroutine. Thus, in our calculations, ALLMAT is used only to calculate characteristic values with all characteristic vectors being calculated from the output of the MFGR subroutine.

NUMERICAL INTEGRATION PROCEDURE

The boundary conditions used in this analysis are the same as those of Brown (References 1, 7 or 8) as well as the basic approach to solving the complete eigenvalue problem. The solution in the boundary layer is accordingly

$$Z_i = C_1 Z_i^{(1)} + C_2 Z_i^{(2)} + C_3 Z_i^{(3)} + C_4 Z_i^{(4)} \tag{9}$$

$$(i = 1, 2, \ldots, 8)$$

where the $Z_i^{(j)}$ denote fundamental solutions defined by the initial conditions

$$Z_i^{(j)}(0) = \delta_{ik} \qquad (j = 1, 2, 3, 4 \text{ and } k = 2j) \tag{10}$$

Attempts to numerically integrate the system of equations using standard numerical integration procedures met with very limited success. Because of parasitic error growth, the four fundamental solutions became very nearly dependent at the edge of the boundary layer. Only the lower branch of the neutral stability curve for $R_\theta < 1000$ could be determined in a straight-forward manner. Brown's method of differential corrections (Reference 13) was then used to extend the range of the calculations. The use of this method made it possible to determine the lower branch out to an $R_\theta$ of about 1500 and the upper branch out to $R_\theta = 900$. In order to calculate a M=5 neutral stability curve for the same range of $R_\theta$ as that of Brown, it was finally necessary to use an improved numerical integration procedure. The Gram-Schmidt orthogonalization procedure (Reference 14, 15, 16, 17, and 18) was applied in order to control parasitic error growth during numerical integration.

The application of the Gram-Schmidt procedure to boundary layer stability problems has been adequately described in the fluid mechanics literature as far as determining eigenvalues is concerned. The determination of eigenfunctions corresponding to the eigenvalues however is not so well described and will be presented here. Conte (Reference 16) presents a description of the application of Gram-Schmidt orthogonalization to determining both eigenvalues and eigenfunctions. Conte notes that the eigenfunctions can be constructed without reintegration from information generated during the orthonormalization process provided certain information is stored at each integration mesh point. Following Conte, the orthonormalization process applied to the system of equations represented by Equations (9) and (10) can be written as

$$\overline{z}_i^{(j)}(y_1) = \sum_{k=1}^{4} z_i^{(k)}(y_1) P_{kj} \qquad \begin{array}{l} (i=1, 2, \ldots, 8) \\ (j=1, 2, \ldots, 4) \end{array} \quad (11)$$

where $y_1$ denotes the first mesh point where the four linearly independent

fundamental solutions $Z_i^{(k)}(y_1)$ obtained by any standard integration procedure are orthonormalized. The elements of the $P_{kj}$ matrix are generated from information obtained during the application of the Gram-Schmidt recursion formulas for orthonormalizing a set of vectors. Using the usual inner (dot) product notation for two vectors, $(\alpha, \beta)$ denoting the inner product of the vectors $\alpha$ and $\beta$, the elements of $P_{ij}$ are given by[*] (Reference 18)

$$P_{ij} = \begin{cases} -\sum_{\ell=i}^{j-1} (\overline{Z}^{(\ell)}, Z^{(j)}) \dfrac{P_{i\ell}}{w_{jj}} & \text{if } i < j \\[4mm] 0 & \text{if } i > j \\[4mm] \dfrac{1}{w_{jj}} & \text{if } i = j \end{cases} \qquad (12)$$

where

$$w_{jj} = (t^{(j)}, t^{(j)})^{1/2} \qquad (13)$$

and

$$t^{(j)} = Z^{(j)} - \sum_{i=1}^{j-1} (Z^{(j)}, \overline{Z}^{(i)}) \overline{Z}^{(i)} \qquad (14)$$

$$\overline{Z}^{(j)} = t^{(j)}/w_{jj} \qquad (15)$$

Equations (13), (14), and (15) together constitute the Gram-Schmidt orthonormalization formulas. Comparisons of Equations (12) through (15) shows that the elements of $P_{ij}$ are available as a byproduct during the orthonormalization process although they are not actually themselves needed to orthonormalize the $Z^{(j)}(y_1)$. If the $P_{ij}$ are formed and stored

---

[*] Conte (Reference 16) incorrectly lists the $P_{ij}$ for $i<j$. His equation for $P_{ij}$ will give the proper result for $j = 1, 2$ and whenever $i=j-1$ but will be incorrect for other $i$ and $j$.

at $y_1$ and if the initial conditions and fundamental solutions are stored at each intermediate integration mesh point, then the solution over the range $0 \le y \le y_1$ can be restored to a common basis by transformation according to Equation (11), that is, by postmultiplication of the fundamental solution matrix at each mesh point and at $y=0$ by $P_{ij}$. The resultant initial condition matrix $\overline{Z}_i^{(j)}(0)$ now represents the initial conditions for each fundamental solution which would yield its corresponding orthonormalized solution at $y_1$ and all intermediate mesh points upon straight-forward integration from $y=0$ to $y=y_1$. The postmultiplied $\overline{Z}_i^{(j)}$ are stored at each mesh point instead of the $Z_i^{(j)}$ and the integration is then continued from the point $y_1$ with the initial conditions $\overline{Z}_i^{(j)}(y_1)$ to the next mesh point, $y_2$, where orthonormalization is desired and where a new $P_{ij}$ matrix is formed and stored. The solution over the range $0 \le y \le y_2$ can again be restored to a common basis by postmultiplication of the fundamental solution matrix at all mesh points between $y=0$ and $y=y_2$ with the new $P_{ij}$ matrix. This process is continued until the edge of the boundary layer ($y=\delta$) is reached at which time a final orthonormalization is performed, $P_{ij}$ at $y=\delta$ is formed and stored, and the $\overline{Z}_i^{(j)}$ matrix at each mesh point between $y=0$ and $y=\delta$ and the initial condition matrix $\overline{Z}_i^{(j)}(0)$ are all postmultiplied by $P_{ij}(\delta)$. The final result of this process is a set of fundamental solutions which are orthonormal at $y=\delta$. These new fundamental solutions can then be linearly combined to satisfy the appropriate combination of initial and final boundary conditions, thus determining the $C_j$ in Equation (9). If the proper values of $\alpha_1$, $\alpha_3$, $c_r$, $c_i$, and R were chosen so that this set of parameters constituted an eigenvalue, then the eigenfunction could be obtained simply by forming the linear combination

$$Z_i = \sum_{j=1}^{4} \overline{C}_j \overline{Z}_i^{(j)} \tag{16}$$

at each mesh point. In actual practice of course the eigenvalues are not known a priori but must be determined by means of an appropriate search

procedure with the consequence that the procedure outlined above is unnecessarily time-consuming since the fundamental solutions are not required at the intermediate mesh points but only at y=0 and y=δ in order to search for the eigenvalues. Therefore, the above procedure is modified so that only the initial condition matrix $Z_i^{(j)}(0)$ is postmultiplied by the $P_{ij}$ matrix each time when the orthonormalization procedure is carried out. This provides sufficient information for the search procedure to be carried out and for the combining coefficients, $\overline{C}_j$, in Equation (16) to be determined. Then after an eigenvalue has been determined, the eigenfunction can be constructed by proceeding backwards from the endpoint y=δ. Recall that at each mesh point where an orthonormalization was carried out the $\overline{Z}_i^{(j)}$ are stored and that this matrix represents the initial conditions used to integrate the fundamental solutions from one orthonormalization mesh point to the next. Also suppose that the interval $(0, \delta)$ was divided into m equal meshes of length h so that $y_n = nh$, (n=1, 2, ... m) and that orthonormalizations were carried out at p points $y_{n_1}, y_{n_2}, \dots, y_{n_p}$. Since the endpoint is one of the orthonormalization points, $\delta = y_{n_p}$ and

$$\overline{Z}_i^{(j)}(\delta) = \sum_{k=1}^{4} Z_i^{(k)}(\delta) P_{kj}(\delta) \tag{17}$$

Let $y_s$ be any mesh point between $y_{n_p}$ and $y_{n_p-1}$. Then applying the same transformations used in Equation (17) to $Z_i^{(j)}(y_s)$, the reconstructed fundamental solution matrix at $y_s$ becomes

$$\overline{Z}_i^{(j)}(y_s) = \sum_{k=1}^{4} Z_i^{(k)}(y_s) P_{kj}(\delta)$$

and the eigenfunction at $y_s$ is given by

$$Z_i(y_s) = \sum_{k=1}^{4} \overline{Z}_i^{(j)}(y_s) \overline{C}_j \tag{18}$$

which can be written as

$$Z_i(y_s) = \sum_{k=1}^{4} Z_i^{(k)}(y_s) \sum_{j=1}^{4} P_{kj}(p)\overline{C}_j(p)$$

or as

$$Z_i(y_s) = \sum_{k=1}^{4} Z_i^{(k)}(y_s)\overline{C}_k(p-1) \qquad (19)$$

$$y_{n_{p-1}} \leq y_s < y_{n_p}$$

where $\overline{C}_k(p-1)$ is defined as

$$\overline{C}_k(p-1) = \sum_{j=1}^{4} P_{kj}(p)\overline{C}_j(p) \quad . \qquad (20)$$

As soon as the point $y_s$ moves to the left of $y_{n_{p-1}}$, the vector $\overline{C}_k(p-1)$ in Equation (19) is replaced by (Reference 16)

$$\overline{C}_k(p-2) = P_{kj}(p-1)\overline{C}_j(p-1) \qquad (21)$$

and

$$Z_i(y_s) = \sum_{k=1}^{4} Z_i^{(k)}(y_s)\overline{C}_k(p-2) \qquad (22)$$

$$y_{n_{p-2}} \leq y_s < y_{n_{p-1}}$$

This process is continued until the initial point y=0 is reached. An immediate check on the accuracy of the eigenfunction so obtained is available at y=0 by comparing the values obtained in the backward resolution with the initial values obtained during the forward integration, that is with the linear combination

$$Z_i(0) = \sum_{j=1}^{4} \overline{Z}_i^{(j)}(0) \overline{C}_j$$

formed at the end of the forward integration. Typically, these values agree to within six significant figures in our calculations.

## CALCULATIONS AND RESULTS

The following comments apply to all of the calculations described in this paper: the mean flow profiles were obtained by solving the compressible flow laminar boundary layer equations using the procedure described by Mack in Section II of Reference 19; the v-component of velocity was calculated by integrating the mean flow continuity equation; the Prandtl number, specific heat, and specific heat ratio were assumed constant; the stagnation temperature was taken to be 100°F; and the bulk viscosity = 0. An integration step size of 0.04 was used with orthonormalizations performed at the end of every two integration steps. The fourth-order Runge-Kutta integration procedure was used for all integrations.

The results of our calculations for M=5 flow over an insulated flat plate at zero incidence are given in Table I. In Figures 1 and 2, these results are compared to Brown's neutral stability calculations as presented in Table 2 of Reference 7. In Figure 3, a comparison is made to Demetriades' M=5.8 data as presented in Reference 2. Also shown in Figure 3 is Brown's neutral stability curve as presented in Figure 6 of Reference 7. While Brown's neutral stability curve represents a reasonable curve-fit to his tabulated results, the scatter in his computed data is large. In addition, his neutral stability wave number and phase velocity calculations shown in Figure 2 exhibit a disturbing amount of scatter. Thus, even without the benefit of new calculations, there is reason to suspect the validity of Brown's results for the case when he used all three momentum equations and the v-terms (his eighth-order system).

Brown also performed calculations with the v-terms included in a sixth-order system using the Dunn-Lin transformation to account for oblique waves (Reference 8). Brown's neutral stability curve for this case, as shown in Figure 1 of Reference 7 is also compared to our calculations in Figure 3. Substantially better agreement is obtained between our calculations and Brown's in this case. This observation lends credence to the conclusion that it is not the addition of the v-terms to the stability equations which is responsible for the marked difference between Brown's sixth-order and eighth order results, but rather that this difference is due either to numerical inaccuracy and/or to the use of an incomplete eighth order system.

Of course, the above discussion says nothing about the validity of our own calculations. To our knowledge, Brown is the only source of compressible flow stability calculations with the v-terms included in the stability equations. Thus, further comparisons can only be made, at this time, to parallel flow results and experimental data. Such a comparison is presented in Figure 4 where our M=4.5 calculations are presented for $v = 0$ and $v \neq 0$. Also shown in Figure 4 are Mack's results and Kendall's measurements which are taken from Figure 3 of Reference 4. Figure 4 shows that the maximum amplification rate calculated with the v-terms included is about 50 percent less than that obtained from both Kendall's experimental measurements and parallel flow calculations. The agreement between Mack's parallel flow calculations ($\psi = 55°$) and ours ($\psi = 60°$) is seen to be quite good although it would be desirable to make a comparison for the same wave angle.

At the present time, we have not performed those calculations for $\psi = 55°$ at M=4.5, although results are available for $\psi = 55°$ at M=5. In Figure 5, these M=5 results are compared to Mack's M=4.5 results and to our calculations with $v \neq 0$. The agreement between these two sets of parallel flow equations is excellent and again, the maximum amplification

rate for the $v \neq 0$ calculations is about 50% less than the maximum parallel flow amplification rate. The comparisons shown in Figures 4 and 5 serve to establish the validity of our calculational procedures. A further check was performed by comparing both first and second mode neutral stability calculations with Mack's. In Figure 6, neutral stability results for $\psi = 0$ and M=4.5 are shown in comparison to Mack's (Reference 20). Here the comparison shows very good agreement. Since the analysis and numerical procedures used to obtain the results presented in this paper are much different than Mack's, the good agreement of our parallel flow results with his provides assurance that the non-parallel flow results presented in this paper can be viewed with confidence. Therefore, on the basis of these comparisons, it must be concluded (1) that Brown's results obtained with his eighth-order system are incorrect; (2) including the v-terms leads to poorer agreement between theory and Kendall's measurements; and (3) our results provide further evidence that Demetriades' M=5.8 measurements cannot validly be used to justify linear stability theory predictions.

The next logical step would be to include the streamwise derivatives of mean flow quantities as well as the v-terms with the expectation that perhaps their influences would counteract each other and that closer agreement with parallel flow results would be obtained. A few preliminary calculations have been performed for M=5 and $\psi = 55°$ with all of these terms included and are presented in Table II. A comparison of these results with Figure 5 shows that the expected result is not obtained; the maximum amplification rate while greater than when only the v-terms are included, is still considerably less than the parallel flow result.

It is interesting to note that while the addition of the v-terms to the stability equations has an appreciable effect on the maximum amplification rate, the effect of these terms on the amplitude distributions is small. Figure 7 shows a comparison of the magnitudes of $f$, $\phi$, and $\pi$ for $v = 0$

and $v \neq 0$ with M=5, $\alpha_1 = 0.04$ corresponding to $\alpha_1 c_r /R \simeq .215 \times 10^{-4}$ in Figure 5. In Brown's method of solution, the strength of the disturbance is specified through $f'(0)$. Following Brown, we have set $f'(0) = 1$. However had we, in the fashion of Mack, set $f(\delta) = 1$, then Figure 7 shows that the maximum values of these amplitude functions would not be appreciably different, since in this case both sets of $|f|$ would be equal to 1 at $y=\delta$ which would cause the peak values of $|f|$ and $|\phi|$ to be more nearly equal for the same disturbance amplitude boundary condition.

## DISCUSSION

If one accepts our calculations to be accurate and Kendall's measurements to be reliable, then the comparisons made in the preceding section lead to the disturbing conclusion that improving the accuracy of the stability equations leads to poorer agreement between theory and experiment. Speculation as to why calculations with a presumably more "exact" system of equations than the parallel flow equations seems to lead to poorer agreement between theory and experiment might center about the following points. (1) When the v-terms (but not the streamwise derivatives of mean flow quantities) are added to the parallel flow equations, a ninth-order system is generated. The assumption that $(v/\alpha_1)\pi''$ is negligible (References 6 and 7) is required in order to reduce the ninth-order system to an eighth-order system, but for M in the range of 4.5 to 5, $v/\alpha_1$ can be of order 1 so that the validity of this assumption can be questioned. (2) Streamwise derivatives of amplitude functions have been neglected but may be of the same order of magnitude as the v-terms and streamwise derivatives of mean flow quantities. (3) The assumption that the amplification rate ($\alpha_{1_i}$ in the spatial formulation or $\alpha_1 c_i$ in the temporal formulation) is constant may be a more restrictive assumption than the parallel flow assumption. (4) Improving the accuracy of the stability equations without at the same time increasing the accuracy of the assumed form of the solution may not necessarily lead to better results.

The amplitude distribution for $|\pi|$ shown in Figure 7 indicates that $v/\alpha_1 \pi''$ might indeed be negligible, although it would be desirable to perform calculations with the ninth-order system in order to fully clarify this point. With regard to the second point, under the assumption that the amplitude distributions are functions of y only, the streamwise derivatives of the amplitude functions can easily be included in the stability equations as is shown in Reference 6. In view of the third and fourth points, however, such an endeavor may not be rewarding. Furthermore, while the evidence in this paper suggests that v-terms and streamwise derivatives of mean flow are unimportant in supersonic boundary layer stability, this evidence is based on a very meager amount of experimental data; measurements at one free stream Mach number, at one wave angle, and at a single Reynolds number. These terms arise because of boundary layer growth and the suspicion lingers that they may be important in flows with more severe boundary layer growth than occurs for flow over an adiabatic flat plate with zero pressure gradient. They may be important even for such a flow at smaller Reynolds numbers where the v-component of velocity is larger and for flows with an adverse pressure gradient, for flows with ablation, and for three-dimensional flows.

## ACKNOWLEDGMENTS

# REFERENCES

1.  W. B. Brown, "Improvements in Compressible Solutions of Stability Theory," in Boundary Layer Transition Study Group Meeting, Vol. II, U.S. Air Force Report BSD-TR-67-213, Vol. II, Section 11 (August 1967).

2.  A. Demetriades, An Experimental Investigation of the Stability of the Hypersonic Laminar Boundary Layer, Memorandum No. 43, Hypersonic Research Project, Guggenheim Aeronautical Laboratory, California Institute of Technology (May 1958).

3.  J. M. Kendall, Jr., "Supersonic Boundary Layer Stability Experiments," in Boundary Layer Transition Study Group Meeting, Vol. II, U.S. Air Force Report BSD-TR-67-213, Vol. II, Section 10 (August 1967).

4.  L. M. Mack, "The Stability of Viscous Three-Dimensional Disturbances in the Laminar Compressible Boundary Layer. Part II," in JPL Space Programs Summary 37-48, Vol. III, California Institute of Technology, pp 167-169 (December 1967).

5.  M. V. Morkovin, Critical Evaluation of Transition From Laminar to Turbulent Shear Layers with Emphasis on Hypersonically Traveling Bodies, U.S. Air Force Report AFFDL-TR-68-149, Air Force Flight Dynamics Laboratory, Wright-Patterson Air Force Base, Ohio (March 1969).

6.  L. I. Boehman, "Compressible Boundary Layer Stability Equations without the Parallel Flow Assumption," in Developments in Mechanics, Vol. 6, Proceedings of the 12th Midwestern Mechanics Conference, University of Notre Dame Press, Notre Dame, Indiana, pp 193-206 (August 1971).

7.  W. B. Brown, "Stability of Compressible Boundary Layers," AIAA J., Vol. 5, No. 10, pp 1753-1759 (October 1967).

8.  G. S. Raetz and W. B. Brown, Theoretical Investigations of Boundary Layer Stability, Part 2, "Stability of Compressible Flow over a Flat Plate," and Part 3, "Numerical Solution of the Complete Three-Dimensional Stability Equations of the Compressible Boundary Layer on a Flat Plate," by W. B. Brown, U.S. Air Force Report AFFDL-TR-64-184, Air Force Flight Dynamics Laboratory, Wright-Patterson Air Force Base, Ohio, pp 89-126 (September 1966).

9.   R. E. Funderlic and J. Rinzel, "ALLMAT, A FORTRAN IV Arbitrary Matrix Eigensystem Solver," SHARE Program Library (August 1968).

10.  M. Esser, Differential Equations, W. B. Saunders Co., Philadelphia, Pennsylvania, pp 202-206 (1968).

11.  W. Kaplan, Ordinary Differential Equations, Addison-Wesley Publishing Co., Reading, Mass., pp 294-295 (1960).

12.  IBM Scientific Subroutine Package (SSP) Version 3 (360 A-CM-03X), IBM Technical Publications Department, White Plains, New York.

13.  W. B. Brown, "Exact Solution of the Stability Equations for Laminar Boundary Layers in Compressible Flow," in Boundary Layer and Flow Control (G. V. Lachmann, ed.), Pergamon Press, Vol. 2, pp 1033-1042 (1961).

14.  R. E. Bellman and R. E. Kalaba, Quasilinearization and Nonlinear Boundary-Value Problems, American Elsevier Publishing Company, New York, New York, pp 98-103 (1965).

15.  A. R. Wazzan, T. T. Okamura, and A. M. O. Smith, "Stability of Laminar Boundary Layers at Separation," The Physics of Fluids, Vol. 10, No. 12, pp 2540-2545 (December 1967).

16.  S. D. Conte, "The Numerical Solution of Linear Boundary Value Problems," SIAM Review, Vol. 8, No. 3, pp 309-321 (July 1966).

17.  R. Betchov and W. O. Criminale, Jr., Stability of Parallel Flows, Academic Press, New York, New York, pp 275-277 (1967).

18.  J. M. Gersting, Jr. and D. F. Jankowski, "The Hydrodynamic Stability of Two Axisymmetric Annular Flows," in Developments in Mechanics, Vol. 6, Proceedings of the 12th Midwestern Mechanics Conference, University of Notre Dame Press, Notre Dame, Indiana, pp 179-192 (August 1971).

19.  L. M. Mack, "Computation of the Stability of the Laminar Compressible Boundary Layer," in Methods of Computational Physics: Volume 4, Academic Press, New York, New York, pp 247-299 (1965).

20.  L. M. Mack, Boundary Layer Stability Theory, JPL Technical Report 900-277 Rev. A., Jet Propulsion Laboratory, California Institute of Technology, Pasadena, California, p 12-38 (November 1969).

# NOMENCLATURE

| Symbol | Definition | Characteristic Measure |
|---|---|---|
| c | phase velocity of disturbance $= c_r + ic_i$ | $U^*_\infty$ |
| $c_v$ | specific heat at constant volume | $c^*_{v_\infty}$ |
| l | velocity disturbance amplitude in $x^*$ direction | $U^*_\infty$ |
| h | velocity disturbance amplitude in $z^*$ direction | $U^*_\infty$ |
| i | unit imaginary number $\sqrt{-1}$ | |
| k | thermal conductivity | $k_\infty$ |
| $\ell$ | characteristic length $= x^*/R$ | |
| M | Mach number | |
| P | pressure | $P^*_\infty$ |
| $R_x$ | Reynolds number $= \rho^*_\infty U^*_\infty x^*/\mu^*_\infty$ | |
| R | $\sqrt{R_x}$ | |
| r | amplitude of density fluctuation | $\rho^*_\infty$ |
| T | temperature $= T^*/T^*_\infty$ | $T^*_\infty$ |
| t | time | $\ell/U^*_\infty$ |
| $U^*_\infty$ | mean free stream velocity | |
| v | mean flow component of velocity normal to wall ($y^*$-direction) | $U^*_\infty$ |
| w | mean flow component of velocity parallel to wall ($x^*$-direction) | $U^*_\infty$ |
| $x^*$ | dimensional distance parallel to wall in direction of free stream flow | |
| x | non-dimensional distance $= x^*/\ell$ | $\ell$ |
| $y^*$ | dimensional distance perpendicular to wall | |
| y | Blasius similarity variable $= y^*R/x^*$ | |
| $z^*$ | dimensional distance parallel to wall in direction transverse to free stream flow | |
| z | non-dimensional distance $z^*/\ell$ | |
| $\alpha_1$ | disturbance wave number i $x^*$ direction | $\ell^{-1}$ |
| $\alpha_3$ | disturbance wave number in $z^*$ direction | $\ell^{-1}$ |
| $\beta$ | angular frequency | $U^*_\infty/\ell$ |
| $\gamma$ | specific heat ratio $= c^*_{p_\infty}/c^*_{v_\infty}$ | |
| $\delta_{ij}$ | Kronecker delta | |
| $\theta$ | amplitude of temperature fluctuation | $T^*_\infty$ |
| $\mu, \mu_1$ | first viscosity coefficient | $\mu^*_\infty$ |
| $\mu_2$ | Lees-Lin definition of bulk viscosity coefficient $= 3/2\xi$ | |
| $\xi$ | coefficient of bulk viscosity, $=0$ for a Stokesian fluid | $\mu^*_\infty$ |
| $\pi$ | amplitude of pressure fluctuation | $P^*_\infty$ |
| $\rho$ | fluid density | $\rho^*_\infty$ |
| $\sigma$ | Prandtl number | |
| $\alpha_1\phi$ | velocity disturbance amplitude in $y^*$ direction | $U^*_\infty$ |

# APPENDIX: ELEMENTS OF THE $a_{ij}$ AND $b_{ij}$ MATRICES

$a_{11} = 1$  $\qquad a_{22} = \mu/R$  $\qquad a_{23} = \dfrac{i\alpha_1^2}{R}\left(\dfrac{1}{3}\mu + \xi\right)$  $\qquad a_{33} = -1$

$a_{34} = \dfrac{-vM^2}{\alpha_1}$  $\qquad a_{43} = \dfrac{\alpha_1}{R}(\ell n\,\bar{T})'\left(\dfrac{4}{3}\mu + \xi\right) + \dfrac{\alpha_1\bar{T}'}{R}\left(\dfrac{4}{3}\dfrac{d\mu}{d\bar{T}} + \dfrac{d\xi}{d\bar{T}}\right) - \dfrac{\alpha_1 v}{T}$

$a_{44} = \dfrac{-1}{\gamma} - \dfrac{M^2}{R}\left(\dfrac{4}{3}\mu + \xi\right)\left[-v(\ell n\,\bar{T})' + 2v' + i\alpha_1(w-c)\right]$  $\qquad a_{43} = \dfrac{v}{R\bar{T}}\left(\dfrac{4}{3}\mu + \xi\right)$

$a_{55} = 1$  $\qquad a_{63} = -\alpha_1(\gamma-1) + \dfrac{2\alpha_1}{R}\gamma(\gamma-1)M^2\left(\xi + \dfrac{4}{3}\mu\right)v'$  $\qquad a_{66} = \dfrac{\gamma k}{\sigma R}$

$a_{77} = 1$  $\qquad a_{83} = \dfrac{i\alpha_1\alpha_3}{R}\left(\dfrac{1}{3}\mu + \xi\right)$  $\qquad a_{88} = \mu/R$  $\qquad b_{12} = 1$

$b_{21} = \dfrac{i\alpha_1}{\bar{T}}(w-c) + \dfrac{1}{R}\left[\mu\left(\dfrac{4}{3}\alpha_1^2 + \alpha_3^2\right) + \xi\,\alpha_1^2\right]$  $\qquad b_{22} = \dfrac{v}{T} - \dfrac{\bar{T}'}{R}\dfrac{d\mu}{dT}$

$b_{23} = \dfrac{\alpha_1 w'}{T} - i\alpha_1^2\dfrac{\bar{T}'}{R}\dfrac{d\mu}{dT}$  $\qquad b_{24} = \dfrac{vM^2w'}{T} + \dfrac{i\alpha_1}{\gamma}$

$b_{25} = -\dfrac{vw'}{\bar{T}^2} - \dfrac{w''}{R}\dfrac{d\mu}{dT} - \dfrac{w'\bar{T}'}{R}\dfrac{d^2\mu}{d\bar{T}^2} + \dfrac{i\alpha_1 v'}{R}\left(\dfrac{2}{3}\dfrac{d\mu}{d\bar{T}} - \dfrac{d\xi}{d\bar{T}}\right)$  $\qquad b_{26} = \dfrac{-w'}{R}\dfrac{d\mu}{dT}$

$b_{27} = \dfrac{\alpha_1\alpha_3}{R}\left(\dfrac{1}{3}\mu + \xi\right)$  $\qquad b_{31} = i$  $\qquad b_{33} = -(\ell n\,\bar{T})'$

$b_{34} = \dfrac{M^2}{\alpha_1}\left[-v(\ell n\,\bar{T})' + i\alpha_1(w-c) + v'\right]$  $\qquad b_{35} = \dfrac{1}{\alpha_1\bar{T}}\left[2v(\ell n\,\bar{T})' - i\alpha_1(w-c) - v'\right]$

$b_{36} = -\dfrac{v}{\alpha_1\bar{T}}$  $\qquad b_{37} = i\dfrac{\alpha_3}{\alpha_1}$  $\qquad b_{41} = i\alpha_1\dfrac{\bar{T}'}{R}\left(\dfrac{2}{3}\dfrac{d\mu}{d\bar{T}} - \dfrac{d\xi}{d\bar{T}}\right)$  $\qquad b_{42} = \dfrac{i\alpha_1\mu}{R}$

$b_{43} = \dfrac{i\alpha_1^2}{\bar{T}}(w-c) + \dfrac{\alpha_1 v'}{\bar{T}} + \dfrac{\mu}{R}\left(\alpha_1^3 + \alpha_1\alpha_3^2\right) - \dfrac{\alpha_1}{R}\left(\dfrac{4}{3}\mu + \xi\right)(\ell n\,\bar{T})''$

$$b_{44} = \frac{vv'M^2}{T} + \frac{M^2}{R}\left(\frac{4}{3}\mu + \zeta\right)\left[-v(\ell n\,\overline{T})'' - v'(\ell n\,\overline{T})' + i\alpha_1 w' + v''\right]$$

$$b_{45} = \frac{-vv'}{T^2} - \frac{v''}{R}\left(\frac{4}{3}\frac{d\mu}{dT} + \frac{d\zeta}{dT}\right) - \frac{v'T'}{R}\left(\frac{4}{3}\frac{d^2\mu}{dT^2} + \frac{d^2\zeta}{dT^2}\right) + \left(\frac{4}{3}\mu + \zeta\right)\frac{1}{RT}\left\{3v'(\ell n\,\overline{T})'\right.$$

$$+ 2v(\ell n\,\overline{T})'' - 2v\left[(\ell n\,\overline{T})''\right]^2 - v'' + i\alpha_1\left[(\ell n\,\overline{T})'(w-c) - w'\right]\right\} - \frac{i\alpha_1 w'}{R}\frac{d\mu}{dT}$$

$$b_{46} = -\frac{v'}{R}\left(\frac{4}{3}\frac{d\mu}{dT} + \frac{d\zeta}{dT}\right) + \left(\frac{4}{3}\mu + \zeta\right)\frac{1}{RT}\left[3v(\ell n\,\overline{T})' - 2v' - i\alpha_1(w-c)\right]$$

$$b_{47} = \frac{i\alpha_3}{R}T'\left(\frac{2}{3}\frac{d\mu}{dT} - \frac{d\zeta}{dT}\right) \qquad b_{48} = \frac{i\alpha_3\mu}{R} \qquad b_{55} = 1$$

$$b_{61} = i\alpha_1(\gamma-1)\left[1 + 2\gamma v'\frac{M^2}{R}\left(\frac{2}{3}\mu - \zeta\right)\right] \qquad b_{62} = -2w'\frac{\mu}{R}\gamma(\gamma-1)M^2$$

$$b_{63} = \alpha_1 C_v(\ell n\,\overline{T})' - 2iw'\alpha_1^2\frac{\mu}{R}\gamma(\gamma-1)M^2 \qquad b_{64} = vC_vM^2(\ell n\,\overline{T})' + v'(\gamma-1)M^2$$

$$b_{65} = \frac{C_v}{T}i\alpha_1(w-c) + \frac{\gamma}{\sigma R}k(\alpha_1^2 + \alpha_3^2) - \frac{T''\gamma}{\sigma R}\frac{dk}{dT} - \frac{\gamma}{\sigma R}(\overline{T}')^2\frac{d^2 k}{dT^2}$$

$$- \frac{\gamma(\gamma-1)M^2}{R}\left\{\frac{d\mu}{dT}\left[\frac{4}{3}(v')^2 + (w')^2\right] + v'\frac{d\zeta}{dT}\right\} - v\frac{C_v}{T}(\ell n\,\overline{T})'$$

$$b_{66} = \frac{vC_v}{T} - \frac{2\overline{T}'\gamma}{\sigma R}\frac{dk}{dT} \qquad b_{67} = i\alpha_3(\gamma-1)\left[1 + 2\left(\frac{2}{3}\mu - \zeta\right)v'\frac{\gamma M^2}{R}\right]$$

$$b_{78} = 1 \qquad b_{81} = \frac{\alpha_1\alpha_3}{R}\left(\frac{1}{3}\mu + \zeta\right) \qquad b_{83} = -\frac{i\alpha_1\alpha_3}{R}T'\frac{d\mu}{dT}$$

$$b_{84} = \frac{i\alpha_3}{\gamma} \qquad b_{85} = \frac{i\alpha_3}{R}v'\left(\frac{2}{3}\frac{d\mu}{dT} - \frac{d\zeta}{dT}\right)$$

$$b_{87} = \frac{i\alpha_1}{T}(w-c) + \frac{\mu}{R}(\alpha_1^2 + \alpha_3^2) + \left(\frac{1}{3}\mu + \zeta\right)\frac{\alpha_3^2}{R} \qquad b_{88} = \frac{v}{T} - \frac{T'}{R}\frac{d\mu}{dT}$$

# TABLE I. COMPUTED EIGENVALUES FOR M=5, $\psi$=55°. v-TERMS INCLUDED IN THE STABILITY EQUATIONS.

| R | $\alpha_1$ | $c_r$ | $c_i$ | $(\alpha_1 c_r / R) \times 10^{+5}$ |
|---|---|---|---|---|
| 3000.00 | .0051 | .6883 | 0 | 0.1180 |
| 2500.00 | .0063 | .7000 | 0 | 0.1770 |
| 2000.00 | .0083 | .7181 | 0 | 0.2982 |
| 1750.00 | .0100 | .7315 | 0 | 0.4171 |
| 1550.00 | .0121 | .7461 | 0 | 0.5829 |
| 1350.00 | .0161 | .7683 | 0 | 0.9174 |
| 1160.00 | .0245 | .8045 | 0 | 1.6989 |
| 1100.00 | .0284 | .8172 | 0 | 2.1058 |
| 1050.00 | .0326 | .8297 | 0 | 2.5800 |
| 1000.00 | .0387 | .8439 | 0 | 3.2629 |
| 975.00 | .0434 | .8529 | 0 | 3.7936 |
| 961.35 | .0520 | .8657 | 0 | 4.6825 |
| 977.20 | .0600 | .8746 | 0 | 5.3700 |
| 930.00 | .0430 | .8539 | -0.00174 | 3.9483 |
| 930.00 | .0460 | .8585 | -0.00135 | 4.2465 |
| 930.00 | .0500 | .8641 | -0.00110 | 4.6457 |
| 930.00 | .0550 | .8703 | -0.00114 | 5.1472 |
| 1050.00 | .0727 | .8853 | 0 | 6.1268 |
| 1200.00 | .0865 | .8940 | 0 | 6.4468 |
| 1300.00 | .0928 | .8973 | 0 | 6.4060 |
| 1000.00 | .1039 | .9023 | 0 | 6.0491 |
| 2000.00 | .1160 | .9068 | 0 | 5.2579 |
| 2500.00 | .1240 | .9095 | 0 | 4.5103 |
| 3000.00 | .1293 | .9111 | 0 | 3.9265 |
| 3500.00 | .1331 | .9121 | 0 | 3.4686 |
| 1550.00 | .0300 | .8129 | 0.01372 | 1.5734 |
| 1550.00 | .0400 | .8361 | 0.01519 | 2.1577 |
| 1550.00 | .0500 | .8532 | 0.01414 | 2.7522 |
| 1550.00 | .0600 | .8664 | 0.01199 | 3.3539 |
| 1550.00 | .0950 | .8968 | 0.00241 | 5.4966 |

TABLE II.  COMPUTED EIGENVALUES FOR M=5, $\psi$=55°,
STREAMWISE DERIVATIVES OF MEAN FLOW
QUANTITIES AND v-TERMS INCLUDED IN THE
STABILITY EQUATIONS.

| R | $\alpha_1$ | $c_r$ | $c_i$ | $(\alpha_1 c_r/R) \times 10^{+5}$ |
|---|---|---|---|---|
| 1550.00 | .0113 | .8244 | 0 | 0.6020 |
| 1550.00 | .0400 | .8582 | .0173 | 2.2148 |
| 1550.00 | .0600 | .8810 | .0161 | 3.4103 |
| 1550.00 | .1230 | .9189 | 0 | 7.2908 |
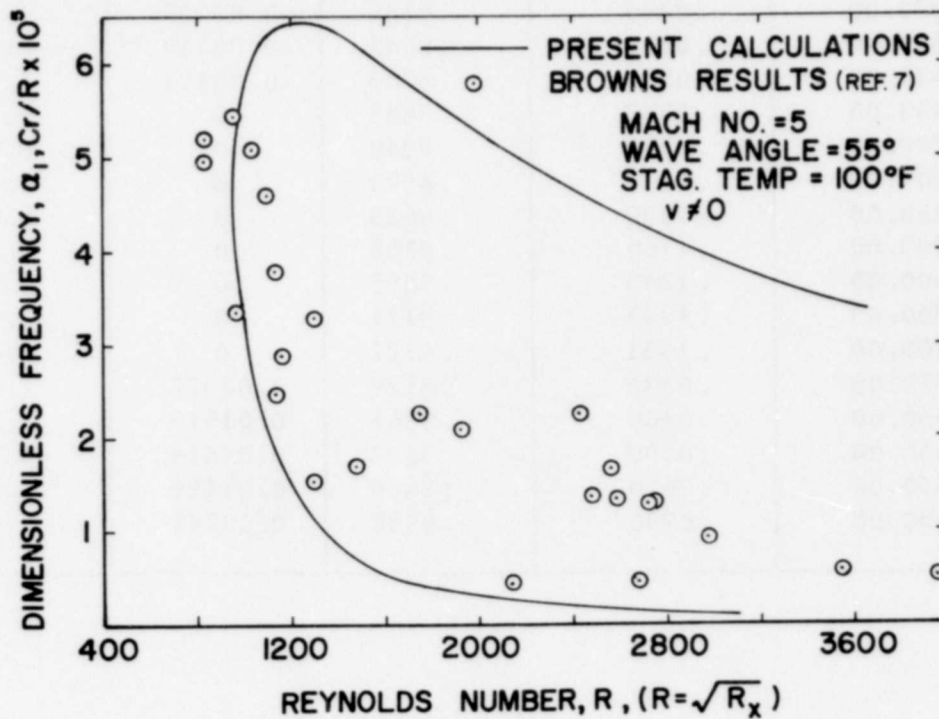


FIG. 1.  First-Mode Neutral Stability Curve. M=5, v-terms
included.
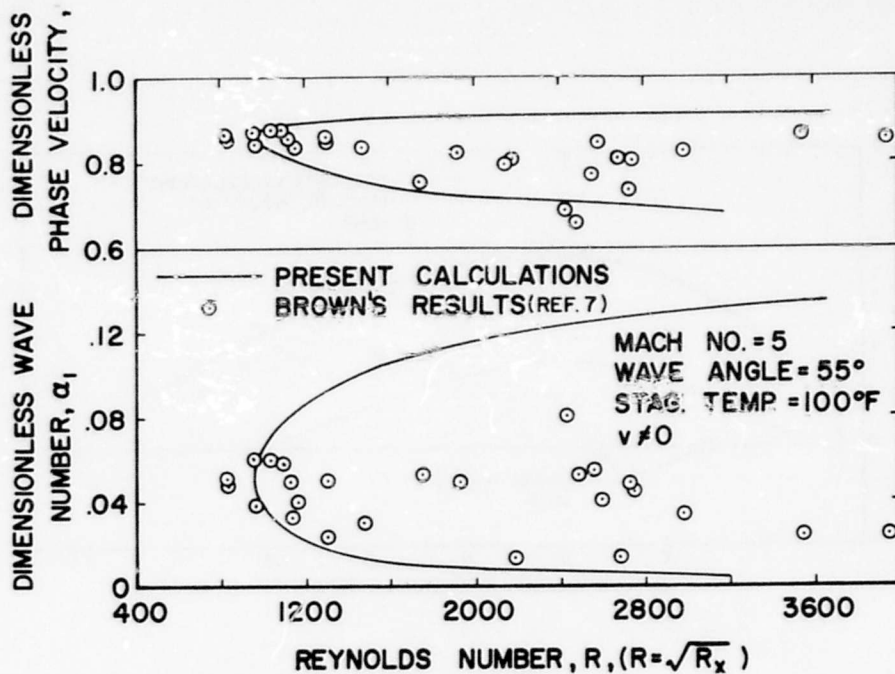
FIG. 2. Neutral Stability Wave Number and Phase Velocity versus Reynolds Number. v-Terms included. M=5.
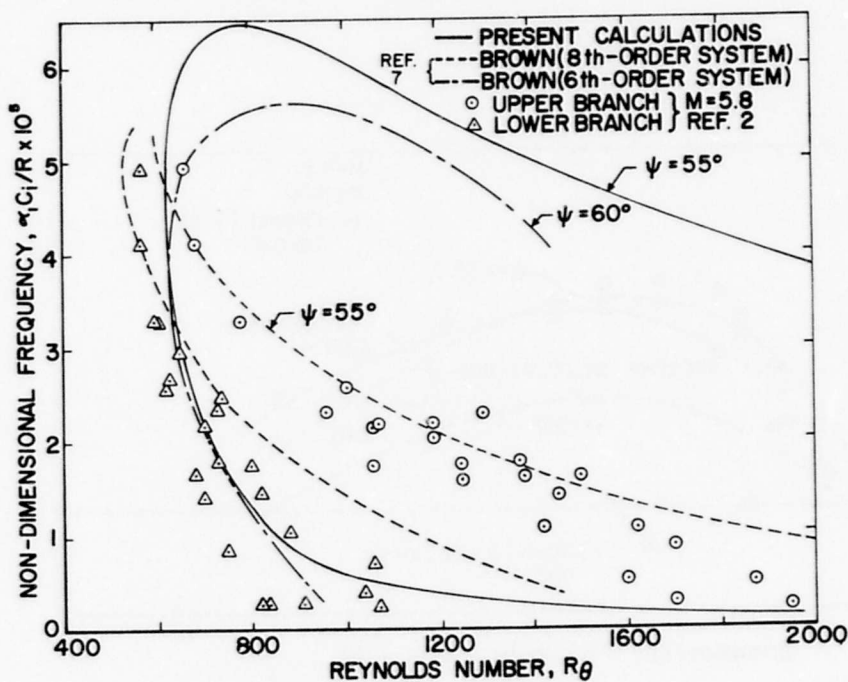


FIG. 3. Comparison of Non-Parallel Flow (v≠0) Neutral Stability Curves for M=5 with M=5.8 Measurements of Demetriades.
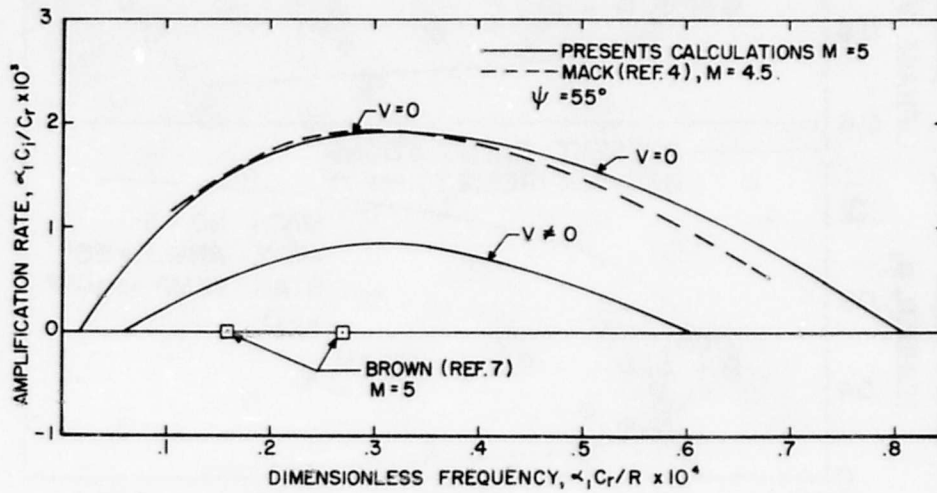
FIG. 4. Comparison of Space Rate of Amplification for v≠0 and v=0
to Mack's Theoretical Results (v=0) and Kendall's Measurements, M=4.5.
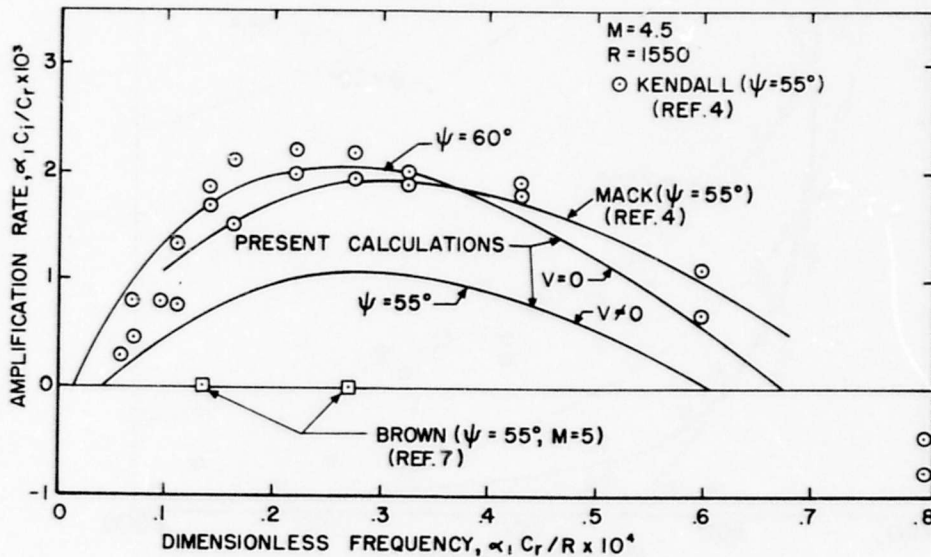


FIG. 5. Comparison of Space Rate of Amplification for v≠0 and v=0 at
M=5, $\psi$=55° to Mack's Theoretical Results (v=0) at M=4.5, $\psi$=55°.

(This page intentionally left blank)

# SECTION 4

## A STUDY OF HYPERSONIC TRANSITIONAL
## BOUNDARY LAYERS
### (Unclassified)

by F.K. Owen and C.C. Horstman

Ames Research Center, NASA
Moffett Field, California 94035

## ABSTRACT

Surface thin film gauges have been used to determine the extent of the transition region, intermittency distribution, and disturbance convection velocities in the boundary layer on a sharp 5° half angle cone at $M_\infty$ = 7.4 in the Ames 3.5-Ft Hypersonic Wind Tunnel. In addition, extensive hot wire correlation and disturbance convection velocity measurements have been obtained in the transitional hypersonic boundary layer on a cone-ogive-cylinder in the same facility. These data suggest that turbulence production in a hypersonic transitional boundary layer is created by highly three-dimensional disturbances originating close to the wall similar to previous observations in incompressible flows.

# INTRODUCTION

In spite of the extensive experimental and analytical work which has been conducted in supersonic and hypersonic transitional boundary layers in recent years, there is still much speculation regarding the detailed structure of and mechanisms influencing boundary layer transition.

Morkovin[1] and Laufer[2] have pointed out that, at high free-stream Mach numbers, the sound field which radiates from the turbulent boundary layers on the wind tunnel walls is a major source of free-stream disturbances and must be considered in all transition experiments. Recently Pate and Schueler[3] have shown that the effects of aerodynamic noise on boundary layer transition may be related to a number of wind tunnel parameters including Mach number and unit Reynolds number. However, the conclusions of Pate and Schueler cannot be extended to all wind tunnel transition data. For example, the transition data of Mateer and Larson[4] show little unit Reynolds number dependence which would not be expected if the effects of aerodynamic noise were dominant. In particular, noise cannot explain the unit Reynolds number effect observed in the ballistic range experiments of Potter[5] where, in the absence of significant free-stream disturbances the variation of transition Reynolds number with unit Reynolds number was comparable to those observed in noise-contaminated wind tunnels. It is apparent that more data are needed to determine the effects of free-stream disturbances on boundary layer transition.

A better understanding of the transition mechanism could be obtained if experiments were designed to obtain a more complete picture of the structure and extent of the transition region together with fluctuation measurements in the free stream rather than the mere determination of a single transition "point" from mean surface measurements, which has usually been the case. Indeed Laufer[6] has pointed out the general failure of experimenters to exploit the advantages of hot wire anemometry for fluctuation measurements. Consequently very little is known about the structure of hypersonic transitional boundary layers.

Since turbulent flows vary not only in time but also in space, their investigation must involve an examination of both the spatial and temporal statistical structure. Space-time correlations can contribute to this study since they give evidence of the heredity and structure of turbulence, as well as the convection velocities of the vorticity and entropy modes relative to the average mass transport velocities. Such measurements have been made in incompressible turbulent boundary layers (e.g., Favre et al.[7]) but, to the authors' knowledge, no such measurements have been reported in hypersonic transitional boundary layers.

The purpose of this investigation was to provide detailed measurements of the structure of hypersonic transitional boundary layers. Data on the intermittency distribution, disturbance convection velocities, and extent of the transition region are presented. Extensive hot wire correlation measurements are also presented. Free-stream fluctuation measurements have also been made in an attempt to determine the influence of free-stream disturbance level on boundary layer transition.

## EXPERIMENTAL DETAILS

### Wind Tunnel

The investigation was conducted in the Ames 3.5-ft Hypersonic Wind Tunnel. In this facility, high-pressure air heated in a pebble-bed heater flows through the 1.067 m-diam test section to low-pressure spheres. Using the nominal Mach 7 contoured nozzle, the test conditions were $T_O = 835°$ K, $P_O = 13-122$ atm, $M_\infty = 7.4$ for the 5° half angle cone experiments and $T_O = 667°$ K, $P_O = 14-28$ atm, $M_\infty = 7.4$ for the cone-ogive-cylinder experiments. The test core diameter was approximately 0.70 m with axial Mach number gradients less than 0.12 per meter. The nozzle had an annular injection slot in its subsonic portion through which helium or air was injected to provide thermal insulation between the nozzle wall and the hot airstream.

### Test Models

All the surface thin film gauge measurements were made on a sharp 5° half angle cone at a wall to free-stream temperature ratio of approximately 0.4. Five thin film

gauges were mounted flush with the model surface at distances between 20.3 and 61 cm from the cone apex.

The hot wire fluctuation measurements were made in the transitional boundary layer on the cylindrical portion of an axisymmetric 10° sharp cone-ogive-cylinder. This test model was 300 cm long and 20.3 cm in diameter. The wall to free-stream temperature ratio was 0.45. Details of the two test models are shown in Fig. 1.

Fluctuation Measurements

The turbulent fluctuations were measured with a constant temperature anemometer system. The frequency response of the system enabled fluctuation scales down to one half of the boundary layer thickness to be recorded and correlated. The ac component of the hot wire and hot film signals, representing the turbulent fluctuations, was recorded on the FM system of a multichannel tape recorder. For the correlation measurements, the signals from two anemometers were recorded simultaneously on two tape recorder channels which had been previously checked for phase differences. The autocorrelation and cross correlation were then obtained by playing back the tapes through an analogue correlator. The filtered correlations were obtained using matched 1/3 octave filters.

Cross correlation measurements involve the correlation of signals from two spatially separated measuring positions, with varying positive or negative time delay of one signal with respect to the other. Thus if $V_1$ $(x_1, y_1, z_1, 0)$ denotes the signal received at one point at time $t = 0$ and $V_2$ $(x_2, y_2, z_2, t)$ denotes the signal received at a second point at time "t" their cross correlation may be defined as

$$R(V_1 V_2) = \frac{\widetilde{V_1 V_2}}{\left(\widetilde{V_1^2}\right)^{1/2} \left(\widetilde{V_2^2}\right)^{1/2}}$$

The space correlation, which involves the comparison of the instantaneous signal received at two spatially separated points is therefore the cross correlation at zero time delay, while the autocorrelation, which involves the comparison of a signal received at

4-4

one measuring station with the signal received at the same point at time "t," is therefore the cross correlation for zero separation.

## DISCUSSION OF RESULTS

### Transition Measurements

Typical variations of the root mean square thin film voltage fluctuations for a range of unit Reynolds numbers are shown in Fig. 2. The curves clearly show a rise from the laminar to the turbulent level with an intermediate peak. Of particular importance is the fact that three distinct points in the transition region can be accurately located: 1) the start of transition, defined as the point where the rms signal begins to increase from its laminar value, i.e., where intermittency begins; 2) the peak rms signal which coincides with the point where the turbulent burst frequency is a maximum (Owen[8]); and 3) the end of transition.

Intermittency measurements in the transition region, obtained by passing the ac components of the hot film signals through a Schmidt trigger circuit, are shown in Figs. 3a and b. There is a close similarity between the intermittency variations in subsonic and hypersonic transitional boundary layers as shown by the good agreement between the present data and the incompressible data of Dhawan and Narashima.[9]

The influence of unit Reynolds number on the magnitude of the transition Reynolds number and the extent of the transition region is presented in Fig. 4. Also shown are previous heat transfer transition onset data obtained on an "identical" model in the same facility.[4] The onset of transition as defined by the heat transfer measurements is much less sensitive than the thin film gauge technique, especially at low unit Reynolds numbers. It is also apparent from Fig. 4 that the heat transfer technique does not provide consistent transition "point" data since the onset of transition is detected at different values of intermittency depending on the unit Reynolds number.

The authors feel that a lot of the scatter in transition data could be attributed to the inconsistent choice of the transition "point" indicated by the many different techniques which are and have been used. A more complete picture of transition

dependence on the various parameters can only be obtained from experiments in which the positions of the beginning and end of transition are accurately determined. It is of interest to note that transition data reported for supersonic and hypersonic flows are not generally based on observations of turbulent spots but rather some macroscopic quantity such as skin friction, heat transfer, or surface pitot pressure, whose departure from laminar values can be detected only when the intermittency is appreciably greater than zero.

## Structure of the Transitional Boundary Layer

Using a hot wire mounted close to the cone-ogive-cylinder model surface ($y/\delta \approx 0.05$) 115 cm from the apex, the beginning and end of transition were determined to occur at tunnel total pressures of 12 and 30 atm, respectively. For reference, the mean velocity profiles obtained from total temperature and pitot pressure surveys at this location are shown in Fig. 5.

Figure 6a shows the autocorrelation of the fluctuation signals midway through transition ($P_o$ = 21 atm) at several positions across the boundary layer. It can be seen from these curves that there is a marked variation of energy distribution with frequency across the boundary layer. The power spectral density variations across the boundary layer obtained by Fourier transformation of the autocorrelation curves are shown in Fig. 6b. It can be seen that the maximum fluctuation energy occurs near the boundary layer edge and decreases as the wall is approached. But, close to the wall there is proportionately more energy associated with the smaller scale disturbances. This "movement" of the relative energy to the smaller scales is believed to be due to the large rates of shear in the wall region. Similar results were also obtained at the two other tunnel total pressures.

The variations of the autocorrelation and power spectral density through the transition region obtained by a surface thin film gauge on the cone model are shown in Figs. 7a and b. The very pronounced change in the autocorrelation after the peak (i.e., $P_o$ = 61 atm) was observed at all gauge locations and is due to the intermittency in the boundary layer. Again it can be seen that there are significant changes in power level

4-6

and distribution with a pronounced energy concentration at the lower frequencies in the transition region. This energy concentration in the transition region is caused by the turbulent bursts passing over the film that change the mean voltage across the film from the laminar to the turbulent level (Owen[8]).

The peaks of the cross correlations obtained for various values of wire separation distance represent the autocorrelation in a reference frame moving with the disturbances or the Lagrangian autocorrelation coefficient. It is therefore a measure of the lifetime of the disturbance pattern as it is swept along with the mean flow. The variation of longitudinal correlation coefficient of the total fluctuation field measured at optimum time delay is shown in Fig. 8. The optimum correlation decreases as the space separation increases. In the case of the filtered turbulent field (Fig. 9) the influence of frequency combines with the influence of separation distance and $y/\delta$. When the separation distance is fixed, the higher the frequency the more the optimum correlation coefficient decreases. This indicates that the smaller scale disturbances are decaying at a faster rate than the larger ones. This more rapid decay of the small scale disturbances explains the selective part played by the longitudinal separation, which reduces their contribution to the correlation coefficient of the total turbulent field as the wire separation increases.

A test of Taylor's hypothesis[10] that turbulence may be regarded as a frozen pattern of eddies being swept past the wire is shown in Fig. 10 for two positions across the boundary layer. The longitudinal space correlations and the autocorrelation measured midway between the two wires are compared. As expected, this comparison shows that Taylor's hypothesis is far from satisfied. However, in the fully turbulent boundary layer, there was good agreement between the auto and space correlations above $y/\delta \approx 0.3$.[11]

The results of a series of filtered cross correlation measurements at two positions across the boundary layer are shown in Fig. 11. Each cross correlation curve reaches a maximum at some value of the time delay other than zero, clearly indicating the presence of convection. A convection velocity of these disturbances may be determined by dividing the separation distance by the time delay at which the maximum of a

particular cross correlation occurs. No variations of convection velocity with wire spacing were observed. This was also the case for the overall and other filtered disturbance convection velocities.

The variation of the disturbance convection velocity relative to the local velocity as a function of disturbance scale is shown for one wire spacing in Fig. 12. The ratio, $U_c/U_\ell$, tends towards unity as the scale ($\lambda_e = U_e/2\pi f$) decreases. Thus the small scale fluctuations are convected close to the local mean velocity. However, as the scale increases the more $U_c/U_\ell$ differs from unity. Near the wall ($y/\delta = 0.25$) the propagation velocities of the disturbances are close to the local velocity whereas they are significantly lower than the local velocity in the outer half of the boundary layer.

The variation of the overall and filtered convection velocity profiles compared to the mean velocity profile is shown in Fig. 13. At a distance from the wall $y/\delta \approx 0.25$ the convection velocities corresponding to the various scales are close to the local fluid velocity ($U_c \approx 0.72 \, U_e$). At greater values of $y/\delta$ the differences increase with the scale. In the outer portion of the boundary layer the large scale disturbances are convected much more slowly than the mean velocity. The transitional surface measurements on the 5° cone (for all disturbance scales) are also shown and can be seen to be in good agreement with the hot wire boundary layer measurements.

The values of the cross correlation coefficient have also been determined for various separation distances normal to the wall as a function of the time delay. Figure 14 shows the resulting filtered correlation coefficients for the case where one hot wire was kept at a fixed distance from the wall ($y/\delta = 0.15$) while the second wire was set at different separation distances directly above the first wire. It can be seen that the correlation reaches a maximum value for an optimum time delay "t" applied to the fluctuations sensed by the probe located farthest from the wall. This optimum time delay, which is a function of the normal separation distance, has been observed previously in an incompressible turbulent boundary layer.[7] These space-time correlations may be interpreted in terms of a disturbance inclination angle to the wall. This angle may be determined by dividing the normal wire separation distance by the product of

the observed time delay and the disturbance convection velocity at that point in the boundary layer. The results (Fig. 15) show that this angle is smallest close to the wall, and increases with increasing distance from the wall. Similar results obtained in the fully developed turbulent boundary layer on the same model[11] are represented by the solid curve on Fig. 15.

This disturbance inclination angle could be interpreted as a disturbance propagation angle, in which case the trajectory of such a disturbance would be similar to that shown in Fig. 15. In the transitional boundary layer the propagation rate across the boundary layer would be considerably faster than in the fully turbulent case. It is also apparent that there is some variation of the propagation angles through the transition region (i.e., as the total pressure changes). Towards the end of transition ($P_O$ = 28 atm) these angles approach the fully turbulent values. The propagation angle of about 20° measured close to the wall may be compared with the incompressible experiments of Kline et al.[12] where ejected streaks were observed to leave the wall layer at an angle of about 10-12°.

Some insight into the three-dimensional structure of these turbulent disturbances may be obtained from Fig. 16 where the results of the variation in lateral correlation across the boundary layer are presented. Again it can be seen that the lateral growth of the disturbances is much greater in the transitional than in the fully developed turbulent boundary layer.[11] Thus, the correlation data suggest that turbulence production in a hypersonic transitional boundary layer may be created by highly three-dimensional disturbances originating close to the wall.

## Free-stream Fluctuation Measurements

Free-stream fluctuation measurements have also been made in an attempt to determine if turbulence generation and transition in the model boundary layer are driven by the free-stream disturbances. By changing the nozzle wall gas injection it is possible to alter the state of the tunnel side wall boundary layer and consequently the free-stream disturbance level without appreciably changing the unit Reynolds number. Thus it is

possible to isolate the effects of changes in the free-stream disturbance level without associated changes in unit Reynolds number.

The undisturbed free-stream power spectra presented in Fig. 17 show comparable changes in magnitude with variations in either unit Reynolds number or tunnel wall boundary layer gas injection. However, transition data obtained with air injection showed no significant differences from the helium injection data (see Fig. 4). If changes in free-stream power spectra are important to the transition process one would expect comparable changes in transition location with gas injection as was found for changes in unit Reynolds number. This is not the case.

The overall free-stream disturbance convection velocity has also been measured and, as shown in Fig. 18, is in good agreement with the extrapolation of the data taken from Laufer.[13] Also shown are the overall disturbance convection velocities in the transitional and turbulent boundary layers on the 5° cone and cone-ogive-cylinder models. Although the convection velocities are somewhat faster in the fully turbulent than in the transitional boundary layer, they are all close to the free-stream disturbance convection velocity. It is also apparent that the boundary layer and free-stream disturbance convection velocities are traveling supersonically relative to the free stream.

The free-stream convection velocities did not vary with scale. Since the disturbance velocities in the transitional boundary layer vary significantly with scale and $y/\delta$, it is not obvious that the free-stream disturbances are driving the boundary layer disturbances.

CONCLUDING REMARKS

The surface hot film results show that a more complete picture of transition dependence on various parameters could be obtained if the onset and extent of the transition region are accurately and consistently determined. The hot wire correlation data suggest that turbulence production in a hypersonic transitional boundary layer is created by highly three-dimensional disturbances originating close to the wall similar to incompressible observations. It is not apparent that these disturbances are driven by the free stream.

# REFERENCES

1. Morkovin, M., "On Supersonic Windtunnels with Low Freestream Disturbances," J. Appl. Mech., Vol. 26, 1959, pp. 319-324.

2. Laufer, J., "Aerodynamic Noise in Supersonic Wind Tunnels," J. Aero. Sci., Vol 28, 1961, pp. 685-692.

3. Pate, S., and Schuler, C., "Effects of Radiated Aerodynamic Noise on Model Boundary Layer Transition in Supersonic and Hypersonic Wind Tunnels," AIAA Journal, Vol. 7, No. 3, 1969, pp. 450-457.

4. Mateer, G. and Larson, H., "Unusual Boundary-Layer Transition Results on Cones in Hypersonic Flow," AIAA Journal, Vol. 7, No. 4, 1969, pp. 660-664.

5. Potter, J.L., "Observations on the Influence of Ambient Pressure on Boundary Layer Transition," AIAA Journal, Vol. 6, No. 10, 1968, p. 1907.

6. Laufer, J., "Thoughts on Compressible Turbulent Boundary Layers," NASA SP-216, 1968, pp. 1-13.

7. Favre, A., Gaviglio, J. and Dumas, R., "Structure of Velocity Space-Time Correlations in a Boundary Layer," Phys. Fluids Suppl., 1967, pp. S138-S145.

8. Owen, F.K., "Transition Experiments on a Flat Plate at Subsonic and Supersonic Speeds," AIAA Journal, Vol. 8, No. 3, 1970, pp. 518-523.

9. Dhawan, S. and Narashima, R., "Some Properties of Boundary Layer Flow during the Transition from Laminar to Turbulent Motion," J. Fluid Mech., Vol. 3, 1958, pp. 418-436.

10. Taylor, G.I., "The Spectrum of Turbulence," Proc. Roy. Soc. A, 1938, Vol. 164, pp. 476-490.

11. Owen, F.K. and Horstman, C.C., "A study of turbulence generation in a hypersonic boundary layer." To be presented at AIAA 10th Aerospace Sciences Meeting, Jan 1972.

12. Kline, S., Reynolds, W., Schraub, F. and Runstadler, P., "The Structure of Turbulent Boundary Layers," J. Fluid Mech., Vol. 30, 1967, pp. 741-773.

13. Laufer, J., "Some Statistical Properties of the Pressure Field Radiated by a Turbulent Boundary Layer," Phys. Fluids, Vol. 7, No. 8, 1964, pp. 1191-1197.

## NOTATION

| | |
|---|---|
| f | frequency |
| M | Mach number |
| p | pressure |
| Re | Reynolds number |
| t | time |
| T | temperature |
| U | velocity |
| V' | rms voltage fluctuations |
| x | distance from model cone apex, along model centerline |
| $\Delta x$ | separation distance in x direction |
| y | distance normal to model surface |
| z | lateral distance around model |
| $\alpha$ | disturbance propagation angle |
| $\gamma$ | intermittency |
| $\delta$ | boundary-layer thickness determined from pitot pressure profiles |
| $\lambda$ | turbulence scale, $U/2\pi f$ |

## Subscripts

| | |
|---|---|
| c | convection |
| e | boundary-layer edge |
| $\ell$ | local |
| o | total |
| w | wall |
| $\infty$ | free stream |

**CONE**

$\theta_c = 5°$

SURFACE THIN
FILM GAUGE

61 cm
50.8 cm
40.6 cm
30.5 cm
20.3 cm

**CONE - OGIVE - CYLINDER**

20.3 cm
DIA.

81 cm RADIUS

TANGENT
POINT

$\theta_c = 10°$

64.4 cm

X, cm

0          50          100          150
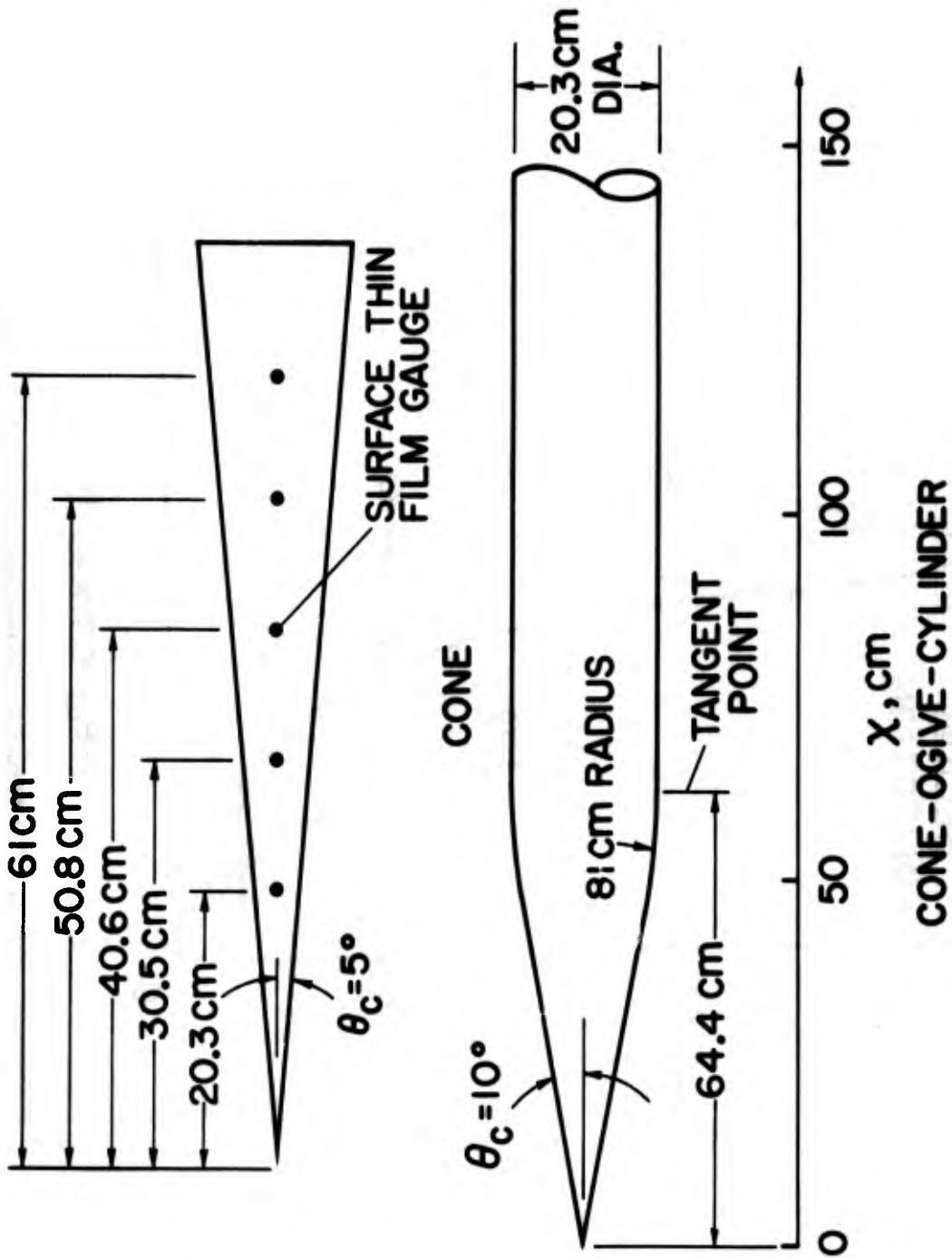
Figure 1.   Test Models
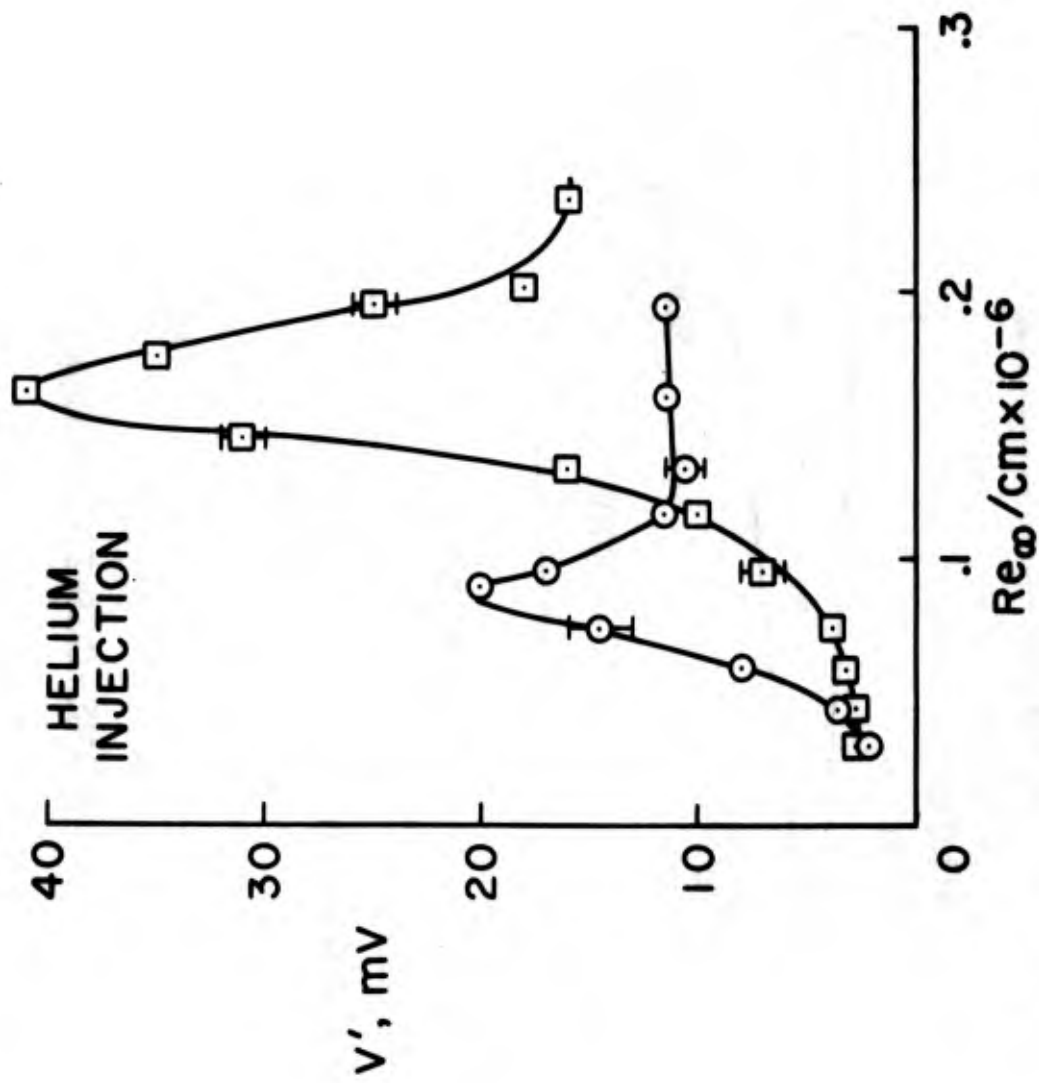
Figure 2. Surface hot film fluctuation measurements through the transition region on a sharp 5° cone
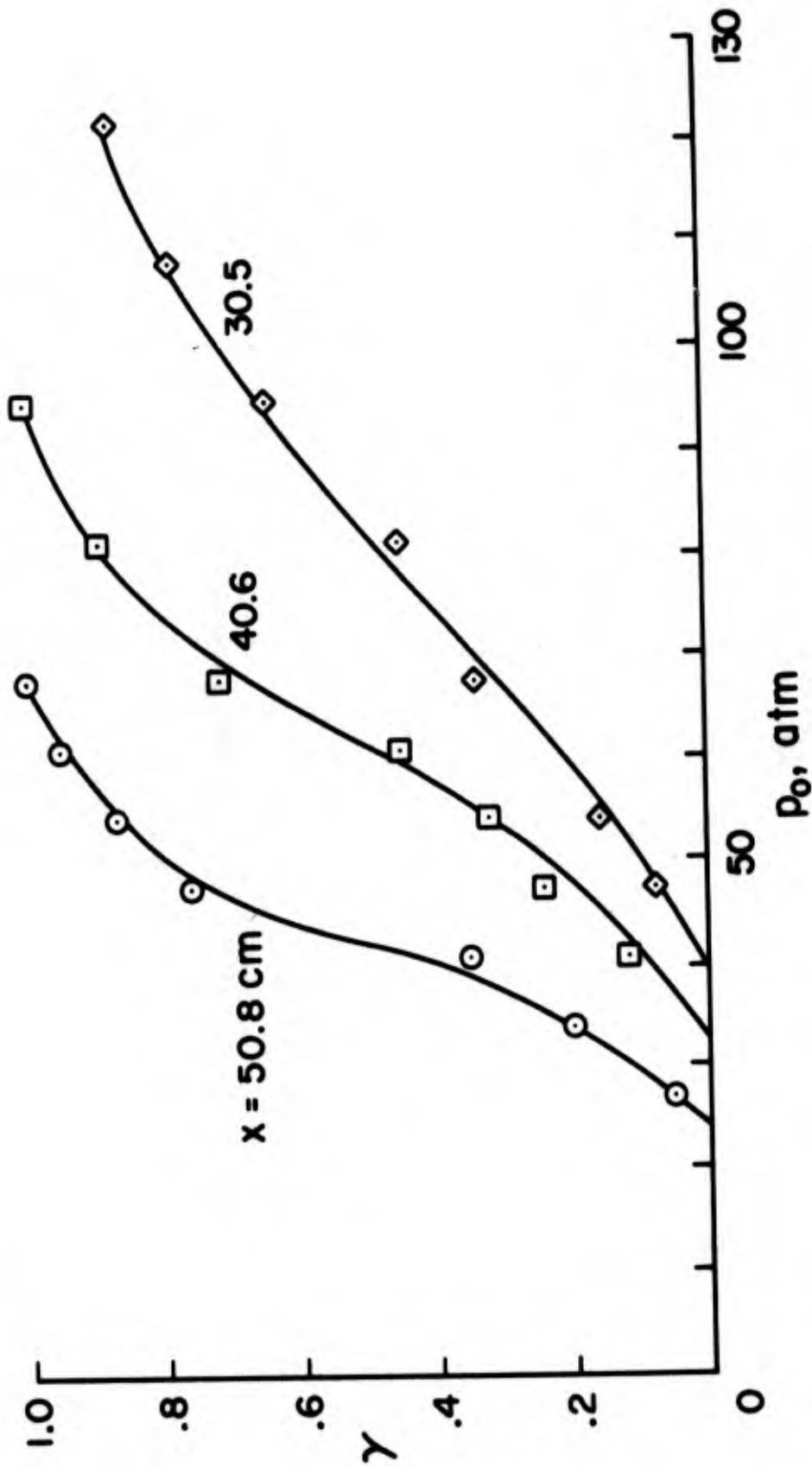
Figure 3. Intermittency distribution through the transitional region on a sharp 5° cone

a. Data
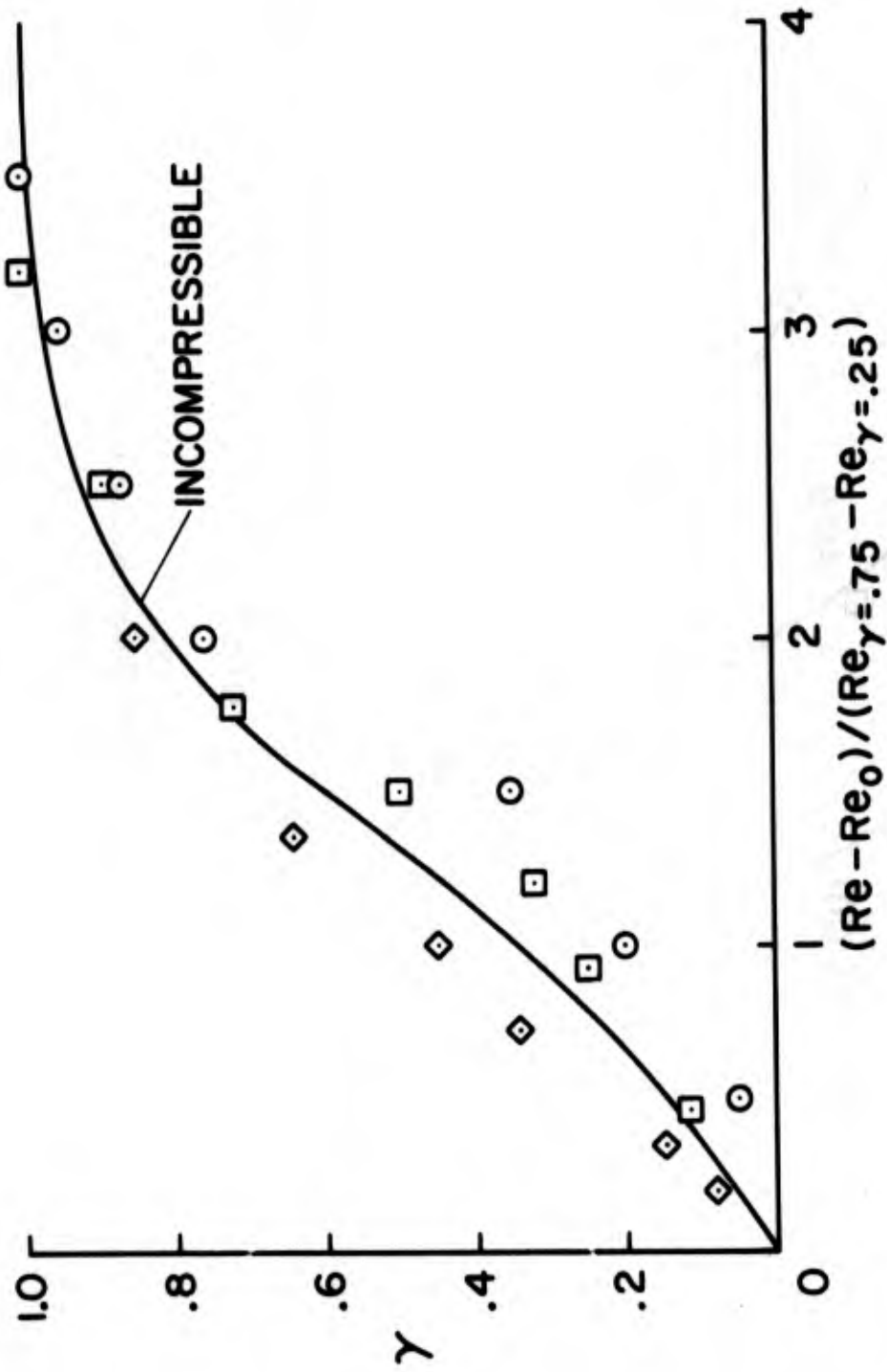
b. Incompressible correlation

Figure 3. Concluded

4-16
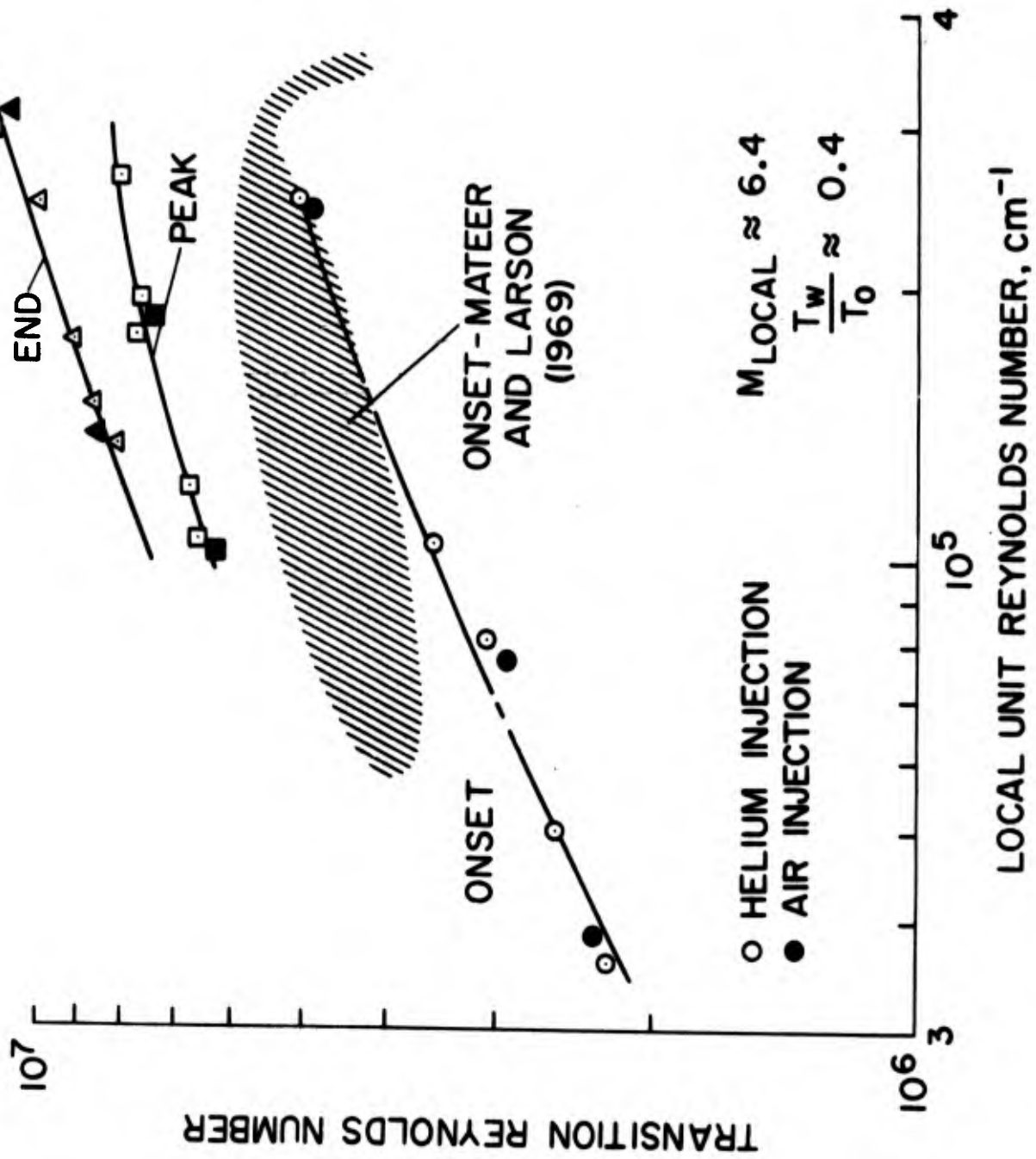
Figure 4. Variation of transition Reynolds number with unit Reynolds number on a sharp 5° cone

4-17
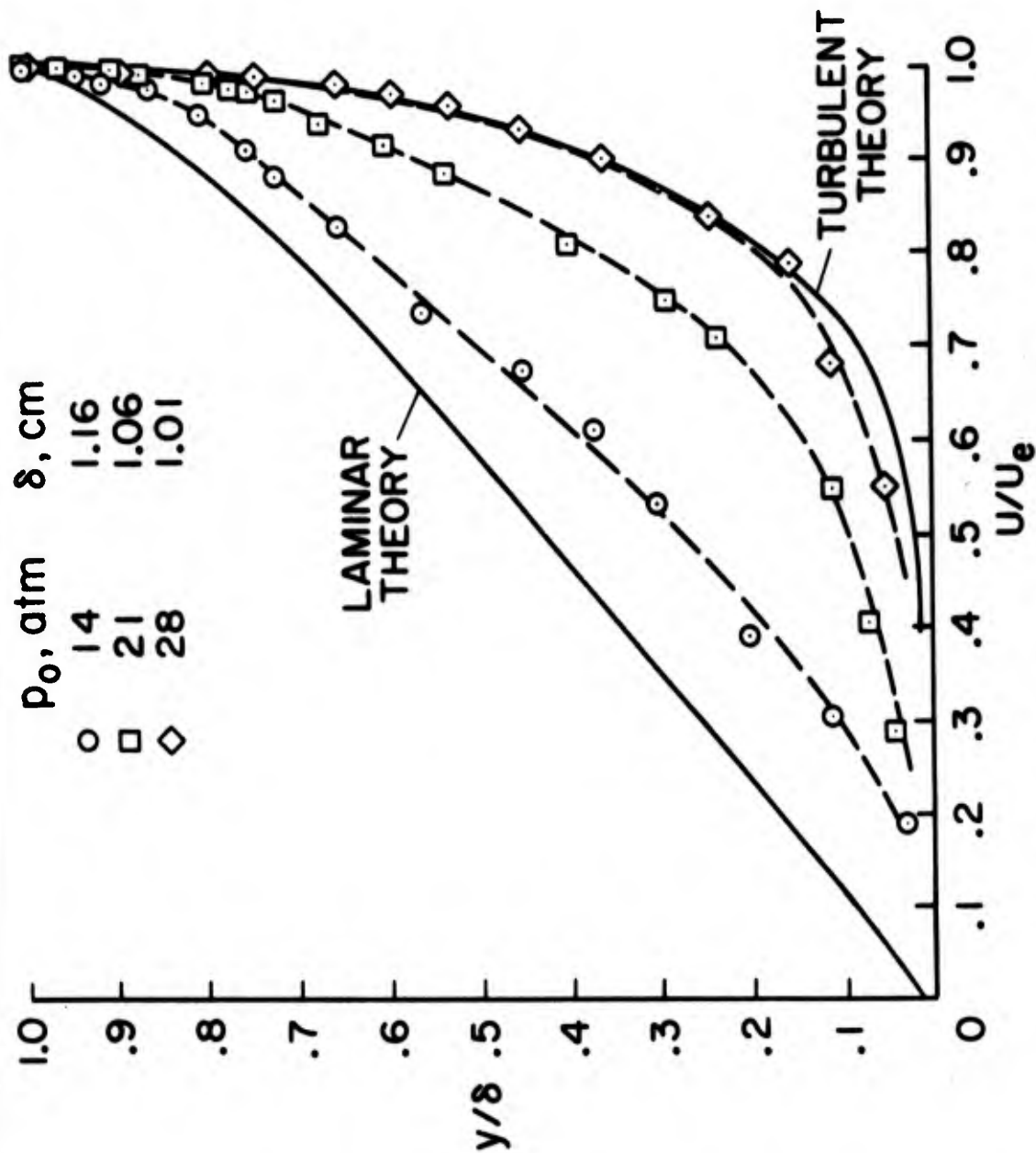
Figure 5. Velocity profiles through the transition region on the cone-ogive-cylinder, x = 115 cm
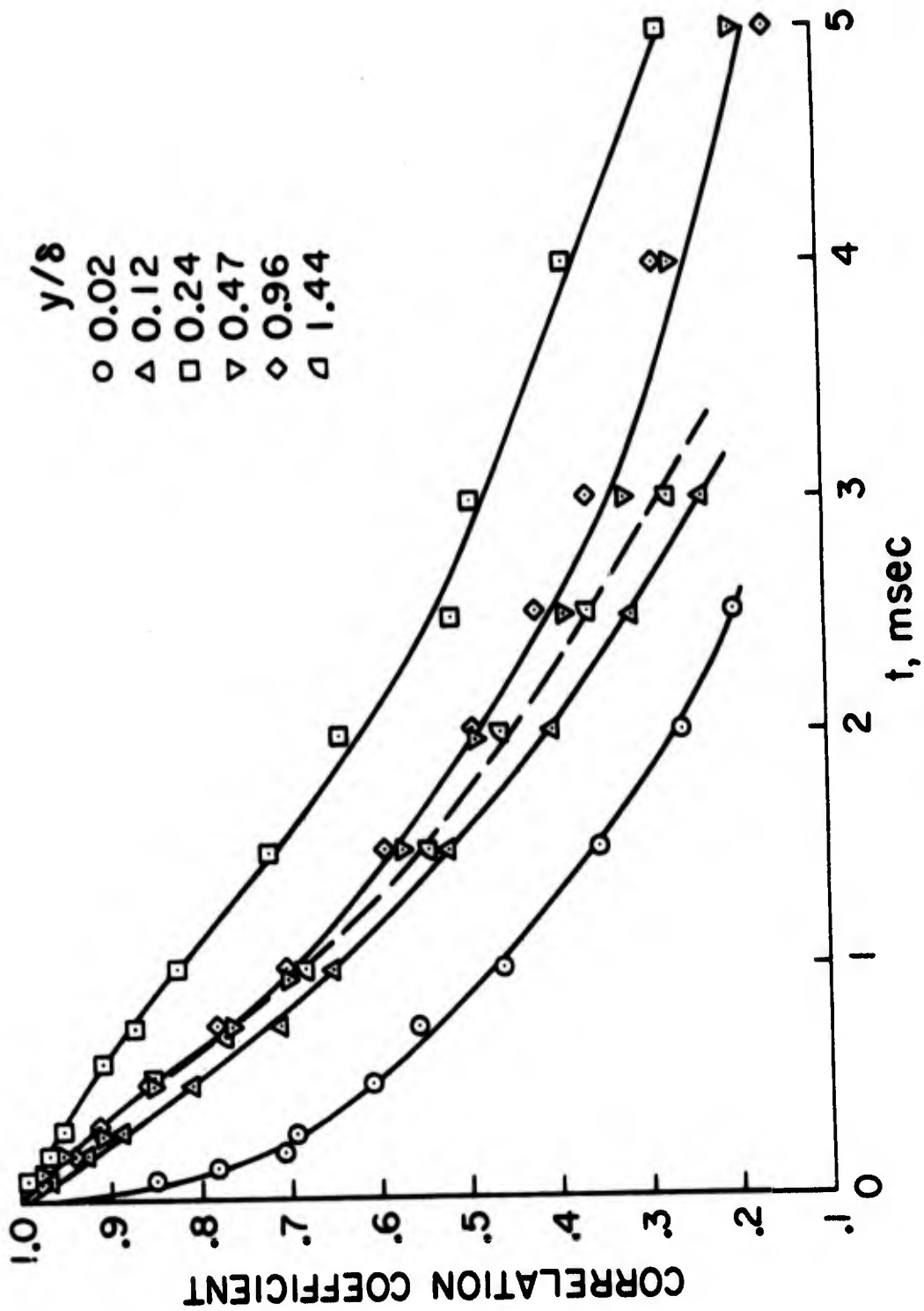
Figure 6. Fluctuating energy distributions through the boundary layer on the cone-ogive-cylinder, $P_0$ = 21 atm, x = 115 cm
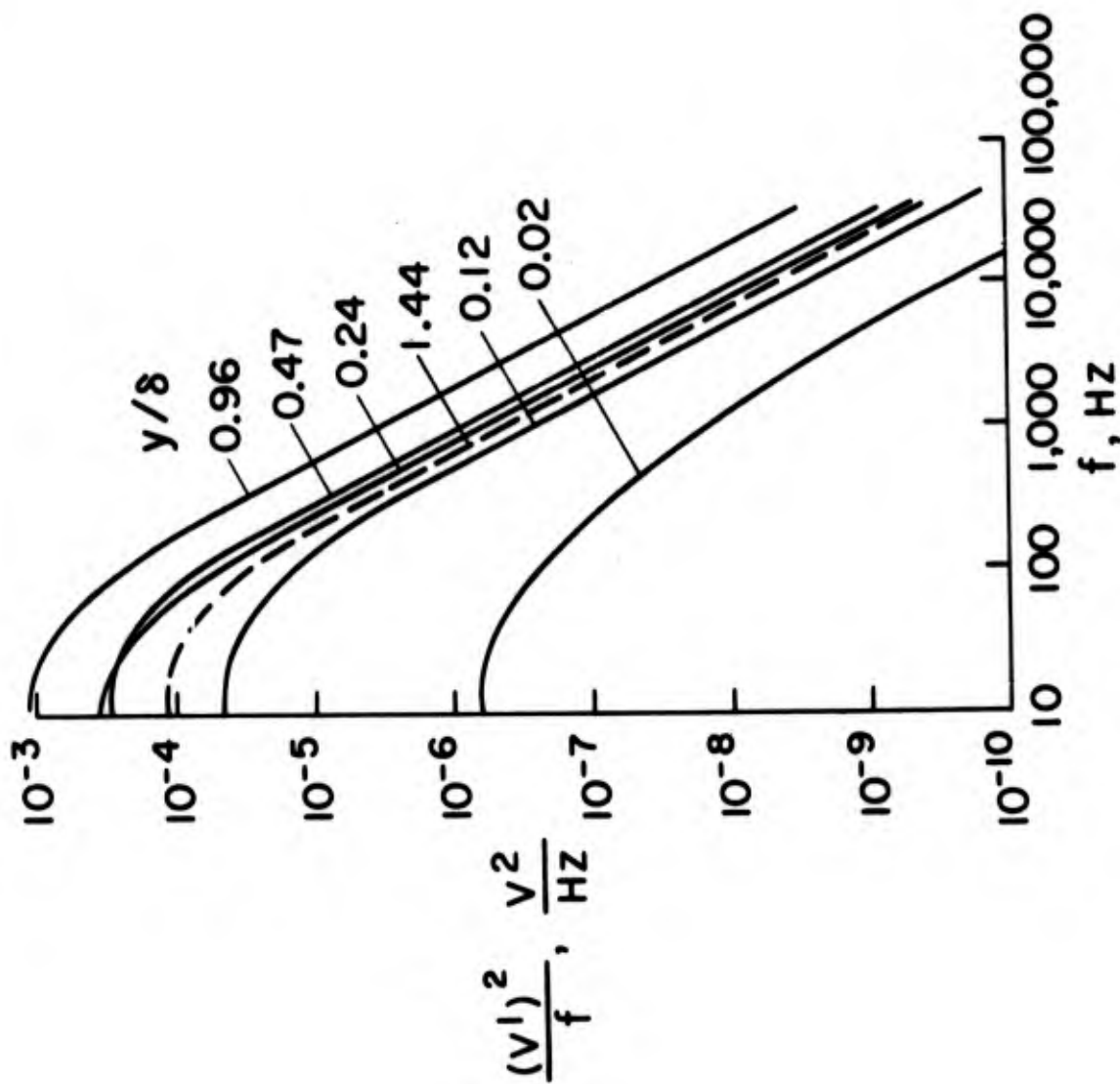
a. Autocorrelation

b. Power-spectral-density

Figure 6. Concluded

4-20
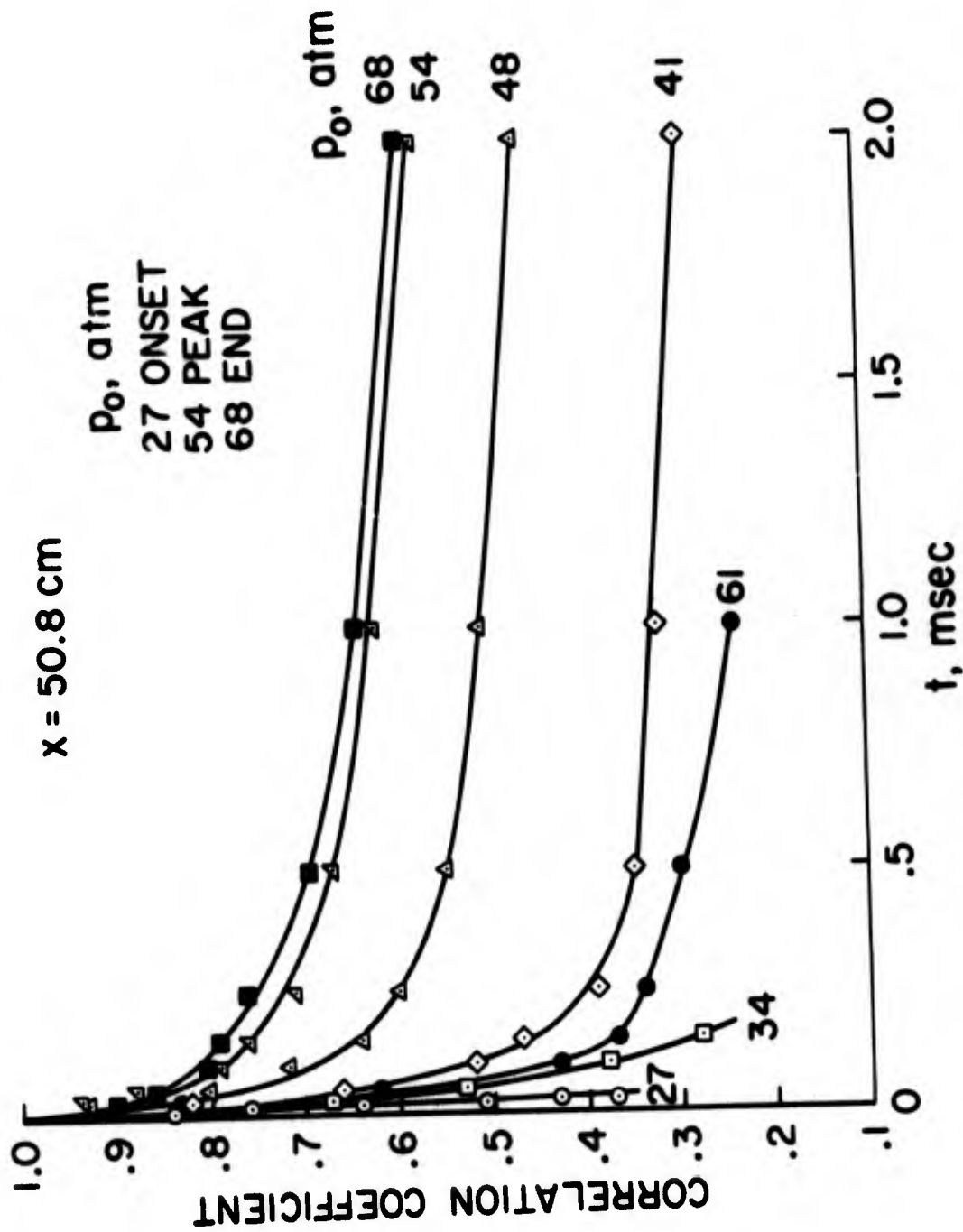
Figure 7. Fluctuating energy distributions through the transition region on the surface of the 5° cone, x = 50.8 cm
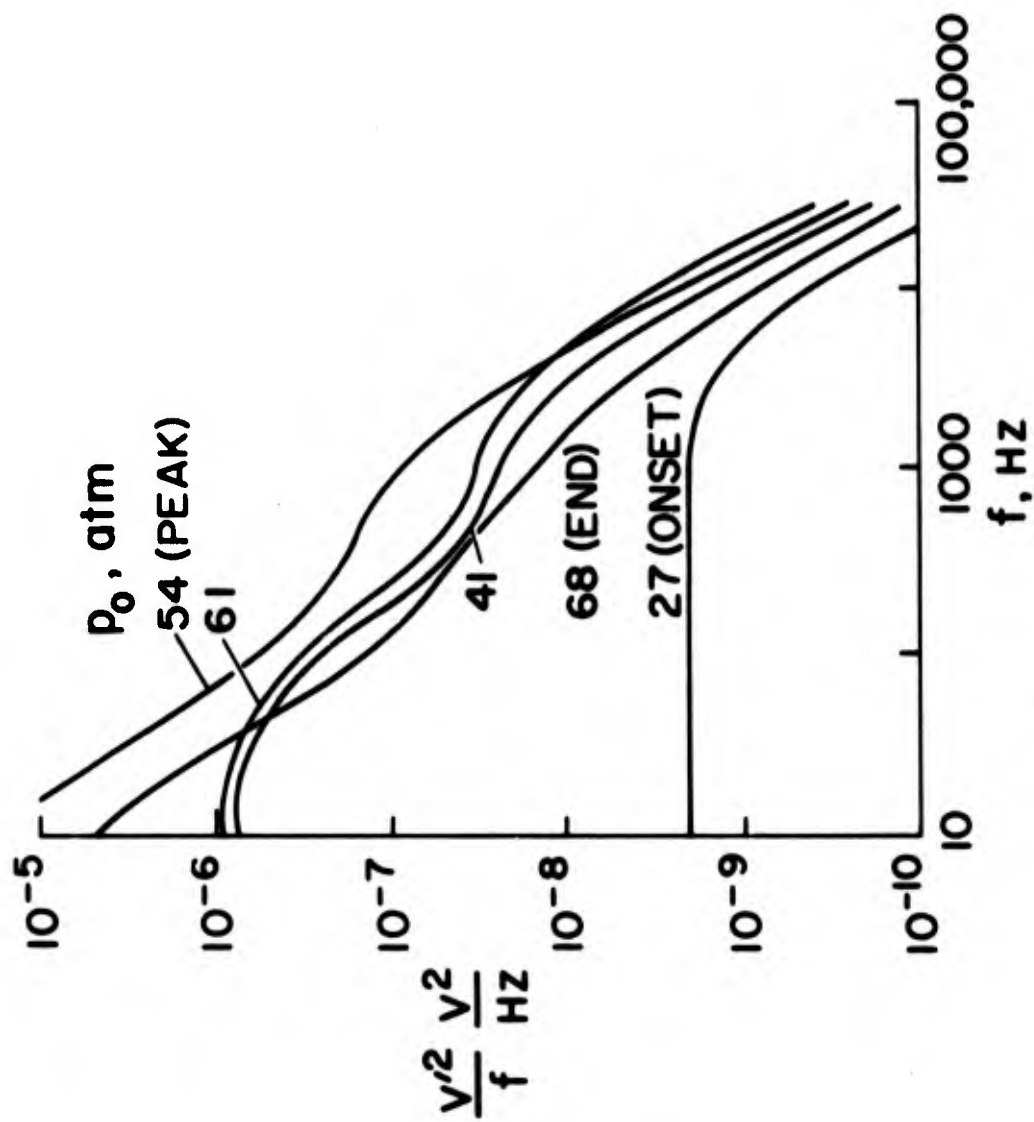
a. Autocorrelation

b. Power-spectral-density

Figure 7. Concluded
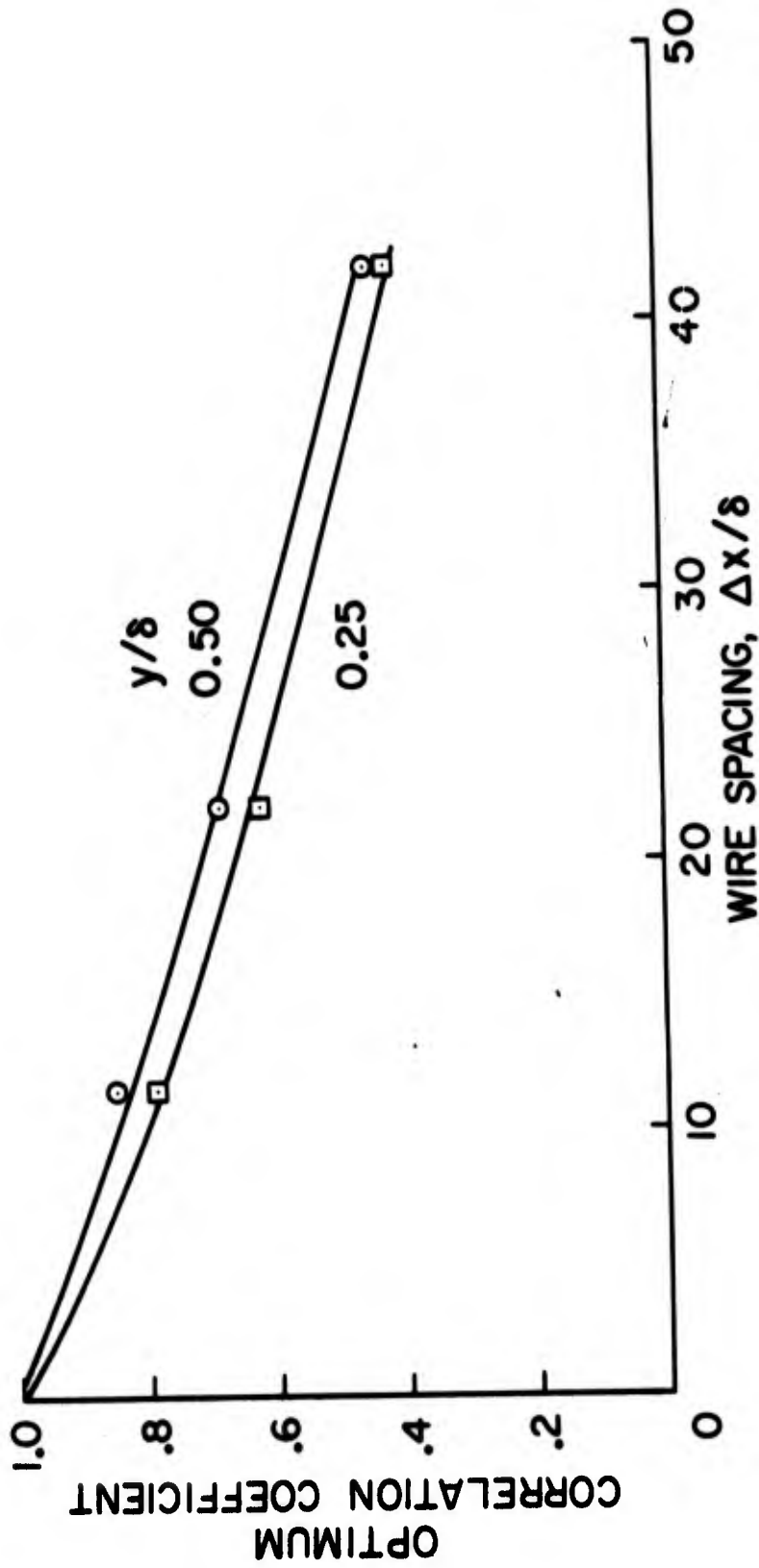
Figure 8. Optimum space-time correlation coefficients–total turbulent field
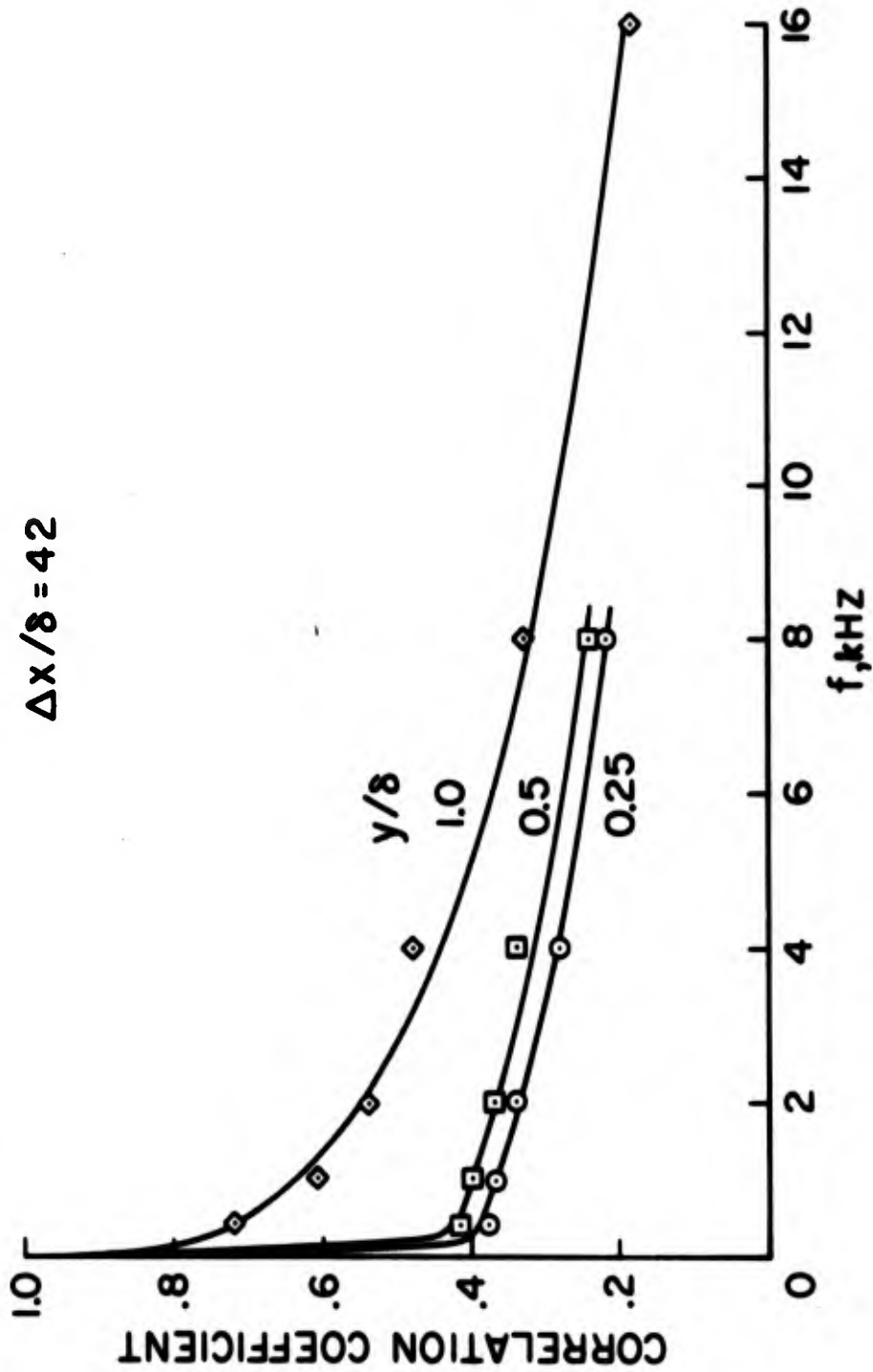
Figure 9. Optimum space-time correlation coefficients-filtered turbulent field

4-24
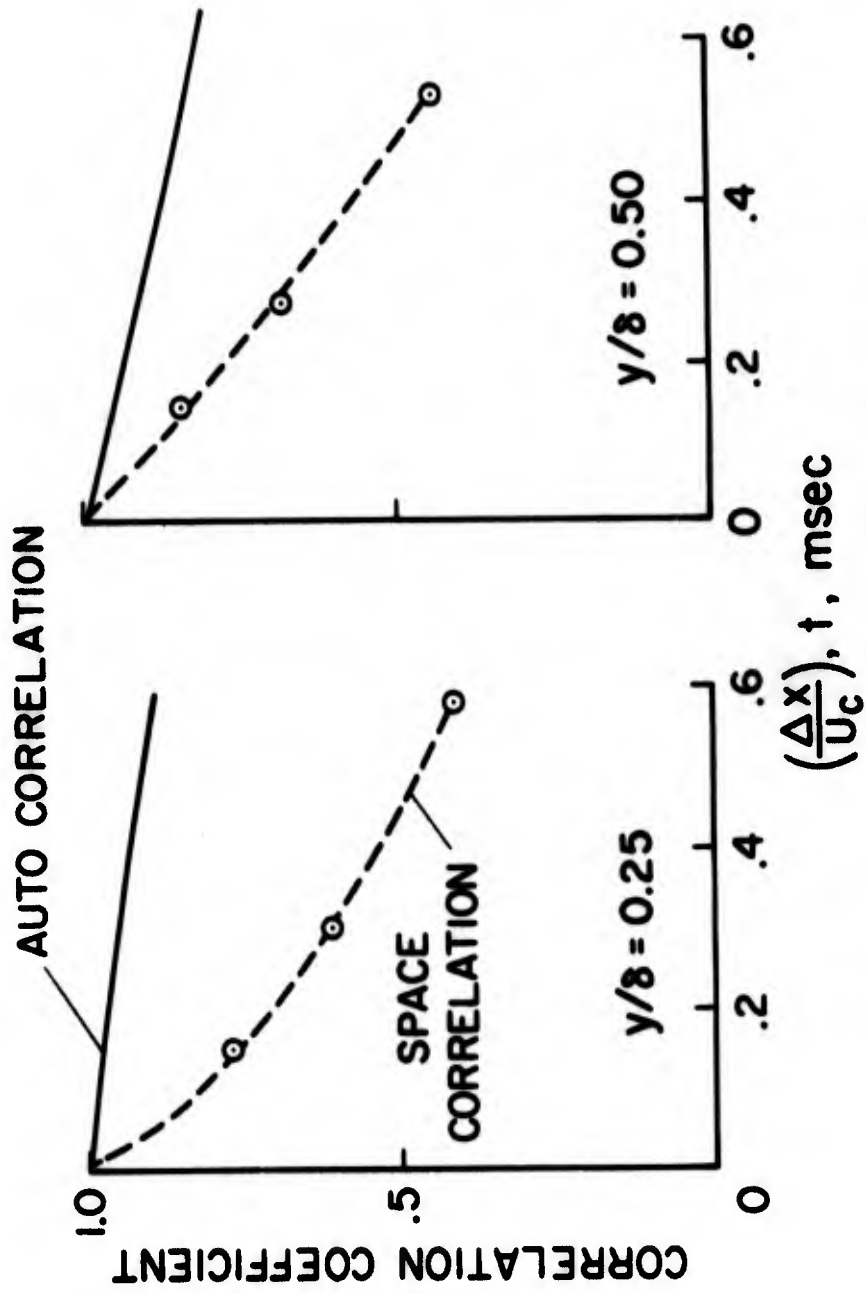
Figure 10. Comparison of autocorrelation and space correlation coefficients
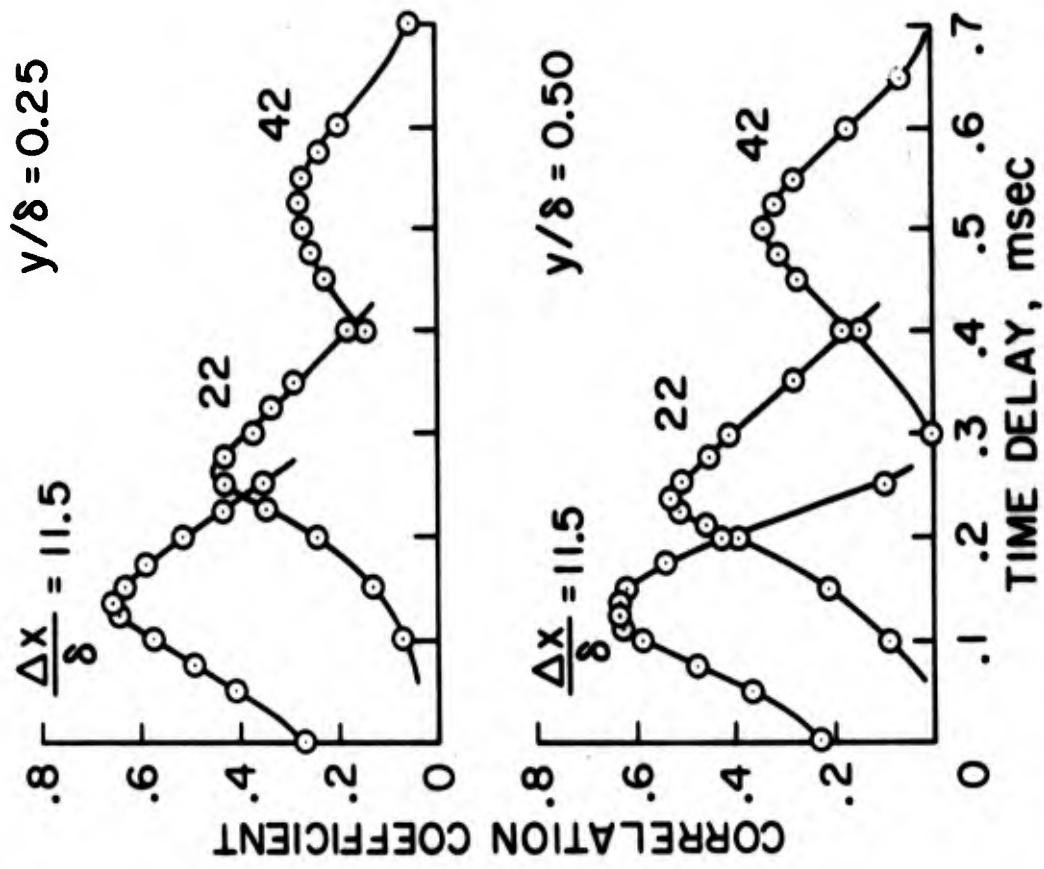
Figure 11. Examples of filtered space-time correlation coefficients – 4 kHz
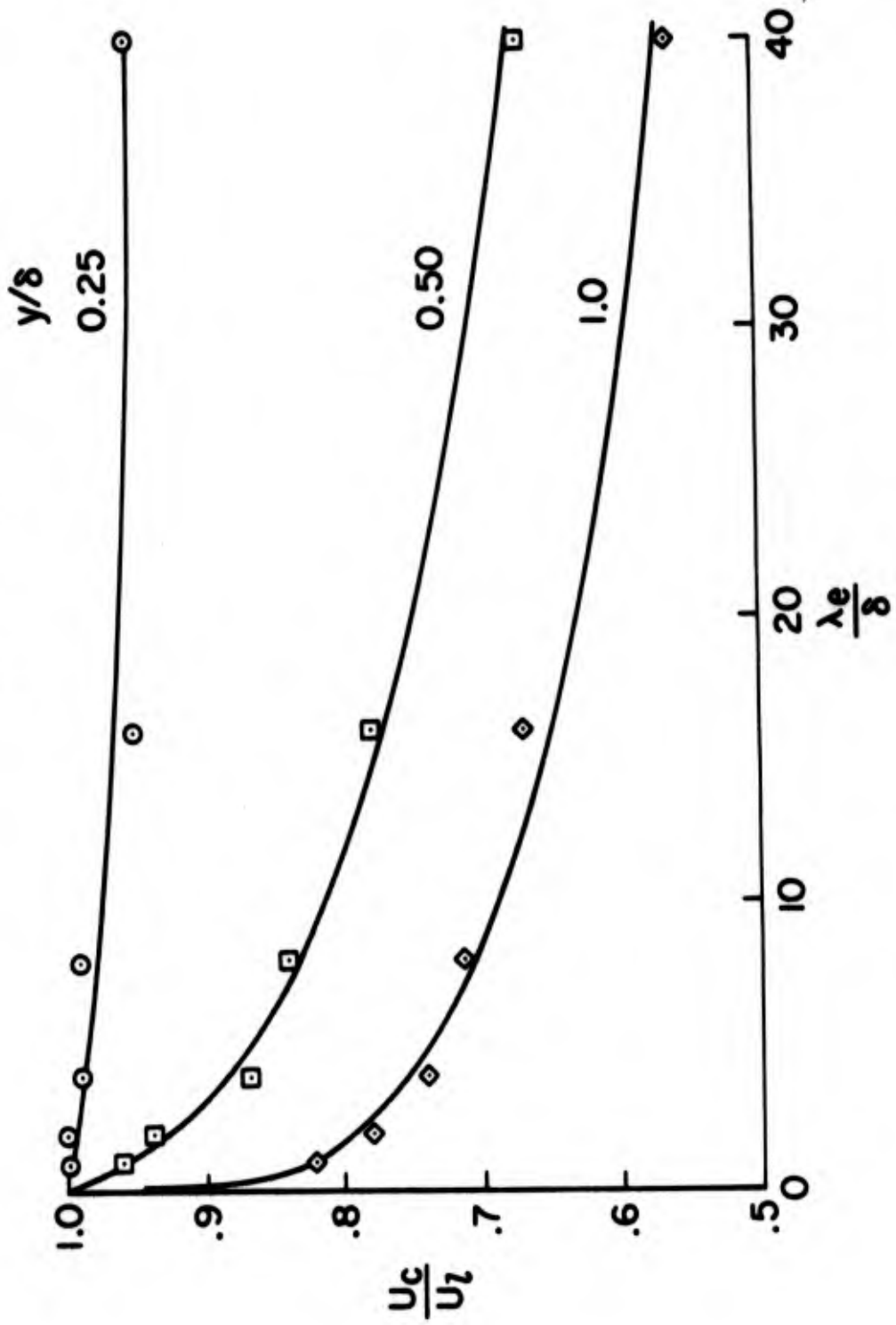
Figure 12. Effect of disturbance scale on convection velocity
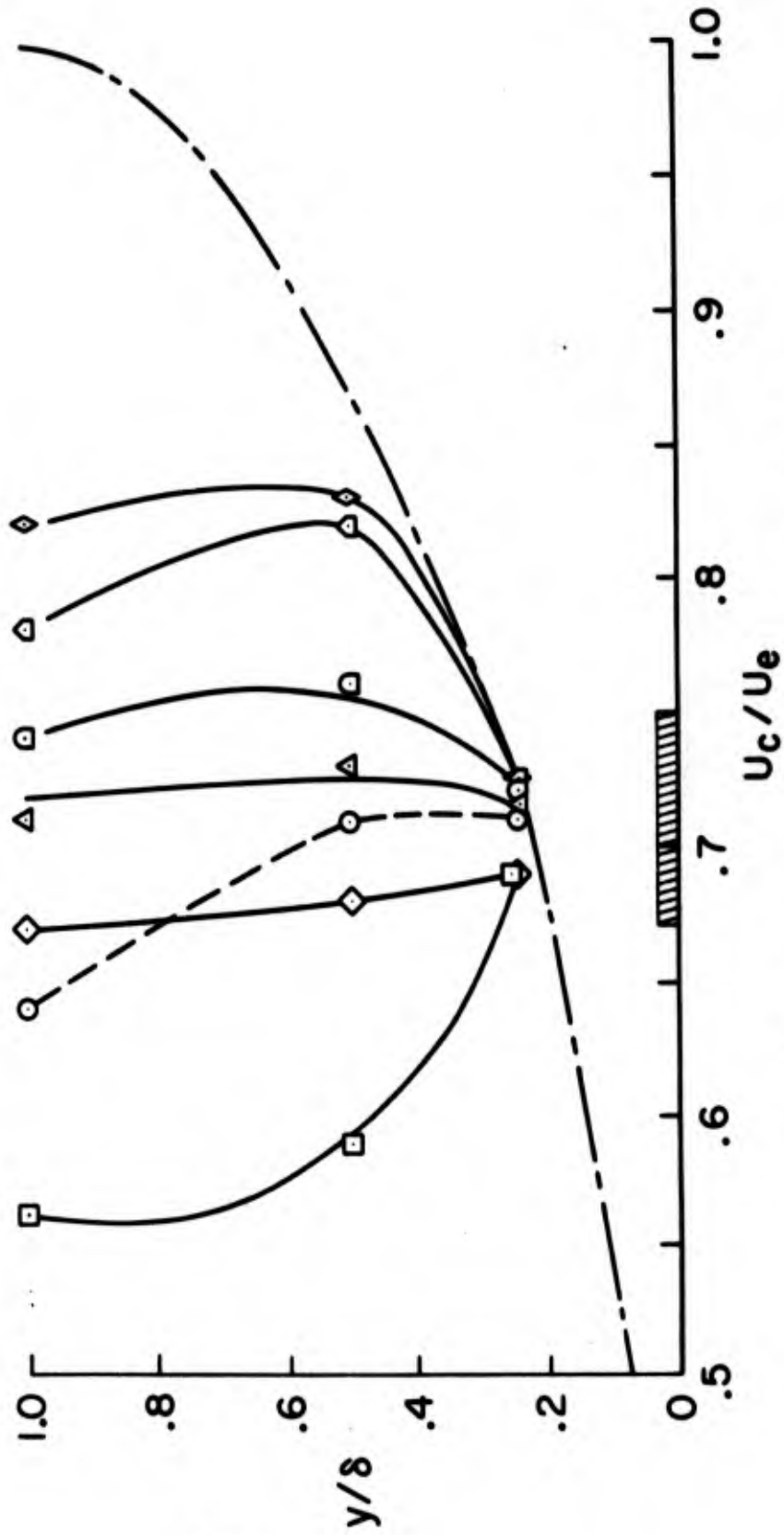
Figure 13. Distribution of disturbance convection velocities across the boundary layer
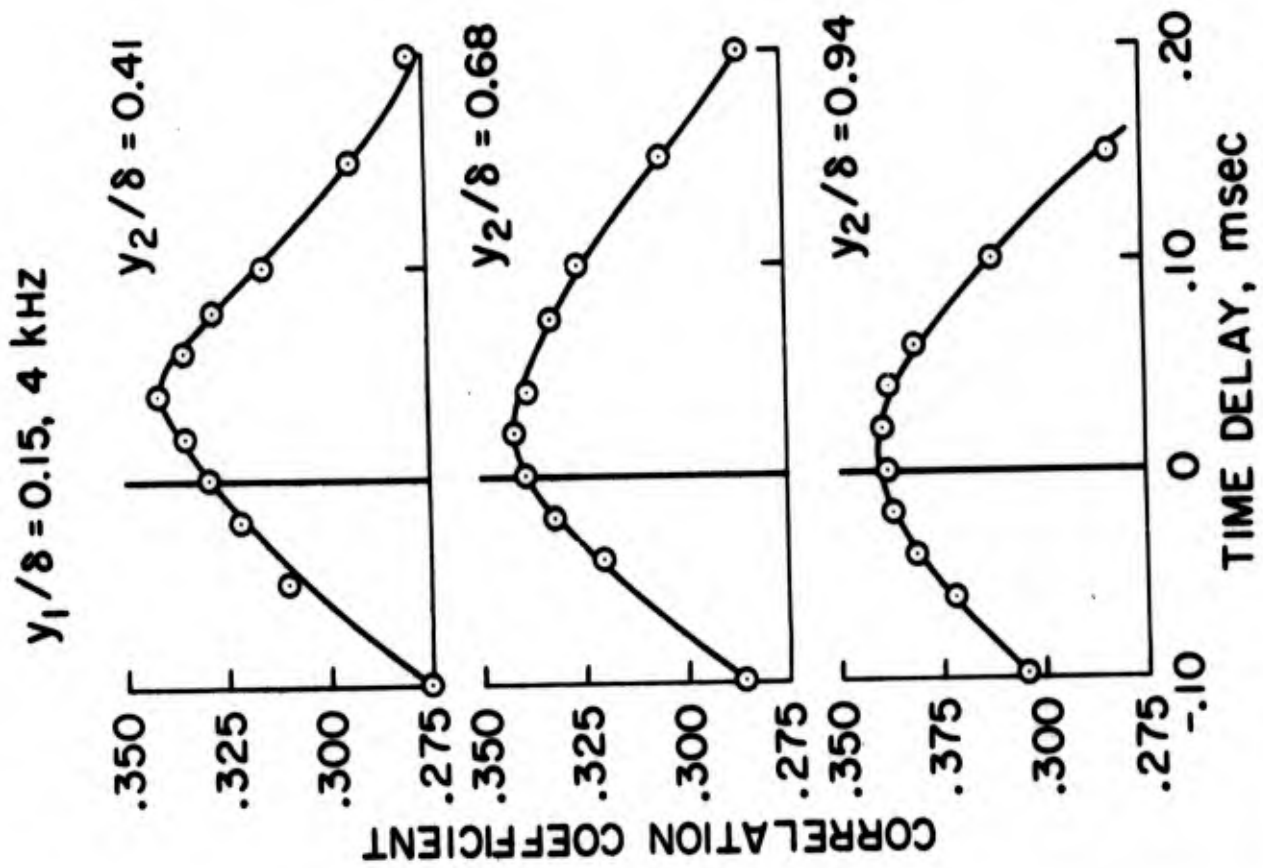
Figure 14. Filtered transverse space-time correlations – 4 kHz
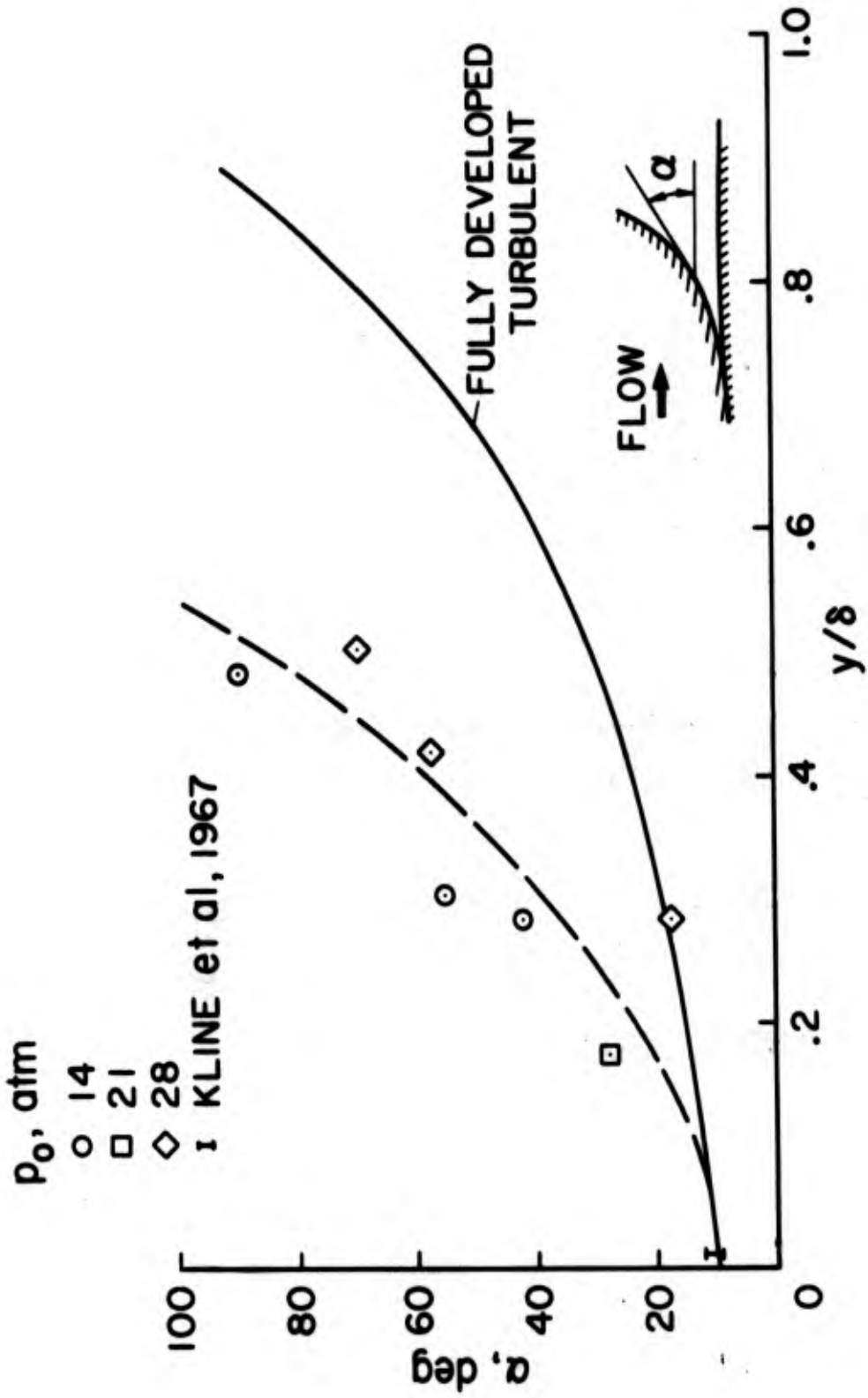
Figure 15.   Disturbance propagation angle
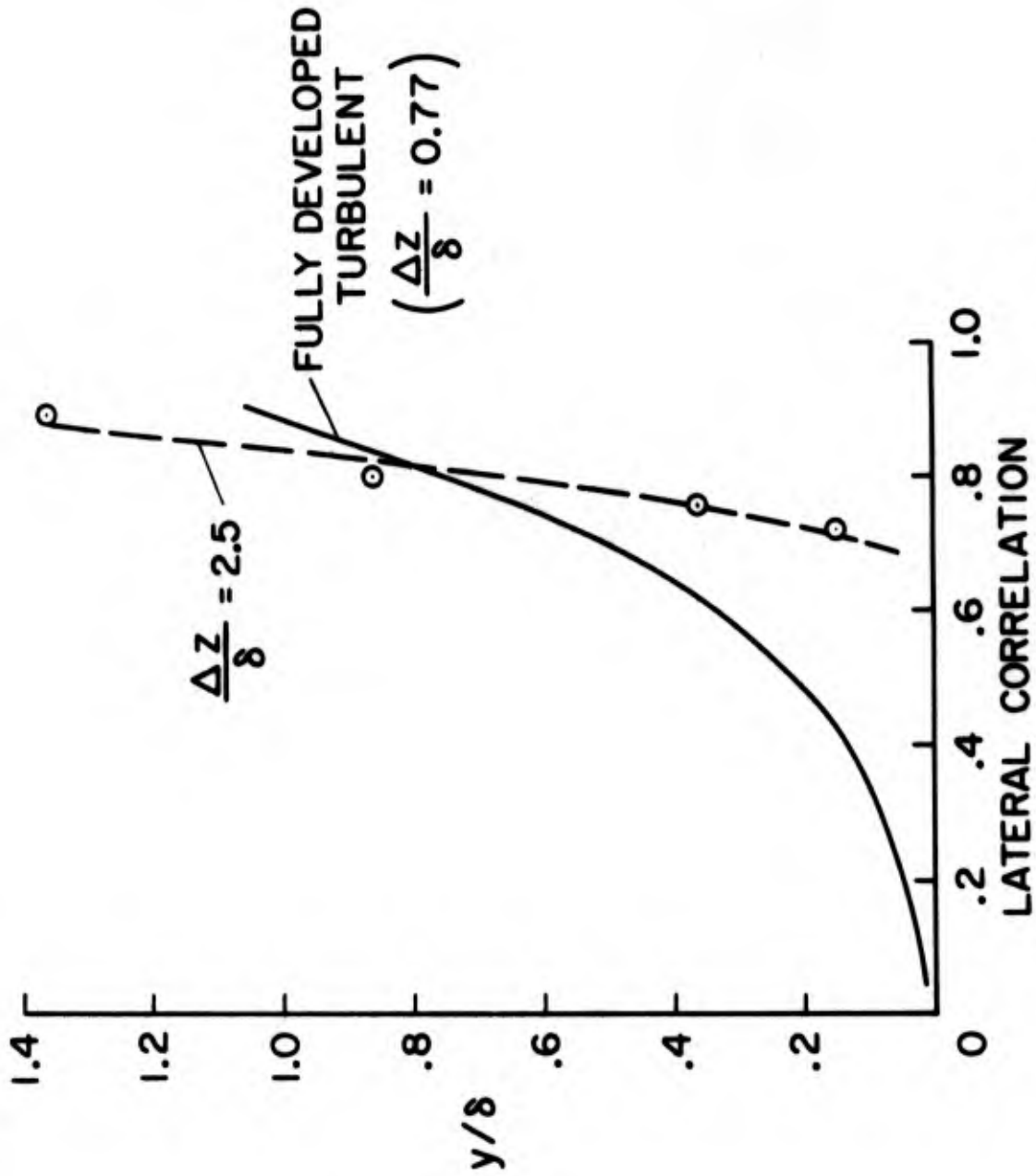
Figure 16.  Variation of lateral correlation across the boundary layer
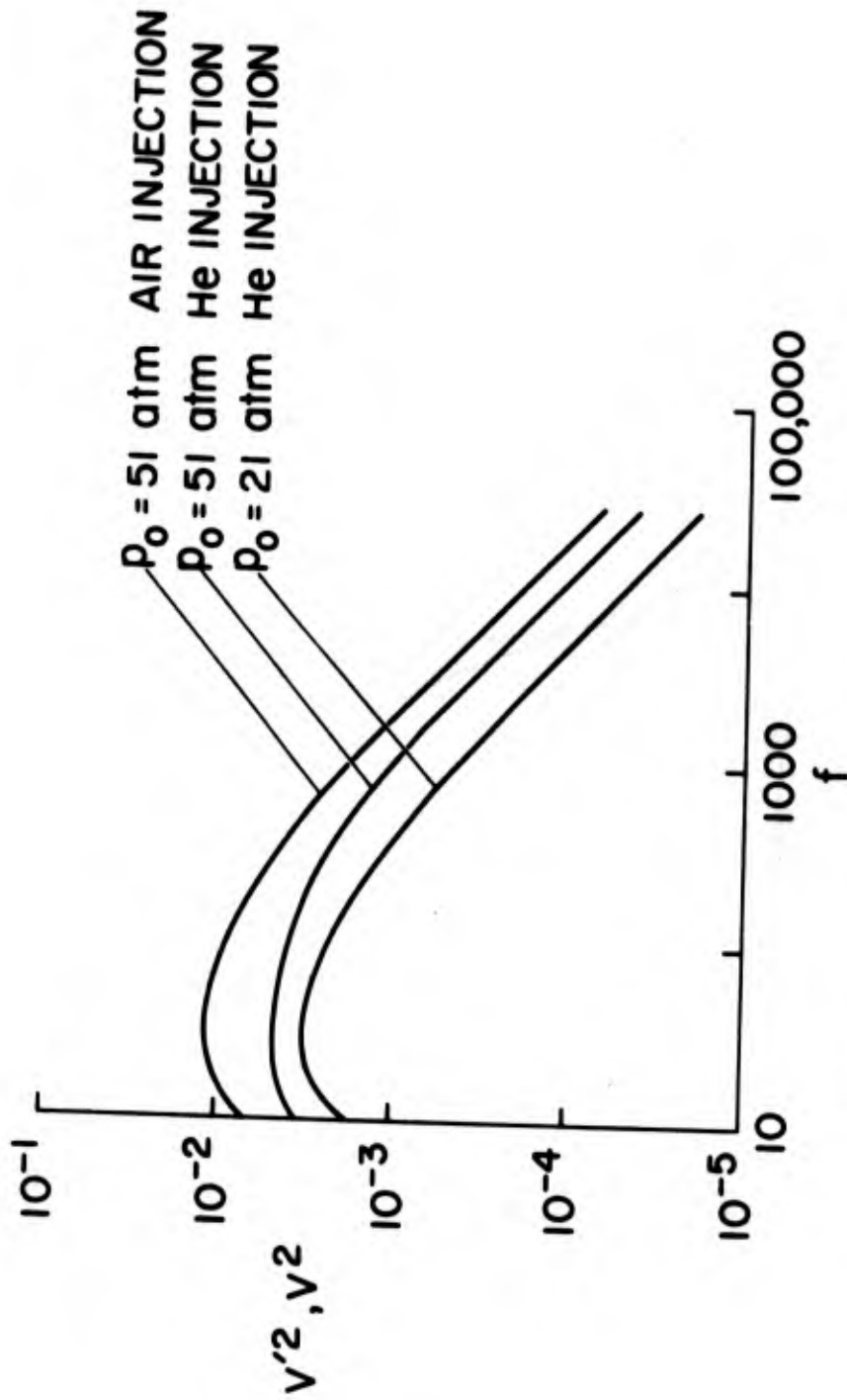
Figure 17. Free stream power-spectra
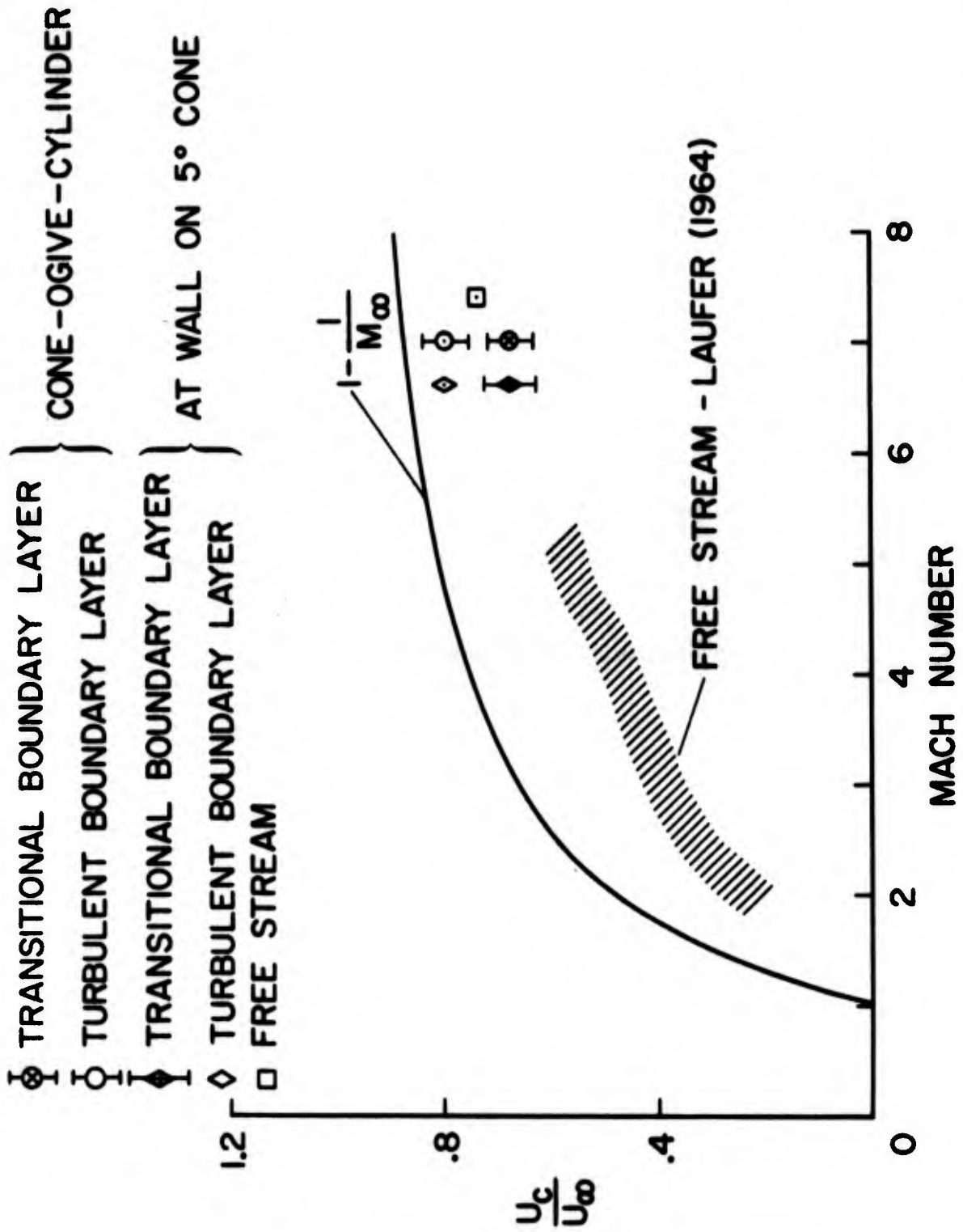
Figure 18. Comparison of disturbance convection velocities

(This page intentionally left blank)

# SECTION 5

## AN ATTEMPT TO CONSTRUCT AN ANALYTICAL MODEL OF THE START OF COMPRESSIBLE TRANSITION*

Coleman duP. Donaldson, Roger D. Sullivan, and John L. Yates
Aeronautical Research Associates of Princeton, Inc.
Princeton, New Jersey

### ABSTRACT

The results of the first step in an attempt to develop a model of compressible transition are reported. The basis of the method goes back to the equations used by Reynolds many years ago to study incompressible viscous instabilities and turbulence. In the work reported here, a simplified linearized version of a set of equations which has been proposed to study complete transitions and turbulent boundary layers in compressible flow are solved by machine computation in order to evaluate the general character of compressible instability that is given by the model. These results are discussed in the light of results obtained from classical stability calculations. Finally, by coupling the instability calculation to the mean flow equation through the Reynolds stress term, the general character of the run-out of instability (as defined by the simplified equations) to the start of transition is investigated. It is shown that the behavior of the critical Reynolds number for instability may be no indication of the behavior of the transition Reynolds number. The paper concludes with recommendations for further numerical studies of compressible transition.

# LIST OF SYMBOLS

| | |
|---|---|
| $a,b$ | dimensionless parameters in model equations |
| $c_f$ | skin friction coefficient |
| $c_p$ | specific heat at constant pressure |
| $c_v$ | specific heat at constant volume |
| $\dfrac{D}{Ds}$ | $\bar{u}^j(\;)_{,j}$ |
| $g_{ij}$ | metric tensor |
| $H$ | see Appendix I |
| $I\tilde{K}$ | see Equation (29) |
| $k$ | thermal conductivity |
| $k_s$ | $\dfrac{\partial \bar{k}}{\partial T}$ |
| $\tilde{k}_1,\tilde{k}_2,\tilde{k}_3$ | $\overline{u_1'^2}$, $\overline{u_2'^2}$, $\overline{u_3'^2}$ , respectively |
| $K$ | $\overline{u_i' u^{1'}}/u_e^2$ |
| $\tilde{K}$ | $\overline{u_i' u^{1'}}$ |
| $\tilde{K}_{max}$ | peak value of $\tilde{K}$ in the boundary layer (see Equation (28) |
| $K_{max}$, IK | dimensionless form of $\tilde{K}_{max}$ and $I\tilde{K}$ (see Equations (30) and (31)) |
| $M_e$ | free stream Mach number |
| $p$ | pressure |
| $\bar{q}$ | average of any quantity $q$ |
| $q'$ | fluctuation of any quantity $q$ |
| $R_z$ | Reynolds number based on free stream velocity and viscosity and distance $z$ where $z = \delta$, $\delta^*$, or $x$ |
| $T$ | temperature |
| $T_w/T_e^o$ | ratio of wall temperature to free stream stagnation temperature |
| $u,v,w$ | velocity components in Cartesian reference frame |
| $u^j$ | j'th covariant component of velocity vector |
| $x,y,z$ | Cartesian coordinate system |

| | |
|---|---|
| $\alpha_1$ | decay constant (see Equation (32)) |
| $\delta$ | boundary layer thickness where $u/u_e = 0.99$ |
| $\delta*$ | displacement thickness |
| $\delta^i_j$ | Kronecker delta symbol |
| $\epsilon_{st}$ | $\bar{u}_{s,t} + \bar{u}_{t,s}$ |
| $\lambda$ | microscale of turbulence |
| $\Lambda$ | macroscale of turbulence |
| $\mu_s$ | $\partial\bar{u}/\partial T$ |
| $\mu, \lambda$ | first and second viscosity coefficients |
| $\rho$ | mass density |
| $\tilde{\sigma}$ | $\overline{u'v'}$ |
| $\tau_{ij}$ | stress tensor (see Equation (4)) |
| $\phi$ | dissipation function (see Appendix I) |

Subscripts

| | |
|---|---|
| e | free stream condition |
| w | wall condition |

# SECTION I

## INTRODUCTION

For many years now, it has been customary to compare the results of boundary layer transition measurements with results obtained from the linearized boundary layer stability theory. While there is no doubt that recent advances in boundary layer stability calculation have added greatly to our understanding of certain aspects of the transition problem, the engineer faced with the design of a new aerospace vehicle has no general tool with which to study his particular case of transition. There are two difficulties. First, there has been no general analytical method which the designer can use to go beyond an evaluation of local boundary layer instability towards actual transition in real environments. Second, the environment in which a given transition is observed has such a profound effect upon the actual Reynolds number at which transition takes place that the scatter in experimentally determined transition Reynolds numbers obscures the effects of more familiar parameters such as local Mach number, wall temperature ratio, and pressure gradient. The general status of the problem has been carefully reviewed by Morkovin (Ref. 1) who has pointed out in detail the many unresolved problems concerning the effect of environment on transition.

In view of this state of affairs, it occurred to the first author of the present paper that an analytical model of transition that would permit certain numerical experiments to be performed would be useful. The effect of the various parameters that are known to affect transition (for example, Mach number, wall temperature ratio, pressure gradient, and external turbulence level) could then be studied systematically. A first attempt at such a model for incompressible flow was published a few years ago (Ref. 2). Since that time, further thought has been given to the modeling of transition with particular emphasis on the case of compressible flow. For this case, results have been obtained with a model which is valid only for the onset of transition. The results of these numerical studies are presented in this paper.

Before going on to present these results, some general observations concerning transition may be in order to help justify the radical departure from traditional studies of boundary layer stability that is taken in this report.

Imagine an experiment in which a measurement has been made of both the local skin friction and the maximum value of the velocity fluctuation correlation $\overline{u'u'}$ within a boundary layer at each position along a flat plate. For this particular test, external disturbances impinging on the boundary layer from the test environment are considered to be negligible compared to small disturbances that are

intentionally introduced into the boundary layer at some
station where the Reynolds number is very low and the boundary
layer is stable to these disturbances.  The result of a set
of such measurements would resemble the plots shown in
Figure 1.  As this figure indicates, the disturbances intro-
duced into the boundary layer would initially result in very
small velocity correlations $\overline{u'u'}$ .  These correlations would,
because of the low local Reynolds number, be damped until such
time as the local boundary layer Reynolds number  $\rho u_e \delta/\mu$

became large enough for the boundary layer to be unstable.
This occurs at approximately the position marked  A  on the
figure.  From the onset of instability at the point  A, the
disturbances grow in magnitude until such time as the maximum
value of the Reynolds stress  $-\rho \overline{u'v'}$  in the boundary layer is
equal to about 10 or 15 percent of the local friction  $\tau_w$  .

This point is marked  B  in the figure.  From this point on,
there is a rapid rise in the surface friction which accompanies
a rapid rise in all the velocity correlations.  This rapid rise
eventually stops after the formation of a typical turbulent
boundary layer.  This point is indicated by the letter  C  in
the figure.  Following this point, the skin friction decreases
with increasing length as the turbulent boundary layer becomes
thicker.

For the hypothetical experiment we have considered here,
we make the following observations:

1.  Classical boundary layer stability theory tells us
something about the behavior of the disturbances that were
introduced into the boundary layer in regions upstream of
position  A  and just immediately downstream of  A .  In
order to apply this theory, we must know the local velocity
profiles, and we must assume that the disturbances that are
present are close to the modal shapes that linear theory
specifies.  For a general test, it can be assumed that we
know the velocity profiles.  However, in cases where signi-
ficant disturbances are continually fed into the boundary
layer from the external environment, the distributions of
disturbance velocity in the boundary layer may be far from
those derived from stability theory.

2.  Stability theory tells us very little about the
behavior of boundary layer disturbances in the region
approaching the point  B  where one observes the start of an
increase in skin friction.  In this report, we shall refer to
the region between point  A , the onset of instability, and
point  B , the onset of transition, as the run-out of the
instability or, simply, the run-out region.

3.  Finally, stability theory tells us nothing about
the flow between points  B  and  C , i.e., about the nature
of the flow in a developing turbulent boundary layer.

Probably the most common definition of the point of transition used in experimental studies is the point B . This point is chosen because it is easy to define and, perhaps, of more importance, it is a point downstream of which aerodynamic heating effects on high-speed vehicles can become truly severe. Thus, the designer of aerospace vehicles is most interested in this point. It is, therefore, unfortunate that classical stability theory only provides the designer with information about point A , and under the rather restricted circumstance where disturbances fed continuously into the boundary layer are small compared to disturbances that are introduced at some point upstream of point A .

Let us examine this latter point in somewhat more detail. In applying stability theory, one picks a point on the surface of a body and from this choice determines the local Mach number $M_e$ , local wall temperature ratio $T_w/T_e^0$ , and the local Reynolds number $\rho_e u_e \delta^*/\mu_e$ . This information, together with the local value of the parameter $(\delta/\tau_w)dp/dx$ permits one to calculate a boundary layer profile that is considered typical of this point on the body.[1] This profile is then used in a stability calculation that freezes this profile for all streamwise positions. For this unchanging profile, the analyst seeks to determine the growth or decay in time of a very special set of sinusoidal waves of length $\lambda$ that travel in the boundary layer at velocity c . For these special waves, one finds, in general, that they are damped for all wave lengths below a certain Reynolds number called the minimum critical Reynolds number and, for higher Reynolds numbers, are amplified for a certain band of wave lengths while damped for other wave lengths. The situation is shown in Figure 2 which is a hypothetical stability plot. In this plot, stability limits for the several different modes of disturbance that might exist in the boundary layer in question are exhibited. For the assumed case, we see there are three regions of instability for three different types of disturbance. In the case of two of these disturbances, the regions of instability overlap. Given a stability diagram such as that shown in Figure 2, it is logical to expect that transition might occur at different Reynolds numbers under different environmental conditions, depending upon the relative strength of disturbances present that might excite the various modes. The problem is, however, even more complicated than this. There may be strong excitations in a given environment that produce disturbances quite different from those given by the eigenfunctions of the linear stability analysis. In this case, what is the effect on the stability diagram? It is probable

---

[1] If a more accurate solution for the boundary layer is available due to the existence of a sophisticated laminar boundary layer growth program, then this profile would be used in the stability calculation.

that one consequence will be a spreading out of the stability
boundaries depending on how much the eigenfunctions are
altered by the foreign disturbances.   The result may
then look something like that shown in Figure 3.   In this
figure, the original instability regions have been smeared
out so that there is a very large region of unstable behavior
at all but the shortest wave lengths.   This behavior is
probably more akin to the behavior of real boundary layers
in wind tunnels and on the nonideal surfaces of real aero-
space vehicles than is the behavior shown in the idealized
case shown in Figure 2.   We might then ask ourselves
whether or not some method could be found that would enable
one to compute a lower bound on all possible modes of distur-
bance, i.e., some curve such as that shown by the reference
line in Figure 3.   The present study is an attempt to develop
an analytical tool to do just that.   The method goes back to
older notions (due to Reynolds, Ref. 3) of computing the growth
of disturbances.   If a successful method can be developed
along the lines pursued here, it would have the distinct
advantage of being able not only to identify the point on a
body at which there could be an onset of instability, point
A , but in its final form, the points  B  and  C  of Figure 1
as well.   The method we have attempted to develop in this
report is not a linear method, so that it permits the user to
investigate numerically the sensitivity of a given boundary
layer to the magnitude of disturbances that might be
introduced.

The advantages set forth above are of such importance
to the designer of aerospace vehicles that the authors have
taken the view that a concerted effort should be made to
develop a numerical tool which can go beyond the classical
stability techniques and provide the engineer with a method
for treating the problem of transition as distinct from the
problem of boundary layer stability.   The present paper
reports our first attempts to develop such an engineering
tool.

## SECTION II

### BASIC EQUATIONS

We take the following differential equations as the basic equations governing the instability and transition to turbulence that we wish to study.

$$\frac{\partial \rho}{\partial t} + (\rho u^j)_{,j} = 0 \tag{1}$$

$$\rho \frac{\partial u_1}{\partial t} + \rho u^j u_{1,j} = -\frac{\partial p}{\partial x^1} + (\tau^j_1)_{,j} \tag{2}$$

$$\rho C_v \left( \frac{\partial T}{\partial t} + u^j T_{,j} \right) = p u^j_{,j} + g^{1j}(kT_{,1})_{,j} + \tau^j_1 u^1_{,j} \tag{3}$$

In these equations,

$$\tau_{ij} = \mu(u_{1,j} + u_{j,1}) + g_{1j}\lambda u^k_{,k} \tag{4}$$

Following the practice introduced many years ago by Reynolds, we now consider the motion under consideration to be made up of a mean and fluctuating part in such a way that any physical quantity $q$ can be written as $q = \bar{q} + q'$ where $\bar{q}$ is the average value of $q$ and $q'$ is the instantaneous fluctuation whose average is zero. We may then write equations for both the mean and fluctuating portions of the motion. These equations for the case of steady state flow are displayed in Appendix I. Here it will suffice to discuss the nature of these equations by means of the example of the continuity equation.

If one puts the expression $\rho = \bar{\rho} + \rho'$ and $u_1 = \bar{u}_1 + u'_1$ into Eq. (1), one obtains

$$\frac{\partial \bar{\rho}}{\partial t} + \frac{\partial \rho'}{\partial t} + (\bar{\rho}\bar{u}^j + \bar{\rho}u^{j'} + \rho'\bar{u}^j + \rho'u^{j'})_{,j} = 0 \tag{5}$$

Taking the time average of this equation yields an equation for the mean density $\bar{\rho}$, namely,

$$\frac{\partial \bar{\rho}}{\partial t} = -(\bar{\rho}\bar{u}^j + \overline{\rho'u^{j'}})_{,j} \tag{6}$$

The equation for the density fluctuation can be found by subtracting Eq. (6) from Eq. (5). One obtains

$$\frac{\partial \rho'}{\partial t} = -(\bar{\rho}u^{j\prime} + \rho'\bar{u}^j + \rho'u^{j\prime} - \overline{\rho'u^{j\prime}})_{,j} \qquad (7)$$

In a like manner, one can obtain equations for $\partial\bar{u}_i/\partial t$ and $\partial u_i'/\partial t$ as well as $\partial\bar{T}/\partial t$ and $\partial T'/\partial t$.

The general character of these equations follows the pattern of Eqs. (6) and (7). In the equation for the mean quantities $\bar{\rho}$, $\bar{u}_i$, and $\bar{T}$, one always finds terms representing the correlations of fluctuating quantities. In the case of the equation for $\rho$, the highest order correlations found are the second order correlations between $\rho'$ and $u_i'$. In the equations for $\bar{u}_i$ and $\bar{T}$, one finds not only the second order correlations $\overline{u_i'u_j'}$, $\overline{\rho'u_i'}$, $\overline{u_i'T'}$, and $\overline{\rho'T'}$ but third-order correlations such as $\overline{\rho'u_i'u_j'}$, $\overline{\rho'T'u_i'}$, etc. (see Appendix I).

Equations for these correlations may be derived. As an example, we may derive an equation for the second-order correlation $\overline{\rho'^2}$ from Eq. (7) if we multiply this equation by $\rho'$ and average. The result is

$$\frac{\partial\overline{\rho'^2}}{\partial t} + \bar{u}^j(\overline{\rho'^2})_{,j} = -2\overline{\rho'^2}\bar{u}^j_{,j}$$

$$- 2\overline{\rho'u^{j\prime}}\,\bar{\rho}_{,j}$$

$$- (\overline{\rho'^2 u^{j\prime}})_{,j}$$

$$- \overline{(2\bar{\rho}\rho' + \rho'^2)u^j_{,j}'} \qquad (8)$$

In a manner similar to that used to derive Eq. (8), one can derive equations for the second-order correlations $\overline{u_i'u_j'}$, $\overline{u_i'T'}$, $\overline{u_i'\rho'}$, etc. For example, the equation for $\overline{\rho'u_i'}$ is derived by multiplying the equation for $\partial\rho'/\partial t$ by $u_i'$, then multiplying the equation for $\partial u_i'/\partial t$ by $\rho'$, and then adding the two results and averaging to obtain the desired equation, namely,

$$\frac{\partial}{\partial t} \, \overline{\rho' u_i'} = \overline{\rho' \frac{\partial u_i'}{\partial t}} + \overline{u_i' \frac{\partial \rho'}{\partial t}} \tag{9}$$

In a like manner,

$$\frac{\partial}{\partial t} \left( \overline{u_i' u_j'} \right) = \overline{u_i' \frac{\partial u_j'}{\partial t}} + \overline{u_j' \frac{\partial u_i'}{\partial t}} \tag{10}$$

The equations for all the simple second-order correlations are displayed in Appendix I.

By a process similar to that just outlined, equations may be derived for third-order correlations. The resulting equations for the case of compressible flow are truly formidable. The system of equations will never be closed by this process for the nonlinear nature of the equations precludes this possibility, even in the case of incompressible fluids. There will always be correlations of order $n+1$ in the equations for the n'th order correlations.

In a program that has been under way at A.R.A.P. for some time, initially under Air Force sponsorship, a fair measure of success has been achieved in computing the development of incompressible turbulent boundary layers by a method called "the method of invariant modeling." In this method, a closure of the set of equations for the mean flow quantities and the second-order velocity correlations is achieved through a modeling of the higher order and pressure correlation terms in these equations using the second-order correlations themselves and two scalar lengths which are related to the integral and miscoscale of the velocity fluctuations. At the present time, the modeling which is being studied to allow one to compute the complete transition and formation of a compressible turbulent boundary layer is given in Appendix II.

The complete set of equations obtained in this way is at present being programmed for solution at A.R.A.P. under NASA sponsorship. A restricted set of equations can be derived from this complete set by which one may perform numerical experiments akin to stability theory that describe the onset of instability as depicted by the model equations. To obtain this restricted set of equations, one eliminates all correlations from the equations in Appendix II for the mean flow variables, and one eliminates all terms of higher than second order in the disturbances from the equations for the second-order correlations. This is done on the basis that the dropped terms are of negligible magnitude at the onset of

instability. When this is done, one obtains the following set of equations for the steady flow of a compressible fluid:

$$(\bar{\rho}\bar{u}^j)_{,j} = 0 \tag{11}$$

$$\bar{\rho}\,\frac{D\bar{u}_1}{Ds} = -\frac{\partial \bar{p}}{\partial x^1} + \bar{\tau}^j_{1,j} \tag{12}$$

$$\bar{\rho}C_p\,\frac{D\bar{T}}{Ds} = \bar{u}^1\,\frac{\partial \bar{p}}{\partial x^1} + \bar{\tau}^j_1\bar{u}^1_{,j} + g^{mn}(k\bar{T}_{,m})_{,n} \tag{13}$$

where $D/Ds = \bar{u}^j(\ )_{,j}$. For a two-dimensional boundary layer flow, this set of equations is reduced, for the usual cartesian coordinate system $(x,y,z)$ $(u,v,w=0)$, to

$$\frac{\partial}{\partial x}(\bar{\rho}\bar{u}) + \frac{\partial}{\partial y}(\bar{\rho}\bar{v}) = 0 \tag{14}$$

$$\bar{\rho}\bar{u}\,\frac{\partial \bar{u}}{\partial x} + \bar{\rho}\bar{v}\,\frac{\partial \bar{u}}{\partial y} = -\frac{\partial \bar{p}}{\partial x} + \frac{\partial}{\partial y}\left(\mu\,\frac{\partial \bar{u}}{\partial y}\right) \tag{15}$$

$$\bar{\rho}C_p\left(\bar{u}\,\frac{\partial \bar{T}}{\partial x} + \bar{v}\,\frac{\partial \bar{T}}{\partial y}\right) = -u\,\frac{\partial p}{\partial x} + \mu\left(\frac{\partial u}{\partial y}\right)^2 + \frac{\partial}{\partial y}\left(k\,\frac{\partial \bar{T}}{\partial y}\right) \tag{16}$$

In this study we shall consider a flat plate flow with Prandtl number one so that Eqs. (15) and (16) possess the particular integral (Crocco's integral)

$$C_p\bar{T} + \frac{\bar{u}^2}{2} = C_1 + C_2\bar{u} \tag{17}$$

Making use of this integral, the mean motion is described by Eqs. (14) and (15) with the additional relationship

$$T = T_w + (T^o_e - T_w)(\bar{u}/u_e) - (T^o_e - T_e)(\bar{u}/u_e)^2 \tag{18}$$

which is obtained from Eq. (17) by applying the boundary conditions on temperature at the wall and at the edge of the boundary layer.

The behavior of small disturbances introduced into the mean flow described by Eqs. (14), (15), and (18) can be studied by means of the small disturbance form of the velocity correlation equation given in Appendix II, namely,

$$\bar{\rho}\bar{u}^j(\overline{u_i'u_k'})_{,j} = - \overline{\rho'u_k'}\,\bar{u}^j\bar{u}_{i,j} - \overline{\rho'u_i'}\,\bar{u}^j\bar{u}_{k,j}$$

$$- \bar{\rho}\,\overline{u_k'u_j'}\,\bar{u}_{i,j} - \bar{\rho}\,\overline{u_i'u_j'}\,\bar{u}_{k,j} - \overline{u_i'u_k'}(\bar{\rho}\bar{u}^j)_{,j}$$

$$- \left(\bar{\rho}b\Lambda^2\sqrt{\epsilon_{st}\epsilon^{st}}\,(\overline{u_i'u^{\ell'}})_{,\ell}\right)_{,k}$$

$$- \left(\bar{\rho}b\Lambda^2\sqrt{\epsilon_{st}\epsilon^{st}}\,(\overline{u_k'u^{\ell'}})_{,\ell}\right)_{,i}$$

$$- a\sqrt{\epsilon_{st}\epsilon^{st}}\left(\overline{u_i'u_k'} - g_{ik}\frac{K}{3}\right) + \bar{\mu}\left[g^{j\ell}(\overline{u_i'u_k'})_{,j\ell} - \frac{\overline{2u_i'u_k'}}{\lambda^2}\right]$$

$$- \frac{\mu s\bar{T}}{\bar{\rho}}\,\overline{\rho'u_k'}\left[g^{j\ell}(\bar{u}_{i,\ell} + \bar{u}_{\ell,i}) - \frac{2}{3}\delta_i^j\bar{u}^\ell_{,\ell}\right]_{,j}$$

$$- \frac{\mu s\bar{T}}{\bar{\rho}}\,\overline{\rho'u_i'}\left[g^{j\ell}(\bar{u}_{k,\ell} + \bar{u}_{\ell,k}) - \frac{2}{3}\delta_k^j\bar{u}^\ell_{,\ell}\right]_{,j}$$

$$+ \bar{\mu}_{,j}\left[g^{jm}(\overline{u_i'u_k'})_{,m} + (\overline{u^{j'}u_k'})_{,i} + (\overline{u^{j'}u_i'})_{,k}\right.$$

$$\left. + g^{jm}\left(\overline{u_i'u_k'} - g_{ik}\frac{K}{3}\right)_{,m}\right] \tag{19}$$

where $\quad \epsilon_{st} = \bar{u}_{s,t} + \bar{u}_{t,s}$

and $\quad K = \overline{u_i'u^{i'}}$

Some time before the start of the present study contract, a program was largely completed which would permit the solution of a simplified version of this equation on A.R.A.P.'s computer. It was felt that this simplified equation contained most of the elements of the compressible instability problem contained in the more complete equation and could be used to successfully study the techniques necessary to obtain accurate solutions of Eq. (19) as well as the general nature of compressible instability by the modeling technique. This simplified equation has been used in this preliminary study. It is obtained from Eq. (19) by setting $\Lambda = \lambda$ and by terms containing the $\overline{\rho' u_i'}$ and $\overline{\rho' u_k'}$ correlations. Some justification can be given for the neglect of the first terms containing $\overline{\rho' u_i'}$ and $\overline{\rho' u_k'}$ in the right-hand side of Eq. (19) in that these terms actually vanish for parallel mean flow and they are not contained in the usual stability analysis. The other terms containing $\overline{\rho' u_i'}$ and $\overline{\rho' u_k'}$ represent the effects of fluctuating viscosity and have been neglected primarily for reasons of economy. If the correlations $\overline{\rho' u_i'}$ and $\overline{\rho' u_k'}$ are left in the equations, a very large number of equations must be solved simultaneously in order to complete the stability calculation. This computation was beyond the capability of A.R.A.P.'s computational facility. In spite of these simplifications, it is felt that the basic problems of computation and general nature of transitions using the modeling technique can be studied with the simplified equation. This equation is displayed below.

$$
\bar{\rho}\bar{u}^j(\overline{u_i'u_k'})_{,j} = -\overline{\bar{\rho}u_k'u^{j'}}\,\bar{u}_{1,j} - \overline{\bar{\rho}u_i'u^{j'}}\,\bar{u}_{k,j} - \left(\bar{\rho}b\Lambda^2\sqrt{\epsilon_{st}\epsilon^{st}}\,(\overline{u_i'u^{\ell'}})_{,\ell}\right)_{,k}
$$

$$
- \left(\bar{\rho}b\Lambda^2\sqrt{\epsilon_{st}\epsilon^{st}}\,(\overline{u_k'u^{\ell'}})_{,\ell}\right)_{,1} - a\sqrt{\epsilon_{st}\epsilon^{st}}\left(\overline{u_i'u_k'} - g_{1k}\frac{K}{3}\right)
$$

$$
+ \bar{\mu}\left[g^{j\ell}(\overline{u_i'u_k'})_{,j\ell} - 2\frac{\overline{u_i'u_k'}}{\lambda^2}\right]
$$

$$
+ \bar{\mu}_{,j}\left[g^{jm}(\overline{u_i'u_k'})_{,m} + (\overline{u_j'u_k'})_{,1} + (\overline{u_j'u_i'})_{,k}\right.
$$

$$
\left. + g^{jm}\left(\overline{u_i'u_k'} - g_{1k}\frac{K}{3}\right)_{,m}\right] \tag{20}
$$

To compute the stability of a boundary layer flow by the present method, we will need equations in the coordinate system $(x,y,z)$ $(u',v',w')$ for the following four quantities: $\overline{u'u'}$, $\overline{v'v'}$, $\overline{w'w'}$, and $\overline{u'v'}$. For the flat plate flow we have considered, the equations obtained from Eq. (20) are as follows:

$$\bar{\rho}\frac{D\tilde{k}_1}{Ds} = 2\bar{\rho}\sigma\frac{\partial\bar{u}}{\partial y} + \frac{\partial\bar{\mu}}{\partial y}\frac{\partial}{\partial y}\left(2\tilde{k}_1 - \frac{\tilde{K}}{3}\right) + a\bar{\rho}\frac{\partial\bar{u}}{\partial y}\left(\frac{\tilde{K}}{3} - \tilde{k}_1\right)$$
$$+ \bar{\mu}\frac{\partial^2\tilde{k}_1}{\partial y^2} - 2\bar{\mu}\frac{\tilde{k}_1}{\lambda^2} \qquad (21)$$

$$\bar{\rho}\frac{D\tilde{k}_2}{Ds} = 2\frac{\partial}{\partial y}\left[b\lambda^2\bar{\rho}\frac{\partial\bar{u}}{\partial y}\frac{\partial\tilde{k}_2}{\partial y}\right] + \frac{\partial\bar{\mu}}{\partial y}\frac{\partial}{\partial y}\left(4\tilde{k}_2 - \frac{\tilde{K}}{3}\right)$$
$$+ a\bar{\rho}\frac{\partial\bar{u}}{\partial y}\left(\frac{\tilde{K}}{3} - \tilde{k}_2\right) + \bar{\mu}\frac{\partial^2\tilde{k}_2}{\partial y^2} - 2\bar{\mu}\frac{\tilde{k}_2}{\lambda^2} \qquad (22)$$

$$\bar{\rho}\frac{D\tilde{k}_3}{Ds} = \frac{\partial\bar{\mu}}{\partial y}\frac{\partial}{\partial y}\left(2\tilde{k}_3 - \frac{\tilde{K}}{3}\right) + a\bar{\rho}\frac{\partial\bar{u}}{\partial y}\left(\frac{\tilde{K}}{3} - \tilde{k}_3\right) + \bar{\mu}\frac{\partial^2\tilde{k}_3}{\partial y^2} - 2\bar{\mu}\frac{\tilde{k}_3}{\lambda^2} \quad (23)$$

$$\bar{\rho}\frac{D\tilde{\sigma}}{Ds} = \bar{\rho}\tilde{k}_2\frac{\partial\bar{u}}{\partial y} + \frac{\partial}{\partial y}\left[b\lambda^2\bar{\rho}\frac{\partial\bar{u}}{\partial y}\frac{\partial\tilde{\sigma}}{\partial y}\right] + \frac{\partial\bar{\mu}}{\partial y}\frac{\partial}{\partial y}(3\tilde{\sigma})$$
$$- a\bar{\rho}\frac{\partial\bar{u}}{\partial y}\tilde{\sigma} + \bar{\mu}\frac{\partial^2\tilde{\sigma}}{\partial y^2} - 2\bar{\mu}\frac{\tilde{\sigma}}{\lambda^2} \quad (24)$$

In this set of equations, $a$ and $b$ are parameters that must be obtained in some way by matching an existing exact computation or by comparison with experiment. The parameter $\lambda$ is essentially the length scale of the disturbances. There is a boundary condition on $\lambda$ that arises from a consideration of the model equations near the surface $y = 0$. At the surface, the model equations (21) through (24) indicate that we must have $\partial\overline{u'_i u'_k}/\partial y = 0$. This, together with the boundary condition $\overline{u'_i u'_k} = 0$ at $y = 0$, leads to the result that $\overline{u'_i u'_k}$ is of the form

$$\overline{u'_i u'_k} = a_2 y^2 + a_3 y^3 + \ldots \tag{25}$$

If this equation is placed in any of Eqs. (21) through (24) we obtain, as the surface is approached

$$0 = 2\mu a_2 - 2\mu a_2 \frac{y^2}{\lambda^2} \tag{26}$$

or

$$\lambda = y \tag{27}$$

In making computations of boundary layer stability by the method being discussed, it has been found that the most unstable cases are those with the largest wave lengths. For this reason we will choose $\lambda = y$ throughout the region of the calculation rather than stopping the growth of $\lambda$ with $y$ when some fixed value of $\lambda$ has been reached. This serves two purposes. First, it should yield a lower limit value of stability Reynolds number for this particular model and, second, it eliminates disturbance wavelength as a parameter in the computations, thereby reducing the number of computations required to obtain critical Reynolds number data in this preliminary study.

# SECTION III

## SELECTION OF MODEL PARAMETERS  a  AND  b

In order to make boundary layer stability calculations using Eqs. (14), (15), and (18) together with Eqs. (21) through (24), the following procedure was originally followed. At some Reynolds number sufficiently below the minimum critical Reynolds number (either assumed, if no information was available, or determined from the calculations after the first few were complete), an arbitrary distribution of small disturbances in $\tilde{k}_1$, $\tilde{k}_2$, and $\tilde{k}_3$ is assumed to exist in an equilibrium laminar boundary layer. The turbulent correlation $-\overline{u'v'} = \tilde{\sigma}$ was initially assumed to be zero. The growth of the mean profile with the coordinate  x  was tracked by the solution of Eqs. (14), (15), and (18). The development of the disturbances in the boundary layer with  x  was computed by means of the simultaneous solution of Eqs. (21) through (24). When this procedure was followed, the following behavior of the disturbances was found. First, there was a period of adjustment in a length  Δx  of the order of 100 boundary layer thicknesses in which the arbitrary disturbances that were introduced adjust themselves to the shapes close to those appropriate for the assumed value of the Mach number and wall temperature ratio as well as trying to achieve a shape appropriate to the local Reynolds number. This latter adjustment was never quite achieved since the local Reynolds number was always changing with  x .[2]

---

[2] For an incompressible boundary layer on a flat plate, the ratio of local Reynolds numbers at two points in the boundary layer may be written

$$\frac{R_{\delta 2}}{R_{\delta 1}} = \sqrt{1 + \frac{25}{R_{\delta 1}}\left(\frac{x_2 - x_1}{\delta_1}\right)}$$

For an adjustment distance of 100 boundary layer thicknesses, the ratio of local Reynolds numbers is

$$\frac{R_{\delta 2}}{R_{\delta 1}} = \sqrt{1 + \frac{2500}{R_{\delta 1}}}$$

in the region near the critical Reynolds number which is approximately 1250. This adjustment distance represents roughly a 73% change in the local Reynolds number since $R_{\delta 2}/R_{\delta 1} = \sqrt{3}$.

Following this initial adjustment, there is usually a region of disturbance decay if the initial Reynolds number was chosen low enough. This decay begins to slacken as the Reynolds number continues to increase until at some Reynolds number the decay ceases and there is an onset of instability. The point at which there is no growth or decay of the disturbance is defined as the critical Reynolds number. Because the equations for the disturbance are linear and are not coupled to the mean flow equations, the behavior just described is independent of the level or intensity of the disturbances. This behavior is shown in Figure 4 in which the nature of the disturbance profiles at several distances downstream of the start of a given calculation is shown. In Figure 5, we show the behavior of two measures of the stability of the boundary layer that are used in what follows for the same calculation shown in Figure 4. These two measures are

(a) the maximum value of the sum of the three energy correlations $\tilde{k}_1$, $\tilde{k}_2$, and $\tilde{k}_3$, namely,

$$\tilde{K}_{max} = \left[\tilde{k}_1(y) + \tilde{k}_2(y) + \tilde{k}_3(y)\right]_{max} \qquad (28)$$

(b) the integral of the energy parameter $\tilde{K}$ throughout the boundary layer, namely,

$$I\tilde{K} = \int_0^\delta (\tilde{k}_1 + \tilde{k}_2 + \tilde{k}_3) \, dy \qquad (29)$$

Figure 5 shows in a very simple way the general behavior of the development of instability as a result of disturbances introduced into a boundary layer. The particular example that is reported in Figures 4 and 5 is for the case of Mach number equal to zero and a wall temperature ratio $T_w/T_e^o = 1$. The values of the model parameters a and b used in these calculations were a = 50 and b = 0. We must now discuss how these values of the parameters a and b were determined.

Since the instability model that is under consideration is a two-parameter model, it is necessary that two separate tests be used to determine the values of the parameters a and b. The two tests that were used were based on a desire to form a connection with classical stability theory for incompressible flow. First, we wished to match the critical Reynolds number found in classical calculations. This number is found to be approximately $R_{\delta*} = 420$ or $R_\delta = 1200$.

Here, $\delta$ is defined as that height at which $u/u_e = 0.99$.

Second, we wished to have a shape of the profile for

$\widetilde{K} = \widetilde{k}_1 + \widetilde{k}_2 + \widetilde{k}_3$ such that it had the general characteristics of the same profile as calculated by classical stability theory. It was originally planned that these calculations would be made in the manner described above, namely, by following the growth of disturbances as the boundary layer developed and $R_\delta$ increased with $x$. As a result of calculations made in this manner, two important conclusions were drawn. First, the value of $a$ can range over a wide spectrum of values, and the critical Reynolds number can be made to be 1200 if $b$ is properly chosen. Second, the value of the critical Reynolds number determined in this way for given values of $a$ and $b$ was too sensitive to the point at which the original disturbances were introduced to accurately pin down the critical Reynolds number. At first it was not known whether this inaccuracy was a result of a lack of precision in the computation or was, indeed, a result of the sensitivity of the physical problem to small variations in modal shape as the critical Reynolds number was passed.

In order to investigate this problem thoroughly and to ensure an accurate determination of the critical Reynolds number, the decision was made to run the program in a mode similar to the way in which classical stability calculations are carried out.

In this mode of computation, the mean profile of the boundary layer is found for the particular case under investigation[3] and the mean velocity profile is then frozen at the particular Reynolds number to be investigated; that is,

$$\bar{u}(x,y;M_e,T_w/T_e^o) \equiv \bar{u}_o(y;M_e,T_w/T_e^o)$$

This assumption also carries with it the condition $\bar{v} = 0$. By this artifice, the mean boundary layer becomes a parallel shear flow of constant $R_\delta$. Disturbances are now introduced into this layer at a given station and the disturbance equations solved for $\bar{u} = \bar{u}_o(y)$ and $\bar{v} = 0$. This computation is conceptually quite similar to the classical stability calculation.

When the program was run in the mode just described, it was found that for any given choice of the parameters $a$ and $b$ an accurate determination of the critical Reynolds number could be made. The method by which this number was found was the following. A mean flow of a given Reynolds number was selected. Disturbances were then introduced into this boundary

---

[3]An outline of the way in which the mean velocity profile is calculated in this mode of operation is given in Appendix III.

layer and their redistribution and growth or decay were
followed by observing the behavior of

$$K_{max} = \tilde{K}_{max}/u_e^2 \qquad (30)$$

and

$$IK = \int_0^\delta (\tilde{K}/u_e^2) \, dy \qquad (31)$$

with  x .  A typical result of such a calculation is shown in
Figure 6.  In this particular case, the disturbances were
damped.  The fact that plots of $K_{max}$  and  IK  ultimately
become straight lines on semilog graph paper indicates that
the disturbances are damped according to the law

$$K_{max} \sim e^{-\alpha_i x} \qquad (32)$$

Here we have used the symbol  $\alpha_i$  to denote the decay constant
in accordance with the usual notation of stability theory.

If one performs a number of calculations such as the
one shown in Figure 6 for several different values of Reynolds
number and the decay rate in each case is noted, a curve
similar to that shown in Figure 7 can be constructed.  It
should be obvious from the nature of this curve that a critical
Reynolds number can usually be determined quite accurately by
means of only three calculations.

While the calculation of critical Reynolds number is quite
straightforward in trying to choose the model parameters  a
and  b , the matching of disturbance distributions to those of
classical theory presents some difficulty.  In classical
theory the modal shapes are a function of both wavelength and
Reynolds number, as well as Mach number and wall temperature
ratio.  Since wavelength no longer appears in the calculations
which are considered in this study, the selection of a parti-
cular modal shape that we wish to match is somewhat arbitrary.
Although it would be desirable to study this point in somewhat
more detail than was permitted under the scope of the study
contract reported here, it was decided that an acceptable
profile for  M = 0  and  $T_w/T_e$ = 1.0  would be one whose maxi-
mum value of  K  for a Reynolds number equal to the critical
Reynolds number, occurred in the neighborhood of  $y/\delta$ = 0.5
and was not too flat a distribution with respect to  y .  In
this rather imprecise (though, we think, not unreasonable)
way, a parameter search was carried out for the Blasius mean
velocity profile to determine the parameters  a  and  b .

By the process described above and after many calculations, during the course of which it was found that it was necessary to perform very precise integrations over distances of the order of 500 boundary layer thicknesses in order to achieve accurate modal shapes and decay rates, it was decided that a satisfactory choice of parameters would be $a = 50$ and $b = 0.01$ . The small value of $b$ was forced on us largely by the requirement that the profile shape be peaked in the neighborhood of $y/\delta = 0.5$ . Perhaps this will be more clear from Figure 8 when we show two $k$ profiles. Both these profiles are for approximately the same $R_\delta$ and $x/\delta$ . One is for the model with $a = 50$ and $b = 0.01$ and the other is for $a = 30$ and $b = 0.05$ . Both models have roughly the same critical Reynolds number. It was felt that the disturbance profile for the case $a = 30$ and $b = 0.05$ was too flat and that the profile for $a = 50$ and $b = 0.01$ was more representative of what happens in actual boundary layers. It is evident that this particular point in choosing a desirable model needs considerably more study.

Once the model $a = 50$ and $b = 0.01$ had been found to meet the initial requirements we had placed on the model, an investigation to find out whether, when $b$ is as small as $0.01$ , the terms which contain it enter the calculations in any significant way was made. Calculations were run for $a = 50$ and $b = 0.001$ and $b = 0$ . For all intents and purposes, the results obtained were the same. On the basis of these results, the final model selected for this study was $a = 50$ and $b = 0$.

# SECTION IV

## CRITICAL REYNOLDS NUMBER CALCULATIONS

Once the selection of parameters in the model equations was complete, an evaluation of the way in which the model described the onset of instability for compressible turbulent boundary layers could be carried out. To do this, calculations were made of critical Reynolds numbers for Mach numbers 0, 3, 6, 9, and 12 for wall temperature ratios ranging from 0.05 to 1.20. The critical values were determined from the amplification curves plotted in Figures 9 through 13.[4] These plots, following the customary procedure for classical stability calculations, are given in terms of the nondimensional parameters $R_{\delta*}$ and $\alpha_1 \delta*$. It will be noted from these figures that the effect of lowering the wall temperature at all Mach numbers, but especially at low Mach numbers, is to lower the critical $R_{\delta*}$. This behavior is emphasized in Figure 14 where we have plotted the critical values of $R_{\delta*}$ read from Figures 9 through 13 as a function of $T_w/T_e^o$. The effect of $T_w/T_e^o$ on $R_{\delta* \, crit}$ shown in this figure is largely due to the effect of wall cooling on the ratio of $\delta*$, the displacement thickness, to $\delta$, the thickness defined by $u/u_e = 0.99$. This is evident from Figure 15 where we have plotted $R_{\delta \, crit}$ versus $T_w/T_e^o$ with external Mach number as a parameter. We note here that there appears to be an adverse effect of wall cooling on $R_{\delta \, crit}$. The favorable effect of Mach number on $R_{\delta \, crit}$ is expected.

The fact that the critical $R_\delta$ for a given Mach number decreases with wall cooling does not imply that the start of instability would move forward on a flat plate as cooling is increased. In fact, the opposite is true, as may be seen from Figure 16 where we have calculated the critical value of $R_x$ corresponding to the critical value of $R_\delta$ given in Figure 15 and plotted these results against wall cooling with Mach number as a parameter. Two things are apparent from this figure.

---

[4]It should be noted here that each data point on each of these figures represents a complete stability calculation such as that shown in Figure 3. Each data point required approximately 2-1/2 minutes of computation time on a CDC-6600 computer. Although it had originally been thought that these production runs could be carried out on A.R.A.P.'s computer (an IBM 1130), it was found that the computation times proved inordinately long, roughly 11 hours per data point. In addition, the 14-digit precision of the CDC-6600 in comparison to the 7-digit precision of the IBM 1130 slightly improved the accuracy of the results.

First, the lowered skin friction attendant to wall cooling at a given Mach number causes the length of boundary layer run required to achieve a given $R_\delta$ to increase sufficiently to more than offset the effect of wall cooling in lowering the critical value of $R_\delta$. Second, the effect of Mach number on the length of run required to achieve instability at a given wall cooling ratio is quite large. For example, at $T_w/T_e^0 = 1.0$ the Reynolds number for instability increases from something like $6.4 \times 10^4$ at $M = 0$ to something like $2.7 \times 10^5$ at $M = 12$.

The amplification information shown in Figures 9 through 13 can be plotted in a way that illustrates an important point and allows another comparison with classical stability theory. In Figures 17 through 21, we have plotted the nondimensional amplification rate $\alpha_1 \delta^*$ divided by $R_{\delta *}$ as a function of $R_{\delta *}$. The ratio $\alpha_1 \delta^*/R_{\delta *} = \alpha_1 \mu_e/\rho_e u_e$ is a direct measure of the amplification of disturbances with x for the case of a constant external flow. It is seen that for each Mach number and wall temperature ratio the amplification increases with $R_{\delta *}$ after the critical Reynolds number has been passed, but appears to approach asymptotically a maximum value at large $R_{\delta *}$. Equivalent curves computed by means of classical stability theory do not approach a maximum value of amplification at large Reynolds number but rather reach a maximum at some finite Reynolds number which is a function of disturbance wavelength and then decrease again at larger Reynolds numbers. The Reynolds number at which maximum amplification takes place increases with increasing wavelength. Although we do not obtain this wavelength-dependent property of classical solutions, the magnitudes of the maximum amplification reached in the present calculations are comparable in magnitude but slightly smaller than those computed by classical stability methods (see, e.g., Refs. 5 and 6). For example, at $M = 0$ and $T_w/T_e^0 = 1$, we find

$$\left( \frac{\alpha_1 \delta^*}{R_{\delta *}} \right)_{max} = -7.4 \times 10^{-6} \quad , \text{ (Ref. 5)}$$

$$= -2.36 \times 10^{-6} \quad , \text{ present method}$$

Also, a comparison of the damping factor $\alpha_1 \delta^*$ found in this study with the results of Mack for other Mach numbers (Ref. 6) indicates that the values calculated here are of the right order of magnitude but are somewhat smaller than classical stability results.

It might be useful to point out here that, for real flows, measurements do not, in general, show the fall-off of amplification with Reynolds number predicted by classical theory.

It is of considerable interest to calculate the final disturbance distributions in the boundary layer as a function of Mach number, wall cooling ratio, and Reynolds number when the boundary layer is very close to neutral stability and when the boundary layer is definitely unstable. These results are shown in Figures 22 through 26 for M = 0, 6, and 12 for the case of an adiabatic wall and for the M = 0 and M = 12 for the case of a highly cooled wall ($T_w/T_e^0$ = 0.05).

It is interesting to note the movement of the region of turbulence production to the outer regions of the boundary layer as the Mach number is increased even for the case of high cooling ratio. One should also note the very significant change in disturbance profile shape with Reynolds number for high cooling rates at Mach number zero. This may well indicate that, for blunt body laminar layers on high speed reentry vehicles where such conditions exist, the actual disturbance profiles may never be able to adjust to their appropriate local shape. This would imply that classical stability theory or the present method run in a mode analogous to classical stability theory is not really adequate for dealing with the stability of such flows. It would be far more appropriate to do stability calculations for such a case using the method devised by Nagel[5] (Ref. 4) with $\bar{u} = \bar{u}(x,y)$ or by the present method in the boundary layer growth mode, i.e., for $\bar{u} = \bar{u}(x,y)$.

---

[5]It is the opinion of the authors of this report that the excellent technique to study compressible boundary layer stability developed by Nagel under Air Force sponsorship a few years ago has received far too little attention. It would appear that many important questions concerning boundary layer stability might be answered by rigorous exercise of the programs developed by Nagel for the Air Force.

# SECTION V

## RUN-OUT CALCULATIONS

Calculation of stability limits such as we have discussed in the previous section are of considerable interest from an academic standpoint. They are not, however, of great importance to the designer of aerospace vehicles. The designer would like to have information concerning the Reynolds number at which skin friction or heat transfer starts to increase as transition actually starts. In addition, he would like to know what the effect of roughness or external disturbance levels would be on this particular Reynolds number. In what follows, we will adopt the most common definitions of transition Reynolds number, namely, that Reynolds number defined by the wetted length at which an increase in skin friction or heat transfer occurs. In our calculations, we will assume that this point can be related to the point at which the maximum value of the turbulent stress correlation $-\rho\overline{u'v'}$ has grown to the point where it is equal to 10% of the local surface skin friction;[6] i.e., the point at which

$$- (\rho\overline{u'v'})_{max} = 0.1\,\tau(0) \qquad (33)$$

If both sides of Eq. (33) are divided by $\rho_e u_e^2/2$ , we obtain

$$\frac{(\bar{\rho}\sigma)_{max}}{\rho_e} = 0.05 C_f \qquad (34)$$

In order to carry out such a computation, the disturbance equations (Eqs. (21) through (24)) are solved in conjunction with the mean flow equations ((14), (15), and (18)). Now, however, we wish to include in some way the effect of the generation of the turbulent stress correlation $- \overline{u'v'}$ on the growth and shape of the boundary layer. To accomplish this, we add this stress to the right-hand side of Eq. (15) so that it becomes

$$\bar{\rho}\bar{u}\,\frac{\partial\bar{u}}{\partial x} + \bar{\rho}\bar{v}\,\frac{\partial\bar{u}}{\partial y} = - \frac{\partial\bar{p}}{\partial x} + \frac{\partial}{\partial y}\left(\bar{\mu}\,\frac{\partial\bar{u}}{\partial y} - \bar{\rho}\,\overline{u'v'}\right) \qquad (35)$$

----
[6] Actually, it would be desirable to choose a somewhat higher number. However, to use the present model calculations in which third-order terms are neglected for stress levels higher than 0.1 would be stretching the applicability of the method past the point where any credibility can be attached to the results.

Time and funding under the research contract reported here permitted us to carry out only a few complete run-out computations. These were made for $M = 0$ with $T_w/T_e^o = 1.0$ and 0.05 for a case of high initial turbulence level and partially carried out for $M = 0$ and $M = 3$ with $T_w/T_e^o = 1.0$ for a case of low turbulence level.

The initial conditions for these runs were those of the boundary layer at the critical Reynolds number as determined from the runs described in the previous section, except that the turbulence intensity was scaled to make $K_{max} = 3 \times 10^{-4}$ for the high level case or $K_{max} = 3 \times 10^{-6}$ for the low level case.

The seven differential equations governing the motion (Eqs. (14), (18), (35), and (21) through (24)) were then solved simultaneously to track the development of the boundary layer in the streamwise direction. Figure 27 shows the results of the high level disturbance calculations for $M = 0$. We note here that the cold wall case was more stable than the insulated wall case as determined by the calculations of the previous section. Thus for $T_w/T_e^o = 0.05$, the run-out calculation starts at $R_{x} = 9.0 \times 10^4$ and for $T_w/T_e^o = 1.0$, it starts at $R_x = 6.5 \times 10^4$. It is immediately obvious from the figure that, although the cold wall case was more stable (in the sense that the critical $R_x$ was higher), transition occurs sooner. The actual Reynolds numbers for transition as we have defined it are $1.45 \times 10^6$ for $T_w/T_e^o = 1.0$ and $6.9 \times 10^5$ for $T_w/T_e^o = 0.05$. The implication of this result is that one should not judge transition by the criterion of boundary layer stability.

The effect of disturbance level on transition can be seen by comparing the results for $M = 0$ and $T_w/T_e^o = 1.0$ shown in Figure 28. Although the run-out calculation for low level disturbance is not complete, it is obvious that transition will occur at a Reynolds number of approximately $2.8 \times 10^6$ which is considerably larger than for high level disturbance. Also obvious from Figure 28 is the fact that transition at Mach number three occurs at higher Reynolds numbers than at Mach number zero, both because the boundary layer is more stable at $M = 3$ and because the amplification rates are smaller. An estimate of transition Reynolds number for $M = 3$ and $T_w/T_e^o = 1.0$ derived from Figure 28 is $R_x = 6 \times 10^6$.

At the start of this program, it was hoped that run-out calculations such as those presented might be made on A.R.A.P.'s IBM 1130 computer. This hope was not realized. In the course

of the study, the requirement for accuracy in these calculations
as a result of the very long integrations that are carried out
precludes the use of a small computer for these studies, both
from the standpoint of accuracy and of time. The run-outs shown
in Figure 28 required 24 and 11 minutes on a CDC-6600 computer
for $M = 0$ and $M = 3$, respectively. This could work out to
some 100 and 46 hours, respectively, on our IBM 1130 computer.
For this reason, only the four run-outs shown in Figures 27 and
28 were completed under this study contract.

# SECTION VI

## COMPARISON WITH EXPERIMENTAL RESULTS

At the start of this program, it was not known whether there would be some relatively simple relationship between critical Reynolds number and transition Reynolds number. In the previous section, it was shown that the problem of transition, as defined by the present model, is such that judgments concerning transition cannot be related to the behavior of the critical Reynolds number. In view of this fact, it is unwise to compare our stability results with measurements of transition.

Had more time and funding been available, it might have been possible to compare our results with detailed measurements of disturbance growth in unstable laminar layers. In the absence of this information, all that we can say at this time is that the amplification rates predicted by classical theory are generally found to be of the right order of magnitude when tested against experimental observations. Here it must be pointed out, however, that the prediction of classical theory that amplification rates decrease after reaching a maximum is, in general, not observed experimentally. Since the maximum amplification rate results found in this study are in general agreement with the maximum rates of classical theory, it is probable that the present results (insofar as stability is concerned) would, in a general way, agree with experiment.

A great deal more work must be done before any conclusions can be drawn concerning the agreement between transition as predicted by modeling techniques and as measured experimentally. If such studies are to be made, it is strongly recommended that the full model equations be programmed and used to make these studies.

Perhaps it will suffice here to present the few quasi-linear run-out computations completed in this study with some experimentally observed transitions. This is done in Figure 29. In this figure, both the stability limits found in this study and the results of the four run-out computations that were made are compared with the general trend of experimental results as taken from numerous sources. The general level and trend of the results is correct as far as can be discerned from the minimal data available.

Perhaps the most important aspect of this figure is that it emphasizes the very significant differences between the behavior of critical Reynolds numbers and transition Reynolds numbers. These differences are due to both disturbance level effects and to the strong effect of wall cooling and Mach number on amplification rates.

It is hoped that, sometime in the near future, sufficient funds can be made available to perform a complete set of run-out calculations in which the effects of disturbance level, Mach number, and wall cooling ratio are studied.

# SECTION VII

## CONCLUSIONS

1.  It appears from the results of a study of a model of transition that a tool useful for the study of compressible transition might be developed.

2.  The method studied yields amplification rates that agree in magnitude with those of classical stability calculations.

3.  The computations show that there is a strong favorable effect of Mach number on wetted length critical Reynolds number as well as transition Reynolds number.

4.  Wall cooling has a favorable effect on critical Reynolds number.

5.  Wall cooling has an unfavorable effect on transition Reynolds number for $M = 0$ and $T_w/T_e^0 = 0.05$ .

6.  It may be concluded that it is unwise to try to directly relate the results of a minimum critical Reynolds number calculation to the prediction of transition Reynolds number.

7.  The present method of simulating transition is capable of giving direct estimates of the effect of disturbances on transition Reynolds number. These disturbances may be introduced either externally, as in the case of wind tunnels, or at the surface of the body, as in the case of ablating surfaces.

## SECTION VIII

## RECOMMENDATIONS

Because of the encouraging results found in the study reported here, it is recommended that:

1. A complete set of run-out calculations be carried out using the preliminary model of boundary layer instability that has been investigated in this report.

2. A complete compressible transition model be programmed and checked out.

3. Once completed, this program should be used to perform an extensive series of numerical experiments on transition. The effects of the following parameters should be investigated:

        (a) Mach number;

        (b) wall cooling;

        (c) continuously applied external disturbances;

        (d) continuously applied surface disturbances.

4. The program should be used to calculate transition for a large number of cases where transition has been measured in carefully documented environments.

# APPENDIX I

## COMPLETE STEADY STATE EQUATIONS

### Mean Density

$$(\bar{\rho}\bar{u}^j)_{,j} = -\overline{(\rho'u^{1\prime})}_{,1}$$

### Mean Velocity

$$(\bar{\rho}\bar{u}^j + \overline{\rho'u^{j\prime}})\bar{u}_{1,j} = -\bar{\rho}\overline{(u_1'u^{j\prime})}_{,j} - \overline{u_1'u^{j\prime}}\;\bar{\rho}_{,j} - \overline{\rho'u_1'}\;\bar{u}^j_{,j}$$

$$- \bar{u}^j\overline{(\rho'u_1')}_{,j} - \overline{(\rho'u_1'u^{j\prime})}_{,j} - \bar{p}_{,1} + \bar{\tau}^j_{1,j}$$

### Mean Temperature

$$(\bar{\rho}\bar{u}^j + \overline{\rho'u^{j\prime}})\bar{T}_{,j} = -(\bar{\rho}\;\overline{T'u^{j\prime}})_{,j} - (\bar{u}^j\overline{\rho'T'})_{,j} - \overline{(\rho'T'u^{j\prime})}_{,j}$$

$$- \frac{\bar{p}}{C_v}\bar{u}^j_{,j} - \frac{\overline{\rho'}}{C_v}\overline{u^{j\prime}_{,j}} + \frac{\bar{\phi}}{C_v} - \frac{\bar{H}}{C_v}$$

### Density Fluctuation

$$\bar{u}^j\overline{\rho'^2}_{,j} = -2\overline{\rho'^2}\bar{u}^j_{,j} - 2\overline{\rho'u^{j\prime}}\;\bar{\rho}_{,j} - \overline{(\rho'^2u^{j\prime})}_{,j}$$

$$- 2\bar{\rho}(\overline{\rho'u^{j\prime}_{,j}}) - (\overline{\rho'^2u^{j\prime}_{,j}})$$

## Density Velocity Correlation

$$\bar{\rho}\bar{u}^j(\overline{\rho'u_i'})_{,j} = -\overline{\rho'^2\bar{u}^j\bar{u}_{1,j}} + 2\overline{\rho'u_i'(\overline{\rho'u^{j'}})_{,j}} - \overline{\rho'u_i'}\;\bar{\rho}\bar{u}^j_{,j}$$

$$- \overline{\rho'u^{j'}(\bar{\rho}\bar{u}_{1,j})} - \overline{u_i'u^{j'}}\bar{\rho}\bar{\rho}_{,j} - \bar{\rho}^2\overline{u_i'u^{j'}_{,j}}$$

$$- \bar{\rho}(\overline{\rho'u_i'u^{j'}})_{,j} - 2\overline{\rho'u_i'u^{j'}}\;\bar{\rho}_{,j} - \overline{\rho'^2u^{j'}}\;\bar{u}_{1,j}$$

$$- 2\overline{\rho'^2u_i'}\;\bar{u}^j_{,j} - \bar{u}^j(\overline{\rho'^2u_i'})_{,j}$$

$$- (\overline{\rho'p'})_{,1} + \overline{p'\rho'_{,1}} + \overline{\rho'\tau^{j'}_{i,j}}$$

## Velocity Correlation

$$\bar{\rho}\bar{u}^j(\overline{u_i'u_k'})_{,j} = -\overline{\rho'u_k'}\;\bar{u}^j\bar{u}_{1,j} - \overline{\rho'u_i'}\;\bar{u}^j\bar{u}_{k,j} - \overline{\bar{\rho}u_k'u^{j'}}\;\bar{u}_{1,j}$$

$$- \overline{\bar{\rho}u_i'u^{j'}}\bar{u}_{k,j} - \overline{u_i'u_k'(\bar{\rho}\bar{u}^j)}_{,j} - (\overline{\bar{\rho}u_i'u_k'u^{j'}})_{,j}$$

$$- (\bar{u}^j\overline{\rho'u_i'u_k'})_{,j} - \overline{\rho'u_k'u^{j'}}\;\bar{u}_{1,j} - \overline{\rho'u_i'u^{j'}}\;\bar{u}_{k,j}$$

$$- \overline{u_i'p'_{,k}} - \overline{u_k'p'_{,1}} + \overline{u_k'\tau^{j'}_{1,j}} + \overline{u_i'\tau^{j'}_{k,j}}$$

## Density Temperature Correlation

$$\bar{\rho}\bar{u}^j(\overline{\rho'T'})_{,j} + \overline{\rho'^2\,u^j}\bar{T}_{,j} = -\bar{\rho}(\overline{T'u^{j'}})\bar{\rho}_{,j} - \overline{\bar{\rho}\rho'T'}\,\bar{u}^j_{,j}$$

$$- \overline{\bar{\rho}\rho'u^{j'}}\,\bar{T}_{,j} + 2\overline{\rho'T'(\rho'u^{j'})}_{,j}$$

$$- \bar{\rho}(\overline{\rho'T'u^{j'}})_{,j} - 2(\overline{\rho'T'u^{j'}})\bar{\rho}_{,j} - \overline{\rho'^2 u^{j'}}\,\bar{T}_{,j}$$

$$- 2\overline{\rho'^2 T'}\,\bar{u}^j_{,j} - \bar{u}^j(\overline{\rho'^2 T'})_{,j} - \bar{\rho}^2\,\overline{T'u^{j'}_{,j}}$$

$$- \overline{\bar{\rho}\rho'T'u^{j'}_{,j}} - \overline{\frac{\rho'p'}{C_v}}\,\bar{u}^j_{,j} - \overline{\frac{\rho'}{C_v}u^{j'}_{,j}}\,\bar{p}$$

$$- \overline{\frac{\rho'p'}{C_v}u^{j'}_{,j}} + \overline{\frac{\rho'\phi'}{C_v}} - \overline{\frac{\rho'H'}{C_v}}$$

## Velocity Temperature Correlation

$$\bar{\rho}\bar{u}^j(\overline{T'u'_i})_{,j} + \overline{\rho'u'_i}\,\bar{u}^j\bar{T}_{,j} + \overline{\rho'T'}\,\bar{u}^j\bar{u}_{1,j} = \overline{T'u'_i(\rho'u^{j'})}_{,j}$$

$$- (\overline{\bar{\rho}T'u'_i u^{j'}})_{,j} - (\overline{\bar{u}^j\rho'T'u'_i})_{,j} - \overline{\bar{\rho}u'_i u^{j'}}\,\bar{T}_{,j}$$

$$- \overline{\bar{\rho}T'u^{j'}}\,\bar{u}_{1,j} - \overline{\rho'u'_i u^{j'}}\,\bar{T}_{,j} - \overline{\rho'T'u^{j'}}\,\bar{u}_{1,j}$$

$$- \overline{\bar{\rho}T'u'_i u^{j'}_{,j}} - \overline{\frac{p'u'_i}{C_v}}\,\bar{u}^j_{,j} - \overline{u'_i u^{j'}_{,j}}\,\frac{\bar{p}}{C_v} - \overline{u'_i\frac{p'}{C_v}u^{j'}_{,j}}$$

$$- \overline{T'p'_{,i}} + \overline{T'\tau^{j'}_{1,j}} + \overline{u'_i\frac{\phi'}{C_v}} - \overline{u'_i\frac{H'}{C_v}}$$

## Temperature Fluctuation

$$\frac{\bar{\rho}\bar{u}^{J}}{2}\,\overline{T'^{2}_{,j}} + \overline{\rho'T'}\,\bar{u}^{J}\bar{T}_{,j} = \frac{1}{2}\,\overline{T'^{2}(\rho'u^{J'})}_{,j} - \overline{\bar{\rho}T'u^{J'}}\,\bar{T}_{,j}$$

$$- \frac{1}{2}\,(\bar{\rho}\overline{T'^{2}u^{J'}})_{,j} - \frac{1}{2}\,(\overline{\rho'T'^{2}\bar{u}^{J}})_{,j}$$

$$- \overline{\rho'T'u^{J'}}\,\bar{T}_{,j} - \frac{\overline{T'p'}}{C_{v}}\,\bar{u}^{J}_{,j}$$

$$- \frac{\bar{\rho}\overline{T'}}{C_{v}}\,u^{J'}_{,j} - \frac{\overline{T'p'}}{C_{v}}\,u^{J'}_{,j} + \frac{\overline{T'\phi'}}{C_{v}} - \frac{\overline{T'H'}}{C_{v}}$$

## Definitions

$$\bar{\tau}^{k}_{j} = \bar{\mu}\left[g^{k\ell}(\bar{u}_{j,\ell} + \bar{u}_{\ell,j}) - \frac{2}{3}\,\delta^{k}_{j}\bar{u}^{\ell}_{,\ell}\right]$$

$$\tau^{k'}_{j} = \bar{\mu}g^{k\ell}(u'_{j,\ell} + u'_{\ell,j}) + \mu'\left[g^{k\ell}(\bar{u}_{j,\ell} + \bar{u}_{\ell,j}) - \frac{2}{3}\,\delta^{k}_{j}\bar{u}^{\ell}_{,\ell}\right]$$

$$\bar{\phi} = \bar{u}^{J}_{,k}\bar{\tau}^{k}_{j}$$

$$\bar{H} = \bar{g}^{k}_{,k}$$

$$\phi' = \bar{u}^{J}_{,k}\tau^{k'}_{j} + \overline{u^{J'}_{,k}\tau^{k}_{j}}$$

$$H' = g^{k'}_{,k}$$

$$\bar{g}_{k} = -\bar{k}\,\frac{\partial\bar{T}}{\partial x^{k}}$$

$$g'_{k} = -\bar{k}\,\frac{\partial T'}{\partial x^{I}} - k'\,\frac{\partial\bar{T}}{\partial x^{I}}$$

# APPENDIX II

## BOUNDARY LAYER MODEL EQUATIONS

Mean Density $(\bar{\rho})$

$$\bar{u}^j \bar{\rho}_{,j} = - \bar{\rho}\bar{u}^j_{,j} - \overline{(\rho'u^{j'})}_{,j}$$

Mean Velocity $(\bar{u}_1)$

$$\bar{\rho}\bar{u}^j \bar{u}_{1,j} = - \overline{\rho'u^{j'}}\bar{u}_{1,j} - (\overline{\bar{\rho}u'_1 u^{j'}})_{,j} - (\overline{\rho'u'_1}\,\bar{u}^j)_{,j}$$

$$+ g^{jk}\left(\Lambda \sqrt{K}\left[(\overline{\rho'u'_1})_{,k} + (\overline{\rho'u'_k})_{,1}\right]\right)_{,j}$$

$$+ \bar{\mu}\left[g^{j\ell}(\bar{u}_{1,\ell} + \bar{u}_{\ell,1}) - \frac{2}{3}\delta^j_1\bar{u}^\ell_{,\ell}\right]_{,j}$$

Mean Temperature $(\bar{T})$

$$\bar{\rho}\bar{u}^j \bar{T}_{,j} = \bar{T}\overline{(\rho'u^{j'})}_{,j} + \left(\frac{\bar{T}}{\bar{\rho}}\bar{u}^j\overline{\rho'^2}\right)_{,j}$$

$$+ g^{jk}\left(\frac{\bar{T}}{\bar{\rho}}\Lambda\sqrt{K}\overline{\rho'^2_{,k}}\right)_{,j} - \frac{\bar{p}}{C_v}\bar{u}^j_{,j}$$

$$+ \bar{\mu}\,\bar{u}^j_{,k}\left[g^{k\ell}(\bar{u}_{j,\ell} + \bar{u}_{\ell,j}) - \frac{2}{3}\delta^k_j\bar{u}^\ell_{,\ell}\right] + g^{jk}(\bar{k}\bar{T}_{,j})_{,k}$$

Density Fluctuation ($\overline{\rho'^2}$)

$$\bar{u}^j \overline{\rho'^2}_{,j} = -2\overline{\rho'^2}\,\bar{u}^j_{,j} - 2\overline{\rho'u^{j'}}\,\bar{\rho}_{,j} + g^{kj}(\Lambda\sqrt{K}\,\overline{\rho'^2}_{,k})_{,j}$$

$$+ \frac{2\bar{\rho}(\gamma-1)}{\gamma\bar{p}}\left\{ \frac{\bar{u}\sqrt{\overline{\rho'^2}}}{\Lambda\sqrt{K}}\,g^{k\ell}\,\bar{u}^j_{,k}\left(\overline{u'_j u'_\ell} - g_{j\ell}\frac{K}{3}\right)\right.$$

$$+ \frac{\mu_s\bar{T}}{\bar{\rho}}\,\overline{\rho'^2}\,\bar{u}^j_{,k}\left[g^{k\ell}(\bar{u}_{j,\ell} + \bar{u}_{\ell,j}) - \frac{2}{3}\delta^k_j\,\bar{u}^\ell_{,\ell}\right]$$

$$+ \frac{\bar{\mu}\sqrt{\overline{\rho'^2}}}{2\Lambda\sqrt{K}}\,g^{j\ell}\left(\overline{u'_\ell u'_k} - g_{k\ell}\frac{K}{3}\right)\left[g^{km}(\bar{u}_{j,m} + \bar{u}_{m,j}) - \frac{2}{3}\delta^k_j\,\bar{u}^m_{,m}\right]\right\}$$

$$- \frac{2\bar{\rho}(\gamma-1)}{\gamma\bar{p}}\,g^{k\ell}\left\{\bar{k}_{,k}\left[\left(\frac{\bar{T}}{\bar{\rho}}\right)_{,\ell}\overline{\rho'^2} + \frac{\bar{T}}{\bar{\rho}}\,\frac{\overline{\rho'^2_{,\ell}}}{2}\right]\right.$$

$$+ \bar{k}\left[\left(\frac{\bar{T}}{\bar{\rho}}\right)_{,\ell,k}\overline{\rho'^2} + \left(\frac{\bar{T}}{\bar{\rho}}\right)_{,\ell}\frac{\overline{\rho'^2_{,k}}}{2} + \left(\frac{\bar{T}}{\bar{\rho}}\right)_{,k}\frac{\overline{\rho'^2_{,\ell}}}{2} + \frac{\bar{T}}{\bar{\rho}}\frac{\overline{\rho'^2_{,\ell,k}}}{2}\right.$$

$$\left.- \frac{g_{k\ell}}{3}\frac{\overline{\rho'^2}}{\lambda^2}\right] + \frac{k_s\bar{T}}{\bar{\rho}}\,\overline{\rho'^2}\,\bar{T}_{,\ell,k} + \bar{T}_{,\ell}\left[\left(\frac{k_s\bar{T}}{\bar{\rho}}\right)_{,k}\overline{\rho'^2} + \frac{k_s\bar{T}}{\bar{\rho}}\frac{\overline{\rho'^2_{,k}}}{2}\right]\right\}$$

$$+ \frac{\bar{\mu}(\gamma-1)\overline{\rho'^2}}{\gamma\bar{p}\,\Lambda\sqrt{K}}\left\{ 2g^{k\ell}\,\bar{\mu}^j_{,k}\left(\overline{u'_j u'_\ell} - g_{j\ell}\frac{K}{3}\right)\right.$$

$$\left.+ g^{j\ell}\left(\overline{u'_\ell u'_k} - g_{\ell k}\frac{K}{3}\right)\left[g^{km}(\bar{u}_{j,m} + \bar{u}_{m,j}) - \frac{2}{3}\delta^k_j\,\bar{u}^m_{,m}\right]\right\}$$

## Density-Velocity Correlation ($\overline{\rho' u_i'}$)

$$\bar{\rho}\bar{u}^j(\overline{\rho' u_i'})_{,j} = -\overline{\rho'^2}\,\bar{u}^j\bar{u}_{1,j} + 2\overline{\rho' u_i'}(\overline{\rho' u^{j'}})_{,j} - \overline{\rho' u_i'}\,\bar{\rho}\bar{u}^j_{,j}$$

$$-\overline{\rho' u^{j'}}(\bar{\rho}\bar{u}_{1,j}) - \overline{u_i' u^{j'}}\,\bar{\rho}\bar{\rho}_{,j}$$

$$+\bar{\rho}g^{jk}\left(\Lambda\sqrt{K}\left[(\overline{\rho' u_i'})_{,k} + (\overline{\rho' u_k'})_{,1}\right]\right)_{,j}$$

$$+2\Lambda\sqrt{K}\,g^{jk}\left[(\overline{\rho' u_i'})_{,k} + (\overline{\rho' u_k'})_{,1}\right]\bar{\rho}_{,j} + \Lambda\sqrt{K}g^{jk}\overline{\rho'^2}_{,k}\bar{u}_{1,j}$$

$$+2\Lambda\sqrt{K}\,\overline{\rho'^2_{,1}}\,\bar{u}^j_{,j} + \bar{u}^j(\Lambda\sqrt{K}\,\overline{\rho'^2_{,1}})_{,j}$$

$$+\left(\bar{\rho}\left(b\Lambda^2\sqrt{\overline{\epsilon_{st}\epsilon^{st}}} + \Lambda\sqrt{K}\right)(\overline{\rho' u^{k'}})_{,k}\right)_{,1}$$

$$-\bar{\rho}\left(a\sqrt{\overline{\epsilon_{st}\epsilon^{st}}} + \frac{\sqrt{K}}{\Lambda}\right)(\overline{\rho' u_i'})$$

$$-\frac{\bar{\rho}^2(\gamma - 1)}{\gamma\bar{p}}\left\{\bar{\mu}g^{k\ell}\bar{u}^j_{,k}\left(\overline{u_j' u_\ell'} - g_{j\ell}\frac{K}{3}\right)_{,1}\right.$$

$$-\frac{\mu_s\bar{T}}{\bar{\rho}}\,\bar{u}^j_{,k}\overline{\rho' u_i'}\left[g^{k\ell}(\bar{u}_{j,\ell} + \bar{u}_{\ell,j}) - \frac{2}{3}\delta^k_j\bar{u}^\ell_{,\ell}\right]$$

$$\left.-\frac{\bar{\mu}}{2}g^{j\ell}\left(\overline{u_\ell' u_k'} - g_{\ell k}\frac{K}{3}\right)_{,1}\left[g^{km}(\bar{u}_{j,m} + \bar{u}_{m,j}) - \frac{2}{3}\delta^k_j\bar{u}^m_{,m}\right]\right\}$$

$$+\frac{\bar{\rho}^2(\gamma - 1)}{\gamma\bar{p}}g^{k\ell}\left\{\bar{k}_{,k}\left[\left(\frac{\bar{T}}{\bar{\rho}}\right)_{,\ell}\overline{\rho' u_i'} + \frac{\bar{T}}{\bar{\rho}}(\overline{\rho' u_i'})_{,\ell}\right.\right.$$

$$\left.+\frac{\bar{T}\sqrt{\overline{\rho'^2}}}{2\bar{\rho}\Lambda\sqrt{K}}\left(\overline{u_i' u_\ell'} - g_{1\ell}\frac{K}{3}\right)\right] + \frac{\bar{T}}{\bar{\rho}}\frac{\overline{\rho' u_i'}}{\lambda^2}\frac{g_{\ell k}}{3}$$

$$+\frac{k_s\bar{T}}{\bar{\rho}}\overline{\rho' u_i'}\,\bar{T}_{,\ell,k} + \bar{T}_{,\ell}\left[\left(\frac{k_s\bar{T}}{\bar{\rho}}\right)_{,k}\overline{\rho' u_i'} + \frac{k_s\bar{T}}{\bar{\rho}}(\overline{\rho' u_i'})_{,k}\right.$$

$$\left.\left.+\frac{k_s\bar{T}\sqrt{\overline{\rho'^2}}}{2\bar{\rho}\Lambda\sqrt{K}}\left(\overline{u_i' u_k'} - g_{1k}\frac{K}{3}\right)\right]\right\} - \frac{\sqrt{\overline{\rho'^2}}}{\Lambda\sqrt{K}}g^{j\ell}\left(\overline{u_i' u_\ell'} - g_{1\ell}\frac{K}{3}\right)\bar{\mu}_{,j}$$

$$-\frac{\mu_s\bar{T}}{\bar{\rho}}\overline{\rho'^2}\left[g^{k\ell}(\bar{u}_{1,\ell} + \bar{u}_{\ell,1}) - \frac{2}{3}\delta^k_1\bar{u}^\ell_{,\ell}\right]_{,k}$$

## Velocity Correlation $(\overline{u_i' u_k'})$

$$\bar{\rho}\bar{u}^j(\overline{u_i' u_k'})_{,j} = -\overline{\rho' u_k'}\,\bar{u}^j \bar{u}_{1,j} - \overline{\rho' u_i'}\,\bar{u}^j \bar{u}_{k,j} - \overline{\bar{\rho} u_k' u^{j'}}\,\bar{u}_{1,j}$$

$$- \bar{\rho}\,\overline{u_1' u^{j'}}\,\bar{u}_{k,j} - \overline{u_i' u_k'}(\bar{\rho}\bar{u}^j)_{,j} + g^{j\ell}\left(\bar{\rho}\Lambda\sqrt{K}\left[(\overline{u_i' u_\ell'})_{,k}\right.\right.$$

$$\left.\left. + (\overline{u_i' u_k'})_{,\ell} + (\overline{u_\ell' u_k'})_{,1}\right]\right)_{,j} + \left(\Lambda\sqrt{K}\bar{u}^j\left[(\overline{\rho' u_i'})_{,k}\right.\right.$$

$$\left.\left. + (\overline{\rho' u_k'})_{,1}\right]\right)_{,j} + \Lambda\sqrt{K}g^{\ell j}\left[(\overline{\rho' u_\ell'})_{,k} + (\overline{\rho' u_k'})_{,\ell}\right]\bar{u}_{1,j}$$

$$+ \Lambda\sqrt{K}g^{j\ell}\left[(\overline{\rho' u_\ell'})_{,1} + (\overline{\rho' u_i'})_{,\ell}\right]\bar{u}_{k,j}$$

$$- \left(\bar{\rho}\left[b\Lambda^2\sqrt{\epsilon_{st}\epsilon^{st}} + \Lambda\sqrt{K}\right](\overline{u_i' u^{\ell'}})_{,\ell}\right)_{,k}$$

$$- \left(\bar{\rho}\left[b\Lambda^2\sqrt{\epsilon_{st}\epsilon^{st}} + \Lambda\sqrt{K}\right](\overline{u_k' u^{\ell'}})_{,\ell}\right)_{,1}$$

$$+ \bar{\rho}\left(a\sqrt{\epsilon_{st}\epsilon^{st}} + \frac{\sqrt{K}}{\Lambda}\right)\left(\overline{u_i' u_k'} - g_{1k}\frac{K}{3}\right)$$

$$+ \bar{\mu}\left[g^{j\ell}(\overline{u_i' u_k'})_{,j,\ell} - 2\frac{\overline{u_1' u_k'}}{\lambda^2}\right] + \bar{\mu}_{,j}\left[g^{j\ell}(\overline{u_i' u_k'})_{,\ell}\right.$$

$$\left. + (\overline{u_i' u^{j'}})_{,k} + (\overline{u_k' u^{j'}})_{,1} + g^{j\ell}(\overline{u_i' u_k'} - g_{1k}\frac{K}{3})_{,\ell}\right]$$

$$- \frac{\mu_s\bar{T}}{\bar{\rho}}\,\overline{\rho' u_k'}\left[g^{j\ell}(\bar{u}_{1,\ell} + \bar{u}_{\ell,1}) - \frac{2}{3}\delta_1^j\bar{u}^\ell_{,\ell}\right]_{,j}$$

$$- \frac{\mu_s\bar{T}}{\bar{\rho}}\,\overline{\rho' u_i'}\left[g^{j\ell}(\bar{u}_{k,\ell} + \bar{u}_{\ell,k}) - \frac{2}{3}\delta_k^j\bar{u}^\ell_{,\ell}\right]_{,j}$$

$$- \left[\left(\frac{\mu_s\bar{T}}{\bar{\rho}}\,\overline{\rho' u_k'}\right)_{,j} + \frac{\mu_s\bar{T}\sqrt{\overline{\rho'^2}}}{2\bar{\rho}\,\Lambda\sqrt{K}}\left(\overline{u_j' u_k'} - g_{jk}\frac{K}{3}\right)\right]$$

$$\cdot\left[g^{j\ell}(\bar{u}_{1,\ell} + \bar{u}_{\ell,1}) - \frac{2}{3}\delta_1^j\bar{u}^\ell_{,\ell}\right] - \left[\left(\frac{\mu_s\bar{T}}{\bar{\rho}}\,\overline{\rho' u_i'}\right)_{,j}\right.$$

$$\left. + \frac{\mu_s\bar{T}\sqrt{\overline{\rho'^2}}}{2\bar{\rho}\,\Lambda\sqrt{K}}\left(\overline{u_j' u_i'} - g_{j1}\frac{K}{3}\right)\right]\left[g^{j\ell}(\bar{u}_{k,\ell} + \bar{u}_{\ell,k}) - \frac{2}{3}\delta_k^j\bar{u}^\ell_{,\ell}\right]$$

# APPENDIX III

## LAMINAR BOUNDARY LAYER PROFILES

To calculate the laminar boundary layer profiles needed in the present study, we follow a similarity method suggested by Lees (Ref. 22) and explored in detail by Back (Ref. 23). The method is outlined below for the special case of unaccelerated flow treated in this report.

Application of the combined Levy-Mangler transformation

$$\eta = \frac{\rho_e u_e}{\sqrt{2\xi}} \int_0^y \frac{\rho}{\rho_e}\, dy \qquad \xi = \rho_e \mu_e u_e x \qquad (III-1)$$

to the boundary layer equations for an unaccelerated perfect gas yields the following ordinary differential equation

$$(Cf'')' + ff'' = 0 \qquad (III-2)$$

where the prime denotes differentiation with respect to $\eta$. For a power law expression for viscosity

$$\frac{\mu}{\mu_e} = \left(\frac{T}{T_e}\right)^n \qquad (III-3)$$

the function $C$ becomes

$$C = \frac{\rho\mu}{\rho_e \mu_e} = \left(\frac{g_w + (1 - g_w)f' - Sf'^2}{1 - S}\right)^{n-1} \qquad (III-4)$$

where

$$g_w = \frac{T_w}{T_{e_o}}$$

$$\qquad (III-5)$$

$$S = \frac{\gamma - 1}{2}\, \frac{M_e^2}{1 + \frac{\gamma - 1}{2} M_e^2}$$

Note that for $n = 1$, we have $C = 1$ and Eq. (III-2) reduces to the Blasius equation. The boundary conditions on (III-2) are the following:

$$f(0) = f'(0) = 0$$

$$\lim_{\eta \to \infty} f'(\eta) = 1 \qquad \text{(III-6)}$$

The velocity profile and other important physical quantities are calculated from the solution of (III-2) as follows:

$$\frac{u}{u_e} = f'(\eta) \qquad \text{(III-7)}$$

$$\frac{T}{T_e} = \frac{g_w + (1 - g_w)f' - Sf'^2}{1 - S} \qquad \text{(III-8)}$$

$$\frac{\delta_{.99} R_x^{1/2}}{x} = \frac{\sqrt{2}}{1 - S} \left[ g_w \eta + (1 - g_w)f(\eta) - S \int_0^\eta f'^2 \, d\eta \right]_{\eta = \eta_{.99}} \qquad \text{(III-9)}$$

$\eta_{.99}$ = value of $\eta$ where $u/u_e = 0.99$

$$\frac{\delta^* R_x^{1/2}}{x} = \frac{\sqrt{2}}{1 - S} \int_0^\infty (g_w + Sf')(1 - f') \, d\eta \qquad \text{(III-10)}$$

$$\frac{\theta R_x^{1/2}}{x} = \sqrt{2} \int_0^\infty f'(1 - f') \, d\eta \qquad \text{(III-11)}$$

$$C_f = \sqrt{\frac{2}{R_x}} \left( \frac{g_w}{1 - S} \right)^{n-1} f''(0) \qquad \text{(III-12)}$$

$$H = \frac{\delta^*}{\theta} \qquad \text{(III-13)}$$

Equation (III-2) was integrated numerically by the Runge-Kutta-Gill method. Following Back, quasi-linearization was used to facilitate application of the boundary conditions. The FORTRAN computer program executes in approximately 6 minutes on the IBM 1130 and in 1.5 seconds on the CDC-6600.
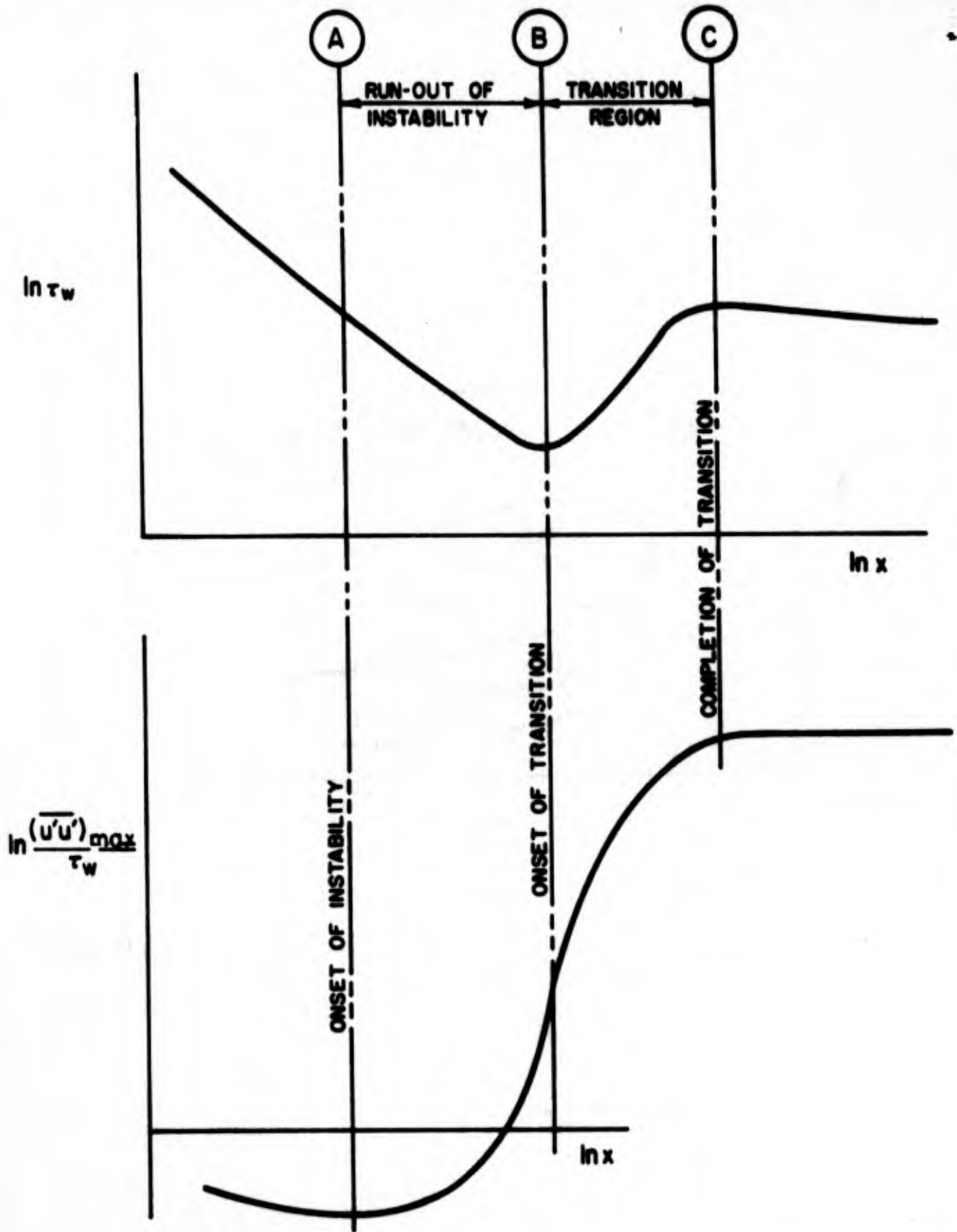
Figure 1. Results of hypothetical measurements of $\tau_w$ and $\overline{(u'u')}_{max}$ for a boundary layer on a flat plate with disturbances introduced upstream of the initial measurements
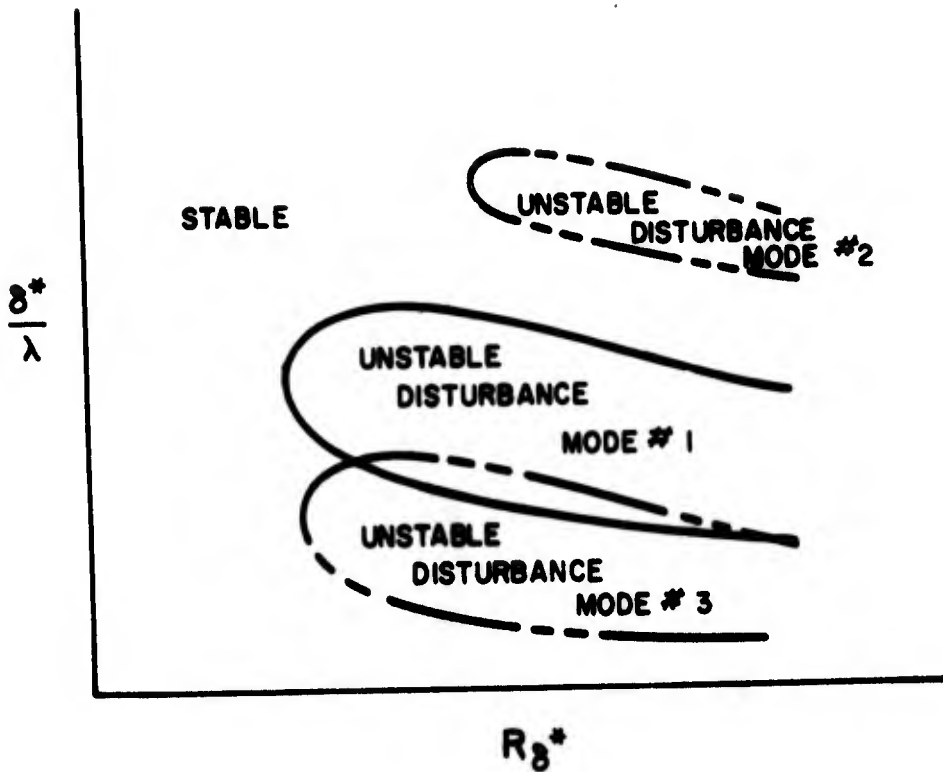
Figure 2. Typical stability diagram in which several different types of disturbance are introduced
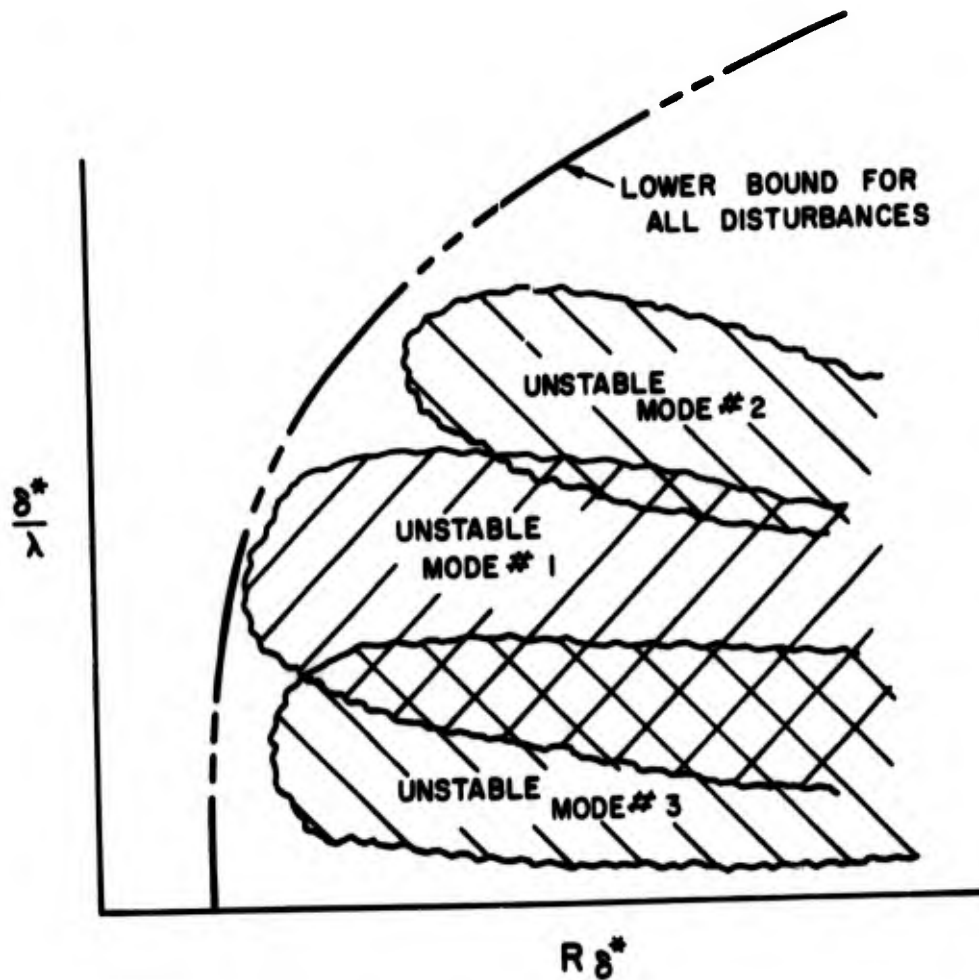
Figure 3. Probable spreading of regions of instability due to environmental effects. A reference line is shown indicating a possible lower bound for all disturbances.
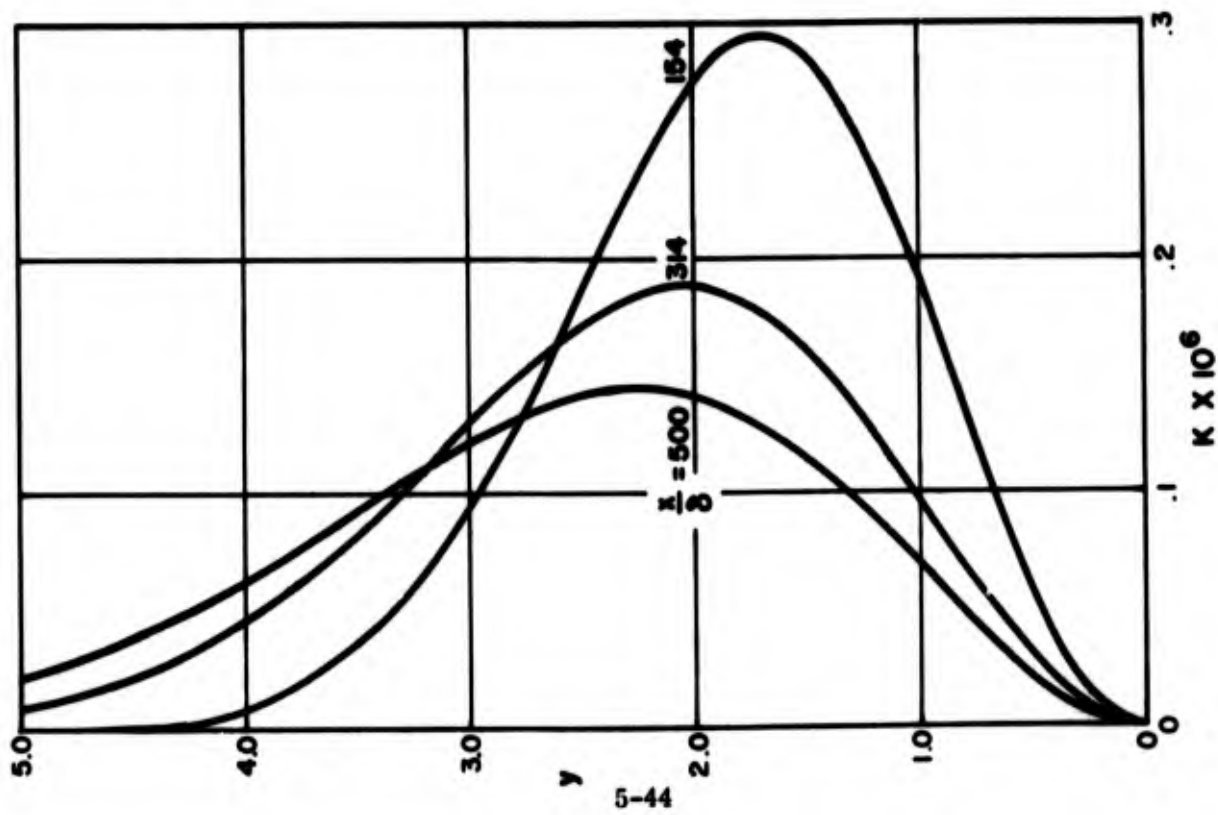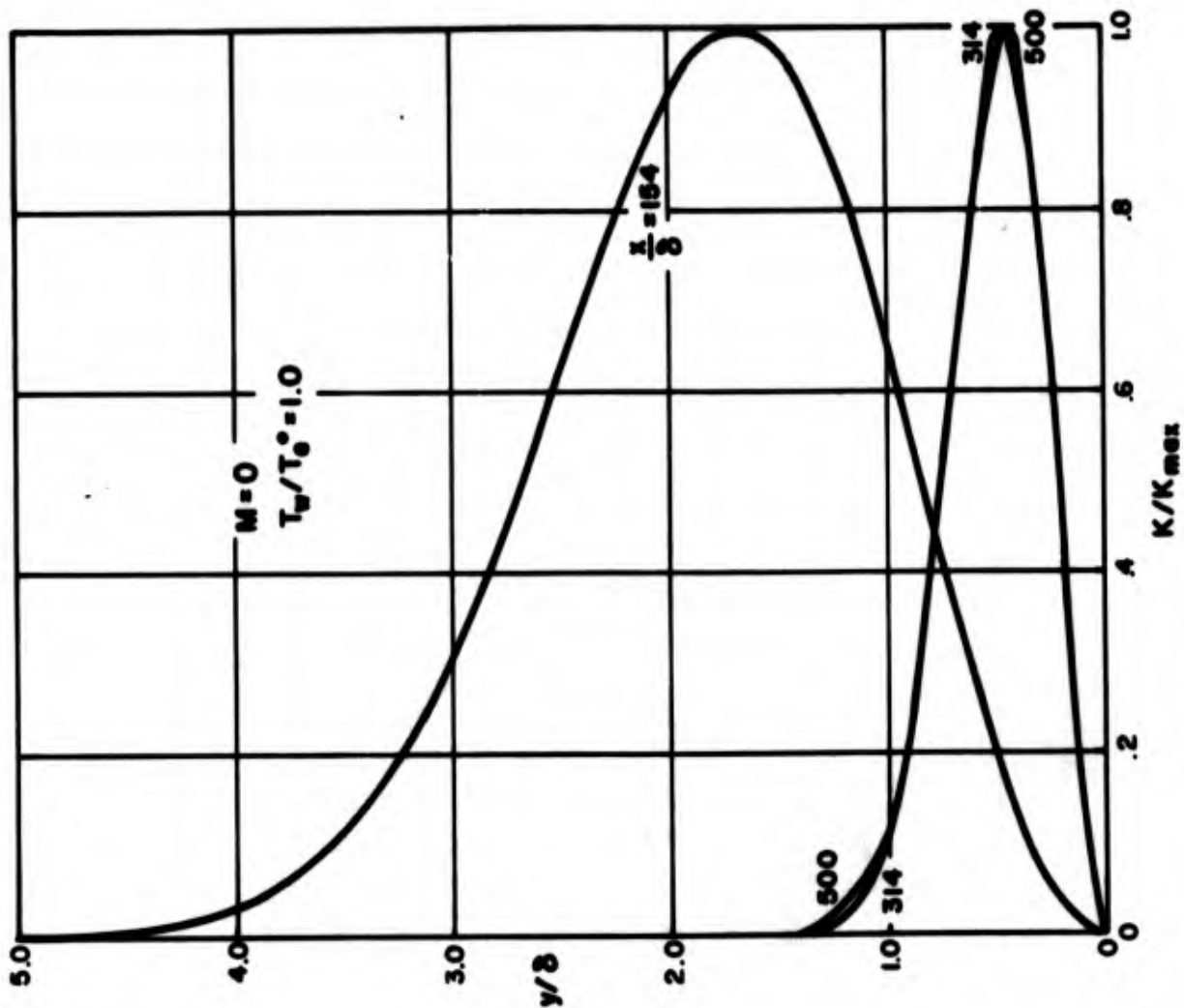
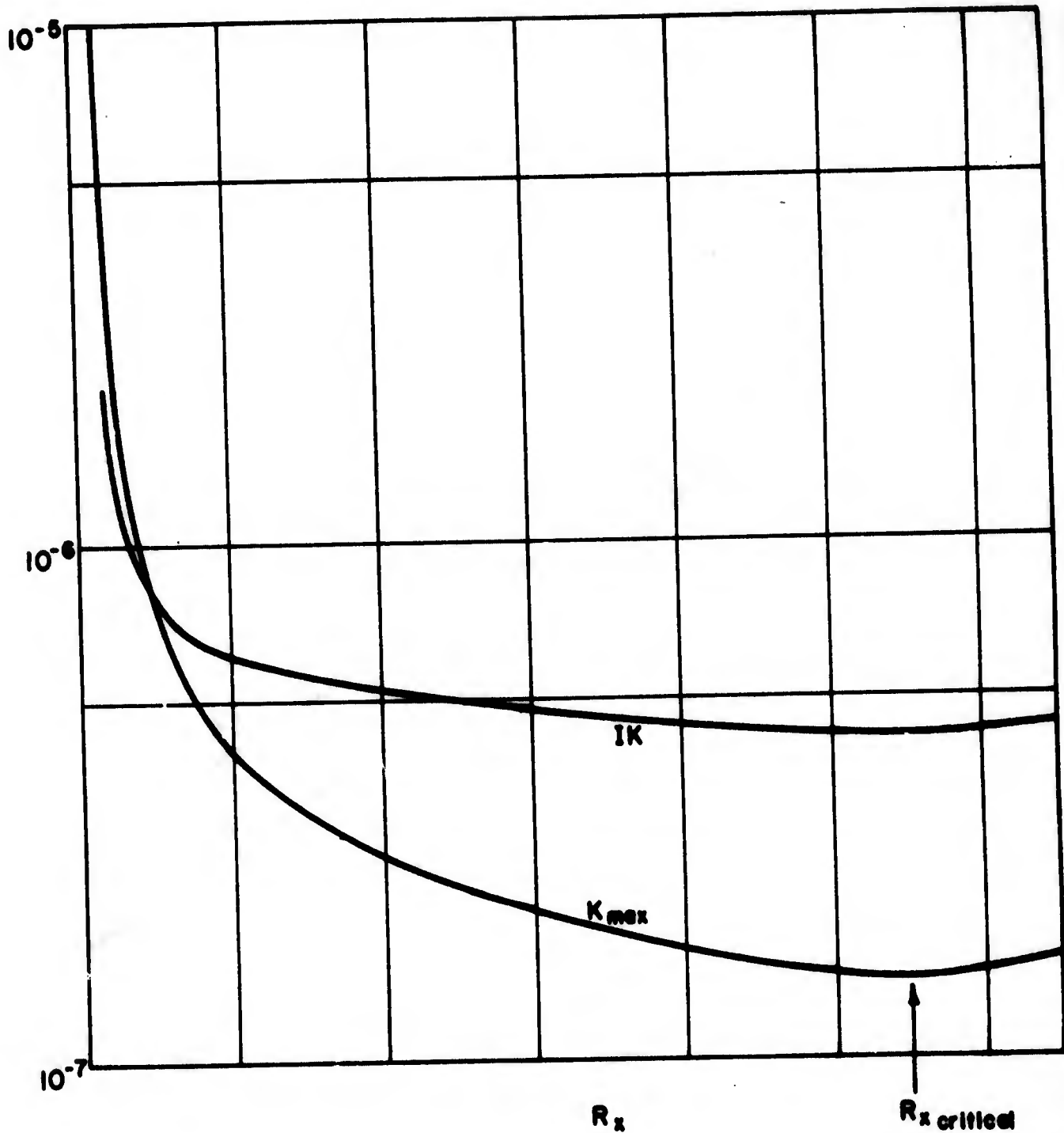Figure 4. Typical behavior of disturbance profiles with $x/\delta$

5-44

Figure 5. Typical behavior of $K_{max}$ and IK with $R_x$ for $M = 0$ and $T_w/T_e^o = 1.0$
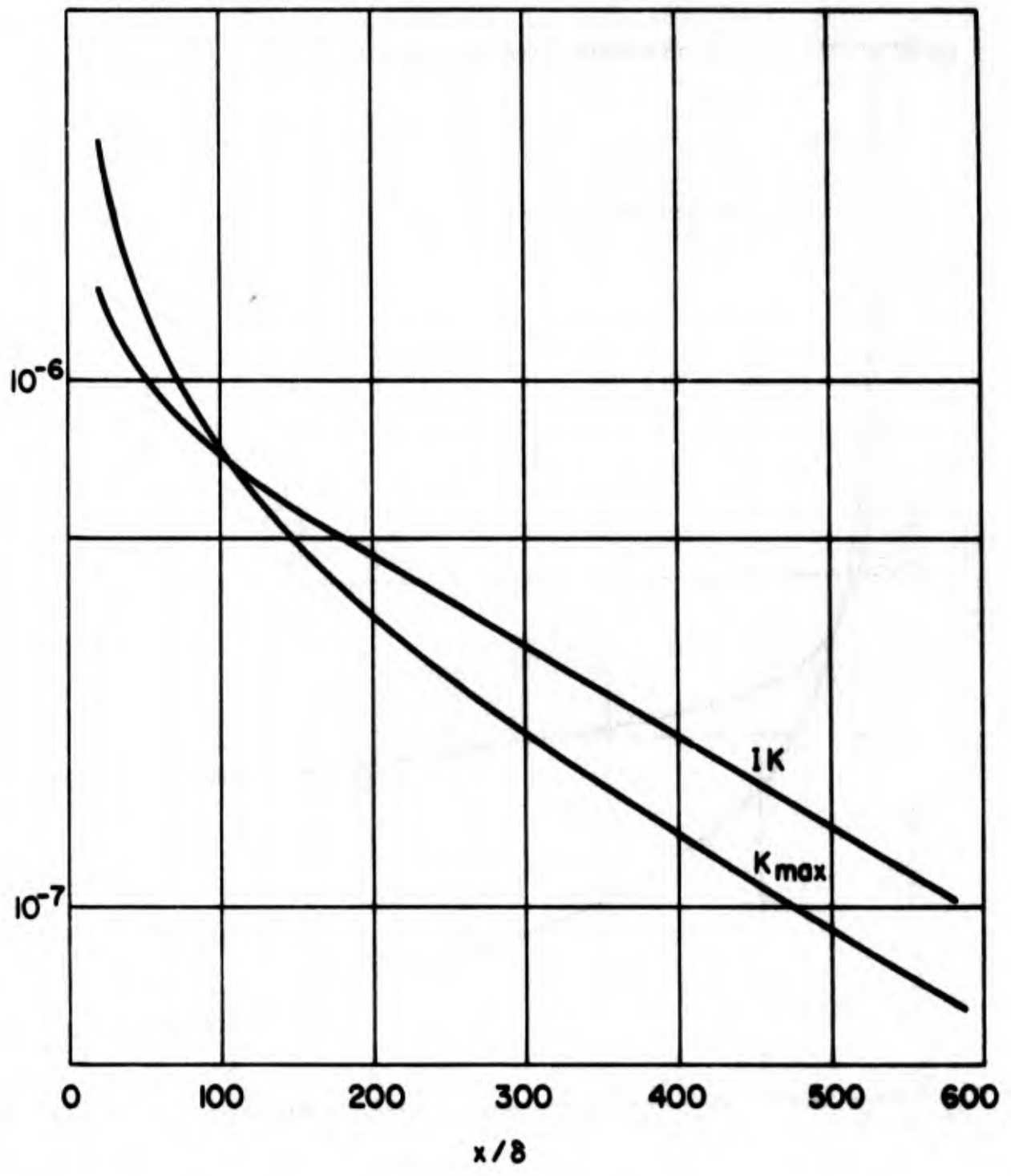
5-45

Figure 6. Behavior of $K_{max}$ and $IK$ after introduction of disturbances for $R_\delta = 600$, $M = 0$, and $T_w/T_e^o = 1.0$
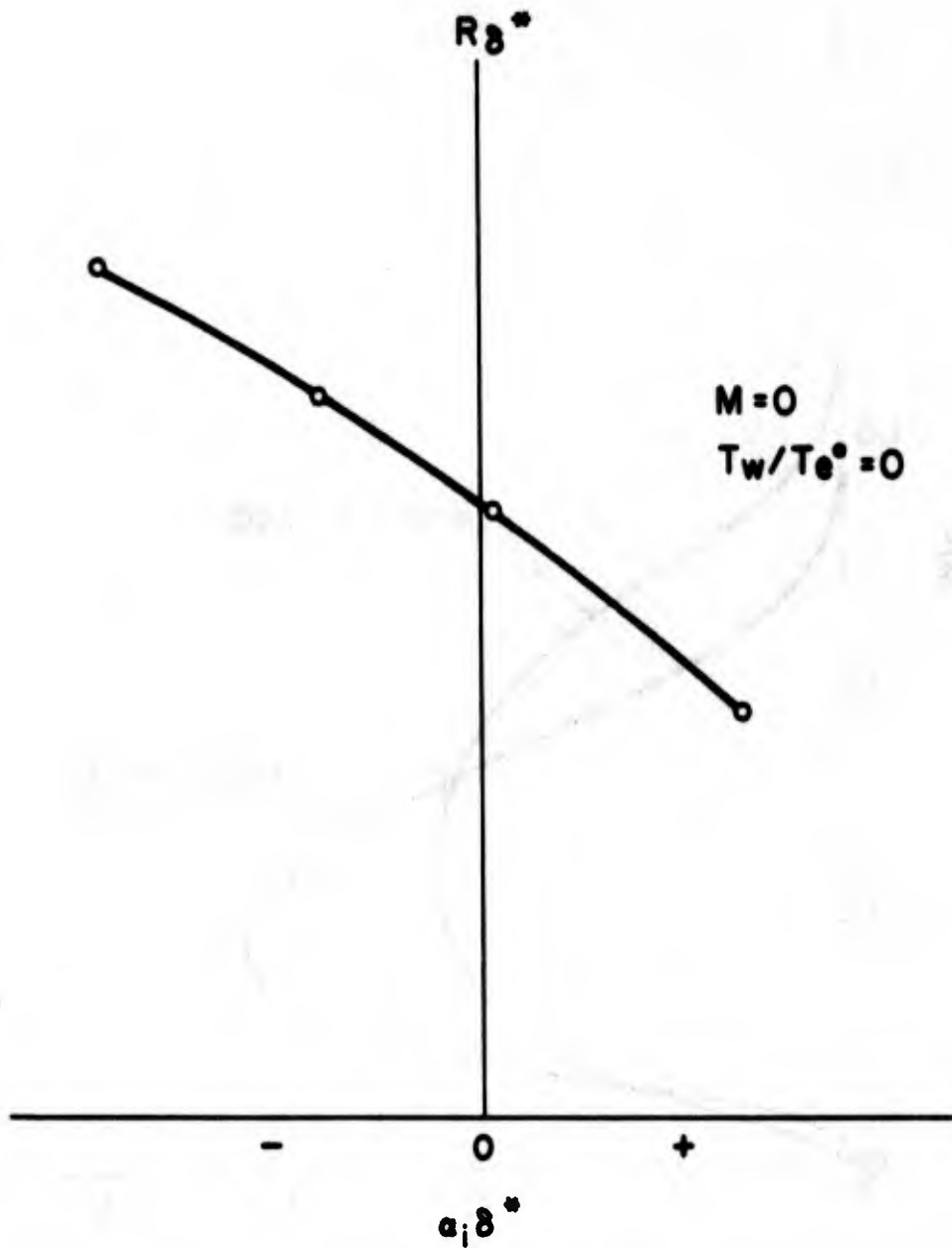
Figure 7. Typical plot used for the determination of the critical Reynolds number $R_{\delta* \text{ crit}} = R_{\delta*}(\alpha_1 \delta* = 0)$
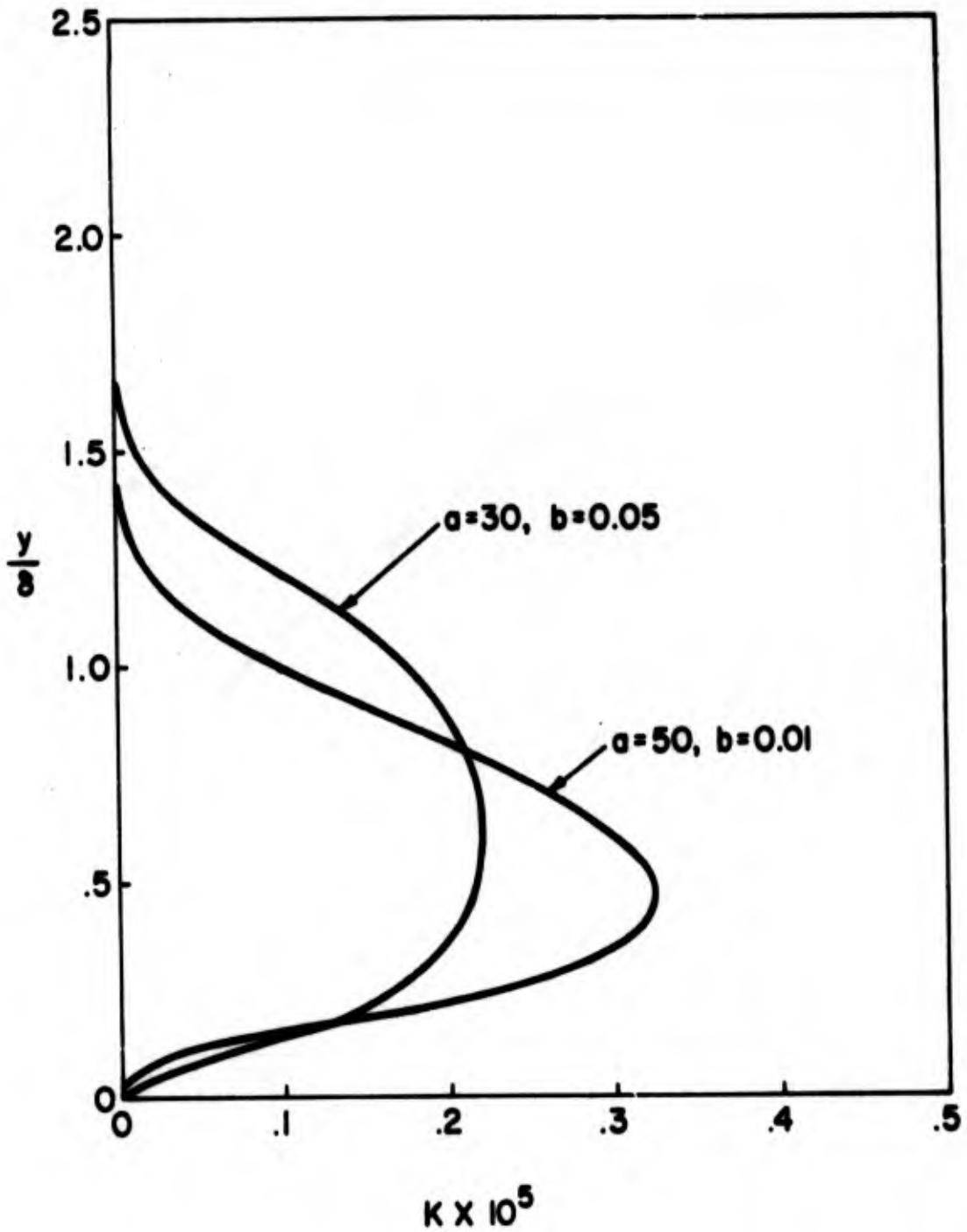
Figure 8. Comparison of typical disturbance distribution shapes for the two models: a = 30, b = 0.05 and a = 50, b = 0.01. $R_\delta \cong 1100$, $x/\delta \cong 30$, M = 0, and $T_w/T_e^o = 1.0$

Figure 9. Amplification $\alpha_1 \delta*$ as a function of $R_{\delta*}$ at $M = 0$ for several wall cooling ratios

5-49

Figure 10.  Amplification $\alpha_1 \delta*$  as a function of  $R_{\delta*}$  at  M = 3 for several wall cooling ratios

5-50

Figure 11.   Amplification $\alpha_i\delta*$ as a function of $R_{\delta*}$ at $M = 6$ for several wall cooling ratios
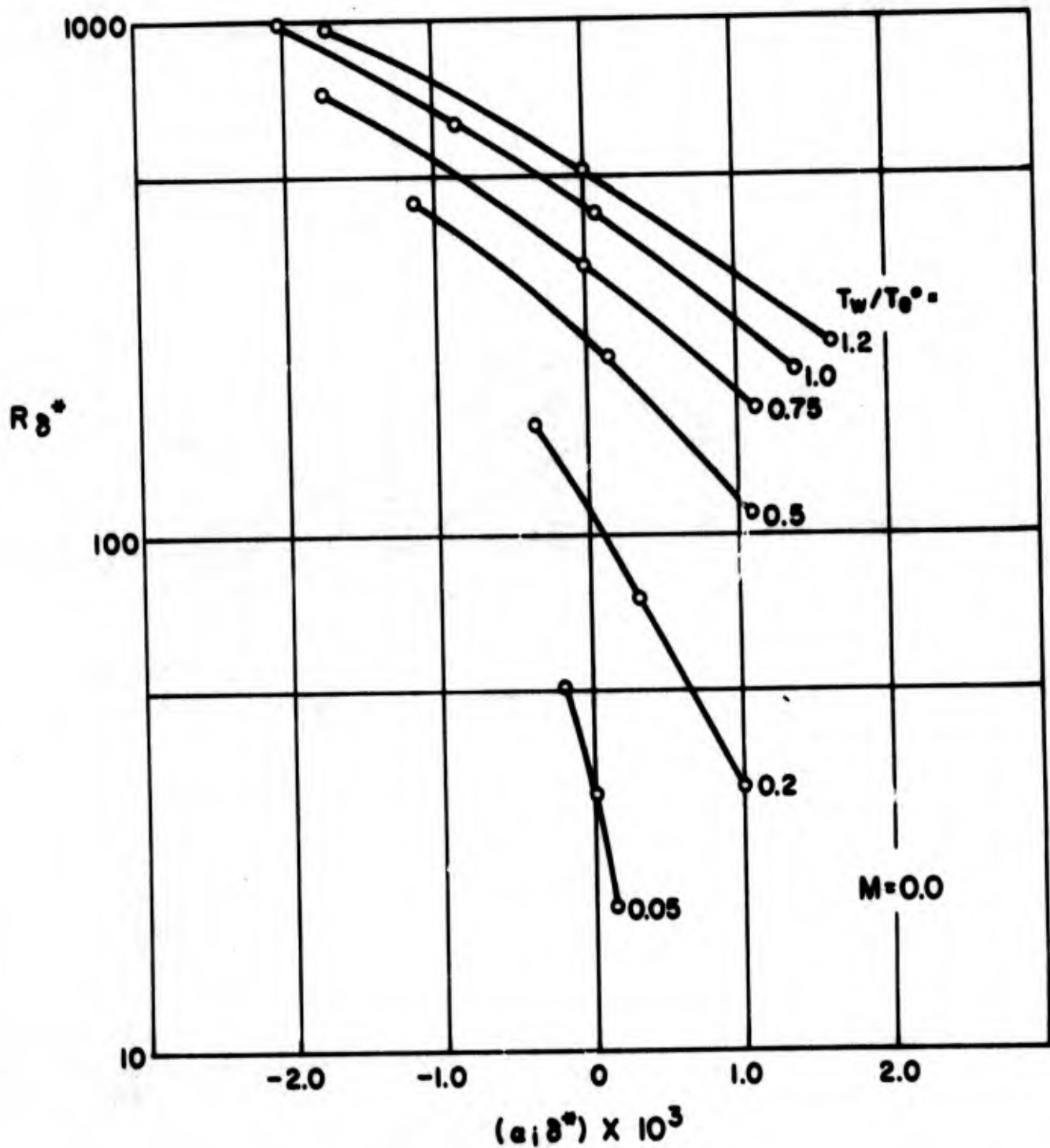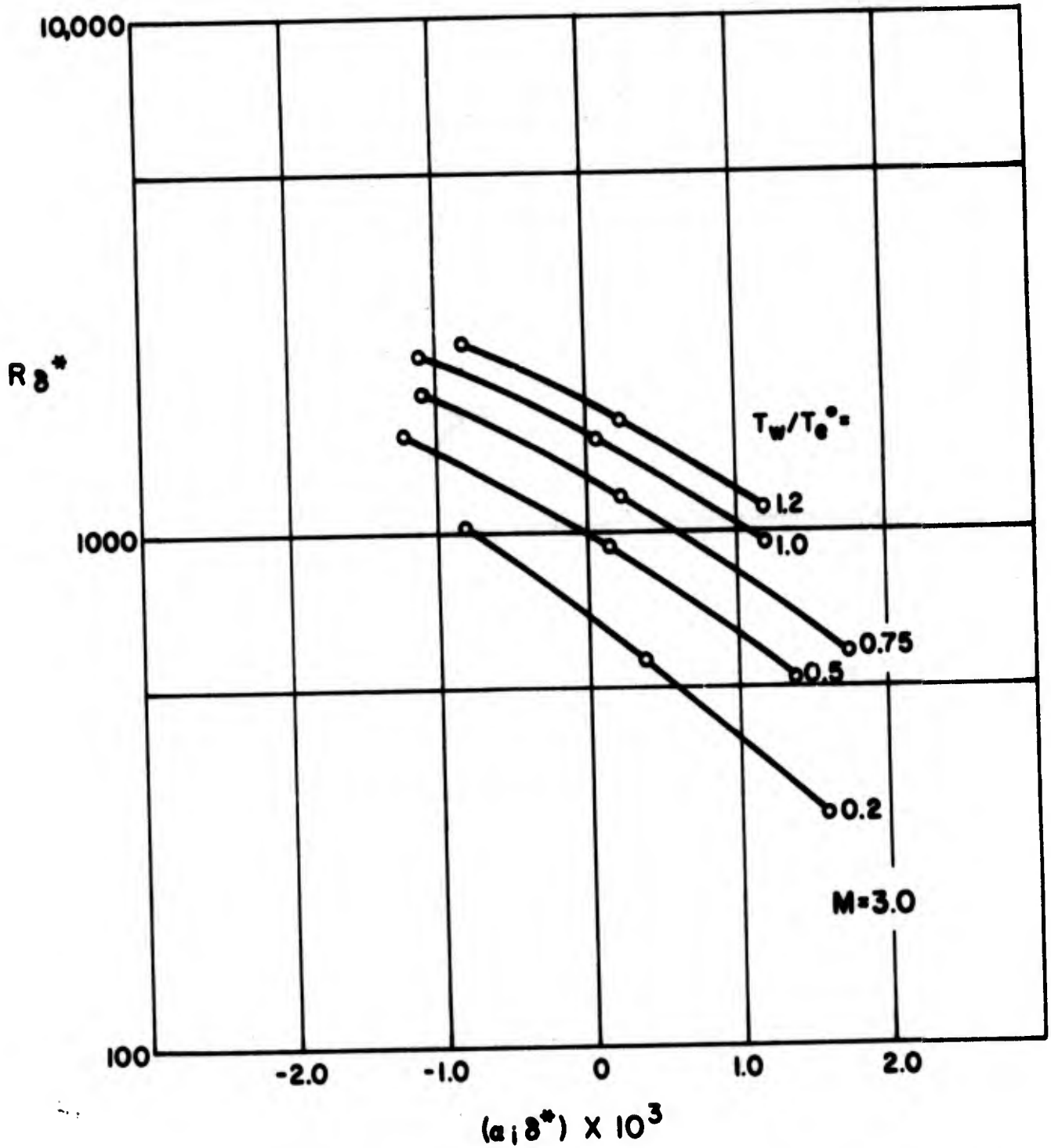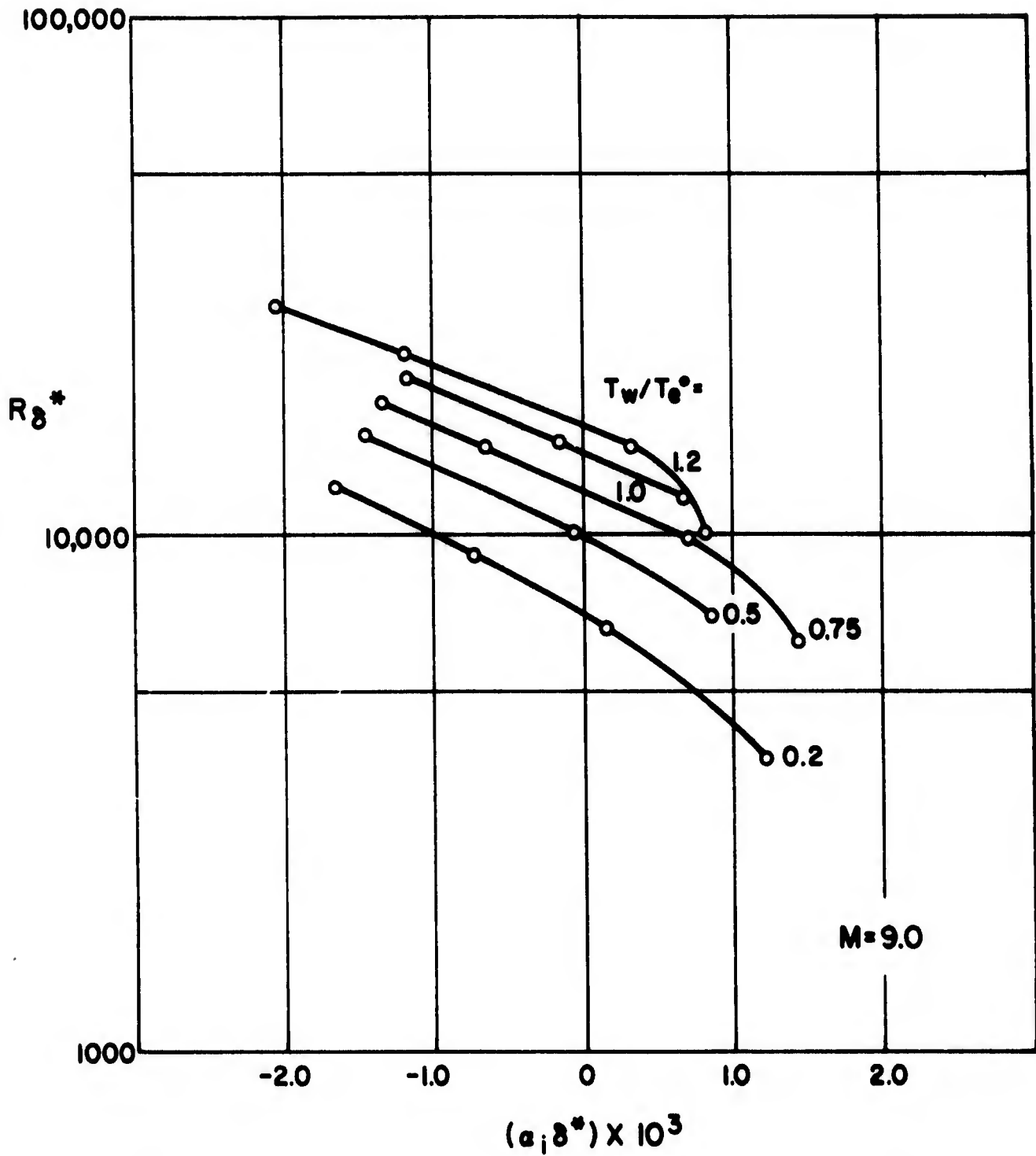
Figure 12. Amplification $\alpha_1 \delta*$ as a function of $R_{\delta*}$ at $M = 9$ for several wall cooling ratios
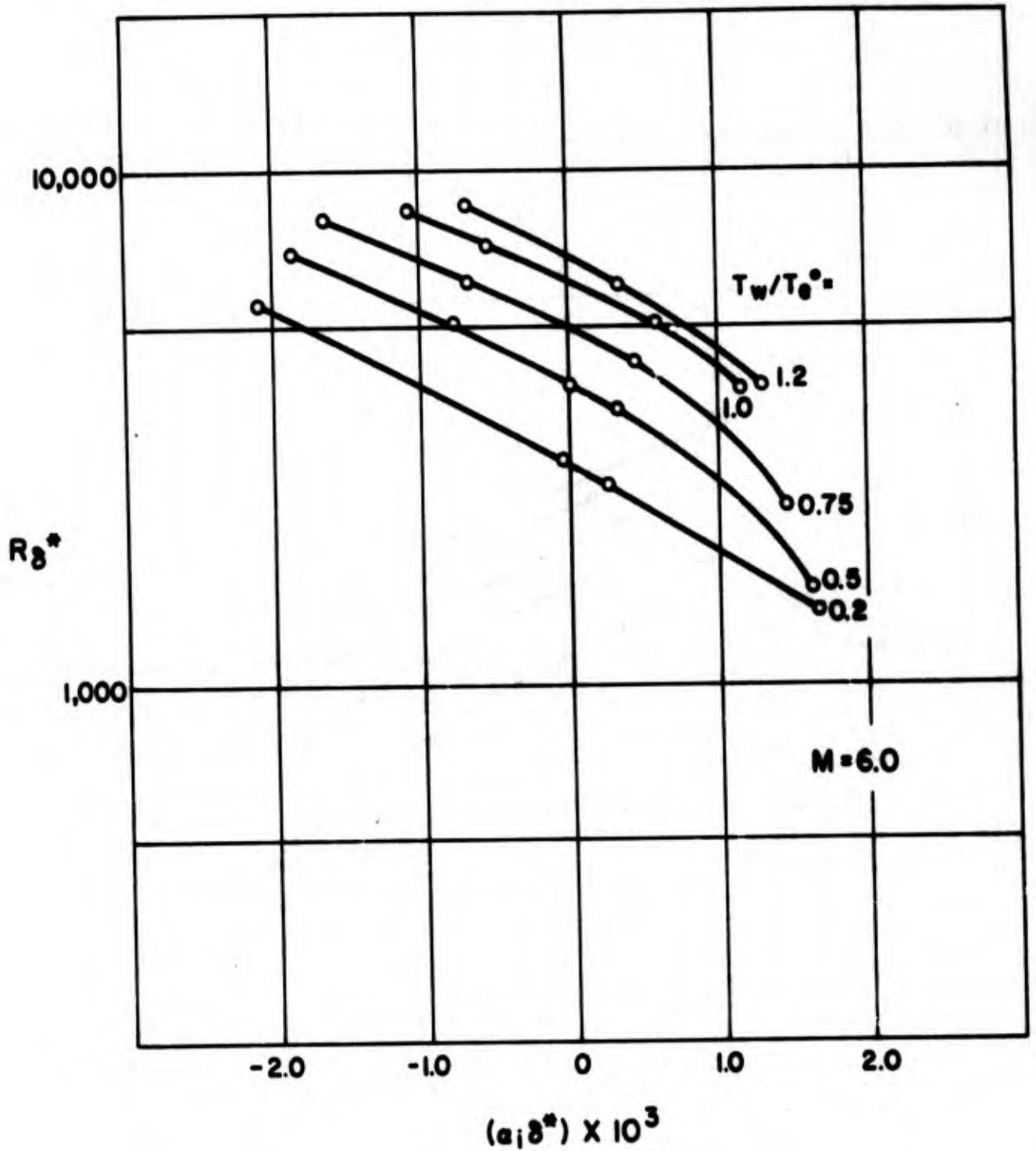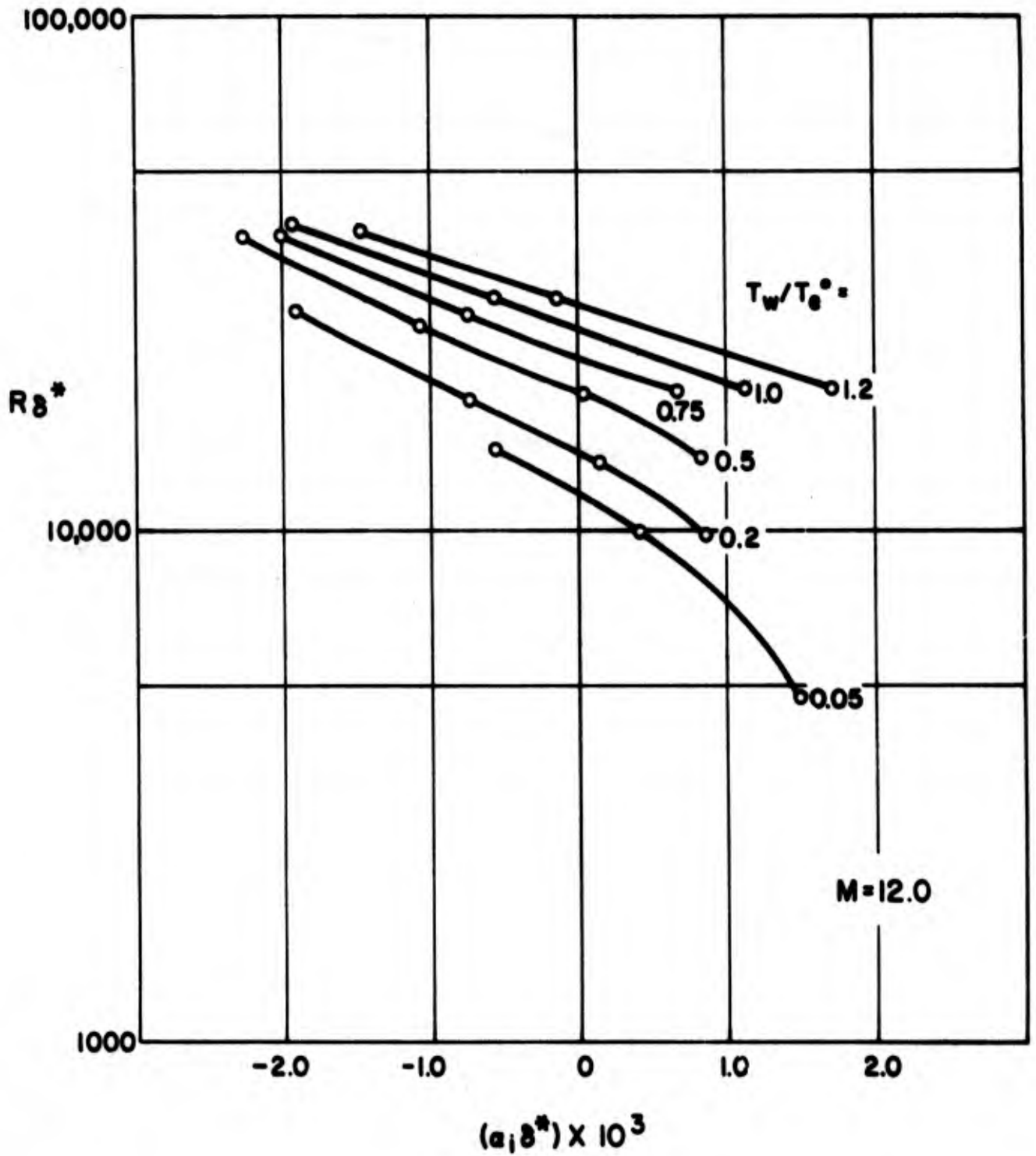
Figure 13. Amplification $\alpha_1 \delta^*$ as a function of $R_{\delta^*}$ at $M = 12$ for several wall cooling ratios
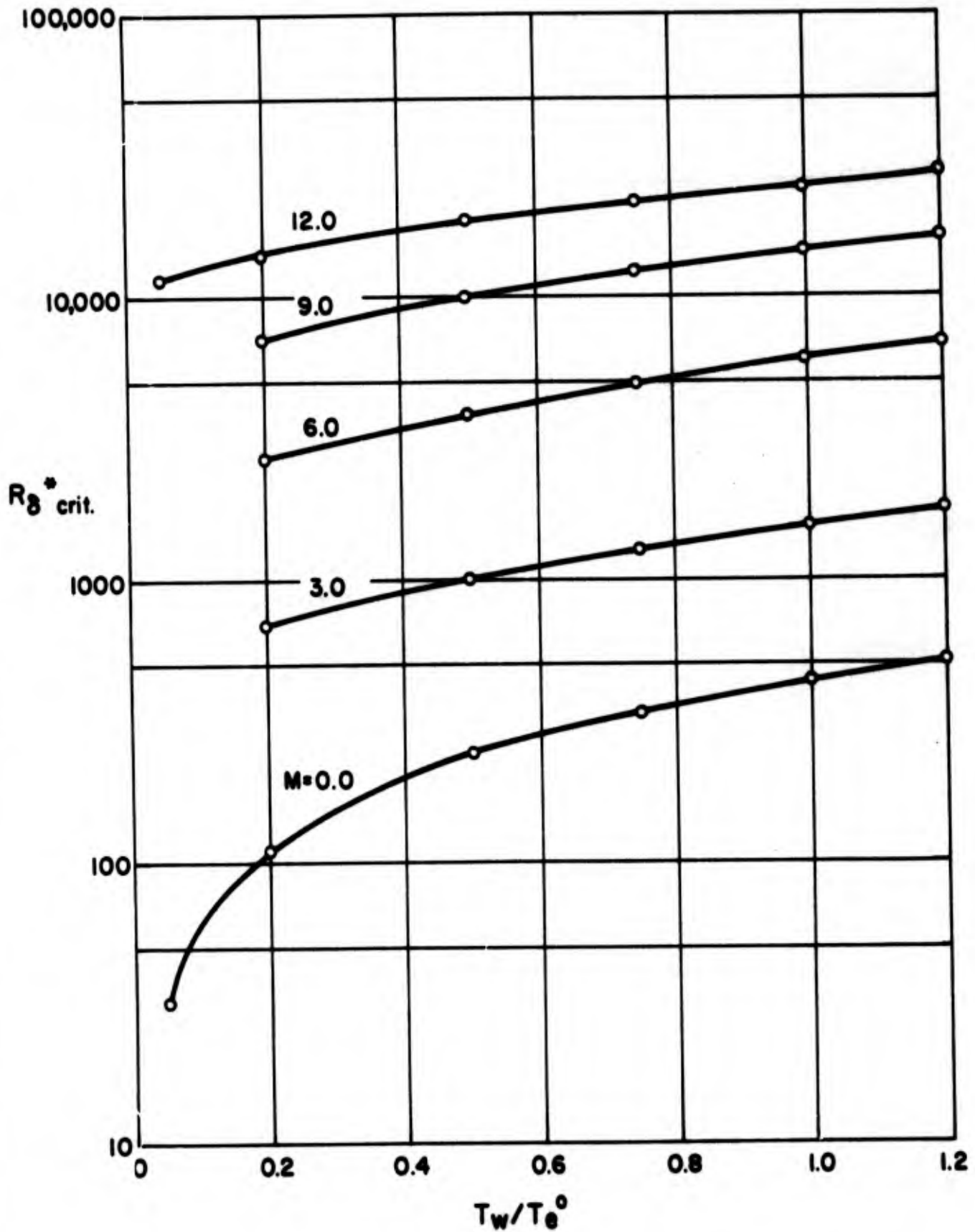
Figure 14.   Dependence of critical Reynolds number based on $\delta^*$ on wall cooling ratio for several Mach numbers
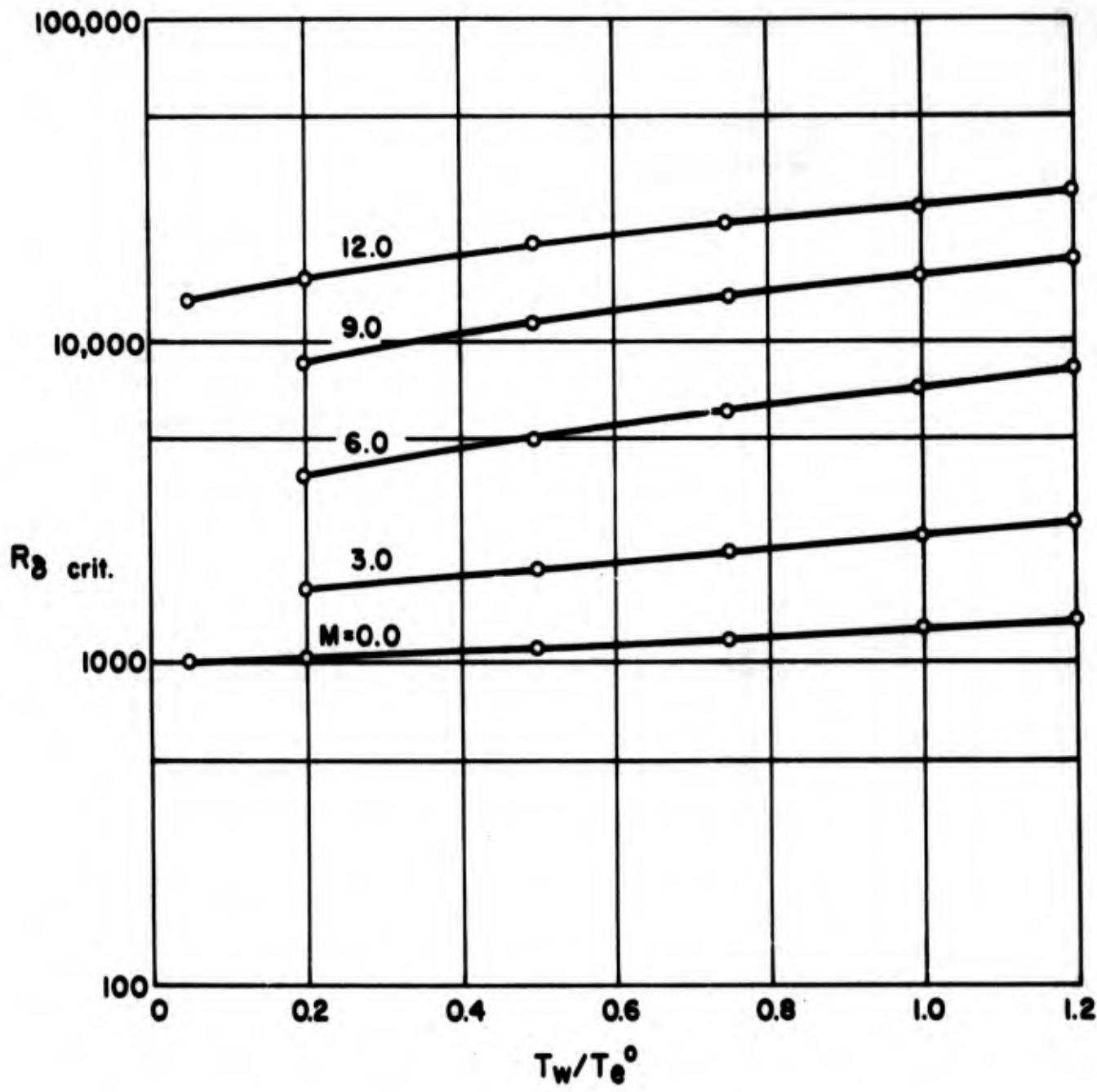
Figure 15. Dependence of critical Reynolds number based on δ on wall cooling ratio for several Mach numbers
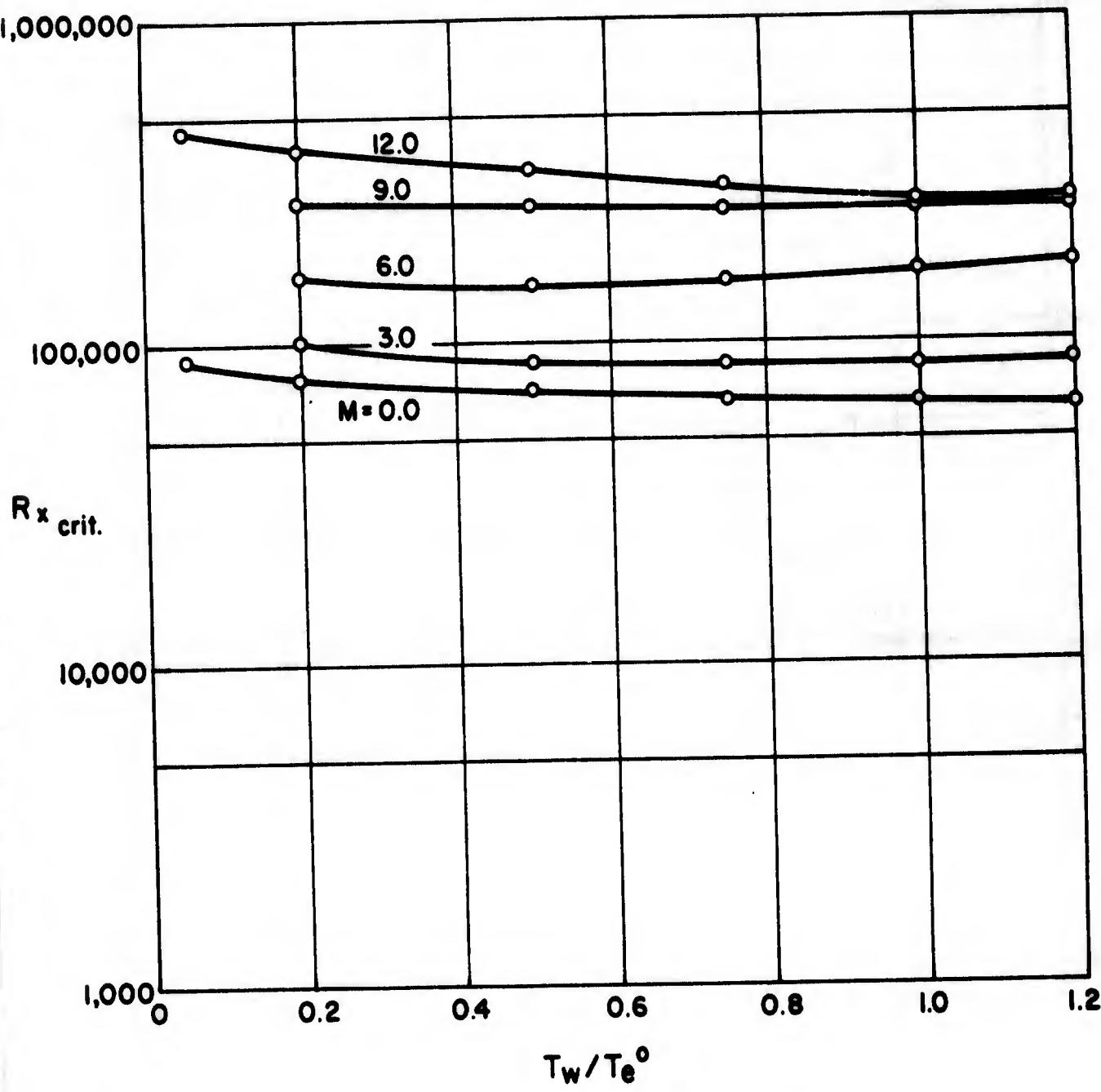
Figure 16. Dependence of critical Reynolds number based on wetted length  x  on wall cooling ratio for several Mach numbers
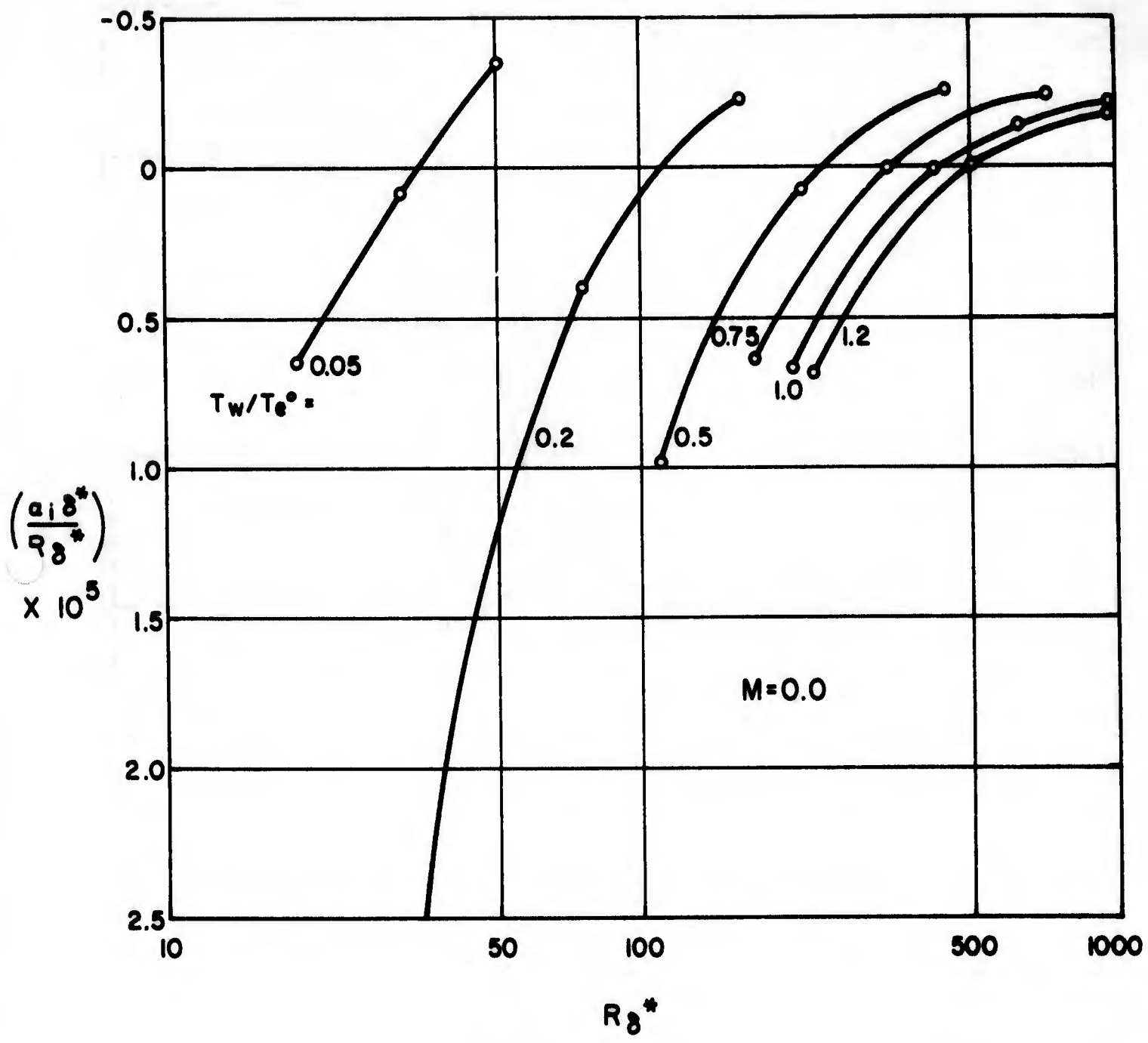
Figure 17. Amplification $\alpha_1\delta^*/R_{\delta*}$ as a function of $R_{\delta*}$ for $M = 0$
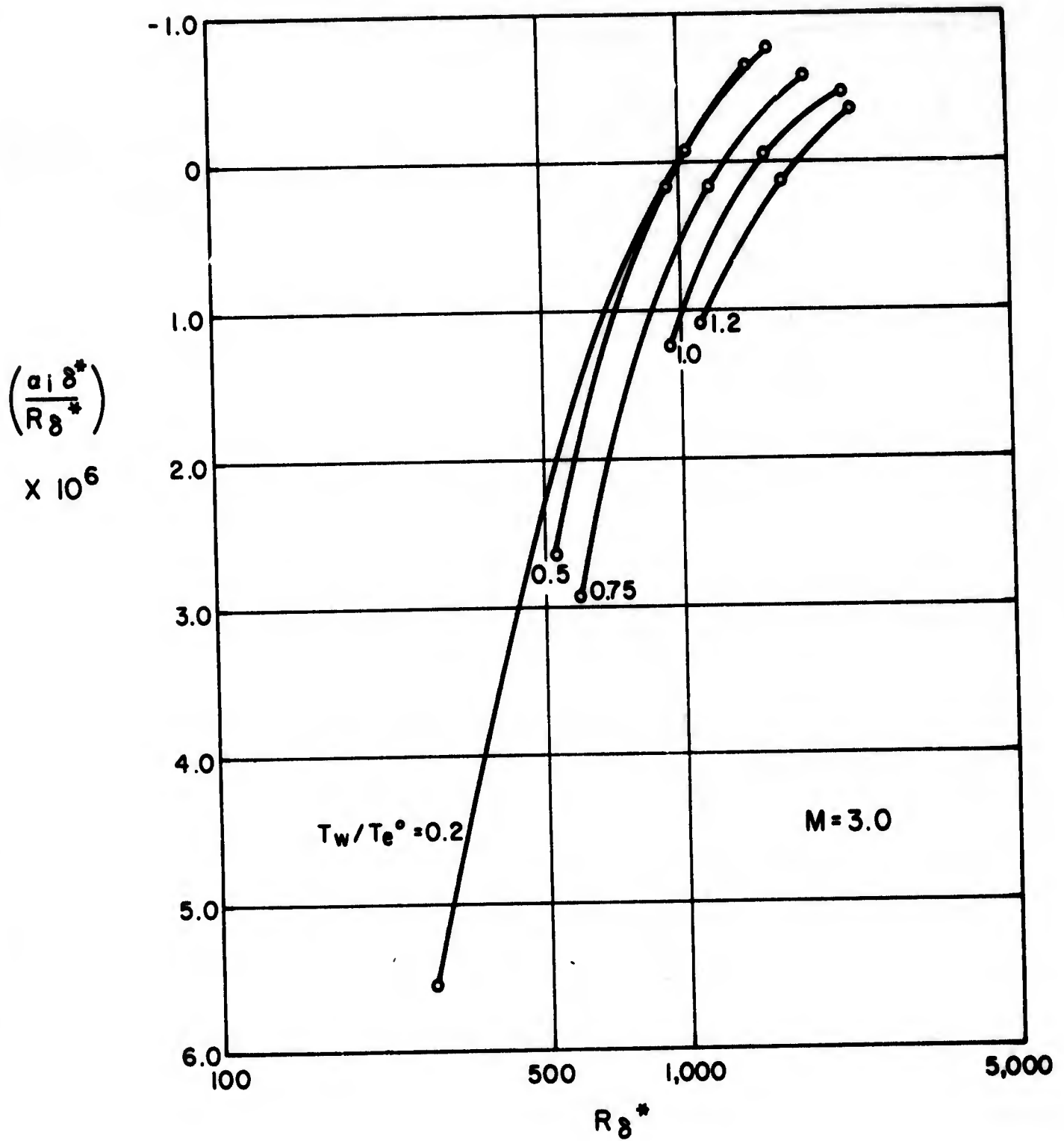
Figure 18. Amplification $\alpha_1 \delta^*/R_{\delta*}$ as a function of $R_{\delta*}$ for $M = 3$

5-58
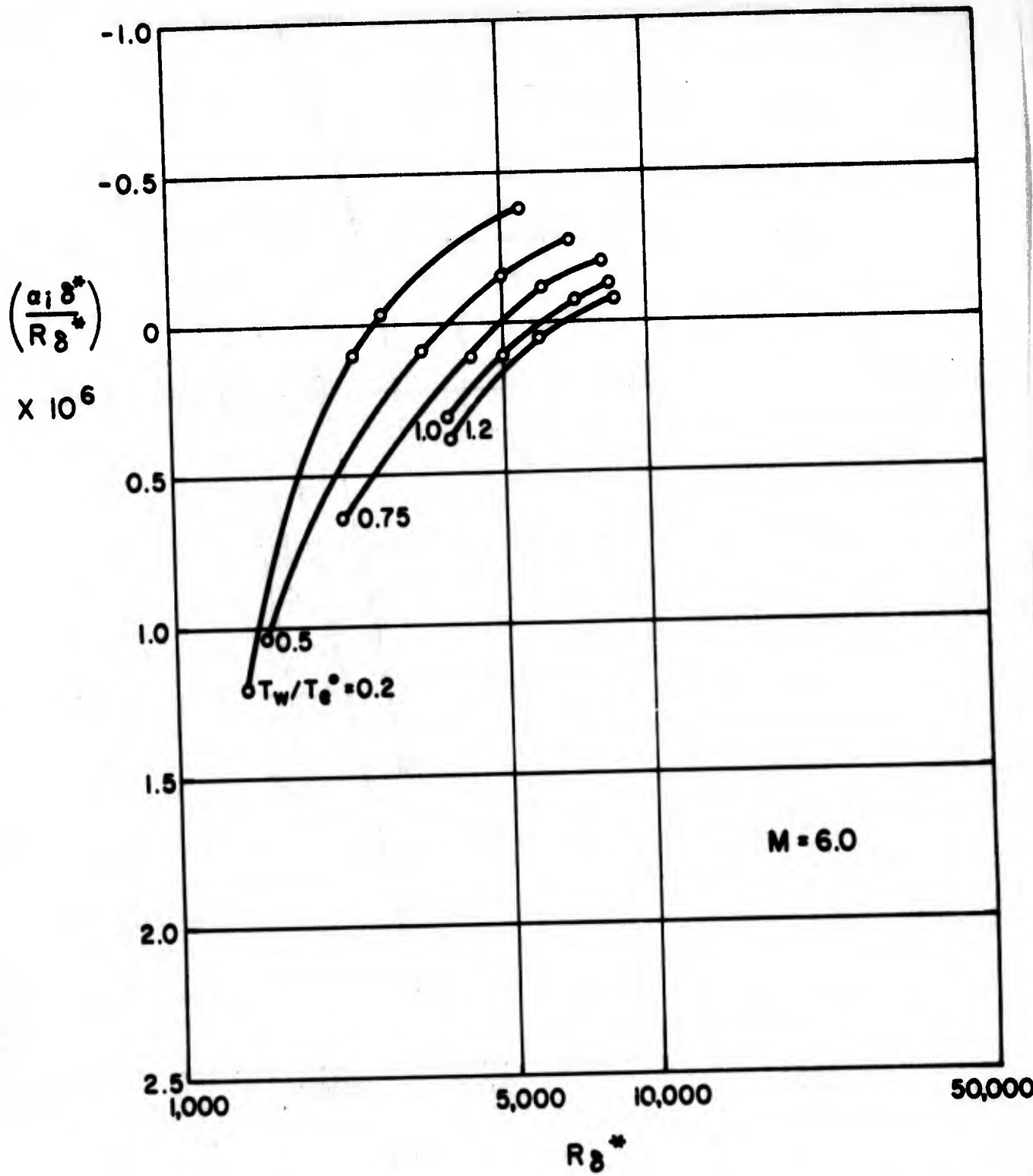
Figure 19.  Amplification  $\alpha_1 \delta^*/R_{\delta*}$  as a function of  $R_{\delta*}$   for  $M = 6$

5-59
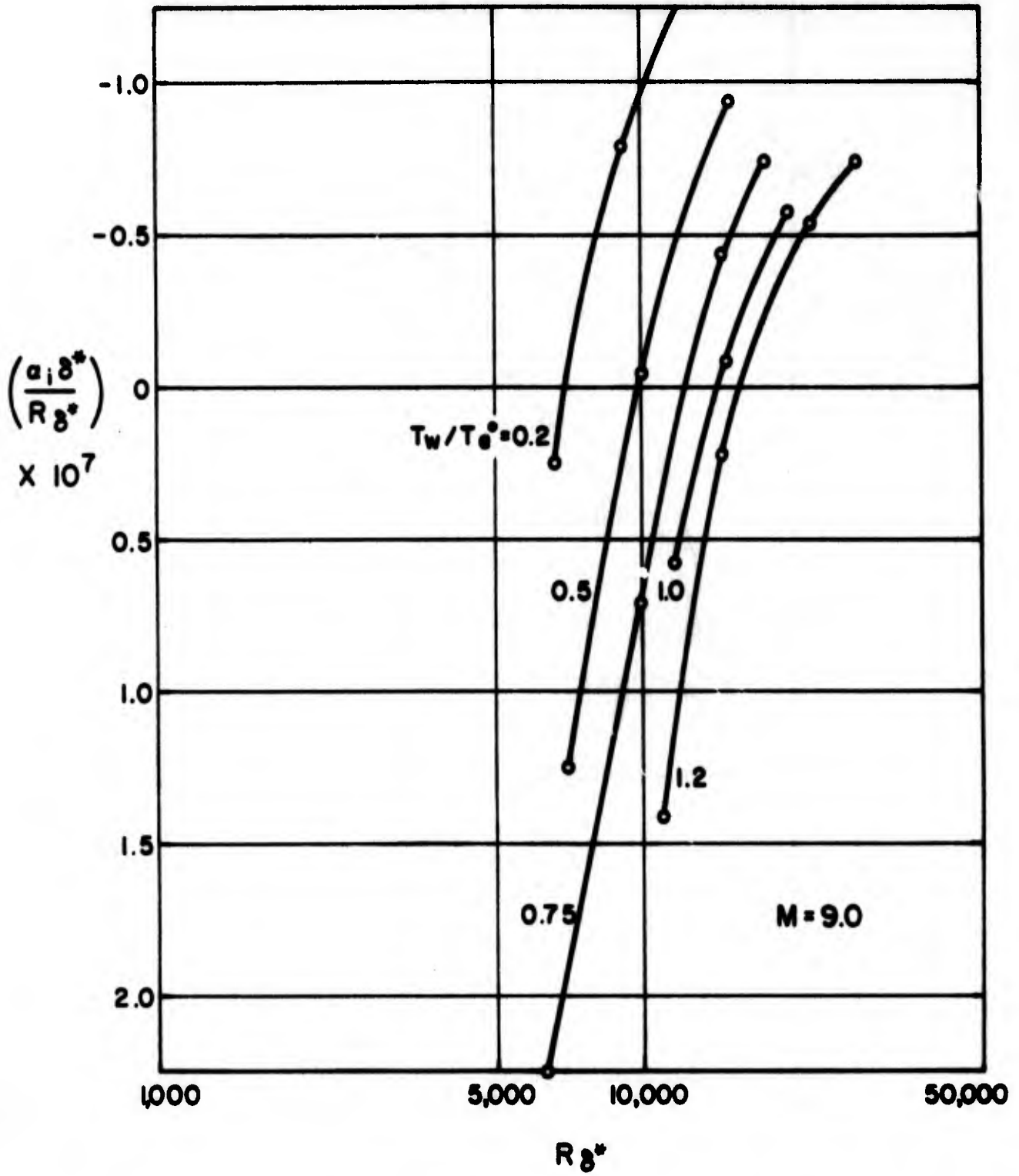
Figure 20. Amplification $\alpha_1 \delta^*/R_{\delta^*}$ as a function of $R_{\delta^*}$ for $M = 9$

5-60
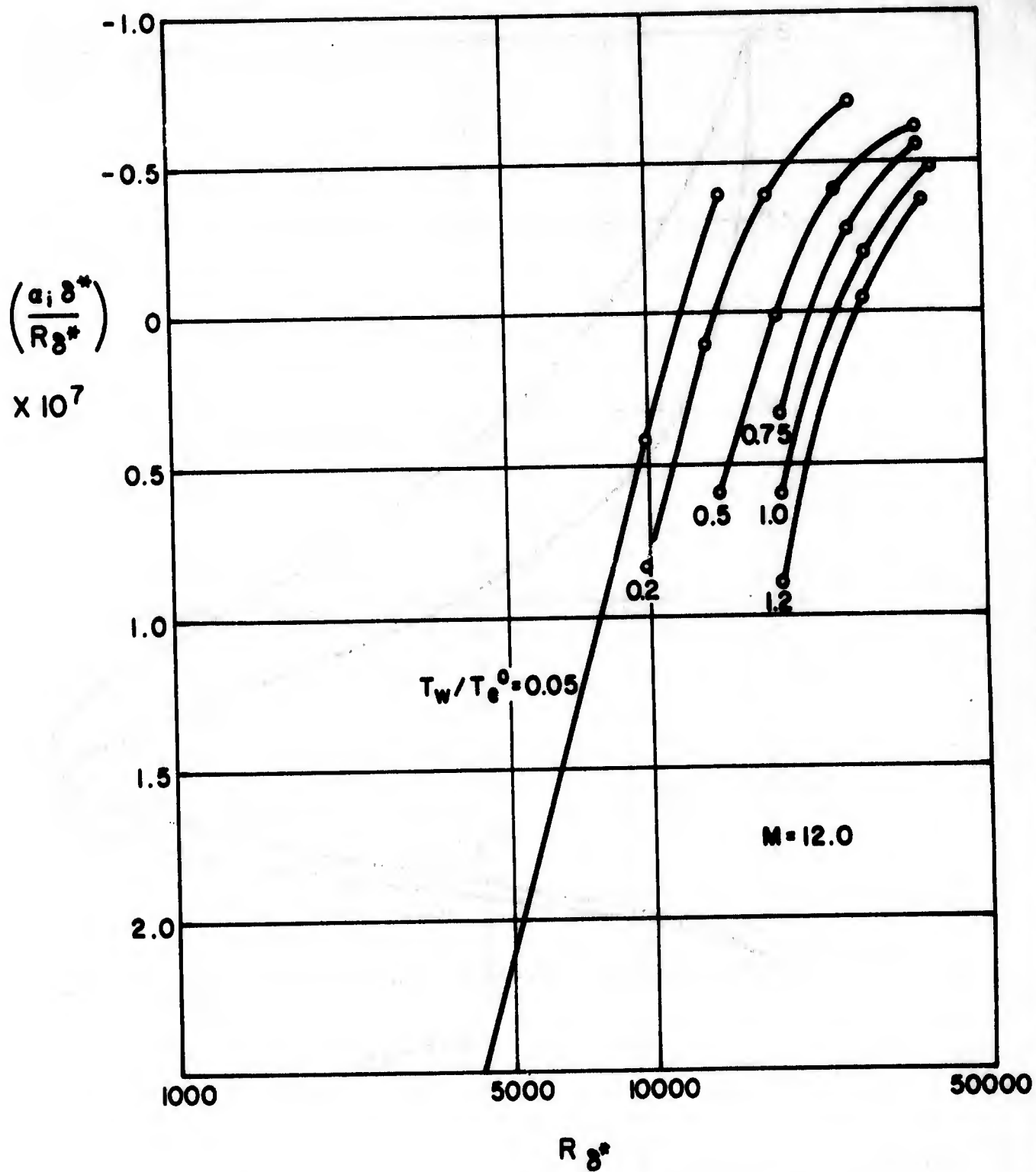
Figure 21. Amplification $\alpha_1 \delta^*/R_{\delta*}$ as a function of $R_{\delta*}$ for $M = 12$
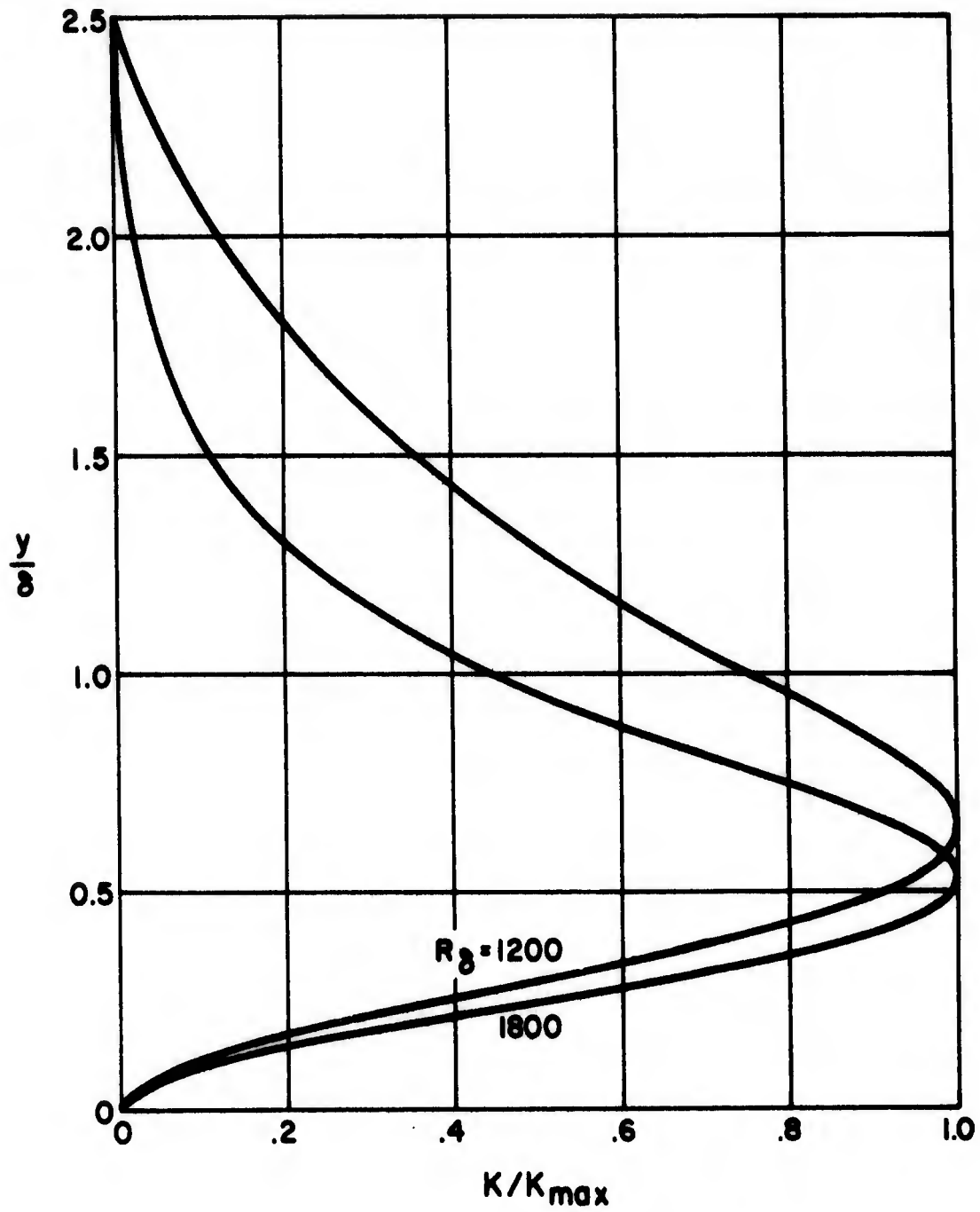
Figure 22. Disturbance shapes for $M = 0$ and $T_w/T_e^o = 1.0$; critical $R_\delta = 1250$
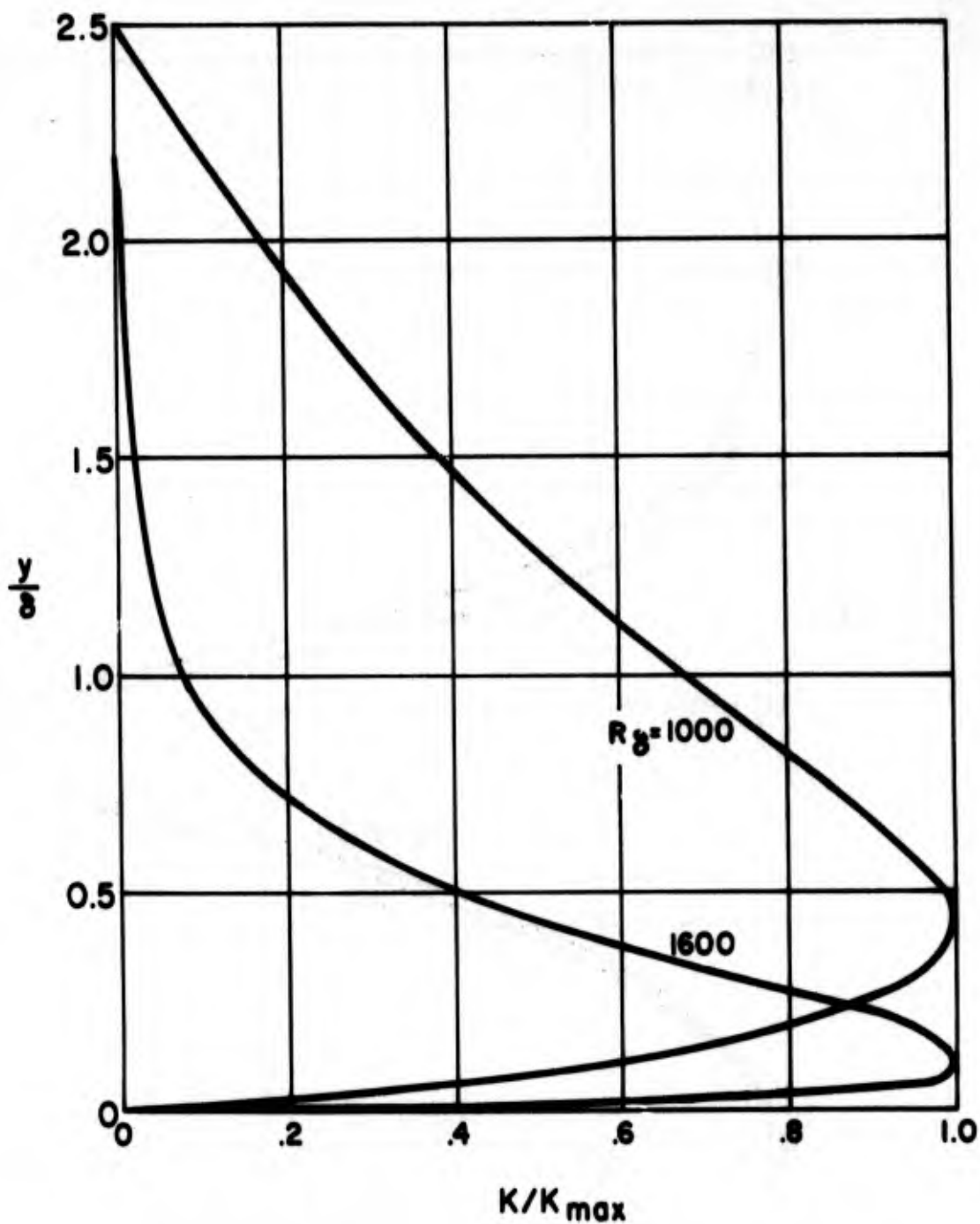
Figure 23. Disturbance shapes for $M = 0$ and $T_w/T_e^o = 0.05$; critical $R_\delta = 1000$
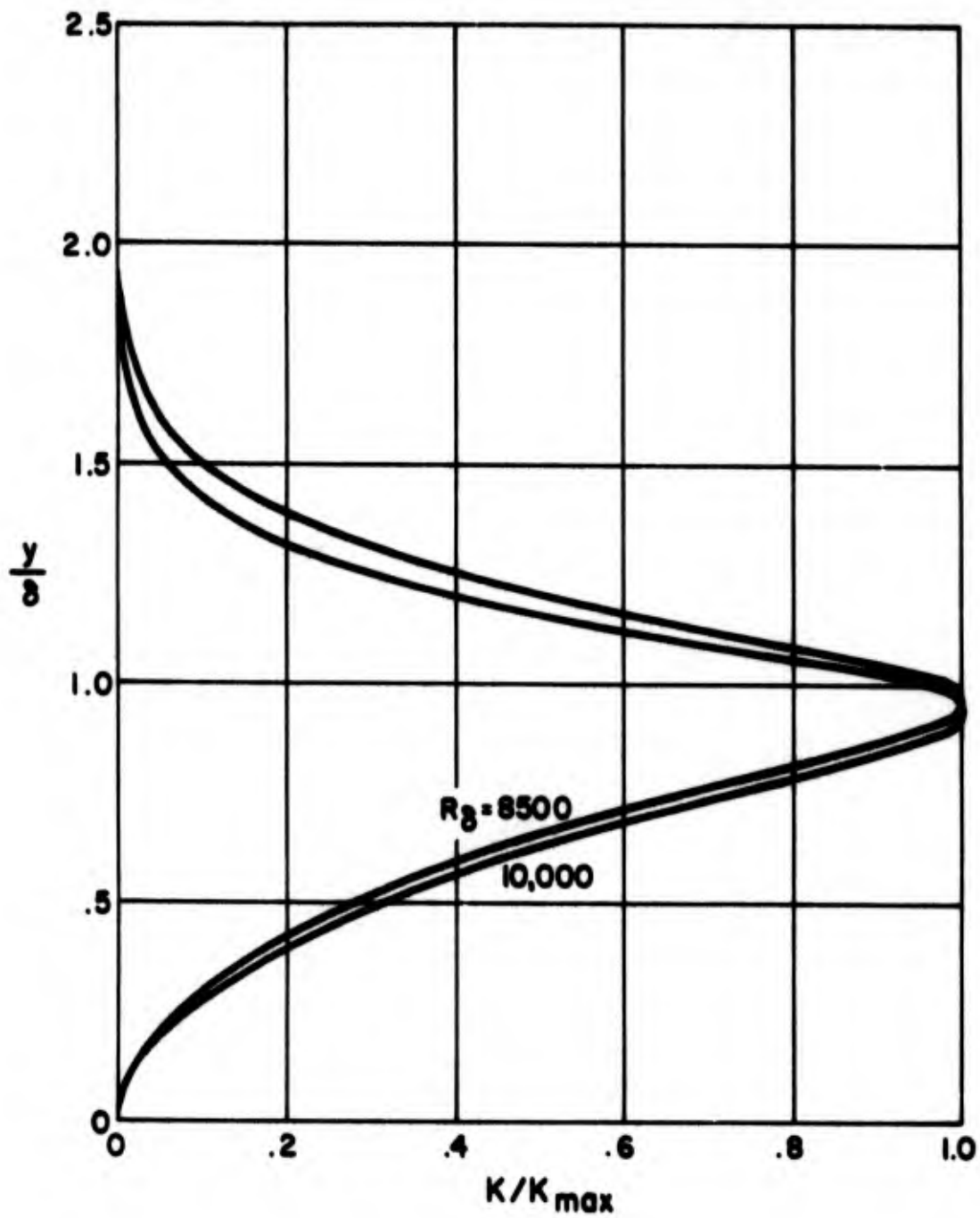
Figure 24.  Disturbance shapes for  $M = 6$  and  $T_w/T_e^o = 1.0$;
critical  $R_\delta = 8000$
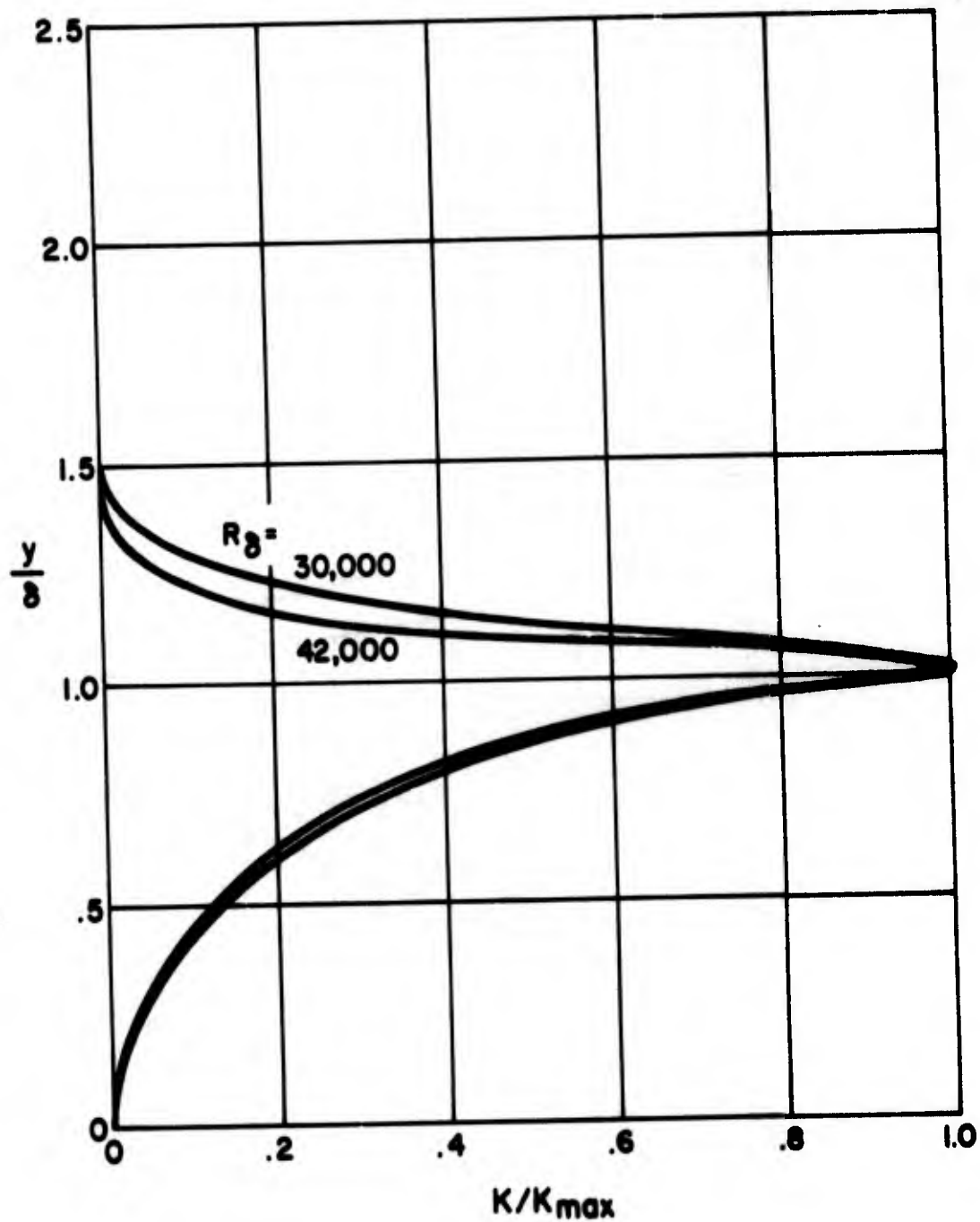
Figure 25. Disturbance shapes for $M = 12$ and $T_w/T_e^o = 1.0$; critical $R_\delta = 29,000$
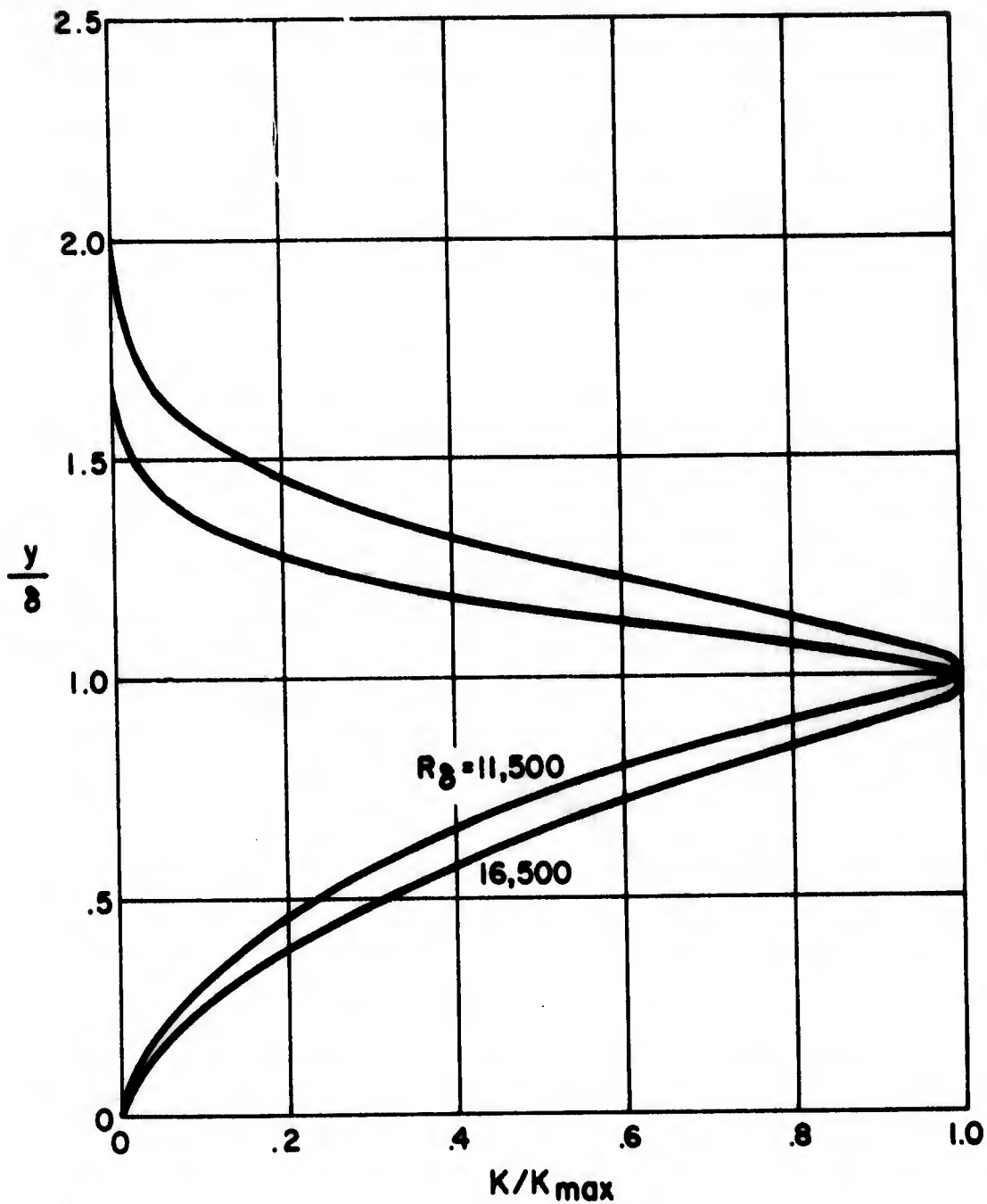
Figure 26. Disturbance shapes for $M = 12$ and $T_w/T_e^o = 0.05$; critical $R_\delta = 13,500$
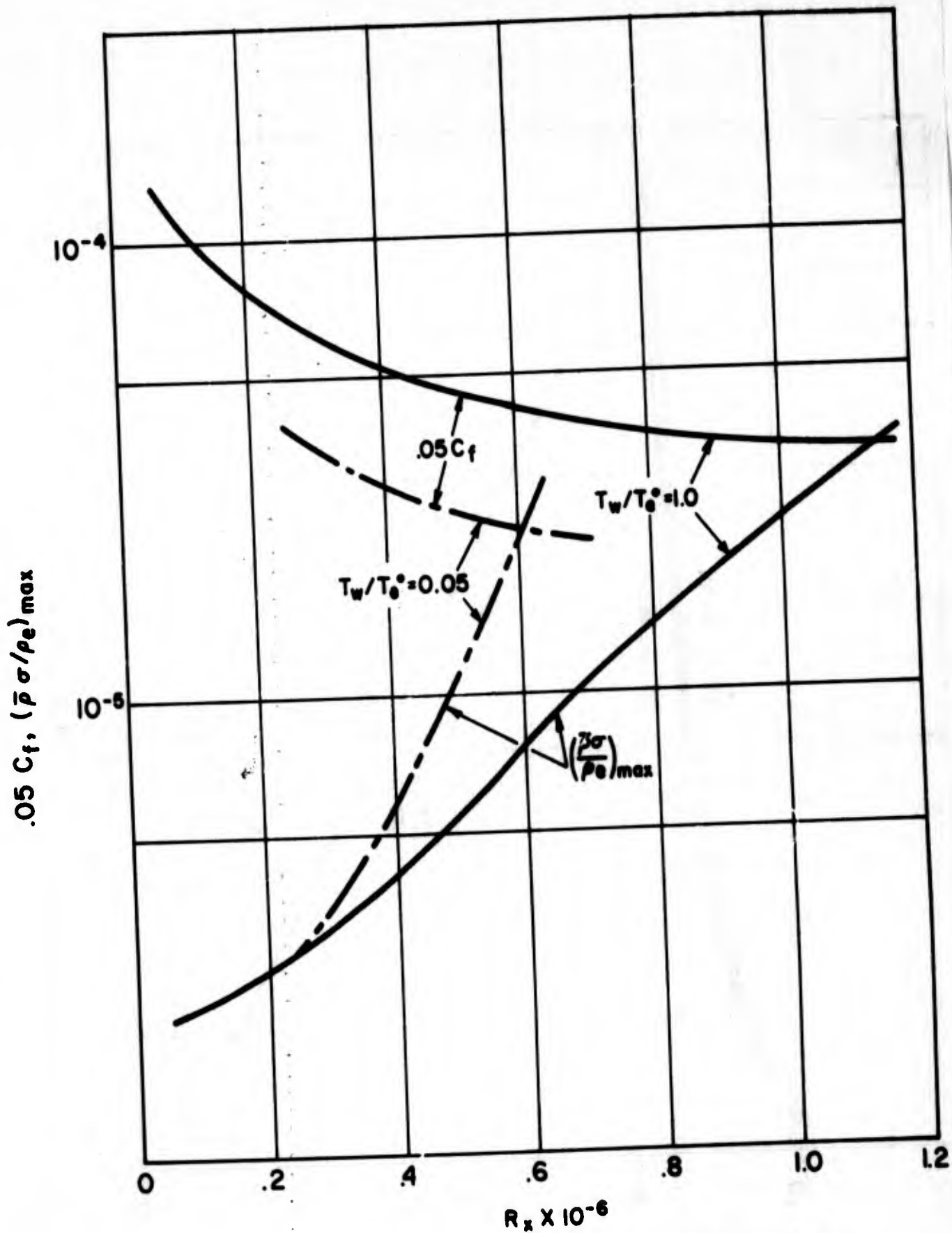
Figure 27.   High disturbance level calculations for   M = 0.
$(K_{max}(0) = 3 \times 10^{-4})$

5-67
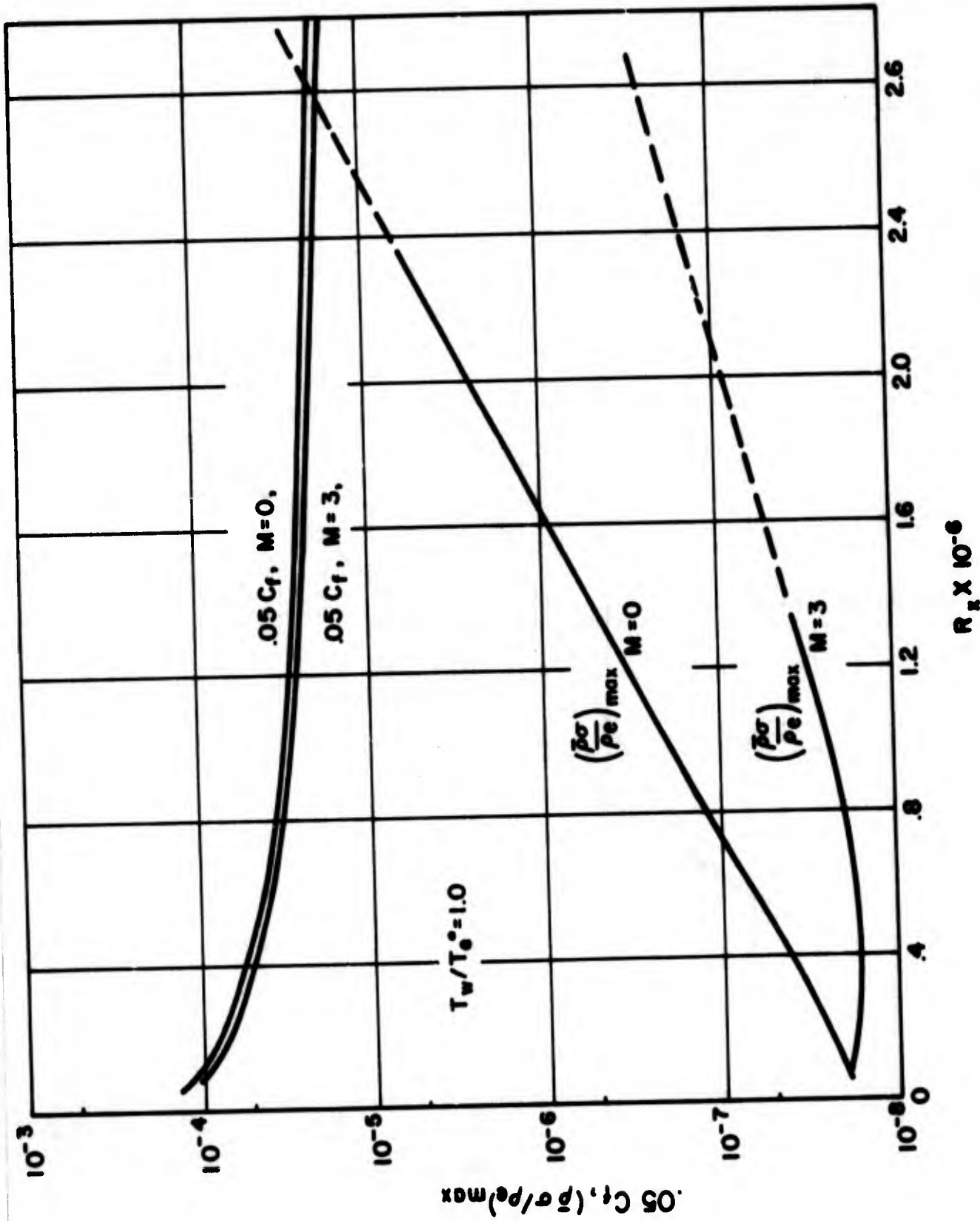
Figure 28. Low disturbance level run-out calculation for $M = 0$ and $M = 3$. $(K_{max}(0) = 3 \times 10^{-6})$
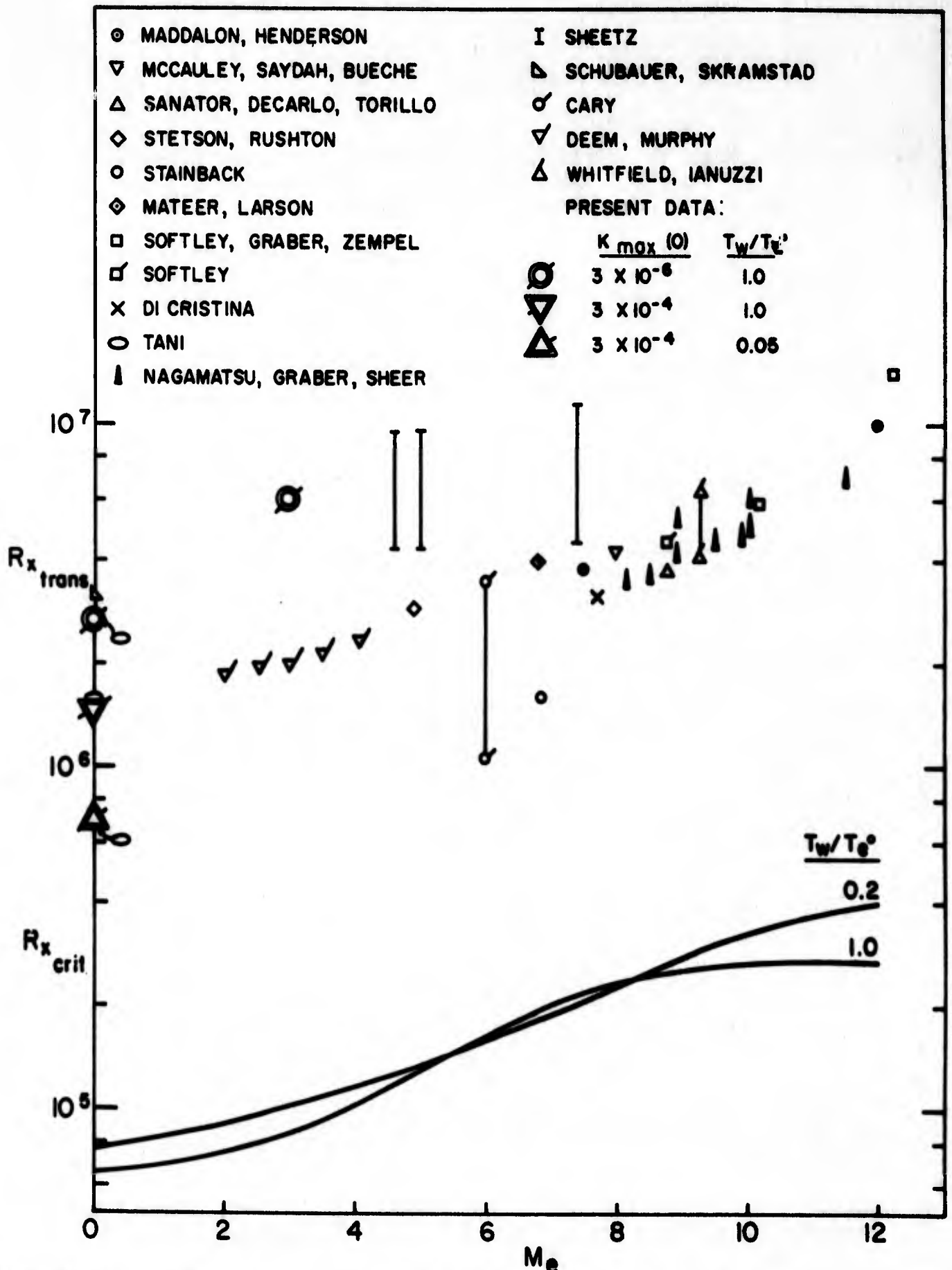
Figure 29. Comparison of present stability calculations for critical $R_x$ and transitional $R_x$ from run-out calculations with experimental results.

5-69

# REFERENCES

1. Morkovin, Mark V.: "Critical Evaluation of Transition from Laminar to Turbulent Shear Layers with Emphasis on Hypersonically Traveling Bodies,"AFFDL-TR-68-149, March 1969.

2. Donaldson, Coleman duP.; Sullivan, Roger D.; and Rosenbaum, Harold: "Theoretical Study of the Generation of Atmospheric Clear Air Turbulence," AIAA Paper No. 70-55, presented at AIAA 8th Aerospace Sciences Meeting, New York, January 1970.

3. Reynolds, Osborne: "On the Dynamical Theory of Incompressible Viscous Fluids and the Determination of the Criterion," Phil. Trans. A186, 1894.

4. Nagel, A.L.; Savage, R.T.; and Wanner, R.: "Investigation of Boundary-Layer transition in Hypersonic Flow at Angle of Attack," AFFDL TR-66-122, August 1966.

5. Wazzan, A.R.; Okamura, T.T.; and Smith, A.M.O.: "Spatial and Temporal Stability Charts for the Falkner-Skan Boundary-Layer Profiles," McDonnell Douglas Report DAC-67086, September 1968.

6. Mack, Leslie R.: "Boundary-Layer Stability Theory," JPL Report 900-277 Rev. A, November 1969.

7. Maddalon, Dal V.; and Henderson, Arthur: "Boundary-Layer Transition on Sharp Cones at Hypersonic Mach Numbers," AIAA Journal, Vol. 6, No. 4, March 1968, p. 424.

8. McCauley, W.D.; Saydah, A.R.; and Bueche, J.F.: "Effect of Spherical Roughness on Hypersonic Boundary-Layer Transition," AIAA Journal, Vol. 4, No. 12, December 1966, pp.2142-2148.

9. Sanator, R.J.; DeCarlo, J.P.; and Torillo, D.T.: "Hypersonic Boundary-Layer Transition Data for a Cold-Wall Slender Cone," AIAA Journal, Vol. 3, No. 4, April 1965, pp. 758-760.

10. Stetson, K.F.; and Rushton, G.H.: "A Shock Tunnel Investigation of the Effects of Nose Bluntness, Angle of Attack, and Boundary Layer Cooling on Boundary Layer Transition at a Mach Number of 5.15," AIAA Paper No. 66-495, Los Angeles, June 1966.

11. Stainback, C.P.: "Some Effects of Roughness and Variable Entropy on Transition at a Mach Number of 8," AIAA Paper No. 67-132, New York, January 1967. See also NASA TN D-4961, January 1969.

12. Softley, E.J.; Graber, B.C.; amd Zempel, R.C.: "Experimental Observation of Transition of the Hypersonic Boundary Layer," AIAA Paper No. 68-39, 1968.

13. Softley, E.J.: "Transition of the Hypersonic Boundary Layer on a Cone: Part II, Experiments at M = 10 and More on Blunt-Cone Transition," GE Space Science Lab., MSD, Document No. GE-TIS-R68SD14, October 1968.

14. DiCristina, V.: "Three-Dimensional Laminar Boundary-Layer Transition on a Sharp 8° Cone at Mach 10," AIAA Journal, Vol. 8, No. 5, May 1970, p. 852.

15. Tani, I.: <u>Boundary Layer Transition</u>, Annual Reviews of Fluid Mechanics, Volume I (Annual Reviews, Inc., Palo Alto, 1969).

16. Nagamatsu, H.T.; Graber, B.C.; and Sheer, R.E.: "Roughness, Bluntness, and Angle-of-Attack Effects on Hypersonic Boundary Layer Transition," J. Fluid Mech., Vol. 24, Part 1, January 1966, pp. 1-31.

17. Sheetz, N.W., Jr.: <u>Boundary Layer Transition on Cones at Hypersonic Speeds</u>, Proc. Navy-NASA-LTV Symposium on Viscous Drag Reduction (Plenum Press 1969).

18. Schubauer, G.G.; and Skramstad, H.K.: "Laminar Boundary Layer Oscillations and Transition on a Flat Plate," NACA Report 909, 1948; J.Research National Bureau of Standards $\underline{38}$, 1947, pp. 251-292; J. Aero. Sci. $\underline{14}$, 1947, pp. 69-78.

19. Cary, A.M., Jr.: "Turbulent Boundary-Layer Heat Transfer and Transition Measurements for Cold Wall Conditions at Mach 6," AIAA Journal, Vol. 6, No. 5, May 1968, pp. 958-959.

20. Deem, R.E.; and Murphy, J.S.: "Flat Plate Boundary Layer Transition at Hypersonic Speeds," AIAA Paper No. 65-128, January 1965.

21. Whitfield, J.D.; and Iannuzzi, F.A.: "Experiments on Roughness Effects on Cone Boundary Layer Transition up to Mach 16," AIAA Journal, Vol. 7, No. 3, March 1969, pp. 465-470.

22. Lees, L.: "Laminar Heat Transfer over Blunt-Nosed Bodies at Hypersonic Flight Speeds," Jet Propulsion, Vol. 26, 1956, pp. 259-269.

23. Back, L.H.: "Acceleration and Cooling Effects in Laminar Boundary Layers - Subsonic, Transonic, and Supersonic Speeds," AIAA Journal, Vol. 8, No. 4, 1970, pp. 794-802.

(This page intentionally left blank)

Ω

# SESSION V

## WORKSHOP COMMITTEE
## RECOMMENDATIONS

Dr. Kenneth Lobb, Chairman

## COMMITTEE A - THEORETICAL APPROACHES

### Dr. Eli Reshotko, Chairman

The items discussed by the Committee on Theoretical Approaches can be listed as shown in Table I. Basically, the theoretical problems that we deal with can be divided into three categories.

The first category is that of linear stability. In this category are described the characteristics of the boundary layer when viewed as a linear oscillator. The items listed in the Linear Stability column of Table I are the factors that affect the boundary layer profiles, hence the characteristics of the oscillator. Category two - receptivity - deals with the input disturbances themselves. It includes the description of how they enter the boundary layer and what their signature is in the disturbance flow. The response of the boundary layer whose characteristics as an oscillator are described by Category One studies to the disturbances listed in Category Two represents the initial linear portion of the transition process. The third category of theoretical approach is that of "transition theory" including non-linear processes. An example of a transition theory is the Donaldson-Yates approach to transition through invariant modeling which was described at this workshop by Dr. Yates. In a transition theory you start from scratch with Navier-Stokes equations assuming an appropriate

# TABLE I

## THEORETICAL APPROACHES

| LINEAR STABILITY | RECEPTIVITY | TRANSITION THEORIES |
|---|---|---|
| (Eigenvalue problems) | (Non-eigenvalue problems) | Invariant Modeling |
| Flat Plate & Cone Temperature level and distribution | External Pressure Fields | Non-linear disturbance equations |
| Pressure Gradient | Free Stream Turbulence | Include distortion of mean flow due to $\tau_{Re}$ |
| Suction and Blowing | Entropy Disturbances | Mode coupling |
| Bluntness | Model Vibrations | Turbulent Energy level approaches |
| Roughness | | |
| Angle of Attack | | |
| Sweep | | |
| Other 3D | | |
| Longitudinal Curvature | | |
| Streamwise Vortices | | |
| Transverse Curvature | | |

disturbance input (and each theory needs some kind of input). Then you let the calculation run as far as you think it can or should go. In addition, you must choose a transition criterion based either on disturbance energy level, a comparison of Reynolds stress with viscous stress or some equivalent criterion. When the calculated quantities reach the point where they satisfy the chosen transition criterion then the transition Reynolds number can be identified from the calculation. Table I lists a number of forms of transition theory and the non-linear elements that enter into them.

Now, let me go back and discuss some of these in a little more detail.
So far the linear stability theories have received the greatest emphasis and
within this category most attention has been given to the zero pressure
gradient cases of the two-dimensional flat plate and cone at zero angle of
attack. Attention has also been given to temperature level in these calcu-
lations but not to axial temperature distribution. There are other factors
which modify the two-dimensional boundary layer (when I say two-dimensional,
I mean also axi-symmetric) in the sense that they modify the profile. In a
linear stability calculation, one studies the stability of a profile so the
key thing with respect to linear stability is that anything that modifies
the profile changes the nature of the amplifier. Factors that change the
profile of a two-dimensional boundary layer are: (Table I, Category 1)
pressure gradient, suction and blowing, bluntness and roughness. We can
also go into three-dimensional problems by introducing, for example, angle
of attack and sweep. Other factors which may change the profiles are longi-
tudinal curvature, streamwise vortices (whether arising from longitudinal
curvature or from other defects or aspects of the geometry) and transverse
curvature.

In Category 2 (Table I) we have the various kinds of disturbances that
may exist and we have to figure out how they couple with the boundary layer.
The information generated to date on the external pressure fields indicates
that they seem to enter rather cleanly from a theoretical point of view.
We do not as yet have as workable a theoretical procedure for introducing
free-stream turbulence and entropy disturbances into the boundary layer.

A-3

The introduction of model vibrations into the theory while conceptually not difficult has yet to be studied.

There has been some progress in developing the elements of some of the non-linear processes and transition theories but not to the point where they are sufficiently independent of empiricism to yield any new information. The empirical elements of these theories are themselves in a state of flux.

The basic objective of people engaged in theoretical work is to understand mechanisms, to understand physically how the elements of a given problem in mechanics work. We have before us in Table I the elements of the transition problem and now we simply have to get busy and start putting them together in an understandable way. From the Committee discussion, the elements that seem most neglected to date are in Category 2 and it is felt that in the immediate period of time there should be concentration on this category. More can, of course, be done in the area of linear stability, particularly for problems other than those involving zero pressure gradient boundary layers. As far as the transition theories go, they are interesting but it is not clear as to what intensity of effort should be put into them at this time. We agree however that there should be no lessening in the effort on transition theories. But if one is seeking to attack theoretically an area which can be most fruitful for understanding of mechanism and for the help that it might give to experimentalists, we feel that the problems to study are those concerned with free-stream turbulence, entropy disturbances, radiated sound, bluntness and roughness.

## COMMITTEE B.    TRANSITION DATA CORRELATION APPROACHES

MR. LEITH POTTER                                    CHAIRMAN

Appropriately, we started by considering the purpose of correlations. We think that's to help the designer and advance the general understanding of the problem. Then we got on to some of the details which I shall review now.

Several of the members felt that improved consistency in the interpretation of the full-scale flight results and uniformly rigorous computation of flow conditions would be big assets. The flight data, of course, come from a number of different types of sensors; e.g., thermocouples are buried differing distances below surfaces, transition is inferred from total drag, from base pressure, etc. I think most of us who don't normally work with those data felt that the reports at this meeting showed a considerable improvement in the quality of the flight data. Nevertheless, people who work on flight data believed that they could be still improved by a more consistent manner of instrumentation and interpretation of the results.

Another point is that it would be a great service to would-be correlators if the data from flights were more widely available. Obviously, it's quite a task to put the flight data in a form that can be used directly for studying correlations of transition. Perhaps the data could be made available to appropriate organizations after screening by a critical group familiar not only with the flight techniques and data interpretation, but also familiar

with transition research. Such a summary booklet should contain all pertinent vehicle and flow conditions. The manner of determining transition location should be defined, or the data given so that the individual worker could make his own determination. The local flow conditions should be included, all calculated in a consistent and suitably rigorous manner. Now this sounds like a big order, but a few people have been doing it. We heard them reporting at this meeting, but we felt that some other correlations or some other ideas about correlation might be forthcoming if others had access to the data. I don't know whether making a body of selected flight data available is feasible, but that's not a problem for committee recommendations. We only suggest that it be considered.

The third point is that we feel that correlations that omit known parameters, or parameters where there is evidence of importance, must be viewed with considerable reserve. Success in collapsing the data is certainly one requirement for a successful correlation, but maybe not the whole story. When parameters that are believed to be important are not included in the correlation, then one wonders how much one can trust the correlation.

Some of the people in our meeting then wanted to list parameters. It's very possible that in our haste we might have forgotten something, but here is our list:

Edge Mach number

Edge unit Reynolds number (or associated quantity)

Wall-to-adiabatic recovery enthalpy ratio (or as Beckwith has pointed out, possibly a more effective parameter is the wall-to-boundary layer edge enthalpy ratio)

Total temperature or total enthalpy may be a factor

Pressure gradients in all three dimensions

Temperature or wall enthalpy gradient

Chemical composition of the boundary layer (that is, the composition of the fluid adjacent to the surface conceivably is a factor, as pointed out by Berkowitz, et al. in this meeting)

Angle of attack

Rate of change of angle of attack

Mass transfer, $\dot{M}$ (blowing or sucking)

Distribution of $\dot{M}$

Surface roughness and waviness

Surface vibration

And I haven't even listed the other factors that might be important in the wind tunnel environment. These are just the things we thought of that are necessary to look at when analyzing flight conditions. It was pointed out too that the correlators often tend to ignore the factor of memory (or the history of the boundary layer) and tacitly assume that the input disturbances of importance are covered by the things that I listed earlier, the local Mach number, Reynolds number, etc.

Two current types of transition problems were emphasized during our discussion, although it is by no means assumed that other cases are solved. One of these recurrent problems is the prediction of transition conditions in the nose region, say for $S/R_N \sim < 5$, where transition is very near the stagnation point. Now the same parameters probably apply there, but the priority or the ordering of the parameters may be different. For example, flow property gradients normal to the surface should not be ignored. There is a need for new data, but we shouldn't ignore the old data which some of our younger associates may not have heard of, such as the X-17 experiments. This stagnation region transition problem merits renewed attention. The same can be said about three-dimensional lifting body flows which give rise to new parameters such as cross-flow Reynolds number, as discussed by Pate and Adams. These subjects have been covered in reported research, but there is not an abundance of data, at least not in the form one would need for correlation purposes.

Finally, it was emphasized that simply succeeding in collapsing the data by taking fractional roots of the parameters and extensive use of log paper is not really the final test. The final test, as someone demonstrated to us during this meeting, is the uncertainty band resulting when the station of transition is predicted in physical coordinates. And so the sensitivity of the parameters is something to consider in evaluating correlations.

- - - - - - - - - - - - - - - - - - - - - - - - - - - - - - - - - - - - - - -

The panel on Flight Test Experiments addressed questions related to
the problems of flight measurements and flight test planning.  First, we
obtained some indication as to what kind of flight measurements are needed,
above and beyond the kind we now make.  Secondly, we attempted to suggest
new forms of flight experiments.  Considerable time was devoted to describing
our problem domain to the panel members.  By "our problem" is meant the
ABRES type of problem.  It was quite surprising to much of the audience that
we were addressing primarily the flow in the first four and five nose radii from
the stagnation point and that we are concerned with the problem of angle of attack.
It was felt that this had been covered during the first day.  It was also quite sur-
prising to most attendees that we were addressing situations where, under the
best of conditions, our boundary layer was a rather strange one; that its thick-
ness, in some of the critical regions was perhaps less or, at best, just slightly
more than the smallest height of some of the roughness being discussed.  People
were shocked that we were talking about boundary layers a few mils in thickness
in the nosecap region and about materials whose inherent roughness is also
several mils.  Indeed, we were not speaking of small roughness buried in the
boundary layer.

It was generally agreed that, when we go to angle of attack and attempt
to obtain data up near the nose region, the present techniques employed, such
as a backface thermocouple measurement, are inadequate.  The approach which
will have to be taken in order to interpret what is going on, or to provide us with
an alternative to flying many vehicles to categorize what is happening, is to use
a complement of ground test data and what would be considered as high-risk
flight test experiments.  By this is meant the following: We may be forced, after
going through a suitable ground test program to try to isolate the main parameters
for our case, to instrument a graphite nose tip, knowing there is a chance that,
purposely, it may fail.  In designing the experiment, we will have to guarantee
that, if the failure of that tip takes place due to the holes that have been drilled or
what have you, the failure will take place at a different altitude regime, say, than
the one at which we want to make our measurements.  Other variations on this,
such as sacrificial skins, also must be considered.  These are felt to be high-risk

experiments. Admittedly, this is a different way of thinking than we are accustomed to. Ordinarily, we design nose tips as best we know how and then tack on the instrumentation without jeopardizing the survivability of the nose tip. The severity of our present situation may justify high-risk experiments such as those described above.

Additionally, there are other points to consider. From the theoretical and ground test people, we need simple scaling laws that will aid in defining our flight instrumentation. Listing all of the possibly important parameters is of little use. The ground test can and should be used, perhaps, to shake out some of these parameters and give us more information as to what we should look for with a limited amount of instrumentation in order to put together any reasonable flight experiment. For example, it may be that we can get all the data we need out of a sphere that is one foot in diameter rather than one inch. In this case, we may be able to configure a flight experiment where we can, indeed, put the instrumentation in a sphere and fly it. We need help in these areas from the ground test and theoretical people. It would seem that one of the basic products of any theory should be scaling laws, even if it does not come out with a number. This is the first thing a theory must give if it is to be of value--some scaling laws that indicate how to plot the data once it is obtained. Hopefully, some of these theories will give us scaling.

Finally, it does not seem improbable to ask that careful calculations be performed for some of the cases where it is felt we have good flight test data. For the most part, this problem has been relegated to the background, and many researchers, for the past ten years, have been working on hypersonic wakes, etc. Techniques that are from ten to fifteen years old are still being used to calculate the laminar flow that should be the thing that all the parameters like receptivities, etc., are feeding on. People are still trying to do transition correlations using locally similar techniques. Present computers allow one to do good laminar flow calculations where there should no longer be a question whether there is a factor of two in predicting displacement thickness or momentum thickness. One can include things like mass addition and the real pressure field. These calculations are difficult, but not necessarily out of scope. They are certainly not out of scope when compared with the cost of running an experiment at a large wind tunnel.

These were the main areas of discussion and, although we were unable to fully answer the questions posed, it was agreed that the problem is sufficiently

critical that we must finally contemplate some higher risk experiments in flight to obtain the proper data.

(This page intentionally left bl..k)

DR. MARK V. MORKOVIN                         CHAIRMAN

Because of unscheduled interference, we "ground-testors" had a rather short and disorganized meeting. Within our group there are strong feelings and some differences of opinion on transition research in ground facilities. I trust that those of our group who may feel that what I report here does not reflect well enough our overall views and needs will speak up at the end and register any omissions or their own separate views.

We started our discussion attempting to respond to Frank Fernandez' Committee C, in particular to the challenge of scaling their flight transition via blunter and larger models (with better spatial resolution) in ground facilities. Immediately, this brought us up against the key problem for meaningful ground tests: identification of the dominant factors or causes for transition on the prototype flights. For, it is the restricted subset of factors which control the specific type of transition mode in the given complex overall environment (Fig. 1 of my "Open Questions", yesterday) which provide the guide to potentially successful ad hoc scaling. Thus we were told just a couple of hours ago that the ABRES type transition on slender bodies with moderate blunting is apparently not sensitive to disturbances in the free stream. This would rule out scaling with amplitude- and size/frequency characteristics of the free-stream disturbances. Since the latter have been identified by Kendall, Pate, and Co. as primary factors in transition on slender bodies in wind tunnels, the essence of the problem of ground simulation has been illustrated in this contrast. To be in the same ball park means that we have to simulate the subset of controlling factors (causes).

In the role of a service group, the ground experimentors need to have the flight people and the designers help to define the likely dominant causes

of ABRES transition, shuttle transition, Project X transition, etc., in order
to be of more direct use to such programs!  Frank's earlier comments and
challenge indicate that there are no viable alternatives to such cross-dis-
cipline cooperation.  The two transition forums organized by our hosts have
laid the groundwork for such cooperation.

Important national programs point us in the direction of the ball park
with a combination of conditions of high unit Reynolds numbers and roughness
with low wall-to-recovery temperatures, $T_w/T_r$, and with or without ablation.
This is a difficult, catch-as-catch-can proposition to be faced by the ex-
perimentors in terms of the peculiarities of their facilities.  As I emphasized
in my presentation, this ball park is unlikely to be truly illuminated until
we understand better the vexing problem of temperature sensitivity - the zigs
and zags of my Figures 3-5.  I have asked Leith Potter to follow me with extra
comments on these conditions of high unit  Reynolds number and low $T_w/T_r$ about
which he has done a lot of thinking in connection with ballistic ranges.

The aforementioned free-stream disturbances in supersonic tunnels con-
taminate the boundary layer on the model so that the significance of tunnel-
observed transition with respect to that in flight must be questioned.  We
feel that testing in contaminated tunnels remains meaningful with respect to
transition mechanisms and mild lower bounds _whenever_ the transition mechanism
or "cause" is clearly dominant.  For instance, strong ablation or strong wall
blowing almost surely override the influence of tunnel wall irradiation, viz.
Stalmach's presentation.  Kendall's documentation of the (relatively slow)
manner in which the disturbances lead to transition supports our communal
feeling that "differential" testing and experimentation in contaminated tunnels
makes some, though limited sense.  Kendall himself demonstrated the "differential"
effects of small blunting of a flat plate, and of small angle of attack on a

slender cone directly in terms of the evolution of the growing boundary-layer fluctuations.

Almost with the same unaminity we felt that for blunt bodies with substantial roughness the tunnel contamination is likely to play a secondary role. The "early" transition process ($R_\theta < 300$) on blunt bodies, especially with high cooling, apparently does not represent "normal" amplification process into which the irradiation from the tunnel sidewalls would significantly couple. Insofar as the ABRES transition includes features of the early blunt-body transition, there could then be some possibility of scaling experiments in wind tunnels. This meeting, I believe, provided extra motivation for the tunnel people to exercise their ingenuity and flex their facilities in this direction.

Our group agreed that a continued effort in definition and spectral classification of free-stream disturbances was desirable in connection with typical transition tests in wind tunnels. While it may bring out additional perplexities, as Bertram's and Owen's reports yesterday exemplified, we feel strongly that such an effort is necessary (though not necessarily sufficient) for the clarification of the embarrassing differences in results between different tunnels.

Despite the preceding several fruitful areas of research in contaminated tunnels, any such transition results remain tainted. We generally support the push towards "quiet tunnels". Besides the Mach 2 and 4 tunnels reported upon by Eli Reshotko on Thursday, there was a feeling that we should be concerned with developing a quiet tunnel with high enough Reynolds number to be able to observe uncontaminated transition at Mach 10-12. This would aim at the important extrapolation of $R_{tr}$ to really hypersonic conditions and its likely uncontaminated dependence on M ($M^{2.5}$, $M^{3.5}$, $M^4$, or what?). Mach 10-12

makes a good target because such conditions remain within the range of
reliable instrumentation as well as of good enough theory: Leslie Mack's
new computer program extends its usefulness to perhaps M ~ 14.

The shortness of our meeting was more than compensated for by the fact
that most of the ground has been carefully considered by the NASA Transition
Committee as described by Eli in his keynote address, and to some extent in
my "Open Questions" presentation (which is an updated version of my status
report to NASA, leading to the formation of that Committee). You-all will
find additional ideas and suggestions in these reports, e.g. concerning the
needed interplay between experiment and theory and between different facil-
ities. Committee D did not really get to the ballistic range questions -
Eli's and Potter's papers report a consensus on the desirable and feasible
experimental targets.

Personally, I would like to commend to you a broader utilization of the
general "spoiler" technique of testing for sensitivity to various parameters
which was used so effectively by Potter in connection with vibration effects
of the ballistic models. For instance, flights through "known" turbulence,
purposely introduced into the ballistic range, would tell us whether the ABRES-
type models "have the right" to be insensitive to free-stream disturbances as
we are told that they are in atmospheric flight. Also, I would be willing to
bet that acoustic radiation from the range sidewalls generated by the sabot
impact (the radiation which Potter showed us how to avoid in his now classic
R/L range studies) makes little difference to the model boundary layer, be-
cause of scale mismatch, leading to negligible receptivity for the disturbances.
On-purpose, sidewall-banging excitation of the free stream with other conditions
unchanged from those of Potter could validate this conjecture, and with it the
many ballistic range tests where the sabot-bang contamination is present. In
other words, perturb for sensitivity those disturbances and parameters that

you cannot reduce: if you can't like them, join them! Even in flight tests, larger bodies can have strips or wedges of their surface covered with known surface roughness while comparable segments retain their normal smoothness. The effects of free-stream disturbances, temperature history, and other parameters, would then be the same and could make the transition diagnosis much more definite. Etc., etc.

This brings us to the desirability of returning periodically to "standard conditions" for checks on repeatability in presence of the large complex of unmeasurable or unmeasured environmental parameters. Bertram's report yesterday on the case of non-repeatability of the results under presumably identical wind-tunnel conditions is not an isolated instance. It only drives home the fact that the twin features of large amplifications and vast number of inputs and modifiers make the transition process non-deterministic as compared to, say, the quasi-deterministic turbulence itself. Several people in our group made strong pleas for systematic extra measurements defining the environment including free-stream spectra and vibrations, so as to minimize and/or explain such discrepancies. Of course, one can go just so far with these expensive and time-consuming techniques without adequate theoretical modeling to provide the conceptual framework. Nevertheless, more can be done at moderate costs, say by monitoring the wind tunnel sidewalls.

Pleas were also heard for redundancy of transition measurements themselves. We have known for some time that as Mach number increases the domains of essentially laminar and highly agitated flow coexist not only in spanwise direction but also in the direction normal to the flow. Bertram's vivid example yesterday underscores the fact that different instruments are "blind" and can give substantially different samplings of the same elephant - hence the plea for redundancy of transition identification.

Several of us feel that the effect of streamwise pressure gradients needs to be tackled more rationally, though we don't know exactly how. In many tunnels one could secure instrument access to the sidewall boundary layer, at least locally, without excessive costs and injury to the test flow. This pressure gradient could tell a great deal about relaminarization and retransition phenomena as a function of the unit Reynolds number. And of course, it would help us to define further the tunnel disturbance environment.

As a group we did not identify any specific experiments and their priorities beyond those of Eli's NASA Transition Committee - and for the same reasons. One can't tell an expert how to play his virtuoso instrument. But one could expect interesting music if the funding officers held out the carrot in the desirable directions...

## DOCUMENT CONTROL DATA - R & D

*(Security classification of title, body of abstract and indexing annotation must be entered when the overall report is classified)*

| 1. ORIGINATING ACTIVITY (Corporate author) | 2a. REPORT SECURITY CLASSIFICATION |
|---|---|
| THE AEROSPACE CORPORATION<br>SAN BERNARDINO OPERATIONS | UNCLASSIFIED |
| | 2b. GROUP |

3. REPORT TITLE

PROCEEDINGS OF THE BOUNDARY LAYER TRANSITION WORKSHOP HELD 3-5 NOVEMBER 1971, Vol IV

4. DESCRIPTIVE NOTES (Type of report and inclusive dates)

Technical Operating Report

5. AUTHOR(S) (First name, middle initial, last name)

W. D. McCauley

| 6. REPORT DATE | 7a. TOTAL NO. OF PAGES | 7b. NO. OF REFS |
|---|---|---|
| 20 Dec 71 | | |

| 8a. CONTRACT OR GRANT NO. | 9a. ORIGINATOR'S REPORT NUMBER(S) |
|---|---|
| F04701-71-C-0172 | TOR 0172(S2816-16)-5 |
| b. PROJECT NO. | |
| c. | 9b. OTHER REPORT NO(S) (Any other numbers that may be assigned this report) |
| d. | SAMSO TR 73-155, Vol IV |

10. DISTRIBUTION STATEMENT

Distribution limited to U.S. Government Agencies Only. (Test & Evaluation) (20 Dec 71) Other requests for this document must be referred to SAMSO/RSSE.

| 11. SUPPLEMENTARY NOTES | 12. SPONSORING MILITARY ACTIVITY |
|---|---|
| | Space & Missile System Organization<br>P.O. Box 92960, Worldway Postal Center<br>Los Angeles, California 90009 |

13. ABSTRACT

The workshop consisted of introductory remarks, a keynote address, four reporting investigation sessions and a session involving all participants on four committees. The objective of the meeting was to make transition specialists aware of the most recent data and techniques for transition prediction and to focus on the solution of design problems associated with boundary layer transition. The first session showed how transition affects reentry vehicle design in terms of nose tip thermostress and ablation, transpiration cooled nosetips, frustum ablation, reentry observables, plasma attenuation, vehicle dynamics and space shuttle design. The second session presented ABRES reentry vehicle transition data and prediction techniques obtained since the previous meeting four years ago. The third session presented recent applications of stability theory, additional confirmation of the theory and work toward transition modeling. In the last session the meeting participants worked on four committees to arrive at recommendations for future efforts on boundary layer transition.

DD FORM 1473 1 NOV 65